Aachener Verfahrenstechnik Series
AVT.CVT – Chemical Process Engineering
Volume 14 (2021)

Robert Gregor Keller geb. Sengpiel

Fenton's Chemistry in Biorefineries

Fenton's Chemistry in Biorefineries

Robert Gregor Keller geb. Sengpiel

DOI: 10.18154/RWTH-2021-06495

Fenton's Chemistry in Biorefineries

Fenton-Prozesse in Bioraffinerien

Von der Fakultät für Maschinenwesen der Rheinisch-Westfälischen Technischen Hochschule Aachen zur Erlangung des akademischen Grades eines Doktors der Ingenieurwissenschaften genehmigte Dissertation

vorgelegt von

Robert Gregor Keller geb. Sengpiel

Berichter:
Univ.-Prof. Dr.-Ing. Matthias Wessling
Prof. Dr. Ir. Earl Goetheer

Tag der mündlichen Prüfung: 17.05.2021

Diese Dissertation ist auf den Internetseiten der Universitätsbibliothek online verfügbar.

Parts of this dissertation have been published. Reproduced with permission from:

Robert G. Keller, Davide Di Marino, Malte Blindert, Matthias Wessling, *Hydrotropic Solutions Enable Homogeneous Fenton Treatment of Lignin*, Industrial & Engineering Chemistry Research, 2020
DOI: 10.1021/acs.iecr.9b06607

Robert G. Keller, Julia Weyand, Jan-Bernd Vennekoetter, Johannes Kamp, Matthias Wessling,
An electro-Fenton process coupled with nanofiltration for enhanced conversion of cellobiose to glucose, Catalysis Today, 2021
DOI: 10.1016/j.cattod.2020.05.059

Titel: Fenton's Chemistry in Biorefineries
Fenton-Prozesse in Bioraffinerien

Autor: Robert Gregor Keller geb. Sengpiel

Reihe: Aachener Verfahrenstechnik Series
AVT.CVT - Chemical Process Engineering
Volume: 14 (2021)

Herausgeber: Aachener Verfahrenstechnik
Forckenbeckstraße 51
52074 Aachen
Tel.: +49 (0)241 8095470
Fax.: +49 (0)241 8092252
E-Mail: secretary.cvt@avt.rwth-aachen.de
http://www.avt.rwth-aachen.de/AVT

Volltext verfügbar: 10.18154/RWTH-2021-06495

Danksagung

Diese Arbeit wäre ohne die Unterstützung von meiner Familie, meinen Freunden und Kollegen nicht möglich gewesen.

Zuerst gilt mein Dank Prof. Dr.-Ing. Matthias Wessling. Matthias, vielen Dank für die bereits lange währende Unterstützung – ich erinnere mich an Gespräche als Hiwi vor der Elektrodialyseanlage des TMFB –, eine zweite Chance nach einem kurzen Abstecher in die Industrie, und vor allem für deine ansteckende Begeisterung für die Forschung.

I would also like to thank Prof. Dr. Ir. Earl Goetheer for agreeing to be the co-chair of my thesis and the challenging while stimulating exam.

Der Deutschen Forschungsgemeinschaft (DFG) danke ich für die finanzielle Förderung im Rahmen der Exzellenzstrategie des Bundes und der Länder – Exzellenzcluster 286 „Maßgeschneiderte Kraftstoffe aus Biomasse“ und Exzellenzcluster 2186 „The Fuel Science Center“ – ID: 39030946 & 390919832.

Susi, dein Einsatz für den Lehrstuhl und deine Begeisterung für die vielfältigsten Aufgaben sind eine Inspiration. Nicht unerwähnt bleiben sollten natürlich die krachenden Feiern, welche den Arbeitsalltag aufgelockert haben.

Sandra, vielen Dank für die unermüdliche Vermessung meiner HPLC Proben. Der mechanischen Werkstatt, allen voran Jürgen, möchte ich für die Geduld danken, mit der auch schlechte Skizzen in hervorragende Bauteile umgesetzt wurden. Helga, Regina und Melda: Die Zusammenarbeit mit euch war mir immer eine Freude. Dem gesamten IT-Team um Jutta, Sascha und Roman danke ich für den unermüdlichen Support.

Mit Susi, Axel und Simon habe ich eine unvergessliche Zeit beim Bau und Umzug des NGP^2 erlebt. Ohne euren Humor hätte es wenig zu lachen gegeben.

Meine Kollegen während der Promotion bin ich dankbar für viele spannende Gespräche rund um die Forschung. Ich bin stolz mit euch zusammen diese Reise bewältigt zu haben. Jan, unsere Diskussionen rund um die Elektrochemie waren immer eine Bereicherung. Vielleicht können wir eines Tages wieder gemeinsam tüfteln. Patrick, ich bin froh, dass du mir bei meinen Eskapaden ins Reich der Biotechnologie und Biofilmbildung beigestanden hast. Davide, dein umfangreiches Wissen im Bereich Biomassenutzung ist bewundernswert und ich bin froh, dass wir zusammen Cellulose und Lignin spalten konnten. Hannah, Bene, Zana, J-Lo, Burkhard: Mit euch war der fachliche Austausch zwar begrenzt, der nicht-fachliche auf Winterschool und anderen Bildungsreisen aber ausgezeichnet. Oded, it was a pleasure working with you.

Meinen vielen Studierenden möchte ich für ihre unermüdliche Arbeit und ihre Motivation danken. Insbesondere möchte ich Daniel Bell, Sebastian Holtwerth, Jan Haussmann, Julia Sablotny, Julia Steeger, Julia Weyand, Julian Sturm, Kassandra Haack, Kilian Popiehn, Malte Blindert, Marcel Welz, Max Franken, Niklas Knaup, Sahel Khanna, Hannah Rosenthal und Karolin Bach erwähnen, welche maßgeblich zum Gelingen dieser Arbeit beigetragen haben.

Mit meinen Freunden und Kommilitonen zusammen konnte ich das Fundament für diese Arbeit legen. Ich würde es als Studium generale bezeichnen, mit lebenslanger Weiterbildung. Ich bin dankbar, dass ich schon gar nicht mehr zählen kann, seit wie vielen Jahren wir in die Casa Kori fahren. Peter und Phil gebührt Dank für die wirtschaftliche Weiterbildung im Handel neben der Promotion.

Meiner Familie, insbesondere meinen Eltern, danke ich für die immer-währende Unterstützung in allen Lebenslagen.

Laura, ohne dich wäre vieles anders und nicht halb so schön. Ich bin sehr glücklich dich an meiner Seite zu haben. Mit dir bleiben alle Herausforderungen, wie zum Beispiel diese Dissertation, immer nur Herausforderungen und werden nie zu Problemen.

Am Ende wird alles gut

KI01 // Oscar Wilde

Contents

Abstract

Today, the energy, industrial, and transport sectors rely heavily on fossil resources as energy and carbon source. An economy based on fossil carbon leads to high emissions of green house gases, such as carbon dioxide, which cause the anthropogenic climate change. In order to prevent a further increase in the average global temperature and combat the adverse impacts it entails, power-to-x technologies and biorefineries are on the rise. Until now, the technological breakthrough of biorefineries is hampered by numerous barriers: For example, harsh chemical pretreatment conditions with the use of harmful solvents for biomass fractionation lead to high investment costs and high complexity due to non-integrated processes.

This thesis presents integrated biorefinery processes based on green solvents, lignin-first conceptualization, and the coupling of electrochemical processes to cellulose depolymerization. Lignin was extracted from beech wood chips by employing hydrotropic and deep eutectic solvents. Subsequently, lignin was depolymerized via Fenton's chemistry in the hydrotropic solvent and coupled with an in situ extraction. Fenton's chemistry was additionally investigated for the depolymerization of cellulose that was studied using the model compound cellobiose. The process was electrified as electro-Fenton and coupled with an in situ membrane separation.

Lignin was extracted with up to 80% yield with deep eutectic and hydrotropic solvents. The highest yields were obtained with high pretreatment temperatures of 120 and 200 °C, respectively, and small wood chip sizes. The lignin that was extracted in a hydrotropic solution was depolymerized to aromatics in the solvent itself. Even though the depolymerization was successful and an in situ extraction was employed, only low amounts of value-added aromatics were obtained. Organic acids were found to be the main product of the depolymerization with a yield of up to 30% based on the initial lignin concentration. Glucose was successfully formed by the depolymerization of cellobiose using Fenton's reagent. However, the selectivity was limited to values below 30% for all parameters tested in this work. With increasing reaction time, the selectivity decreased continuously due to the oxidation of glucose by Fenton's reagent. Thus, a nanofiltration separation stage was coupled to the (electro-)Fenton process. Experimental and simulation results demonstrated that the separation prevents overoxidation of glucose while simultaneously retaining the reactant cellobiose and the catalyst iron in the Fenton reactor.

This thesis emphasizes the need for integrated processes in biorefineries. Electrochemical processes provide the opportunity to drive reactions by an electrical potential that is powered by renewable electricity. When using Fenton's chemistry for the formation of value-added compounds a strong focus must be laid on in situ separation techniques to prevent degradation of the target products.

Zusammenfassung

Die derzeitige auf fossilen Rohstoffen basierende Wirtschaft verursacht einen hohen Ausstoß an Treibhausgasen wie Kohlenstoffdioxid. Als technologische Alternativen können Bioraffinerien und sogenannte Power-to-X Prozesse eingesetzt werden. Der kommerzielle Durchbruch von Bioraffinerien wird bislang durch Hemmnisse wie hohe Investitionskosten durch den Einsatz korrosiver Medien, oder auch durch den Einsatz toxischer Lösungsmittel und nicht integrierter komplexer Prozesse verhindert.

In der vorliegenden Dissertationsschrift wird ein integrierter Bioraffinerieprozess untersucht, welcher auf grünen Lösemitteln basiert, eine chemische Ligninnutzung untersucht und die Cellulosedepolymerisierung mittels einem elektrochemischen Verfahren behandelt. Ausgehend von Buchenholz wurde Lignin mit hydrotropen Lösemitteln und sogenannten "Deep Eutectic Solvents" extrahiert. Anschließend wurde das Lignin unter Einsatz des Fenton-Prozesses in der hydrotropen Lösung depolymerisiert und die entstehenden Produkte in situ extrahiert. Der Fenton-Prozess wurde in seiner elektrifizierten Variante, dem sogenannten electro-Fenton, für die Depolymerisierung von Cellulose eingesetzt. Eine gekoppelte Membranstufe ermöglichte eine in situ Abtrennung des Zielmoleküls Glukose.

Der Einsatz von "Deep Eutectic Solvents" und hydrotropen Lösungen ermöglichte Ligninextraktionsausbeuten von bis zu 80%. Die höchsten Ausbeuten konnten bei hohen Temperaturen von 120 und 200 °C und einer kleinen Holzspangröße erzielt werden. Das mittels Hydrotropen extrahierte Lignin wurde im Lösemittel selber zu Aromaten depolymerisiert. Auch mit einer in situ Extraktion der werthaltigen Produkte blieb deren Ausbeute gering. Das Hauptprodukt der Fenton-Depolymerisation waren organische Säuren mit einer Ausbeute von bis zu 30%. Bei der Depolymerisation von Cellobiose mittels electro-Fenton-Prozess entstand Glukose mit einer Selektivität von maximal 30%. Cellobiose wurde als Modellsubstanz für Cellulose eingesetzt. Mit fortschreitender Reaktionsdauer sank die Selektivität, da die reaktiven OH-Radikale des Fenton-Prozesses das Produkt Glukose abbauten. Simulationen und Experimenten zeigten, dass eine in situ Abtrennung der Glukose mittels Nanofiltration eine konstant hohe Selektivität unter Rückhalt des Eduktes Cellobiose und des Eisenkatalysators ermöglichen kann.

Diese Arbeit verdeutlicht die Notwendigkeit integrierter Prozesse in Bioraffinerien. Elektrochemische Prozesse, elektrifiziert durch erneuerbare Energien, können in Bioraffinerien integriert werden und zur Sektorkopplung beitragen. Mittels Fenton-Prozess können Polymere wie Lignin oder Cellulose zu werthaltigen Produkten abgebaut werden, allerdings sollte ein starker Fokus auf die in situ Abtrennung eben dieser gelegt werden.

1. Introduction

Increasing greenhouse gas (GHG) concentrations in the atmosphere continue to change the world climate [Mass2018]. Immediate action is required for the average global temperature increase to remain below 1.5 ℃ compared to pre-industrial levels [Mass2018]. In 2019, the major contributors in Germany for GHG emissions of an estimated 805 $Mt_{CO2\ eq.}$ were the energy (31%), industrial (23%), and transport sector (20%) [Umwe2020]. The "Klimaschutzplan 2050" of the German government sets a goal to reduce the emissions — depending on the individual sectors by 26 % to 42 % — until the first milestone in 2030 is reached [BMU2016]. These goals were fixed in a national law in 2019 [Deut2019].

Power-to-X (P2X) technologies based on renewable electricity are regarded as enabling technology on the road towards a sustainable energy future [Ausf2019]. Electrochemistry couples the energy, industrial, and transport sector. Thus, sustainable electrochemical processes facilitate the inevitable electrification of said sectors [Schi2017; Lewi2006; Orel2018]. To achieve the large-scale use of electrochemistry, diverse obstacles such as catalyst and cell development, up-scaling, and product separation need to be tackled [De L2019]. A promising route to achieve (partial) substitution of fossil resources is the valorization of lignocellulosic biomass — the world's largest renewable carbon source — to contribute to a sustainable future [Robe2017; Chan2018]. A carefully established biomass-based economy can close the carbon cycle and mitigate the emission of carbon dioxide to the atmosphere while avoiding fuel-food conflicts [Robe2017]. In a lignocellulosic biorefinery, woody biomass is disintegrated into its primary constituents cellulose,

hemicellulose, and lignin [Wage2019, pp. 2–4]. Subsequently, the fractions are valorized via different process routes [Wage2019, pp. 2–4]. Rising interest can be recognized in the field of electrochemical transformations with bio-based molecules [Vedo2020; Akha2020]. This synergetic coalescence of biorefineries and electrochemistry is coined *electrobiorefinery* [Harn2018]. Up to date, obstacles in the biomass supply chain, the process steps, and the product recovery need to be addressed [Chan2018; Rege2018].

This thesis aims for the development of an integrated biomass fractionation coupled with a subsequent cellulose and lignin conversion through (electro-)chemical conversion techniques that are cost-efficient and environment-friendly. Two promising chemical fractionation approaches using hydrotropic and deep eutectic solvents are investigated. Subsequently, the (electro-)Fenton process is applied for the degradation of the lignin and cellulose fractions to value-added chemicals in integrated processes. An overview of this thesis is given in Figure 1.1, which highlights the investigated unit operations and their combination to a viable process chain.

The fundamentals of biorefineries, cellulose, and lignin valorization, electrochemical conversions, the (electro-)Fenton process, and separation strategies for the products are reviewed in **Chapter 2**. As a first process step, the extraction of lignin from beech wood chips is presented in **Chapter 3**. The influence of wood chip size and temperature on the lignin dissolution with two hydrotropic and two deep eutectic solvents was studied. The enzymatic digestibility of the solid pretreatment residues was assessed. Size exclusion chromatography, scanning electron microscopy, computer tomography, and NMR techniques supplement information on the structure of the extracted lignin and the remaining solid.

Oxidative lignin depolymerization and valorization is a commonly used technique to obtain value added compounds from the biopolymer. **Chapter 4** presents a new approach: Fenton's chemistry, which produces OH radicals, was used for the degradation of lignin in hy-

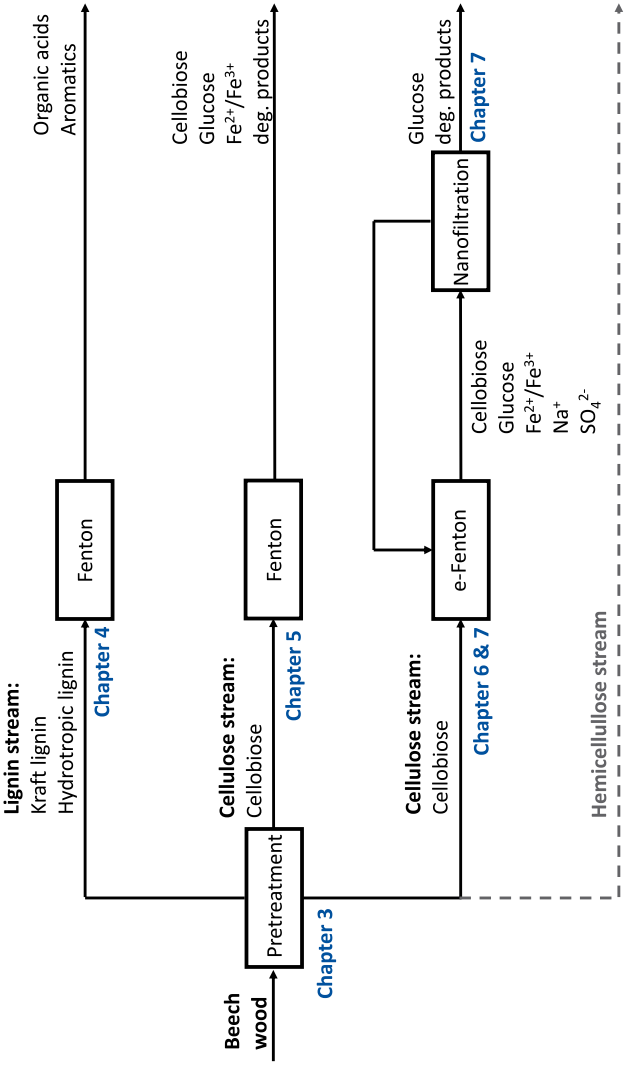

Figure 1.1.: Overview of the investigated process chains of this thesis.

drotropic solvents. In a first step, Kraft lignin was degraded in the hydrotropes to study the influence of the hydrogen peroxide concentration and the pH value on the molecular weight distribution. Degradation products were identified and quantified with GC analysis and liquid chromatography. An in situ extraction of aromatic products into an organic solvent is presented as a strategy to prevent degradation of the products. Finally, the hydrotropic lignin from **Chapter 3** was used in the Fenton process to demonstrate the viability of the process chain.
Cellulose, which is a polymer of glucose, makes up for the highest proportion of the beech wood constituents. The monomer glucose is a viable substrate for the fermentation to value-added chemicals. As a possible alternative to the costly state of the art enzymatic hydrolysis of cellulose to glucose, the Fenton process is presented in **Chapter 5**. The model compound cellobiose functions as well defined substrate to study the influence of a broad range of process parameters on the conversion and selectivity towards glucose: the cellobiose, ferrous iron, and hydrogen peroxide concentration are varied. Additionally, the influence of dissolved oxygen, the chelator dihydroxybenzoic acid, and the salt sodium sulfate is investigated.

The electro-Fenton process represents the electrification of the Fenton process, in which hydrogen peroxide is produced electrochemically in situ and the catalyst ferric iron is reduced to ferrous iron at the cathode to enhance the reaction rate. **Chapter 6** presents tubular and planar electrochemical reactors that are capable of producing hydrogen peroxide and can thus be employed in the electro-Fenton process. In addition to the geometry of the electrodes, different catalysts, a polymeric binder, the operating voltage, the gas flow rate, the gas flow mode, and different spacers for the liquid channel of the electrolyzer are investigated. The experimental parameters are summarized in Figure 1.2. The most promising reactor from **Chapter 6** is subsequently utilized for the electro-Fenton in **Chapter 7** to convert cellobiose to glucose. Findings from **Chapter 5** are compared to the electrified process. Subsequently, the electro-Fenton process is coupled to an in situ membrane filtration to prevent oxidation of the

product glucose by OH radicals. Different commercial and self-made membranes are tested for the separation of glucose from cellobiose and ferrous iron. The experimental findings are transferred to a mathematical model, which is then used to demonstrate the potential of a continuous electro-Fenton process with coupled membrane separation for a steady high selectivity towards glucose. An overview of the investigated parameters is given in Figure 1.2.

The most important findings of the thesis are compiled in **Chapter 8**. The implications of the use of Fenton's chemistry for cellulose and lignin degradation are discussed. The developed electrochemical reactors, especially for an application in the electro-Fenton process, and a combination with in situ separations, are assessed on a level beyond biorefinery applications. Finally, challenges for future work are identified.

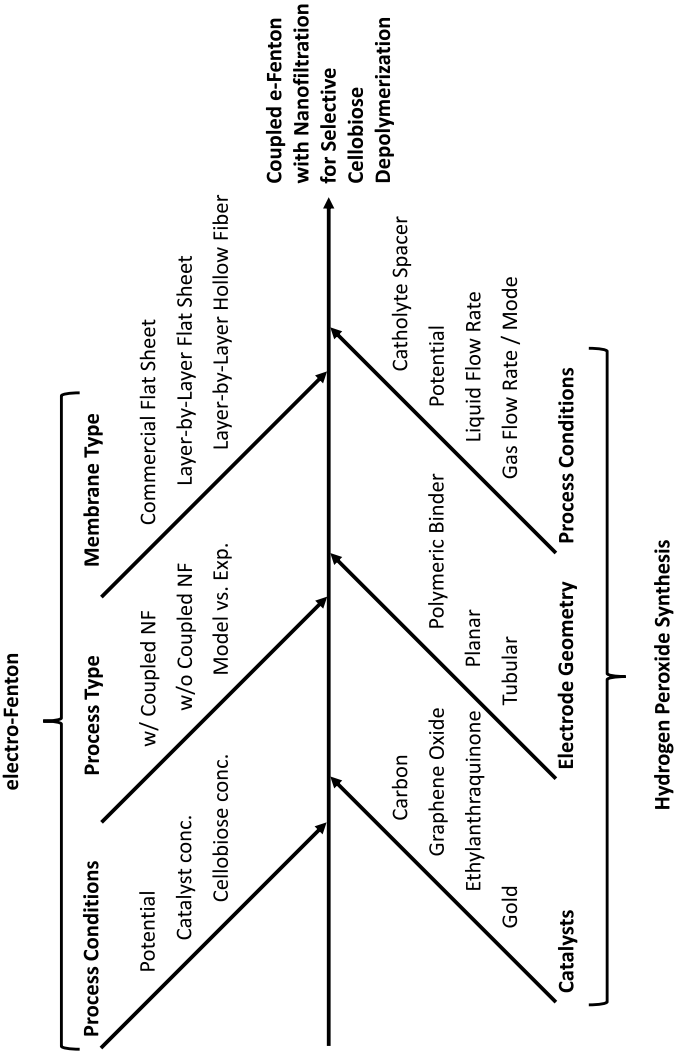

Figure 1.2.: Experimental parameters investigated in Chapters 6 and 7.

Previous Publications in Student Theses

This thesis's content and results emanate from research conducted under the affiliation and position of the author as research fellow and PhD candidate at RWTH Aachen University. The position is associated with the Chair of Chemical Process Engineering. The work comprises data based on the following student theses:

- Malte Blindert, Master's thesis, 29.09.2017, *Hydrotropic solutions for Fenton depolymerization of lignin*
- Indra Marth, Bachelor's thesis, 13.07.2019, *Tuning reaction parameters towards a selective conversion of cellobiose to glucose via Fenton process*
- Marcel Welz, Bachelor's thesis, 24.04.2017, *Optimizing the hydrogen peroxide synthesis in an electrochemical membrane reactor by variation of process parameters*
- Daniel Bell, Master's thesis, 08.12.2016, *Optimization of tubular CNT-based gas diffusion electrodes for hydrogen peroxide synthesis*
- Julia Weyand, Master's thesis, 03.12.2018, *Combining electro-Fenton with layer-by-layer polyelectrolyte membranes for continuous glucose production from cellobiose*
- Sebastian Holtwerth, Master's thesis, 31.03.2019, *Optimization of CNT microtubes as gas diffusion electrodes and incorporation into a tubular electrochemical membrane reactor*
- Sahel Khanna, Bachelor's thesis, 13.03.2016, *Separating cellobiose and iron ions from glucose via nanofiltration*
- O. Altunok, M. Becker, S. Holtwerth, A. Schmitz, J. Schulze, Verfahrenstechnische Projektarbeit, 13.02.2017, *Depolymerisation von Cellulose unter Anwendung des Elektro-Fenton-Prozesses*

1

2. Fundamentals

Parts of this chapter have been published as:
Robert G. Keller, Davide Di Marino, Malte Blindert, Matthias Wessling *Hydrotropic Solutions Enable Homogeneous Fenton Treatment of Lignin*, Industrial & Engineering Chemistry Research, 2020
DOI: 10.1021/acs.iecr.9b06607

Robert G. Keller, Julia Weyand, Jan-Bernd Vennekoetter, Johannes Kamp, Matthias Wessling *An electro-Fenton process coupled with nanofiltration for enhanced conversion of cellobiose to glucose*,
Catalysis Today, 2021
DOI: 10.1016/j.cattod.2020.05.059

2.1. Biomass and Biorefineries

One promising route to achieve (partial) substitution of fossil resources is the valorization of biomass in biorefineries [Robe2017; Chan2018]. In this regard, the valorization of lignocellulosic substrates is attractive, because lignocellulose represents the world's largest renewable organic carbon source [Schu2018; Hube2006]. The definition of biorefineries highlights integrated processes and use of all of the constituents of biomass:

> A biorefinery is characterised by an explicitly integrative, multifunctional overall concept that uses biomass as a diverse source of raw materials for the sustainable generation of a spectrum of different intermediates and products (chemicals, materials, bioenergy/biofuels), whilst including the fullest possible use of all raw material components. Co-products can also be food and/or feed. These objectives necessitate the integration of a range of different methods and technologies. The biorefinery process chain consists essentially of the pre-treatment and preparation of biomass, as well as the separation of biomass components (primary refining) and the subsequent conversion and processing steps (secondary refining). ([Wage2012])

Biorefineries are classified depending on the raw material, platform, products, and processes. The platform, e.g., biogas, syngas, or lignocellulosic components, is most frequently used for classification. In the latter type, a lignocellulosic feed, such as woody biomass, is disintegrated in the primary refining step into the major components cellulose (40-50%), hemicellulose (20-30%), and lignin (20-30%) [Silv2015], see Figure 2.1. Subsequently, the intermediates are valorized via different process routes [Wage2012, pp. 50–54]. In addition to the three major constituents, low molecular weight components such as extractives and inorganic substances as well as minor carbohydrate fractions such as pectins and starch are found in biomass to a much lesser

extent [Sixt2006, p. 22]. The carbohydrate fractions of cellulose and hemicellulose are most often depolymerized to fermentable sugars via cost-intensive enzymatic hydrolysis [Ashr2017]. A subsequent fermentation then yields value-added products [Wage2012, pp. 50–54]. Lignin, on the other hand, is often only thermally valorized given its recalcitrance and heterogeneity. However, lignin is the world's largest renewable source for aromatics and for a successful implementation of biorefineries in the world, more value must be derived from lignin besides the generation of heat [Abu-2020]. For successful commercialization of biorefineries challenges in the biomass supply chain, the process steps, and the product recovery need to be overcome [Chan2018; Rege2018].

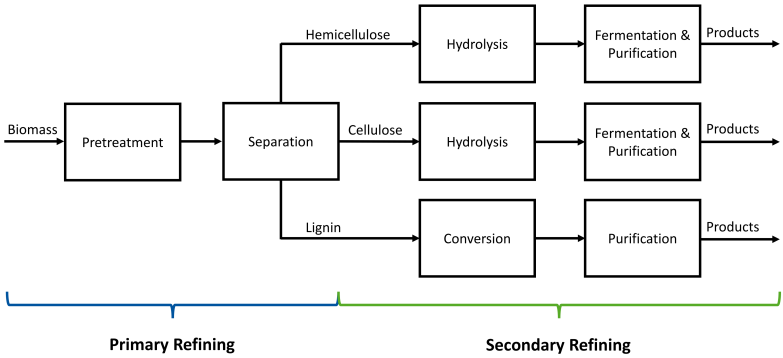

Figure 2.1.: Sketch of a lignocellulose biorefinery with primary and secondary refining.

2.1.1. Pretreatment of Biomass

Different techniques and processes exist for biomass pretreatment and fractionation. For a long time, the main goal of biomass pretreatment was to give enzymes access to the plant carbohydrates to convert them to fermentable sugars [Silv2015; Chan2018]. However, because a viable biorefinery must also utilize lignin, so-called *lignin-first* approaches are gaining attention, in which the valorization of lignin is regarded

as equally important [Abu-2020]. Silveira et al. [Silv2015] give a comprehensive overview of the different categories of pretreatment technologies. As described previously, a suitable pretreatment is imperative to overcome physical and chemical barriers, and to access and separate the major constituents cellulose, hemicelluloses, and lignin. The recalcitrance of biomass is caused by the recalcitrant polymers themselves, but also to the structure, in which cellulose is the framework, hemicelluloses the matrix, and lignin the encrusting material [Sixt2006, p. 41]. The complex structure of lignocellulose is depicted in Figure 2.2. Available pretreatment methods can be categorized as physical, biological and chemical pretreatments, which each offer a spectrum of distinct subprocesses, see Figure 2.3. The effectiveness of each technology is highly influenced by the type of biomass. Currently, hydrothermal and dilute acid/base pretreatments are predominant in industry. Alternatives such as Organosolv or dilute ammonia still require additional development [Wage2019, pp. 177–185]. Many pretreatments are limited by high costs for corrosion resistant vessels, harmful solvents, or slow kinetics. Thus, it is necessary to utilize green chemicals in the preatreatment steps and, in the best case, mitigate effluent streams to the environment [Silv2015].

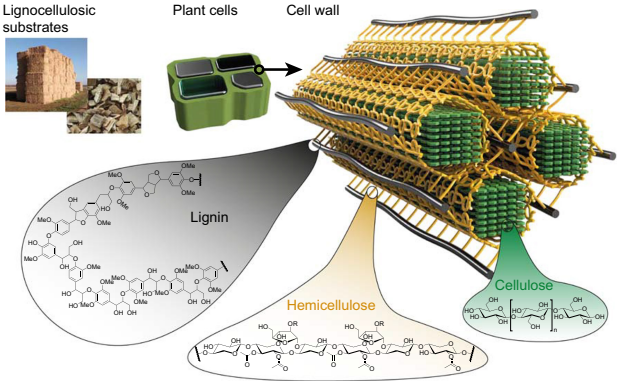

Figure 2.2.: The structure of lignocellulose. Reprinted with permission from Brethauer et al. [Bret2020]. © 2020, Springer Nature.

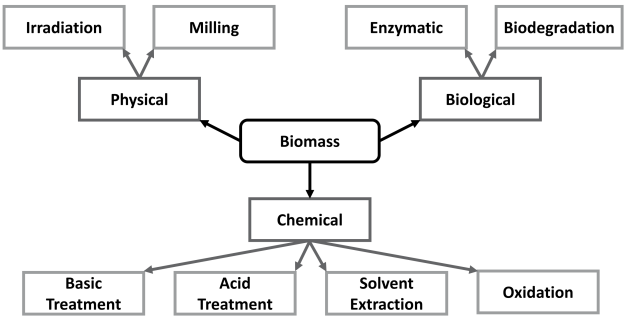

Figure 2.3.: Classification of pretreatment methods according to Silveira et al. [Silv2015]

Hydrotropic Solutions and Deep Eutectic Solvents for Lignin Extraction

Carl A. Neuberg introduced the term *hydrotropy* in 1916 as he observed anionic organic salts to tremendously increase the solubility of otherwise poorly soluble solutes [Dhap2015]. Today, hydrotropes are defined as a class of water-soluble amphiphiles with surface-active properties. Often, they have an aromatic ring structure with a sulfate, sulfonate, or carboxylate group. In contrast to surfactants, they do not aggregate in ordered structures, e.g., spherical micelles, and have a rather short but bulky and compact hydrophobic part [Subb2012]. If the concentration is increased above the so-called *minimum hydrotrope concentration* (MHC), self-aggregates form. In an effort to move towards green chemicals for pretreatment methods [Silv2015], hydrotropic aqueous solutions are a promising chemical pretreatment candidate, as they are cost-effective, nontoxic, and environment-friendly [Subb2012]. Many applications for hydrotropic solutions have been proposed such as the development of pharmaceutical formulations, detergent solutions, food stuffs, paint industry, coatings, plastic additives, alterations in reactions kinetics, selective separations, electrochemical reactions and lignin dissolution [Subb2012; McKe1946]. Lignin can be dissolved up to $350\,\mathrm{g\,L^{-1}}$. Although early interest was raised for wood frac-

tionation utilizing hydrotropic solutions [McKe1946; Proc1971], only recently efforts have increased to evaluate the potential of hydrotropes for biorefinery purposes [Fard2013; Ma2018b; Chen2017; Wang2019]. In comparison to other pretreatment methods, the degradation of cellulose is mitigated, because the hydrotropic solution is pH neutral [McKe1946]. Hydrotropes have been shown to potentially increase the enzymatic digestibility in comparison to pretreatment methods such as hydrothermal pretreatment and organosolv pretreatment [Mou2017]. Additionally, hydrotropic solutions can be easily recovered: after lignin extraction the solution can be diluted until lignin precipitates [McKe1946].

Deep Eutectic Solvents (DES) are a family of ionic fluids. A DES is a mixture of two or three Lewis or Brønsted acids (hydrogen-bond donor) and bases (hydrogen-bond acceptor), which form a eutectic solution with a lower melting point than the individual components. Compared to ionic liquids, DES's have similar physico-chemical properties, but are generally less cost-intensive and often environment-friendly [Zhan2012; Smit2014]. DES's are applied in the field of metal processing, electrochemistry, environmentally benign alternatives for synthesis, gas absorption, biotransformations, and biorefinery applications [Zhan2012; Smit2014; Vigi2015]. Compared to conventional chemical solvents for biomass processing, DES's offer potential advantages inhibiting water reactivity, stabilizing carbohydrates and furanic derivatives, decreasing polyol visocosity, and increasing enzymatic compatibility [Vigi2015]. As the family of DES's is very large, the potential benefits need to be assessed for each application. Franisco et al. [Fran2012] studied the dissolution of lignin, cellulose, and starch in different DES's. Lignin was generally well dissolved with up to 14.9 wt.-% in a maleic acid/proline mixture, while cellulose solubility was negligible. As DES's are also suitable solvents for the conversion of lignin [Di M2016] and carbohydrates [Vigi2015], integrated biorefinery processes are attainable. However, compared to the high dissolution of pure lignin, lignin extraction from biomass was found to be low and needs to be investigated in more detail [Fran2012].

2.1.2. Lignin Valorization

Lignin is a recalcitrant biopolymer, which is nowadays often only valorized thermally [Abu-2020]. The economic feasibility and the sustainability of biorefineries can be improved by not only valorizing cellulose and hemicellulose, but also lignin, which constitutes up to 30% of biomass [Schu2018]. Lignin is an amorphous, three-dimensional biopolymer, which is embedded in the cellular walls of land plants. A random and radical polymerization of the three primary monomers (monolignols), p-coumaryl-, coniferyl- and sinapyl-alcohol results in the highly-branched structure of lignin, characterized by several carbon-carbon and carbon-oxygen bonds, see Figure 2.4 [Zakz2010; Schu2018]. The precise composition of lignin molecules differs notably depending on the source (softwood, hardwood, grass, etc.) [Pu2008]. Due to its structure, lignin is chemically and enzymatically highly stable. Uncertain reactivity and heterogeneity impede the degradation of lignin [Argy2016; Stie2016a]. Lignin represents the largest renewable source of aromatic compounds and consequently numerous valorization processes have been proposed [Abu-2020; Zakz2010][Sixt2006, pp. 30–31]. Even though many attempts have been made to gain value-added chemicals and materials from lignin [Zakz2010], several challenges remain such as non-integrated processes as well as low product selectivity and concentration [Behl2016]. Recently, lignin-first approaches are gaining attention, in which lignin utilization is considered in the process design phase. The goal of the lignin-first approach is to extract lignin from the biomass matrix without changing the chemical structure of lignin and avoiding condensation to more recalcitrant structures [Abu-2020]. Valorization of lignin can be achieved through lignin-based functional materials, including mechanically reinforced composites [Kai2016], antioxidants and antimicrobial agents [Yang2018b], carbon fibers [Shi2018], phenol-formaldehyde resins [Ma2018a], and biomedical materials [Figu2018]. Another approach addresses the depolymerization of lignin to value-added products, especially aromatic compounds and carboxylic acids [Di M2019b]. Eligible processes are generally divided in cracking, hy-

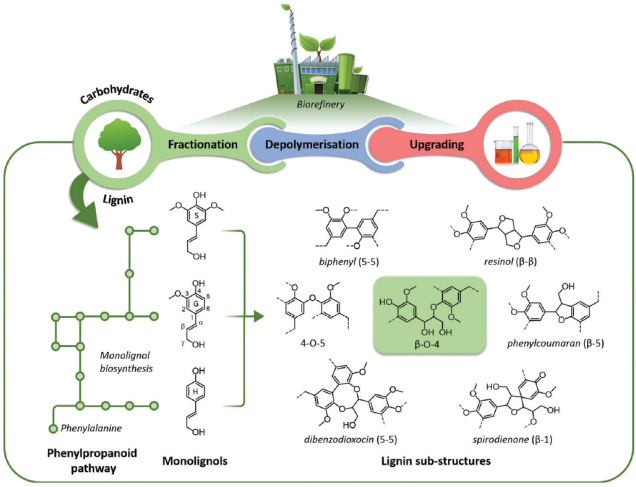

Figure 2.4.: Monolignols produced by the phenylpropanoid pathway and the resulting lignin sub-structures with characteristic bonds. Reproduced from [Schu2018] with permission from The Royal Society of Chemistry.

drolytic, reductive, and oxidative processes [Chat2014]. Even though a general technical feasibility was shown, several challenges remain such as non-integrated processes, low selectivity, low product concentrations, harsh reaction conditions in terms of temperature and pressure, as well as difficult separation and purification [Behl2016].

2.1.3. Cellulose and Hemicellulose Valorization

Cellulose is the world's largest renewable polymer resource with up to 10^{10} to 10^{11} tons produced via photosynthesis each year [Klem2005b]. It is a linear homopolymer, which consists of anhydroglucose units (AGU) linked by β-1,4-glycosidic bonds. Each neighbouring AGU is rotated by 180° and thus, two AGU form the repeating unit cellobiose. Cellobiose represents the basic unit of cellulose, which can therefore be considered to be a isotactic polymer of cellobiose, see Figure 2.5.

The degree of polymerization varies depending on the biomass source and is between 300 - 1700 in the case of wood, and 800 - 10000 in the case of cotton and plant fibers [Klem2005a]. The cellulose molecule is terminated on one end by an AGU unit with reducing end, and on the other by a non-reducing end. Due to the ability of cellulose to form intra- and intermolecular hydrogen bonds, the polymer develops crystalline and amorphous regions [Sixt2006, pp. 25–27]. In the lignocellulosic biorefinery, a biochemical conversion of the carbohydrate fractions is the most frequently applied route [Wage2019, p. 8]. After a suitable pretreatment, lignin is separated from the cellulose and hemicellulose stream. Often, also cellulose and hemicellulose are processed separately. As state of the art, the enzymatic hydrolysis is employed for cellulose conversion to glucose, because it potentially offers high sugar yields, high sugar selectivity, little side products, mild operation conditions, low energy costs, and low environmental impacts [Chan2018; Yang2011]. The crystallinity of cellulose, the content and distribution of residual lignin and hemicellulose, porosity and particle size are important parameters that affect the enzymatic digestibility of the homopolymer [Park2010]. The depolymerization product glucose can be subsequently fermented to value-added products [Dean2008]. Nonetheless, enzymes are a major cost driver in biorefineries [Ashr2017]. Alternative depolymerization techniques include acid, alkaline, hydrothermal, oxidative, and mechanocatalytic treatments [Yun2008; Lute2014; Schu1978].

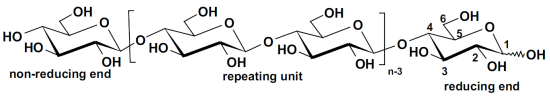

Figure 2.5.: Molecular structure of cellulose. The repeating cellobiose unit is shown in brackets. Reprinted with permission from John Wiley and Sons [Sixt2006, p. 25]. © John Wiley and Sons (2006).

In contrast to cellulose, hemicellulose is a branched heteropolymer, consisting of a multitude of different sugar monomers (pentoses, hexoxses, hexuronic acids, deoxy-hexoses), with a degree of polymerization

of up to 200 [Sixt2006, p. 28]. Hemicelluloses are more susceptible to hydrolysis than cellulose and can readily be transferred to, e.g., a biochemical transformation after pretreatment in the liquid stream [Wage2019]. Recently, electrochemical conversion of carbohydrates attracts increasing attention due to benefits arising from the use of renewable energy, an increase in production efficiency, and a decrease in negative environmental impacts [Vedo2020].

2.1.4. Fenton's Reagent for Biomass Valorization

In nature, brown rot fungi employ the non-enzymatic Fenton chemistry for the biodegradation of plant cell walls [Aran2012]. Arantes et al. [Aran2012] describe that cellulose, and hemicellulose may be degraded through fragmentation or oxidative cleavage. The same authors report that Fenton's chemistry cleaves the β-O-4 ether bonds of lignin and occurs in the natural breakdown of lignocellulose in nature [Aran2012]. Inspired by nature, Fenton processes are integrated into biorefineries: a preceding Fenton treatment improves the enzymatic hydrolysis [Jeon2016; He2015]. Additionally, the complete solubilization of cellulose by Fenton chemistry was demonstrated in the 1960s by Halliwell et al. [Hall1965]. The conversion of cellulose to glucose via Fenton-related processes is gaining attention and is proposed as an alternative to the enzymatic hydrolysis [Kwon2012; Wang2011; Meng2011; Yang2014]. Similarly, the degradation of lignin to organic acids and aromatics is investigated as an alternative oxidative valorization method [Ma2014; Zeng2015; Sagu2018; Kell2020; Bhan2015; Kent2015; Kent2018]. A detailed overview of previous works is presented in Chapters 5, 7 and 4.

2.2. Electrochemistry

2.2.1. Basic Principles

In electrochemical reactors, chemical reactions are driven by the transfer of electrons at electrode-electrolyte interfaces. A typical electrochemical reactor encompasses an anode and a cathode for oxidation and reduction reactions, respectively. To facilitate the passage of charge inside the electrochemical cell, ion-conducting electrolytes and separators are employed. Figure 2.6 depicts an electrochemical cell for hydrogen peroxide synthesis, where H_2O is oxidized at the anode and O_2 is reduced to H_2O_2 at the cathode. Electrochemical

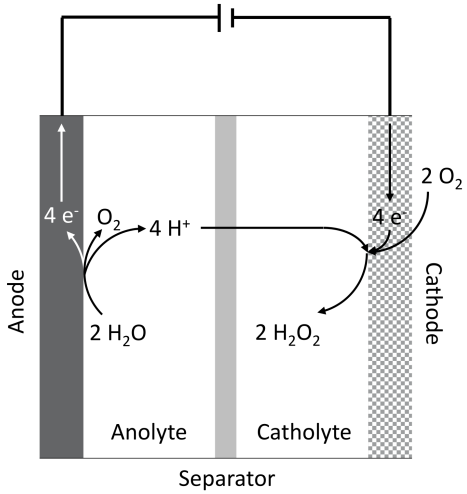

Figure 2.6.: Sketch of an electrochemical cell for hydrogen peroxide synthesis.

reactions take place spontaneously if the change in Gibbs Free Energy of the overall reaction is negative. In this case, one speaks of a galvanic cell and chemically stored energy is converted to electrical energy. If the Gibbs Free Energy is positive, an external potential

needs to be applied via a current source in order to drive the reaction of the so-called electrolytic cell. Efficient electrochemical cells require active and selective catalysts on the electrodes, highly ion conductive electrolytes and separators, and efficient mass and heat transfer at the (reactive) interfaces. The overall cell reaction for the electrochemical hydrogen peroxide synthesis is

$$O_2 + 2\,H_2O \longleftrightarrow 2\,H_2O_2 \tag{2.1}$$

with a Gibbs Free Energy of $\Delta G^0_{H2O2} = 206\,\mathrm{kJ\,mol^{-1}}$ at standard conditions[1]. Thus, this reaction is driven by an applied electrical potential in an electrolytic cell. The Gibbs Free Energy is connected to the cell potential via

$$|\Delta G| = -z * F * |E| \tag{2.2}$$

where F is the Faraday constant, z the stoichiometric number of electrons, and E the cell potential. The equilibrium cell potential for the hydrogen peroxide synthesis at standard conditions is consequently 0.535 V. However, in practice the applied cell potential to drive the reaction will be higher due to, e.g., ohmic resistances of the electrolytes, membrane and electrodes, and overpotentials at the electrodes. Overpotentials, such as charge-transfer or mass-transfer overpotentials, describe the deviation from the equilibrium potential required to drive the reaction [Faul2002, p. 7].

The overall cell reaction in eq 2.1 can be split up two so-called half-cell reactions. The Gibbs Free Energy ΔG of a half-cell reaction

$$\nu_O O + ze \longleftrightarrow \nu_R R \tag{2.3}$$

in which ν_i are the stoichiometric coefficients, z is the stoichiometric numbers of electrons, e the electronic charge, O the oxidized and R

[1] Standard conditions are $T = 25\,^{\circ}\mathrm{C}$, $p = 100\,\mathrm{kPa}$, $a_i = 1$ according to A. J. Bard, J. Jordan, and R. Parsons, Eds., "Standard Potentials in Aqueous Solutions," Marcel Dekker, New York, 1985 [Bard1985, p. 2]

the reduced species, is

$$\Delta G = \Delta G^0 + RT \ln \frac{a_R^{\nu_R}}{a_O^{\nu_O}} \tag{2.4}$$

where ΔG^0 is the Gibbs Free Energy at standard conditions. Thus, the half-cell potential of the reaction in eq 2.3 is described via the Nernst equation by connecting eqs. 2.2 and 2.4 to

$$E = E^0 + \frac{RT}{zF} \ln \frac{a_O^{\nu_O}}{a_R^{\nu_R}} \tag{2.5}$$

with E^0 as standard potential. The activity of the species a_i are connected to the concentrations c_i or partial pressure p_i of the reactants via the activity coefficients

$$\begin{aligned} a_i &= \gamma \frac{c_i}{c_0} \\ a_i &= \gamma \frac{p_i}{p_0} \end{aligned} \tag{2.6}$$

with c_0 and p_0 as standard concentration and pressure. The standard potential of the reduction of O_2 to H_2O_2 is 0.695 V vs. SHE, and the standard potential of the water oxidation is 1.229 V vs. SHE. Because it is impossible to measure a single half-cell potential experimentally, the standard potentials are referenced towards a well-defined electrode reaction, the standard hydrogen electrode (SHE). Equation 2.5 shows that the half-cell potentials change if the concentration, activity coefficient, partial pressure, or temperature of a reaction change.

The current efficiency η_{CE} of an electrochemical reaction describes how much of the total current is utilized to drive the desired reaction. For the hydrogen peroxide synthesis, the current efficiency can be calculated with the following equation

$$\eta_{CE} = \frac{n_{\mathrm{H_2O_2},measured}}{n_{\mathrm{H_2O_2},theoretical}} \tag{2.7}$$

where $n_{H2O2,measured}$ represents the molar amount of experimentally

measured H_2O_2, whereas $n_{H2O2,theoretical}$ represents the theoretically attainable molar amount of H_2O_2. $n_{H2O2,theoretical}$ can be calculated with Faraday's law

$$Q = zFn_{H2O2,theoretical} \tag{2.8}$$
$$It = zFn_{H2O2,theoretical}$$

with Q as passed charge, I as current and t as time. The current I is frequently normalized to the geometrical surface area of the electrode and named current density, which allows a facile comparison of the results obtained in different studies. For reactions involving a gaseous reactant, the stoichiometric excess factor λ is an important parameter, defined as

$$\lambda = \frac{\dot{n}_{O2} zF}{I} \tag{2.9}$$

and describes the excess of, e.g., oxygen supplied to the electrode in relation to the stoichiometrically required oxygen.

2.2.2. Electrochemical Reactors and Electrodes

An electrochemical reactor generally consists of anode, cathode, electrolytes, and a separator, e.g. an ion exchange membrane. Anode and cathode must ensure a high electrical conductivity, chemical and mechanical stability, and a high electrochemical activity [Schm2012, pp. 239–240]. When gaseous reactants with a low solubility in the electrolyte are used, as is the case in the H_2O_2 synthesis, so-called gas diffusion electrodes (GDEs) can significantly enhance the rate and selectivity of the reaction. In comparison to solid, non-porous electrodes, GDEs create a three-phase-boundary between gas phase, electrocatalyst, and liquid electroyte. Thus, mass transfer limitations due to limited solubility of gases can be circumvented by a direct transport of the gaseous reactant to the reaction interface. The structure of GDEs is thoroughly explained in [Zhan2008]. In brief, a gas

diffusion electrode is a porous multicomponent structure. It contains a top layer, which is the catalyst layer (CL) where the electrochemical reactions takes place. Often, the CL contains the catalyst, an ionomer, and a substrate such as carbon black particles. The catalyst layer must thus ensure contact to the electrolyte and gas phase by being electrically and ionically conductive, porous, and provide a high electrochemical activity. Because many catalysts are expensive, the loading should be as low as possible. The catalyst layer is placed on a microporous layer (MPL), which is responsible for electrolyte management and reactant supply. Last, a macro-porous substrate layer (SL) provides mechanical and chemical stability, high electronic and heat conductivity, high porosity, and adequate wettability. The electrolyte and ion exchange membranes must have a high ionic conductivity to reduce ohmic losses, and be chemically inert. Additionally, the ion exchange membranes should have a high permselectivity for the desired main charge-carrying ion, while retaining reaction products and reactants. In general, many electrochemical reactors are designed with planar electrodes and membranes, as depicted in Figure 2.6. However, tubular reactors can provide numerous advantages compared to their planar counter-part such as a higher power and packing density, and lower manufacturing costs [Perc2020; Gend2014a; Gend2014b].

2.2.3. Electrochemical Hydrogen Peroxide Synthesis

Hydrogen peroxide (H_2O_2)is a chemical with numerous applications such as industrial bleaching, wastewater treatment, chemical synthesis, and fuel cell technologies [Perr2019; Camp2006]. Additional application and technology fields are being developed and the world capacity increases steadily [Perr2019; Ciri2016]. From the 1990s, where H_2O_2 was produced with a capacity of 1.5 Mt, the annual production reached 5.5 Mt in 2015 [Ciri2016]. In 2005, 95% of H_2O_2 was produced via the so-called *anthraquinone process*, which belongs to the group of organic autooxidation processes (*AO process*) [Camp2006]. Up to

date, alternative routes like the direct or electrochemical synthesis do not play a significant role in industry [Goor2019]. AO processes marked the breakthrough for industrial high capacity production of H_2O_2 [Goor2019] and the modern AO process was developed in the 1930s by Riedl and Pfleiderer for I.G. Farbenindustrie AG [Ried1939]. Due to challenges such as waste generation, mass transfer limitations in the hydrogenation and oxidation reactors, organic contamination of the product and by-product formation, alternative approaches for the direct or electrochemical synthesis may provide advantages [Camp2006]. Additionally, electrochemical approaches can be operated decentralized, at ambient pressure and temperature [Kotr2008] and contribute to the electrification of the chemical industry via sustainable energy conversion technologies [Schi2017; Lewi2006; Orel2018]. The synthesis of H_2O_2 via an electrochemical route was observed by Meidinger [Meid1853] in 1853 during the electrolysis of sulfuric acid. In this indirect route, peroxodisulfuric acid is formed and subsequently hydrolyzed to H_2O_2 and sulfuric acid [Goor2019]. After further development, this process was implemented in Austria by the Konsortium für Elektrochemische Industrie in 1908 [Goor2019]. Nowadays the focus is on the direct cathodic reduction of O_2 to H_2O_2, which was first reported by Traube in 1882 [Trau1882].

Paramount characteristics of electrochemical reactors for the H_2O_2 synthesis are

- the type of catalyst: metals, transition metals, metal alloys and metal oxides [Kim2018; Perr2019], carbon materials [Hasc2016], quinones and their derivates [Song2008], and metal complexes [Fuku2012]
- the type of reactor: trickle bed, fuel cell like or one-side buffered [Perr2019; Camp2006; Fuku2012; Foll1995]
- the type of separator: ion exchange membrane or diaphragm [Foll1995]

The electroreduction of O_2 may yield H_2O or H_2O_2, mainly depending on the catalyst [Song2008; Tara1983]. Unwanted side and competing reactions to the two-electron reduction reaction (eq 2.10), e.g., as described by the comprehensive work on oxygen electrochemistry by Tarasevich, Sadkwoski, and Yeager [Tara1983] and Song and Zhang [Song2008], are the four-electron oxygen reduction reaction (eq 2.11) and reduction of H_2O_2 (eq 2.12).

$$O_2 + 2\,H^+ + 2e^- \longleftrightarrow H_2O_2 \qquad E^0 = 0.695\text{V vs. SHE}^2 \tag{2.10}$$

$$O_2 + 4\,H^+ + 4e^- \longleftrightarrow 2\,H_2O \qquad E^0 = 1.229\text{V vs. SHE}^2 \tag{2.11}$$

$$H_2O_2 + 2\,H^+ + 2e^- \longleftrightarrow 2\,H_2O \qquad E^0 = 1.763\text{V vs. SHE}^2 \tag{2.12}$$

Not only electrochemical side reactions decrease the selectivity for H_2O_2, but also the decomposition of H_2O_2

$$H_2O_2 \longrightarrow H_2O + (1/2)\,O_2 \tag{2.13}$$

$$H_2O_2 + HO_2{}^- \longrightarrow H_2O + O_2 + OH^- \tag{2.14}$$

$$H_2O_2 + X^n \longrightarrow X^{n+1} + OH^- + OH^\bullet \tag{2.15}$$

where the self-decomposition in eq 2.13 is often truly a base-catalyzed decomposition (eq 2.14) or a metal-catalyzed decomposition as in eq 2.15 [Qian2002; Perr2019; Abel1952]. Qiang et al. [Qian2002] demonstrated that the stability of H_2O_2 strongly decreases above a pH of 9 and at elevated temperatures. In practice, H_2O_2 is stabilized by organic or inorganic compounds [Goor2019].

[2]Standard potentials taken from A. J. Bard and L. R. Faulkner "Electrochemical Methods: Fundamentals and Applications", Jon Wiley and Sons, New York, 2001 and A. J. Bard, J. Jordan, and R. Parsons, Eds., "Standard Potentials in Aqueous Solutions," Marcel Dekker, New York, 1985 [Faul2002, p. 809][Bard1985]

Catalysts

In principal, H_2O_2 can be obtained through the oxidation of H_2O at the anode, see eq 2.12. Catalysts for the cathodic reduction of O_2 to H_2O_2 must be highly selective, as thermodynamics favor the four-electron ORR, which is apparent by the standard electrode potentials of eqs 2.10 and 2.11 [Kim2018; Perr2019; Verd2014]. Additionally, the catalysts should have a high activity for low catalyst loadings, a high energy efficiency as well as long-term stability [Verd2014]. A frequently employed descriptor for the catalyst activity is the Sabatier volcano, which correlates the overpotential of the electrochemical reaction to the binding energy of an intermediate, which is OOH* (* refers to the surface adsorbed species) in the case of the two-electron ORR [Verd2014]. If the intermediate is bound to strongly, a four-electron ORR takes place. If the binding energy is too low, the catalyst fails to form sufficient OOH* from O_2 [Verd2014]. E.g., gold binds the intermediate weakly and is highly selective, but not highly active for H_2O_2 [Perr2019]. A key for achieving a high selectivity is the coordination of adsorbed oxygen on the catalyst. In general, a side-on or end-on coordination of oxygen is possible, see Figure 2.7 [Tara1983; Yeag1976]. An end-on coordination favors H_2O_2 formation, as the O–O bond cannot dissociate in this case [Perr2019]. Thus,

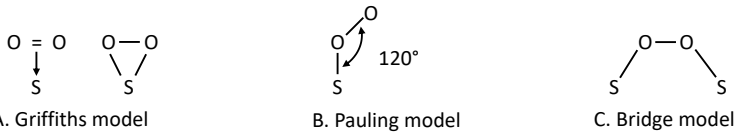

Figure 2.7.: Coordination of oxygen on substrates. Based on Yeager et al. and Tarasevich et al. [Yeag1976; Tara1983]

.

a frequently employed approach for metal and metal alloy catalysts is to isolate active catalyst centers, which are highly active, e.g., Pd or Pt, but are not selective enough as bulk material [Verd2014; Perr2019]. As state of the art catalysts, Pd-Hg and Pt-Hg enable

the highest activity in acidic media and graphene-based catalysts in caustic media [Verd2014; Siah2013; Park2014; Jirk2011; Zhen2016; Lee2012]. Recently, a moderately reduced graphene oxide catalyst was developed by Kim et al. [Kim2018], which shows the highest reported mass activity in caustic conditions with basically no overpotential and close to 100% selectivity. Current densities and overpotentials of the most active catalysts can be seen in Figure 2.8. In general, gold and carbon catalysts catalyze the two-electron ORR well in caustic media, while they are sluggish in acidic media [Yeag1984; Tara1983]. Many catalysts show a more or less pronounced dependence of the H_2O_2 formation on the pH value and the origin of this effect is still under debate [Yang2018a]. Yang et al. [Yang2018a] propose that the barrier preventing the dissociation of adsorbed intermediates such as OOH^* or $H_2O_2{}^*$ is lower in caustic than in acidic media. Thus, only the weakest binding catalysts in caustic media, carbon-based catalysts, show high activities and selectivities at high pH values. Further, Yang et al. [Yang2018a] hypothesize that pH-dependent rearrangement of the electrical double-layer may be connected to the observed trends, similar to recent findings for H_2 evolution [Lede2017]. As mentioned before, the self-decomposition of H_2O_2 is enhanced at high pH values [Qian2002]. Thus, the electrochemical H_2O_2 is attractive in the acidic environment [Agla2007; Yang2018a].

Reactors

Presumably, the only process on industrial scale for the cathodic reduction of oxygen is the *Huron-Dow process*, which was first piloted in the pulp industry in Muskogee, USA [Goor2019; Foll1995]. Historically, the electrochemical H_2O_2 production was especially interesting for the pulp and paper industry, as a) H_2O_2 was needed in high quantities to replace chlorine and b) a mixture of caustic soda and H_2O_2 can be directly transferred from the electrolyzer to, e.g., the *Kraft process* [Foll1995]. The Huron-Dow process is characterized by a trickle-bed reactor operated with an alkaline solution

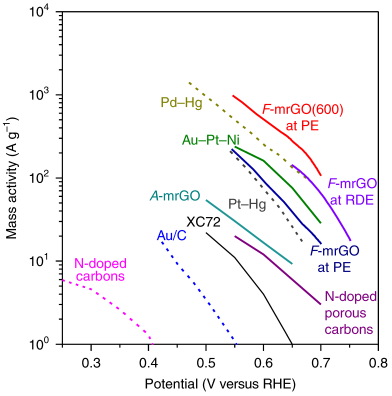

Figure 2.8.: Mass activity of different catalysts for H_2O_2 electrosynthesis based on data from literature [Kim2018]. Reprinted with permission from Springer Nature Customer Service Centre GmbH: Springer Nature, Nature Catalysis, *Efficient H_2O_2 generation using reduced graphene oxide-based oxygen reduction electrocatalysts*, Kim, H.W., Ross, M.B., Kornienko, N., Zhang, L., Guo, J., Yang, P., McCloskey, B., © (2018)

[McIn1984; McIn1985; Dong1990; Foll1995]. The cathode is a packed bed of graphite particles, which are covered with a high-surface carbon with fluorpolymer binder. Anolyte and catholyte are separated by a polypropylene microporous separator, which feeds caustic soda to the reduction compartment. The oxygen, which is converted to H_2O_2, is supplied by the OER at the anode. In order to produce H_2O_2 concentrations of 3 wt.-% to 4 wt.-%, the caustic soda to H_2O_2 ratio must be at least 1.6. At lower ratios, the current efficiency decreases, because the perhydroxyl ion and the hydroxyl ion both migrate and diffuse towards the anode, where they are oxidized [Foll1995]. An excess of hydroxyl ions ensures the preservation of perhydroxyl ions [Foll1995; Olom1979]. Typically, a current density of 65 mA cm^{-2} is reached at a cell potential of 2.3 V with a current efficiency of 95%. Over a six month operation period, this efficiency declined to 80% [Foll1995]. Gupta and Oloman [Gupt2006] replaced the particulate electrode by a carbon felt and introduced a perforated bipolar plate, which ensured direct passage of anodically generated oxygen towards the

cathode. This design enables a high current density of 120 mA cm^{-2} at a cell potential of 1.8 V. However, the current efficiency was rather low at 60% and the caustic soda to H_2O_2 ratio was high at above two. Muddemann et al. [Mudd2020] showed that a carbon-based gas diffusion electrode in combination with a cation exchange membrane as separator between anode and cathode enables a Faraday efficiency above 90% at cell voltages between 1.5 V to 3.5 V at pH 14 and 15 °C. The caustic soda to peroxide ratio was approximately 2:1. The membrane prevented cross-over of H_2O_2 to the anode. The caustic soda concentration in the product stream can be reduced, if an acidic anolyte is used. However, a higher cell voltage is the consequence [Foll1995]. In principal, oxygen and air can be used as feed for the cathode. Muddemann et al. [Mudd2020] reported high CE for air and pure oxygen, but the cell voltage was significantly higher if air was used.

An electro-Fenton process typically requires an acidic solution of H_2O_2, which is described in detail in Section 2.2.4. For this type of H_2O_2 product stream, the caustic soda in the catholyte needs to be replaced with salt as supporting electrolyte, e.g., sodium sulfate or sodium chloride, which is usually acidified to a pH of 3. The use of a carbon-based GDE and a cation exchange membrane as separator have shown promising results. Giomo et al. [Giom2008] investigated a pilot plant with a Vulcan XC-72 coated gas diffusion electrode. A catholyte compartment separated the cathode from the cation exchange membrane and the anode. After 19 h of operation, a H_2O_2 concentration of 0.13 M was achieved at 56 mA cm^{-2}. This corresponds to a CE of 70%. Agladze et al. [Agla2007] also employed a gas diffusion electrode, catholyte gap and cation exchange membrane. They showed, that sodium chloride can be advantageous to sodium sulfate due to a low price and higher conductivity. A H_2O_2 concentration of approximately 0.3 M at 50 mA cm^{-2} was reached, which corresponded to about 85% CE. Recently, a liquid electrolyte-free cell was constructed for the generation of pure H_2O_2. The outstanding characteristics of the reactor were achieved by employing a cation exchange membrane at the anode side - for the migration of protons - and an anion exchange membrane

on the cathode side - for the migration of perhydroxyl anions. The two ions migrate towards a central compartment and form H_2O_2. The central compartment is additionally filled with a porous ion exchange resin which renders a supporting electrolyte obsolete. Up to 20 wt.-% H_2O_2 at 200 mA cm^{-2} and 90% CE were reached [Xia2019].

These examples from literature show that an electrochemical reaction system for the production of H_2O_2 needs to be tailored to the envisaged utilization. The current efficiency for carbon-based catalysts depends on the functional groups of the carbon [Kim2018; Hasc2016; Assu2011], the type of electrolyte [Hasc2016], the pH value [Mudd2020; Hasc2016], the temperature [Mudd2020] and process engineering parameters such as liquid and gas feed flow rate [Mudd2020], which are in turn influenced by the reactor design.

2.2.4. The Fenton and electro-Fenton Process

The so-called Fenton reaction is a process for the generation of hydroxyl radicals using ferrous iron (Fe^{2+}) and H_2O_2. In the Fenton reaction, H_2O_2 reacts with ferrous iron to produce OH radicals and ferric iron as described in eq 2.16. Subsequently, ferric iron can be reduced by H_2O_2 (eq 2.17) to close the catalytic cycle. The reaction was discovered in 1894 by the British chemist H.J.H. Fenton and the mechanism was unravelled in a series of studies by Barb et al. [Fent1894; Barb1949; Barb1951a; Barb1951b]. Hydroxyl radicals are powerful oxidants and degrade a variety of molecules [Pign2006; Bril2009].

$$Fe^{2+} + H_2O_2 \longrightarrow Fe^{3+} + HO^{\bullet} + OH^- \tag{2.16}$$

$$Fe^{3+} + H_2O_2 \longrightarrow Fe^{2+} + HO_2{}^{\bullet} + H^+ \tag{2.17}$$

$$Fe^{3+} + e^- \longleftrightarrow Fe^{2+} \tag{2.18}$$

$$Fe^{2+} + HO^{\bullet} \longrightarrow Fe^{3+} + OH^- \tag{2.19}$$

$$H_2O_2 + HO^{\bullet} \longrightarrow HO_2{}^{\bullet} + H_2O \tag{2.20}$$

Today, the Fenton reaction is mostly employed in advanced oxidation processes in the wastewater industry [Bril2009; Pign2006]. In the pulp, paper, and biorefinery context, Fenton's chemistry is investigated as a delignification step [Makh2008]. Increasing research is conducted in order to use the oxidative (pre)treatment as a technology in biorefineries [Kato2014].

In the electro-Fenton process, H_2O_2 is produced at the cathode through the reduction of oxygen, see equation 2.10 [Bril2009]. Additionally, ferric iron can be reduced electrochemically, see equation 2.18 [Bril2009]. In general, the advantages of the electro-Fenton process compared to the Fenton process are an increased iron regeneration rate and a localized H_2O_2 production [Pign2006; Bril2009]. Carbon materials are frequently employed as catalysts in the electro-Fenton process as they are nontoxic, have a high overpotential for H_2 evolution and a low catalytic activity for H_2O_2 decomposition. Additionally, carbon materials are characterized by a high mechanical stability, electrical conductivity, and chemical resistance [Bril2009]. Often, gas diffusion electrodes are used in electro-Fenton processes to mitigate a negative influence of the low oxygen solubility in aqueous electrolytes. The main operating parameters that affect the electro-Fenton process are the pH value, the applied current, the catalyst concentration, the electrolyte, temperature and initial organics concentration [Plie2015]. In order to prevent the precipitation of ferric iron, pH values below three must be employed [Pign2006]. Additionally, the pH value should be above 2.5, to prevent a decrease in reaction rate [Plie2015]. The pH range can be extended, if the iron catalyst is immobilized in a solid state. The process is coined heterogeneous electro-Fenton [Plie2015]. The applied current should be as high as possible. However, if a certain threshold is reached parasitic reactions diminish the efficiency of the process [Plie2015]. In the Fenton reaction, a peroxide-to-iron molar ratio of 100 to 1000 is recommended [Pign2006]. If the iron concentration is high, the conversion of H_2O_2 to OH radicals is high. However, if the concentrations of OH radicals is too high, scavenging reactions occur. Similarly, H_2O_2 can scavenge OH radicals [Plie2015]. Starting with ferrous iron can lead to very high initial degradation

rates, which result from an eruption of radicals. After this initial phase, the reaction rate decreases [Pign2006]. As in any electrochemical reaction, the supporting electrolyte in electro-Fenton processes ensures a high ionic conductivity and thus, mitigates ohmic losses in the cell. However, many inorganic ions may also show adverse affects on the process by leading to iron precipitation, scavenging of OH radicals and coordination to ferric iron [Pign2006]. Sulfate, for example, does not scavenge OH radicals but coordinates with ferric iron, reducing the reaction rate. Bromide and chloride ions, on the other hand, scavenge OH radicals [Pign2006]. An increase in temperature generally increases reaction rates in the Fenton process [Plie2015]. However, a rising temperature also leads to an increase in H_2O_2 self-decomposition and a decrease in O_2 solubility [Qian2002].

2.3. Membrane Separation Processes

Membranes are used as semi-permeable barriers in separation processes driven by a (partial-)pressure, electric field, or concentration gradient. The separation is achieved based on size-exclusion and solution-diffusion mechanisms, as well as electro-static interactions. In this thesis, nanofiltration (NF) will be investigated to purify a mixture of low molecular weight compounds and ions.

With the help of nanofiltration membranes, retention of molecules above approximately 200 Da can be achieved, which corresponds to a molecule size of 1 nm. Additionally, nanofiltration separates ions based on their ionic charge and size. Generally, multivalent ions are retained to a higher degree than monovalent ions. Polymeric and ceramic NF membranes are utilized in processes for the separation of monovalent from divalent ions (e.g., water softening), for the separation of organic molecules from salts (e.g., water treatment), and for the separation of low molecular weight from high molecular weight compounds (e.g., wine purification). Typically, NF is operated between 3 bar to 30 bar, which is in between ultrafiltration and reverse osmosis. The separation

of the solutes is dependent on the trans membrane pressure (TMP), solute concentrations, type of membrane and temperature. [Meli2007, pp. 285–308]

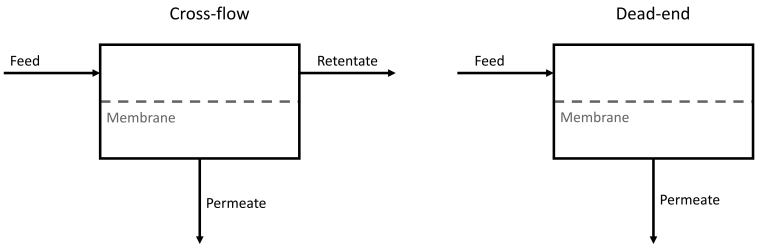

Figure 2.9.: Membrane module operation in cross-flow and dead-end mode.

Membrane modules are operated either in cross-flow or dead-end mode, whereas cross-flow is preferred to mitigate mass transport limitation such as concentration polarization. The trans membrane pressure, the driving force of nanofiltration, is calculated as

$$\Delta p_{TMP} = \frac{p_{feed} + p_{retentate}}{2} - p_{permeate} \tag{2.21}$$

Key performance indicators of membranes are the permeability P, the selectivity S, and the retention R. The permeability is calculated as

$$P = \frac{Q}{A_{membrane} \Delta p_{TMP}} \tag{2.22}$$

where Q is the volumetric permeate flow and $A_{membrane}$ the membrane area. The selectivity and retention are calculated as

$$S_{i,j} = \frac{c_{i,permeate} / c_{j,permeate}}{c_{i,retentate} / c_{j,retentate}} \tag{2.23}$$

$$R_i = 1 - \frac{c_{i,permeate}}{c_{i,retentate}} \tag{2.24}$$

with c_i as the concentration of the individual solutes.

An emerging technology in the field of nanofiltration is the fabrication of so-called *layer-by-layer polyeelectrolyte membranes*. Layer-by-layer (LbL) polyelectrolyte membranes are fabricated through deposition of polyelectrolyte multilayers (PEM) on a charged membrane support. In an alternating fashion, positively and negatively charged polyelectrolytes are deposited on the support, each pair creating a so-called bilayer. Through variation of , e.g., the number of deposited layers, the polyelectrolytes themselves and salt addition the rejection of solutes can be tailored to the desired application [Groo2015; Ilya2015; Juri2015; Sany2015; Jose2014].

3. Wood Pretreatment with Hydrotropic Solutions and Deep Eutectic Solvents

Parts of this chapter have been published as:
Robert G. Keller, Davide Di Marino, Malte Blindert, Matthias Wessling *Hydrotropic Solutions Enable Homogeneous Fenton Treatment of Lignin*, Industrial & Engineering Chemistry Research, 2020
DOI: 10.1021/acs.iecr.9b06607

Within a collaborative research project parts of this chapter are also a constituent of: Davide Di Marino, "Extraction and Electrochemical Valorization of Lignin in Novel Electrolytes", Ph.D. dissertation, RWTH Aachen University, 2019

3.1. Introduction

The conversion of cellulose, hemicellulose and lignin relies on efficient processes, which fractionate lignocellulosic biomass into the individual constituents. The currently available pretreatment methods can be categorized in physical, biological, and chemical methods. The individual strategies can be combined to utilize synergies. Up to date, research in all areas is pursued, because, e.g., biological processes suffer from slow kinetics and chemical treatments from high costs for corrosion resistant equipment. In general, viable methods should minimize the generation of inhibitors, ensure a high carbon efficiency, provide a pure accessible lignin stream, and minimize energy consumption. [Silv2015]

In this chapter, a lignin-first approach is investigated in order to provide a lignin rich stream for a subsequent Fenton treatment. Even though long known as a solvent for lignin [McKe1946; Proc1971], hydrotropic solvents have only recently attracted attention again in biorefinery pretreatment steps [Fard2013; Ma2018b; Chen2017; Wang2019]. Deep eutectic solvents have emerged as a new family of solvents at the beginning of the century [Smit2014]. Hydrotropes and deep eutectic solvents (DES) are an alternative to ionic liquids or mineral acids, which are frequently applied for biomass pretreatment [Tade2011; Tang2017]. In comparison to ionic liquids, hydrotropes and deep eutectic solvents may be more cost competitive [Subb2012; Smit2014]. An advantage of hydrotropes over DES is their recyclability through precipitation of the solute below the minimum hydrotrope concentration [Wang2019; Ma2018b]. Possible low-temperature operation and simple chemistry are another benefit [Ma2018b; Proc2015]. Gabov et al. [Gabo2013; Gabo2014; Gabo2017] investigated the fractionation of birch wood and sugarcane bagasse at temperatures of 150 °C in the hydrotrope sodium xylene sulfonate. According to Gabov et al. [Gabo2014], the lignin underwent substantial changes through the pretreatment. Hemicellulose was removed from the lignin matrix. Recently, Chen et al. [Chen2017] reported the near-complete disso-

lution of wood lignin in a hydrotropic solution of p-toluenesulfonic acid at a temperature of 80 ℃ in less than two hours. After the biomass fractionation, the sugar fraction was successfully hydrolyzed, the lignin was precipitated, and the hydrotrope recycled by crystallization. The study by Chen et al. [Chen2017] highlights the potential of hydrotropes in a biorefinery context and was extended in a recent study to produce lignocellulosic nanofibrils, lignin nanoparticles, and furfural [Ma2018b] and a flow-through reactor was established [Wang2019]. Deep eutectic solvents have been shown to increase the enzymatic hydrolysis of pretreated biomass [Proc2015] and many different DES are well suited to dissolve lignin [Fran2012].

This chapter investigates the capabilities of two hydrotropic solvents and two deep eutectic solvents for their ability to dissolve lignin from beech wood. In addition to the different solvents, the influence of temperature and particle size on the lignin extraction yield was investigated. Further, the enzymatic digestibility of the solid residue was evaluated.

3.2. Experimental

3.2.1. Lignin Extraction from Beech Wood

For the hydrotropic solvents, lignin was extracted from beech wood with sodium cumene sulfonate (SCS) and sodium xylene sulfonate (SXS) solutions of 400 g/L hydrotrope concentration. Beechwood of particle size d_p 1 mm to 3.15 mm was mixed with the hydrotrope solution in the ratio of 1:20 $w_{wood}/w_{solution}$. The pretreatment of wood was then performed in a high pressure stirred tank reactor (BR-300 Berghof GmbH) at temperatures of 120 ℃, 150 ℃, and 200 ℃. The pretreatments lasted 6 h, excluding heating and cooling the reactor for 20 min. There was no pressure regulation; the pressure in the vessel was the vapor pressure of the mixture.

A cholin chloride–oxalic acid DES with the molar ratio 1:1 and a cholin chloride–lactic acid DES with the molar ratio 1:10 was used. For the DES pretreatments, a glas piston was filled with the solvent and subsequently preheated to temperatures of 80 ℃, 100 ℃, and 120 ℃. After the temperature was reached, the wood chips were added to the solution for 6 h, which was continuously stirred. A reflux condenser was placed at the outlet of the piston to condense vapors. Beechwood of particle size d_p 0.038 mm to 2.8 mm was mixed deep eutectic solvents in the ratio of 1:20 $w_{wood}/w_{solution}$.

The lignin extraction yield was calculated based on the measurements of extracted lignin via UV-Vis and gravimetric measurements. The lignin content of the raw biomass was 31.2 wt.-% , based on acid hydrolysis of wood (41.2 wt.-% glucose, 22.0 wt.-% xylose), extractives determination via Soxhlet extraction (5.2 wt.-%), and ash content via TGA measurement (0.4 wt.-%).

Chemicals

Kraft lignin (370959), sodium hydroxide (NaOH, 98%), and SXS (90%) were purchased from Sigma-Aldrich. SCS (93%) was purchased from Julius Hoesch. Cholin chloride, lactic acid and oxalic acid were supplied by Sigma-Aldrich. The pH was adjusted with sulfuric acid (H_2SO_4, 75%) from Carl Roth. Beech wood chips were supplied by Wilhelm Eder. The wood chips were dried at 50 ℃ prior to use. All chemicals were used without further purification and adjusted to the desired concentrations with deionized water.

3.2.2. Analytics

Determination of the Lignin Molecular Weight Distribution

The average molecular weight of the different lignin fractions was determined using size exclusion chromatography (SEC). Lignin samples were precipitated by the addition of 0.01 M H_2SO_4 with a dilution ratio of 1:10 v:v, centrifuged (4083 g) for 30 min and the precipitated solid was freeze-dried. For SEC analysis, the solid residue was resuspended in 2 mL of 1 M NaOH. The measurements were performed using an Agilent 1200 system equipped with a UV-Vis detector at a wavelength of λ= 280 nm. The eluent was 0.1 M NaOH (99 % , Sigma Aldrich) in water (HPLC grade, Carl Roth) with addition of 0.01 wt.-% sodium azide (NaN_3, extra pure, Merck). The internal standard was a 12.5 g/L glucose monohydrate solution (Merck). One pre-column (8 x 50 mm) and three MCX gel columns (8 x 300 mm) were used at a flow rate of 1.0 mL/min at 40 °C. The diameter of the gel particles was 5 µm, the nominal pore widths were 1000 $\AA$ for the three columns. Calibration was performed using narrowly distributed poly(styrene sulfonate) standards (Polymer Standards Service).

Determination of the Lignin Concentration

Lignin concentrations were determined by UV-Vis measurements with a Thermo Scientific Genesys 10S UV-Vis-Spectrophotometer (Thermo Fisher Scientific Inc, USA). After the pretreatment, 5 mL of the supernatant was collected in a Falcon tube and diluted 1:10 v:v with 0.01 M H_2SO_4. Afterwards the sampled was stored for 12 h and lignin precipitated. The solution was then centrifuged (4083 g) for 10 min to separate the solids from the liquid phase. The supernatant was removed and the remaining solids were washed two times with 30 mL, respectively 20 mL, 0.01 M H_2SO_4 and each time the supernatant was discarded after 10 min of centrifugation at 4083 g. The remaining solids were freeze dried and redissolved in 1 mL of 1 M NaOH vor

the UV-Vis measurement. The calibration curve was established with Kraft lignin in 1 M NaOH.

Determination of the Chemical Linkages of Lignin

Lignin contained in the liquid phase was precipitated by addition of sulfuric acid or water, centrifuged, and freeze-dried, as described before. 2D Heteronuclear Single-Quantum Coherence (HSQC) NMR measurements were conducted to characterize the type of lignin chemical linkages. The details of the measurement can be found in [Dabr2015].

Enzymatic Hydrolysis

Cellulases from *Trichoderma reesei* (Aq. solution, 700 Units/g, Sigma Aldrich) were mixed with a buffer solution. The resulting mixture was composed of 85.95 vol.% 100 mM sodium acetate buffer solution at pH 4.8 and 14.05 vol.% of cellulases. Reaction tubes were placed in a thermo mixer (HLC-Heating Mixer MHR, Ditabis, Germany) at 45 ℃ and 1000 rpm. The hydrolysis was started by mixing 1 mL of enzyme solution with 0.1 g of biomass sample. Biomass samples, which were pretreated with DES or hydrotropic solvents, were washed twice with dilute sulfuric acid to remove residual solvent. Samples sugar concentration determination were taken after 30 min, 4 h, 24 h and 48 h. The samples were rapidly cooled in ice to stop the reaction. A HPLC Agilent 1100 equipped with an organic acid resin column and precolumn with RI detector and 0.8 ml/min 5 mM sulfuric acid as eluent was used for sugar quantification.

Surface and Volume Analysis of Wood Chips

A Bruker Skyscan 1272 with 50 kV and 200 μA was used for computer tomography scans of the biomass. A Hitachi SEM S 3000 was used

for scanning electron microscopy to determine the surface changes of the wood structure.

3.3. Results and Discussion

Lignin was extracted from beech wood in 400 g/L hydrotropic solutions of sodium cumene sulfonate and sodium xylene sulfonate for 6 h between 120 °C to 200 °C and in different deep eutectic solvents between 80 °C to 120 °C. The deep eutectic solvents were: cholin chloride–lactic acid and cholin chloride–oxalic acid. Figure 3.1 shows a quantification of the extracted lignin by means of UV-Vis and gravimetric measurements for the two different hydrotropic salts and the three investigated temperatures, namely 120 ℃, 150 ℃ and 200 ℃. With an increase in temperature up to 200 ℃ a lignin yield of 80 - 90% can be reached. The results are in line with the literature, e.g., Gabov et al. [Gabo2014], who extract 91% of spruce wood lignin with SXS at 170 ℃. Overall, there is no significant difference between the lignin extracted with SXS and SCS. Figure 3.2 shows beech wood pretreatment in lactic acid and oxalix acid based DESs. The yield again rises with temperature, whereas the lactic acid DES is superior to the oxalic acid DES. The lactic acid based DES additionally outperforms the hydrotropic solutions, especially if very small wood particles of $\leq 38\,\mu m$ were used. Small particle sizes help the dissolution of lignin due to an increased surface area [Schä2018]. Acid hydrolysis measurements qualitatively confirmed the lignin extraction yields.

The enzymatic hydrolysis of the hydrotropic pulp reveals that low temperatures yield the highest sugar concentration, see Figure 3.3. Apparently, some kind of inhibitor is formed at high temperatures, e.g., sugar degradation products. Another possibility could be the redeposition of highly condensed lignin residues on the cellulose. Even though lignin is nearly completely extracted from the beech wood at 200 ℃, the enzymatic hydrolysis is greatly hampered.

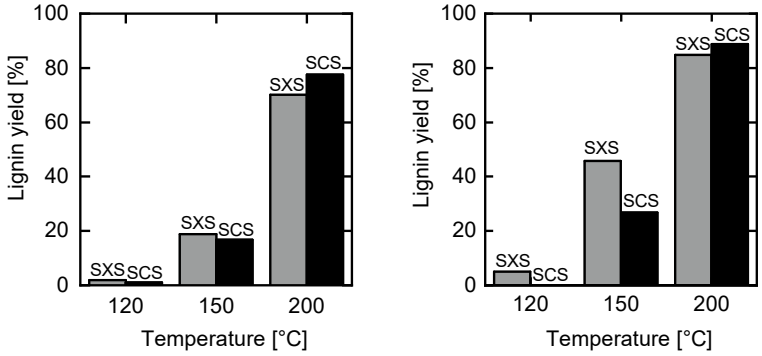

(a) Quantification via UV-Vis. **(b)** Gravimetric quantification.

Figure 3.1.: Quantification of extracted lignin relative to absolute lignin content in raw beech wood with SCS/SXS pretreatment at 120, 150 and 200 °C for 6 h.

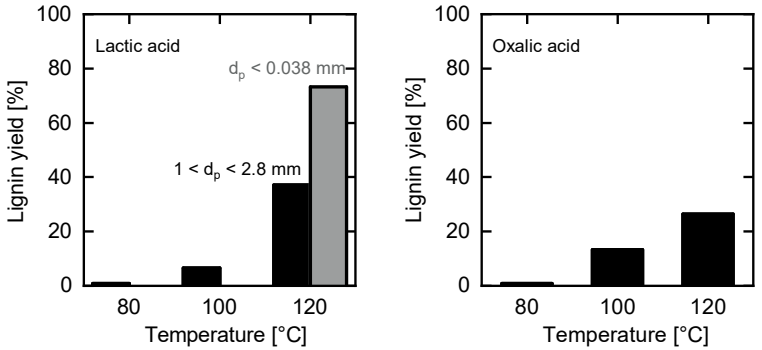

(a) Pretreatment in a lactic acid based DES. **(b)** Pretreatment in a oxalic acid based DES.

Figure 3.2.: Quantification (UV-Vis) of extracted lignin relative to absolute lignin content in raw beech with wood deep eutectic solvents at 80, 100 and 120 °C for 6 h

.

Mou et al. [Mou2017] studied the influence of a hydrotropic treatment on the enzymatic digestibility compared to an organsolv treatment. In this study, a positive effect of the hydrotropic pretreatment was observed. However, no variation of temperature was reported. Thus, it may be beneficial to operate at low temperatures with a different hydrotrope, which is capable of high lignin yields [Chen2017; Ma2018b; Wang2019]. The low xylose yield can additionally be explained by another effect: xylan is extracted and hydrolyzed during hydrotropic pretreatments [Gabo2014; Gabo2013; Ma2018b]. Thus, the available xylan may have dissolved during the pretreatment leading to a low enzymatic yield [Mou2014]. After pretreatment with the deep eutectic solvents, the enzymatic digestibility is very low. Di Marino [Di M2019a] showed that the enzymatic digestibility of DES pretreated wood is not enhanced compared to raw wood if a low temperature pretreatment of 80 °C is applied. An increase in temperature may additionally lead to an increase of inhibitory substances as is the case in acid hydrolysis [Silv2015]. In this chapter, the glucose yield of the enzymatic hydrolysis after pretreatment at 120 °C is even below that of raw beech wood. Residues of the solvent may impede the enzymatic hydrolysis [Di M2019a]. The CT and SEM images in Figures 3.4 and 3.5 visualize the effect of pretreatment temperature. With increasing temperature, the wood structure becomes more and more disintegrated due to the lignin removal.

The SEC molecular weight distributions of the extracted lignins in dependence of temperature and solvent and wood particle size are shown in Figure 3.6 and 3.7. Figure 3.6a) shows the results from the extraction using SXS and Figure 3.6b) from the extraction using SCS. For all the curves, two main peaks can be recognized: a low molecular weight peak at around 100 Da and a high molecular weight peak, which shifts depending on the temperature. For both hydrotropes, a higher temperature pushes the high molecular weight peak from 1000 Da up to 4000 Da, indicating that high molecular weight lignin can only be extracted in high quantities at temperatures higher than 150 ℃. Additionally, just as in the molecular weight distribution for Kraft lignin (see Figure 4.5a), an additional characteristic peak at 400 Da

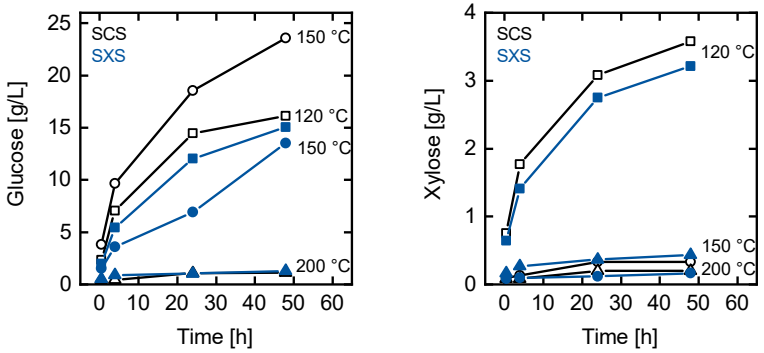

(a) HPLC results for the glucose concentration during the enzymatic hydrolysis of hydrotropic (SCS) beech wood.

(b) HPLC results for the xylose concentration during the enzymatic hydrolysis of hydrotropic (SCS) beech wood.

Figure 3.3.: HPLC results for the sugar concentration during the enzymatic hydrolysis of hydrotropic (SCS and SXS) beech wood.

can be observed. In general, the trend of a higher lignin yield at higher temperatures is the same for DESs, see 3.2. Interestingly, it can be seen in Figure 3.7 that a smaller particle size — i.e. a high surface area — of wood does not shift the curve of the distribution of the molecular weight significantly. Thus, a smaller particle size enables higher lignin dissolution, but the average molecular weight of the dissolved lignin polymer chain does not change. High molecular weight lignin can be extracted independently of the wood chip size with the parameters tested in this thesis. Table 3.1 summarizes the average molecular weight of the hydrotropic, DES and Kraft lignins and confirms the observations of the SEC molecular weight distributions.

Lignins extracted by SXS at different temperatures show differences in characteristic bonds as demonstrated by 2D HSQC measurements in Figure 3.8. The aliphatic ethers region is intensified at 150 °C compared to 120 °C, indicating the influence of the temperature on the typology of extracted lignin. By raising the temperature to 200 °C, the ether region shows less intense signals. This may

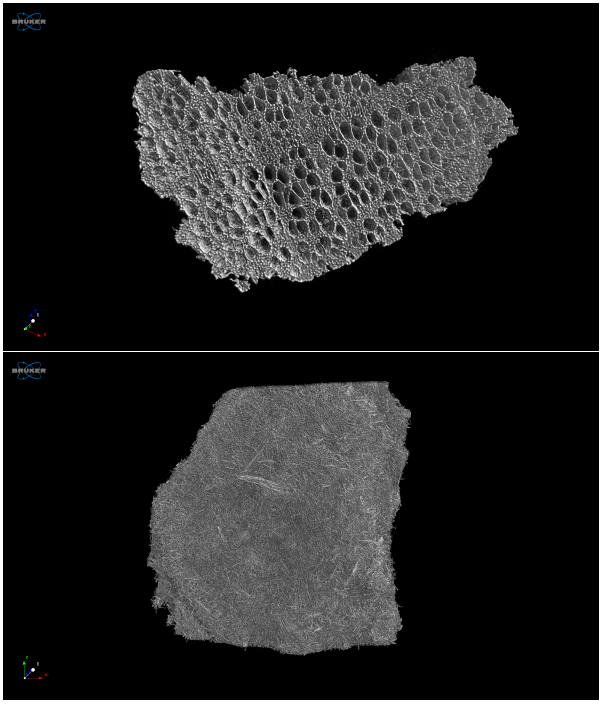

Figure 3.4.: Computer tomography images of raw beech wood (top) and beech wood after treatment in SCS at 200 °C for 6 h (bottom).

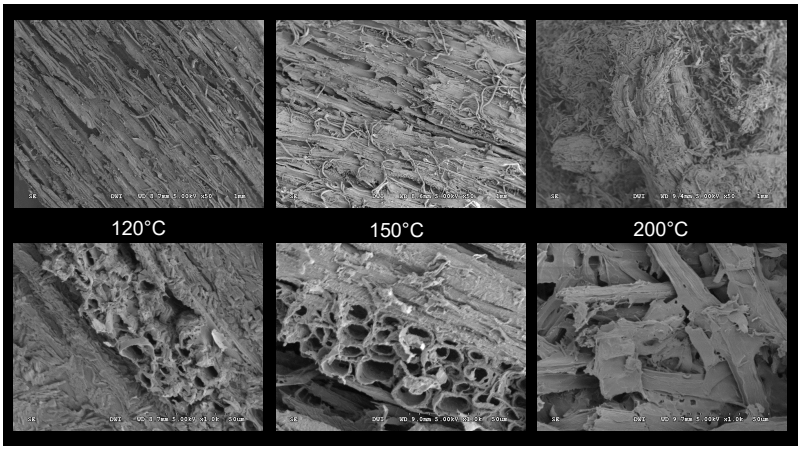

Figure 3.5.: SEM images of beech wood after treatment in SCS at 120, 150 and 200 ℃ for 6 h.

be due to the cleavage of the ether bonds, triggered by the high temperature, as suggested by Rinaldi et al. [Rina2016]. Gabov et al. [Gabo2014] also report the cleavage of β-O-4 bonds through hydrotropic lignin extraction, whereas Wang et al. [Wang2019] show that β-O-4 bonds can be preserved under the right conditions, e.g., a low pretreatment temperature. A similar behavior can be observed for the SCS experiments in Figure 3.9, although the NMR measurement at 120 ℃ could not be performed due to an insufficient amount of extracted lignin. The ether bonds contents in lignin are known to be a crucial factor affecting most of the valorization processes [Schu2018]. In fact, several catalysts are able to cleave ether bonds selectively and generate aromatic monomers as products [Dabr2015]. Researchers have proposed a mechanism in which OH-radicals are involved in the cleavage of the β-O-4 bonds [Ma2014; Zhao2010; Zeng2015] and Arantes et al. [Aran2012] have identified β-O-4 cleavage as one of the main chemical changes occuring in lignin upon attack of OH radicals. These studies indicate that a high β-O-4 content in lignin is favorable for degradation via OH radicals. Additionally, for Fenton's chemistry may also cleave C-C bonds [Klet2017]. Thus, with the parameters

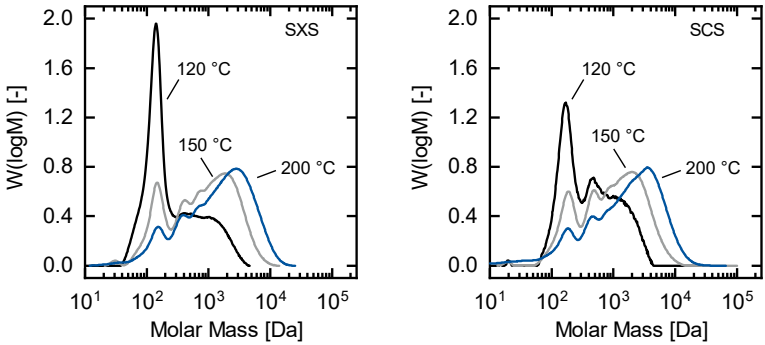

(a) Molar mass distribution of extracted lignin after wood pretreatment in SXS.

(b) Molar mass distribution of extracted lignin after wood pretreatment in SCS.

Figure 3.6.: Molar mass distribution of lignin extracted in a pretreatment with SXS, respectively SCS, at 120, 150 and 200 °C for 6 h.

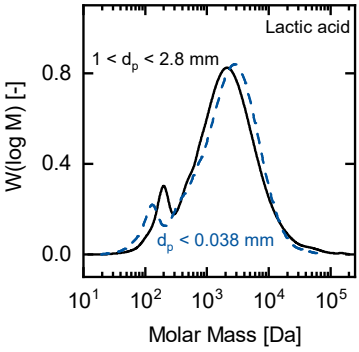

Figure 3.7.: Molar mass distribution of lignin extracted in a pretreatment with lactic acid based DES at 120 °C for 6 h.

tested in this chapter, a hydrotropic pretreatment at 150 ℃ is the most promising route.

Table 3.1.: Average molecular weight M_w and polydispersity D of hydrotropic, DES, and Kraft lignin.

	SCS			**SXS**		
Temperature [℃]	120	150	200	120	150	200
M_w [g/mol]	774	1597	2903	459	1356	2449

	Lactic Acid DES	**Lactic Acid DES** $\leq 38\,\mu m$
Temperature [℃]	120	
M_w [g/mol]	3740	3489

	Kraft
Temperature [℃]	as received
M_w [g/mol]	3702

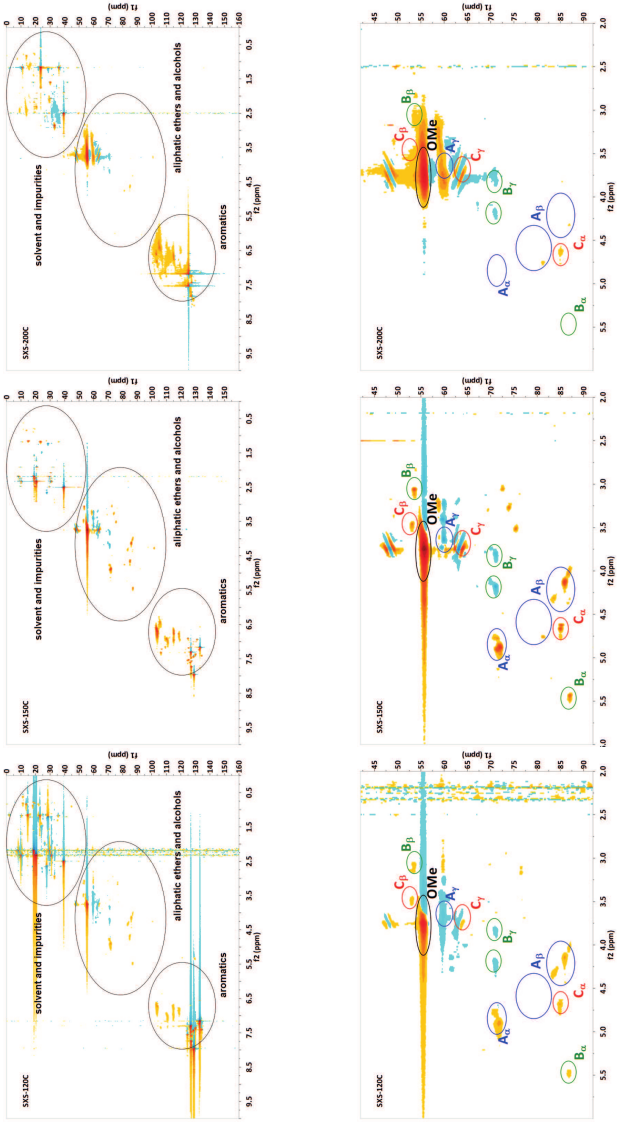

Figure 3.8.: 2D-NMR of hydrotropic lignin (SXS) for pretreatment temperatures of 120, 150 and 200 °C.

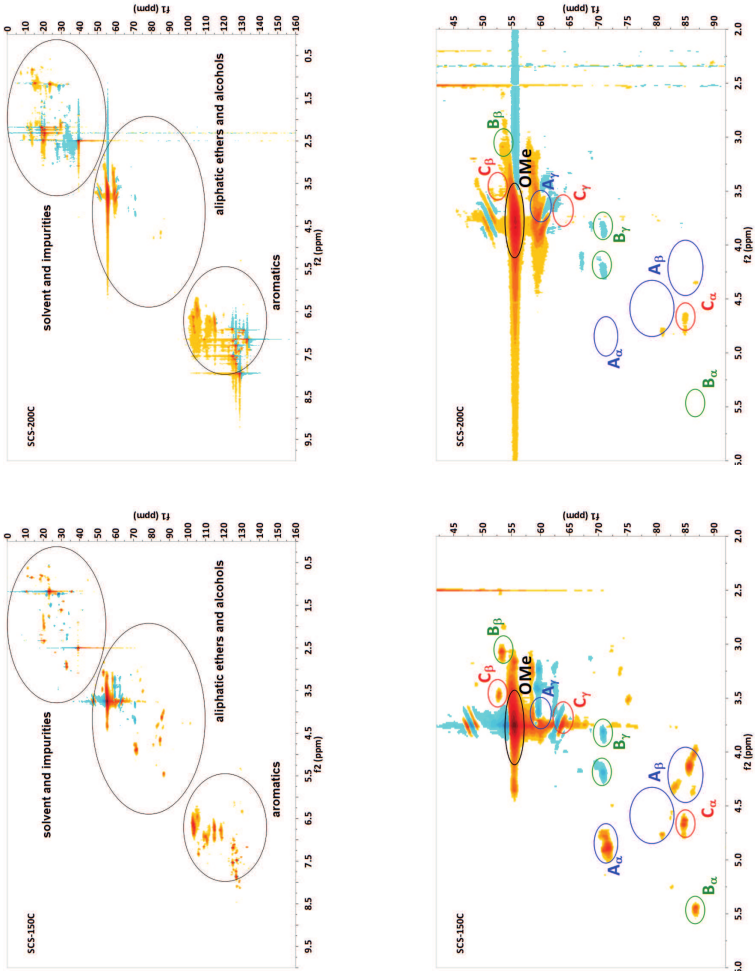

Figure 3.9.: 2D-NMR of hydrotropic lignin (SCS) for pretreatment temperatures of 150 and 200 °C.

3.4. Conclusion and Outlook

The dissolution of lignin is viable with hydrotropes (SCS, SXS) and deep eutectic solvents based on cholin chloride with either lactic acid or oxalic acid. High temperatures led to high lignin extraction yields. With hydrotropic solvents, up to 80-90% lignin extraction was reached at 200 °C. No significant difference between SCS and SXS was observed. Lactic acid is superior to oxalic acid. Up to 40% of lignin was dissolved at 120 °C. A reduction of wood particle size to less than 38 µm enhanced the extraction to close to 80%. With increasing pretreatment temperature, the average molecular weight of the dissolved lignin increased. The DES pretreated biomass showed a very poor enzymatic conversion, possibly due to the formation of inhibitors at high temperatures and the DES adsorption on the biomass. The hydrotropic solvents SCS and SXS proved to be superior in terms of enzymatic digestibility, especially when moderate pretreatment temperatures between 120 °C to 150 °C were applied. At 200 °C no enzymatic conversion of the residue was observed. NMR measurements showed that the β-O-4 content of lignin was especially high, when lignin was extracted from beech wood at 150 °C. These linkages can be cleaved upon OH radical attack through Fenton's chemistry [Aran2012]. Thus, 150 °C can be identified as best pretreatment temperature for the substrate and hydrotropic solvent chosen in this chapter.

Overall, the hydrotrope shows the most promising pretreatment characteristics: Lignin can be dissolved with high yields from biomass and the enzymatic digestibility is ensured. Additionally, the hydrotropic solution can be directly utilized in a Fenton treatment, which will be elucidated in detail in Chapter 4. Solutions of deep eutectic solvents an lignin, on the other hand, can be directly utilized in the electrochemical depolymerization of lignin [Di M2016]. In future, the solid residue must be characterized more thoroughly to understand the low enzymatic digestibility. Further, the fate of the hemicelluloses must be elucidated and valorization strategies must be

developed. At last, the overarching goal of a lignin-first biorefinery concept is the preservation of the original lignin functionalities and bonds. The NMR studies in this work showed that a low pretreatment temperature is favorable to achieve this goal. In future, a further decrease in pretreatment temperature can be achieved by substituting the hydrotrope with, e.g., p-toluensulfonic acid.

Acknowledgements Karolin Bach is acknowledged for her experimental support.

4. Depolymerization of Lignin with Fenton's Chemistry

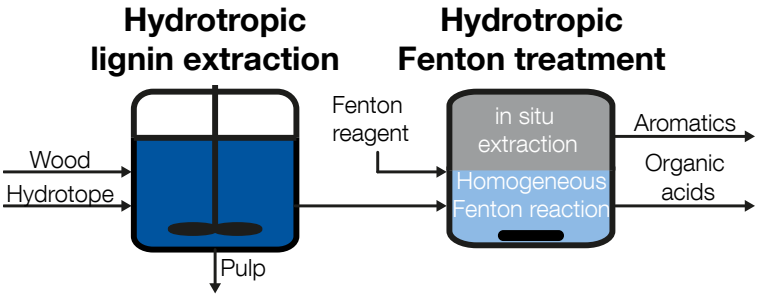

Parts of this chapter have been published as:
Robert G. Keller, Davide Di Marino, Malte Blindert, Matthias Wessling *Hydrotropic Solutions Enable Homogeneous Fenton Treatment of Lignin*, Industrial & Engineering Chemistry Research, 2020
DOI: 10.1021/acs.iecr.9b06607

Within a collaborative research project parts of this chapter are also a constituent of: Davide Di Marino, "Extraction and Electrochemical Valorization of Lignin in Novel Electrolytes", Ph.D. dissertation, RWTH Aachen University, 2019

4.1. Introduction

In biorefineries, renewable resources are converted to value-added chemicals. During processing of lignocellulose and lignin, the lignin structure is modified by base-catalyzed, acid-catalyzed, reductive, oxidative and thermal processes [Schu2018]. Oxidative lignin treatment is known to degrade lignin [Schu2018]. In particular, Fenton's chemistry has been shown to cleave β-O-4 bonds of lignin and to occur in the natural breakdown of lignocellulose [Aran2012]. Thus, degradation through Fenton's chemistry may prove to be a feasible alternative to the established processes.

A major drawback for lignin depolymerization via Fenton's reaction is the acidic pH value of at least 3, which is required to prevent the precipitation of iron hydroxides [Pign2006]. Usually, lignin cannot be dissolved in aqueous solutions at a pH of 3. Thus, most studies are conducted using lignin suspensions, organic solvents, and heterogeneous catalysts. Bentivenga et al. [Bent1999; Bent2003] performed lignin depolymerization in a mixture of acetonitrile-ethanol and observed lignin modification, polymerization, and degradation. Subsequently, recycled paper was treated with Fenton's reagent and successfully degraded. Zeng et al. [Zeng2015] depolymerized organosolv hardwood lignin in supercritical ethanol at 7 MPa and 250 °C after pretreating the lignin with Fenton's reagent in a suspension with ethanol. Mono- and oligomeric aromatics, phenols and dicarboxylic acids (DCA) were detected and a considerable yield of up to 60% bio-oil was achieved. Further, Zeng et al. [Zeng2015] suggest that the Fenton process cleaves β-ether bonds between lignin residues and lignin recondensation is depressed by the formation of a lignin-iron chelating complex. Sagues et al. [Sagu2018] extended the work of Zeng et al. [Zeng2015] and pretreated sweet sorghum bagasse with Fenton's reagent before depolymerization in supercritical ethanol (150 °C, 6.5 MPa). They detected six valuable monomers with a maximum yield of 19.1 wt.-% . Bhange et al. [Bhan2015] used the Fenton reaction to delignify lignocellulosic biomass in an aqueous solution without adjusting the

pH. They demonstrated that catalyst and reactant concentration need to be chosen carefully in order to degrade lignin and cellulose efficiently. Cronin et al. [Cron2017] adopted an approach of Ma et al. [Ma2018a] and depolymerized lignin at pH 4 under mild conditions with hydrogen peroxide and chalcopyrite as heterogeneous catalyst. Even though DCAs were produced, the yield compared to the lignin dry weight was low. Cronin improved the method by switching to an alkaline electrolyte and using percarbonate as catalyst. At high temperatures of 200 ℃ the DCA yield was improved by 85%. One reason for this observation might be the solubility of lignin in alkaline environment. Kent at al. studied the breakdown of lignin films and the conversion into water-soluble polymers [Kent2015; Kent2018]. In another approach, a high yield of carboxylic acids was reached with alkaline solubilized lignin and electrochemical oxidation [Di M2019b].

This chapter aims to improve the promising approaches reported in literature by employing an environment-friendly solvent that dissolves lignin at room temperature, independently of pH, and that is also suitable as a medium for subsequent treatment by Fenton's reagent. First, the influence of the hydrotropic solvent and the iron catalyst on the lignin degradation is presented. Then, the degradation of Kraft lignin with a coupled in situ extraction of low molecular weight aromatic products is presented in dependence of the hydrogen peroxide flow rate and the pH value. Subsequently, lignin, which was extracted from beech wood with environment-friendly hydrotropic solvents in Chapter 3, was used as substitute for Kraft lignin in the Fenton process. Hence, this chapter proposes a two-stage process for biomass pretreatment and lignin valorization in a hydrotropic solution.

4.2. Experimental

4.2.1. Fenton Experiments

Batch Reactor Setup

Batch experiments for Fenton treatment of lignin were performed in a beaker with 100 mL solution volume to study the influence of Kraft lignin dissolution (with and without hydrotropic salt) and Fenton chemistry (with and without iron catalyst) at room temperature. The concentration of the hydrotrope sodium cumene sulfonate (SCS) was $400\,\mathrm{g\,L^{-1}}$, and Kraft lignin was added to $5\,\mathrm{g\,L^{-1}}$. The pH value of the solutions was adjusted to 3 with H_2SO_4. Following other Fenton studies with lignin, the catalyst concentration of iron sulfate ($FeSO_4$) was adjusted to 1 mM [Esca2005; Kent2015]. The different reaction parameters are listed in Table 4.1. In each experiment, samples were taken for gas chromatography-mass spectrometry (GC-MS) and size exclusion chromatography (SEC) after 0 h, 1.5 h, 3 h, and 4.5 h, followed by the addition of 100 μL of 30 wt.-% hydrogen peroxide (H_2O_2).

Table 4.1.: Reaction parameters for the batch experiments.

Batch exp. nr. [-]	**SCS concentration** [g/L]	**Fe^{2+} concentration** [mM]
1	400	0
2	0	0
3	400	1
4	0	1

Continuous Reactor Setup

A sketch of the reactor setup for the continuous Fenton reaction is depicted in Figure 4.1. Experiments were performed at room temperature with $5\,g\,L^{-1}$ Kraft lignin and with lignin extracted from wood chips. The aqueous phase (150 mL Volume, $400\,g\,L^{-1}$ hydrotrope, pH 2 or 3, 1 mM $FeSO_4$) was recirculated with a pump through the organic phase (Methyl isobutyl ketone, MIBK) to extract aromatics. A Schott bottle served as the reaction vessel. The reaction mixture was circulated using a peristaltic pump (Ismatec, ISM831C) at $40\,mL\,min^{-1}$. The in situ extraction was performed with 150 mL MIBK. By means of a syringe pump (Harvard Pump 11 Elite) and a long cannula, 30 wt.-% H_2O_2 was injected with a flow rate of either 1 or $2\,mL\,h^{-1}$ into the aqueous lignin phase for three hours. The aqueous solution was agitated with a magnetic stirrer. Gas chromatography (GC) and size exclusion chromatography (SEC) samples were taken from the organic phase as well as SEC and liquid chromatography (LC) samples from the aqueous phase. To demonstrate the feasibility of the integrated two-step process consisting of pretreatment and valorization, additional experiments were performed with hydrotropic lignin from Chapter 3. The hydrotropic lignin solution was diluted 1:4 v/v to $100\,g\,L^{-1}$ SCS, $FeSO_4$ was added (1 mM), and the pH was adjusted to 2 with H_2SO_4.

Chemicals

$FeSO_4$ (99.0%), H_2O_2 (30%), Kraft lignin (370959), Methyl isobutyl ketone (99%), NaOH (98%), SXS (90%), sodium sulfite (Na_2SO_3, 98-100%) and 2-methyltetra-hydrofuran (2-MTHF, 99%) were purchased from Sigma-Aldrich. SCS (93%) was purchased from Julius Hoesch. The pH was adjusted with H_2SO_4 (75%) from Carl Roth. All chemicals were used without further purification and adjusted to the desired concentrations with deionized water.

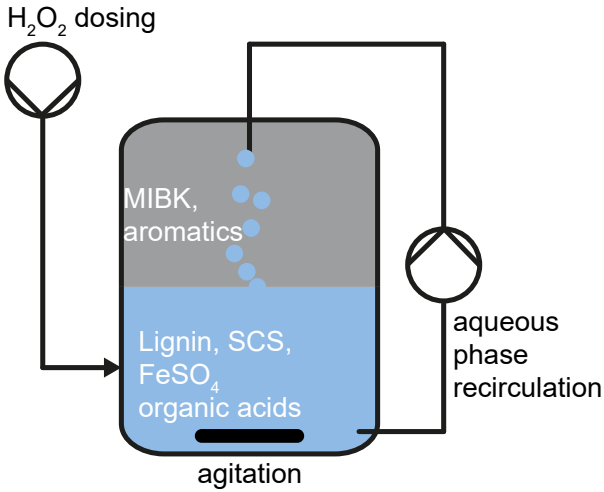

Figure 4.1.: Process sketch of the continuous reactor setup for Fenton treatment of lignin in a hydrotropic solution. Hydrogen peroxide was continuously added to the reaction vessel. The aqueous phase was recirculated through the organic phase for aromatic product extraction.

Sample Preparation

Lignin samples for SEC from the batch experiment were prepared according to Chapter 3. For the SEC analysis of the continuous experiments, 2 mL of the aqueous lignin phase were diluted with 2 mL of deionized water or 3 wt.-% Na_2SO_3 and 16 mL of 1 M sodium hydroxide solution. Na_2SO_3 was initially used as quenching agent for the Fenton reaction [Kwon2012]. However, the addition of NaOH also stops the reaction and renders the Na_2SO_3 obsolete. Na_2SO_3 does not change the SEC results significantly compared to water, see Figure 4.2. One milliliter of the diluted sample was then transferred into a vial for analysis by SEC. Furthermore, for the analysis of organic acids a sample of the aqueous phase of the experiments with hydrotropic lignin was diluted 1:10 v:v with NaOH and analyzed according to the procedure described in the next section and in Di Marino et al. [Di M2019b]. For the analysis of the organic phase by means of GC-MS, 1 mL of sample was transferred into a vial. The GC analysis of the organic phase was performed according to the procedure described in subsequent sections. The concentrations of the compounds listed in Table 4.2 were measured. The remaining sample volume after GC analysis was mixed with 1 mL of 1 M sodium hydroxide solution for SEC.

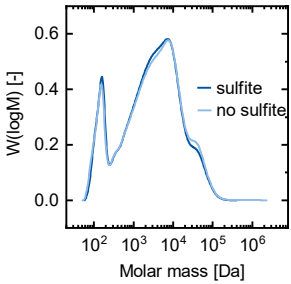

Figure 4.2.: Comparison of SEC results for samples after 4.5 h of reaction time, which were either quenched or not quenched with sodium sulfite before 1 M NaOH was added.

4.2.2. Analytics

Details on the SEC analysis for the moleclar weight distribution can be found in Chapter 3.

Aromatics Quantification

Gas chromatography mass spectrometry (GC-MS) (Agilent 6890 and N-Agilent 5975 MSD) equipped with a J&W 122-0132 DB-1MS capillary column (30 m, 0.25 mm n.d., film 0.25 mm) was performed in order to detect the monomers and oligomers produced during the electrochemical depolymerization and subsequent extraction. Helium was applied as carrier gas with an initial flow of 0.8 mL/min. The initial temperature of the GC oven was 50 ℃ for 1 minute; thereafter the temperature was increased to 120 ℃ with a rate of 15 $^{\circ}\mathrm{C}\,\mathrm{min}^{-1}$, and finally 280 ℃ were reached with a rate of 25 $^{\circ}\mathrm{C}\,\mathrm{min}^{-1}$. The two temperatures were kept constant for 6 and 2.5 minutes, respectively. All identified products by GC-MS measurements (see Table 4.2) were quantified by external calibration curves, for which chemicals were purchased by Sigma-Aldrich with the purest available grade.

Organic Acids Quantification

The amount of organic acids in the depolymerized lignin samples was determined by a method based on reversed-phase liquid chromatography coupled to electrospray ionization quadrupole time-of-flight mass spectrometry (LC-ESI-Q-ToF-MS) as described in Di Marino et al. [Di M2019b].

Table 4.2.: Products quantified via GC.

Nr.	Compound	Chemical formula
1	α-methylstyrene	C_9H_{10}
2	guaiacol	$C_7H_8O_2$
3	p-cumenol	$C_9H_{12}O$
4	phenylacetic acid	$C_8H_8O_2$
5	4-hydroxybenzaldehyde	$C_7H_6O_2$
6	eugenol	$C_{10}H_{12}O_2$
7	vanillin	$C_8H_8O_3$
8	4-hydroxyacetophenone	$C_8H_8O_2$
9	acetovanillone	$C_9H_{10}O_3$
10	syringaldehyde	$C_9H_{10}O_4$
11	acetosyringone	$C_{10}H_{12}O_4$
12	bisphenol-A	$C_{15}H_{16}O_2$

4.3. Results and Discussion

4.3.1. Batch Fenton Reaction in Hydrotropic Solutions

Batch experiments were performed to investigate the influence of lignin dissolution (hydrotrope vs. no hydrotrope) and Fenton's chemistry (iron catalyst vs. no iron catalyst). Based on the change in the average molecular weight an assessment of the effectiveness in terms of average molecular weight reduction of lignin can be established. Figure 4.3 a) shows that lignin dissolution by addition of the hydrotropic salt SCS and subsequent Fenton chemistry (H_2O_2 and Fe^{2+}) yield a much higher apparent depolymerization compared to systems without hydrotrope or Fenton's reagent. In the two systems without SCS, in which lignin is not dissolved but suspended, the decrease of the relative average molecular weight is 20-25%. The presence of iron (II) sulfate in a system without SCS has a minor influence on the molecular weight reduction, even though the catalyst

enables the generation of OH-radicals (Equation 2.16), which are strong oxidants and have been reported to depolymerize suspended biomass or lignin [Bhan2015; Ma2018a; Cron2017]. In this work, the amount of added hydrogen peroxide was rather low. Thus, the accessibility of lignin — provided by dissolution in the hydrotrope — seems to enhance the depolymerization. Considering the two systems with sodium cumene sulfonate (SCS) where lignin is dissolved, there is a clear difference in the reduction of the average molecular weight. In the presence of $FeSO_4$, apparent depolymerization of lignin occurs as a result of the Fenton reaction. The average molecular weight is reduced by more than 60%. The molecular weight distribution of experiment 3 is shown in Figure 4.3 b). On the other hand, the system without $FeSO_4$ shows a constant molecular weight. Overall, the analysis of the above-mentioned data was demanding, as the sample preparation involved multiple steps, and the precipitation of lignin from the hydrotropic solutions was challenging. Additionally, experiments were performed where the samples were not precipitated before analysis and the average molecular weight reduction was not as pronounced. The SEC results in Figure 4.4 add additional weight to the proposed hypothesis. They compare an experiment with SCS and hydrogen peroxide, but with and without the addition of the iron catalyst. The SEC samples, in this case, were drawn directly from the solution and prepared according to the procedure described for the continuous reactor setup, which means that no precipitation step was involved. As before, the effect of iron is clearly visible. Even though the depolymerization is not as pronounced, a substantial increase in low molecular weight compounds can be observed. From these results we conclude that the Fenton treatment relies on two factors:
a) OH radicals attack lignin more effectively than hydrogen peroxide
b) dissolution of lignin improves the accessibility of the substrate.

Table 4.3.: Total GC yield of aromatics of the batch depolymerization of Kraft lignin.

No. of experiment	**Total GC yield**
-	wt.-%
1	0.70
2	0.29
3	2.97
4	0.12

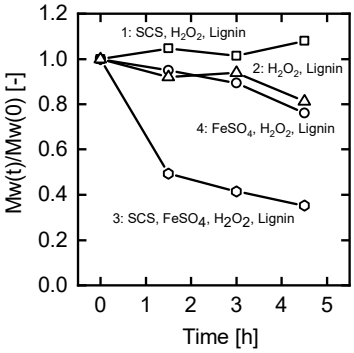

(a) Relative molecular weight over reaction time.

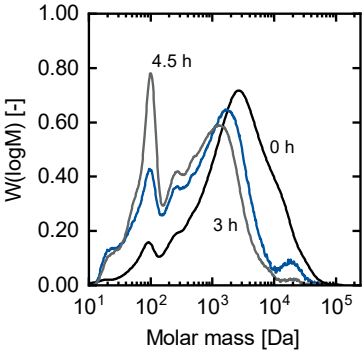

(b) SEC results for the batch Fenton experiment Nr. 3: SCS, $FeSO_4$, H_2O_2 and lignin

Figure 4.3.: Batch Fenton treatment of lignin with and without catalyst and hydrotrope. The experimental conditions were: $5\,g\,L^{-1}$ Kraft lignin , $0\,g\,L^{-1}$ or $400\,g\,L^{-1}$ SCS, 0 mM or 1 mM $FeSO_4$, addition of 100 μL of 30 wt.-% H_2O_2 after sampling at 0 h, 1.5 h, 3 h.

The aqueous supernatants were examined with GC-MS for aromatics after lignin precipitation and extraction . Experiments 1, 2 and 4 from Table 4.1 show a very low yield of aromatics, which was less than 1 wt.-% . Moreover, the detected aromatics originate from the raw lignin and no increase in concentration could be observed over time. Experiments 2 and 4 permit only limited yield due to the poor accessibility of lignin in the suspended state. Although a reduction in the average molecular weight can be seen, no appreciable yield of aromatic monomers could be detected. In experiment 3, an overall yield of 3 wt.-% was detected. The yields for the different experiments are summarized in Table 4.3. The analysis of the supernatants revealed a maximum concentration of about 115 mg/L for p-cumenol. However, in the case of guaiacol, for example, a decrease in concentration was observed with progressive reaction: The unselective nature of OH-radicals leads to overoxidation. Cleavage of the ring structure results in the loss of aromaticity and the formation of alcohols, ketones, or acids [Zazo2005]. As a remedy to this challenge, the batch addition of H_2O_2 was substituted by a continuous addition with combined in situ extraction.

4.3.2. Continuous Fenton Reaction in Hydrotropic Solutions

Kraft lignin was dissolved in hydrotropic solutions and treated in the continuous reactor setup with in situ extraction to study the influence of varying process conditions such as pH value and hydrogen peroxide flow rate. Figure 4.5 a) shows the treatment of $5\,g\,L^{-1}$ Kraft lignin in $400\,g\,L^{-1}$ SCS, pH 3 and 1 mM $FeSO_4$. H_2O_2 (30 wt.-%) was continuously added with $1\,mL\,h^{-1}$, or $2\,mL\,h^{-1}$. After 4 h of reaction time, an increase in low molecular weight compounds (LMWC) can be observed. The LMWC, which are detected at ca. 25 mL elution volume, correspond to molecular weights of less than 300 Da. As will be shown in the next paragraphs, the group of LMWCs consists of guaicaol, p-cumenol, vanillin, acetovanillone and acetosyringone, but

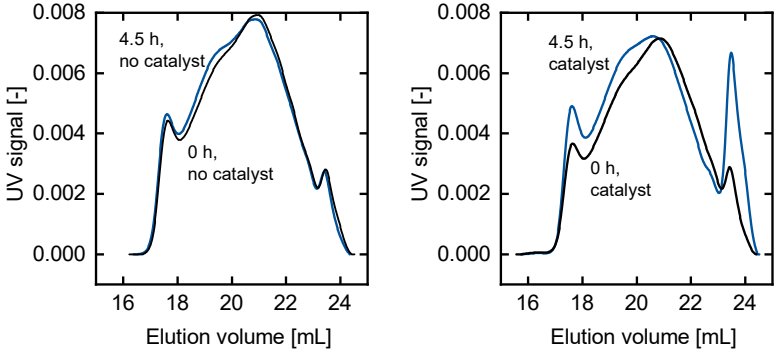

(a) SEC results of a batch experiment with 5 g L^{-1} lignin in 400 g L^{-1} SCS, pH 3 and the addition of 100 μL of 30 wt.-% H_2O_2.

(b) SEC results of a batch experiment with 5 g L^{-1} lignin in 400 g L^{-1} SCS, 1 mM $FeSO_4$, pH 3 and the addition of 100 μL of 30 wt.-% H_2O_2 after 0h, 1.5 h and 3h.

Figure 4.4.: SEC results for the batch Fenton treatment of 5 g L^{-1} Kraft lignin with and without the iron catalyst.

also organic acids such as oxalic acid. A higher flow rate of H_2O_2 yields more hydroxyl radicals, as can be seen from eq 2.16, and consequently, more degradation products can be formed. Correspondingly, for medium elution volumes of 23 mL (medium molecular weight compounds, 300 Da $< M_{MMWC} <$ 5000 Da, MMWC) a decrease in concentration is observed. Additionally, polymerization to high molecular weight compounds is apparent (HMWC), which correspond to an elution volume $<$ 21 mL and a molecular weight $>$ 5000 Da, see Figure 4.5 a). Similar trends were observed in other studies with oxidative depolymerization, e.g., by Stiefel et al. [Stie2016b]. As the Fenton process employs radicals, condensation of lignin fragments is possible [Schu2018]. After a certain degree of polymerization is reached, mainly depolymerization takes place [Stie2016b]. Additionally, it has to be kept in mind that a Fenton treatment may alter the aromatic structure of lignin [Kent2015].

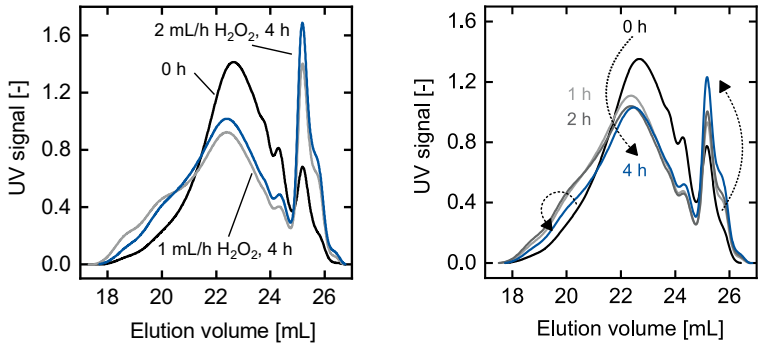

(a) Elugram for the reaction at pH 3 with different H_2O_2 flow rates.

(b) Elugram of the reaction at pH 2 with a flow rate of $2\,mL\,h^{-1}$ H_2O_2.

Figure 4.5.: SEC results of the continuous Fenton treatment of $5\,g\,L^{-1}$ Kraft lignin in $400\,g\,L^{-1}$ SCS and 1 mM $FeSO_4$.

4

In general, pH 3 is the optimum pH value for Fenton's chemistry which is among other factors due to the poor solubility of Fe^{3+} at pH values greater than 3 [Pign2006]. In this work, the precipitation of iron was observed even at pH 3, which is attributed to the presence of SCS in the reaction solution. A decrease of the pH value to 2 overcame the limitations and did not show any precipitation. Accordingly, all further experiments were carried out at this value. In Figure 4.6 the molecular weight distribution and elugram for the continuous treatment of $5\,g\,L^{-1}$ Kraft lignin in $400\,g\,L^{-1}$ SCS, pH 2, 1 mM $FeSO_4$ 30 wt.-% H_2O_2 with $1\,mL\,h^{-1}$, respectively $2\,mL\,h^{-1}$, are shown. They are qualitatively similar to the results for pH 3. SEC samples throughout the reaction time in Figure 4.5 b) show how polymerization, depolymerization, and extraction take place simultaneously. While LMWCs at an elution time of 25 min are continuously formed through bond scission, HMWCs polymerize until 2 h of reaction time, after which a decrease in concentration can be observed. As especially aromatic LMWCs are unstable in the highly oxidative environment of Fenton's chemistry [Schu2018], the presented process concept involves

an in situ extraction to the organic phase. The molar mass distribution in Figure 4.7 a) shows that lignin compounds between 30 - 3000 Da are extracted by MIBK. The extracted compounds are formed by the Fenton depolymerization but are also present in raw Kraft lignin as the sample of 0 h demonstrates. The concentration of the LMWC increases continuously over the course of the experiment. With the help of a blank experiment, the behavior of the SEC results in Figure 4.6 can be understood in more detail. In the blank experiment, no hydrogen peroxide was added to the aqueous phase. Figure 4.8 compares the elugrams of the aqueous and organic phase of an experiment with and without H_2O_2. As can be expected, the organic phase extracts low and medium molecular weight compounds from lignin over the course of the reaction. The compounds are present in raw lignin, but are also formed during depolymerization. Thus, the peak for MMWCs at 23 mL in the aqueous phase decreases in both the blank and Fenton experiment over the course of the reaction. However, in the aqueous phase it is apparent that depolymerization due to radicals forms LMWC as the peak at 25 mL increases compared to the start of the experiment and the blank, see Figure 4.8 a). Additionally, in the organic phase one can observe that the peak at 24 mL visible in the blank experiment is almost not detectable in the Fenton experiment. It is hypothesized that these compounds are degraded by Fenton's reagent.

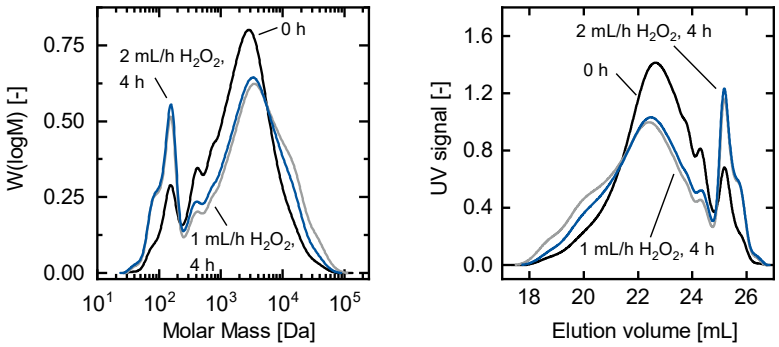

(a) Molar mass distribution **(b)** Elugram

Figure 4.6.: SEC results for continuous Fenton treatment of $5\,\mathrm{g\,L^{-1}}$ Kraft lignin in $400\,\mathrm{g\,L^{-1}}$ SCS, pH 2, 1 mM $FeSO_4$ and different hydrogen peroxide flow rates.

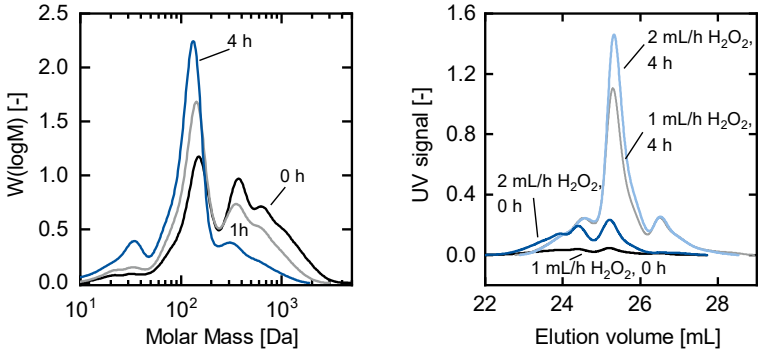

(a) Molar mass distribution of the organic phase over the reaction time. **(b)** Elugram of the organic phase for different H_2O_2 flow rates.

Figure 4.7.: SEC results of the organic extractant phase over the reaction time of a continuous Fenton treatment of $5\,\mathrm{g\,L^{-1}}$ Kraft lignin in $400\,\mathrm{g\,L^{-1}}$ SCS, pH 2, 1 mM $FeSO_4$

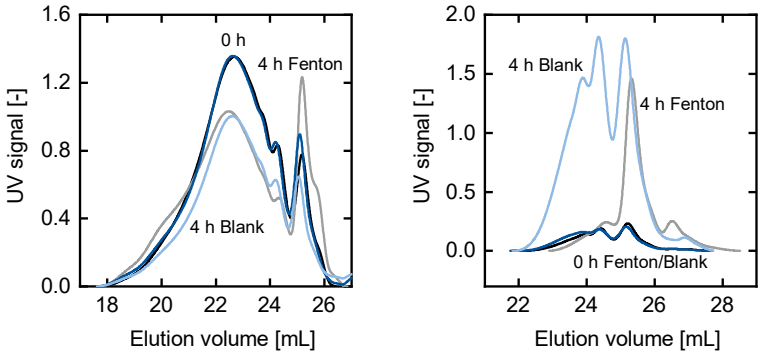

(a) Comparison of SEC elugrams of the aqueous phase of blank experiment and of the Fenton experiment.

(b) Comparison of SEC elugrams of the organic phase of blank experiment and of the Fenton experiment.

Figure 4.8.: Comparison of SEC elugrams of the blank experiment and of the Fenton experiment.

A higher hydrogen peroxide addition leads to a slightly higher concentration of LMWCs in the organic phase, as shown in Figure 4.7 b). However, the concentration of LMWCs at the beginning of the experiment is also higher for the higher flow rate. Thus, a more detailed investigation of the extract phase was carried out by means of a gas chromatography-mass spectrometry for quantification. The GC was calibrated with the compounds listed in Table 4.2. Of all the compounds, only guaicaol, p-cumenol, vanillin, acetovanillone and acetosyringone were detected in concentrations > 1 mg/L in the GC samples taken from Fenton experiments after 4 h. The concentrations measured for the samples from the Fenton reaction were corrected with partition coefficients between MIBK and the aqueous phase, which were measured in separate experiments to obtain the total concentration ("sample") in the organic and aqueous phase. Additionally, two blank experiments were conducted to correct for degradation products from SCS and extractives from lignin: One experiment, where no lignin was added to detect degradation products of SCS ("SCS blank") and one experiment, where no H_2O_2 and $FeSO_4$ were added to detect

compounds extracted from raw lignin ("lignin blank"). Thus, the "corrected sample" represents the sample value minus the two blank values. SCS degradation products were mainly p-cumenol and acetosyringone. It has been shown previously that SCS can be mineralized by radicals generated in electrochemical, photochemical, and photoelectrochemical reactors [Osie2013]. From the data of this study, it was not possible to calculate the amount of degraded hydrotrope, because not all degradation products were measured. Nonetheless, it seems imperative for future studies to increase the lignin to hydrotrope ratio significantly in order to obtain more lignin degradation products and less hydrotrope degradation products. The highest share of the total detected GC products is accounted for by extracted lignin as can be seen in Figure 4.9 a), which indicates that the formation of monomer products and the extraction of products from lignin is faster than the degradation of SCS. The main products detected in the lignin

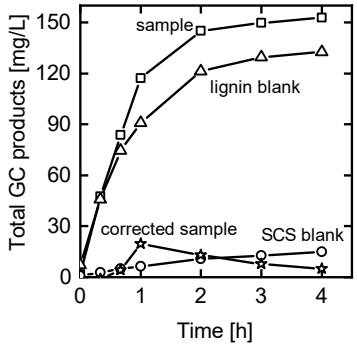

(a) Total GC product yield over time at $1\,mL\,h^{-1}$ H_2O_2, corrected by products extracted from lignin (lignin blank) and degradation products from SCS (SCS blank).

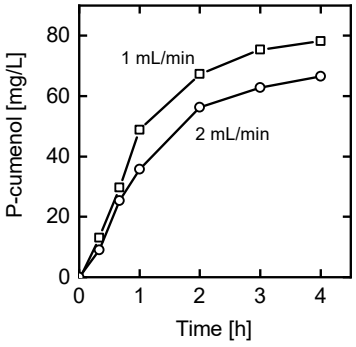

(b) P-cumenol yield over time in dependence of the H_2O_2 flow rate.

Figure 4.9.: Yield of GC products for Fenton reaction of lignin ($5\,g\,L^{-1}$) in $400\,g\,L^{-1}$ SCS, 1 mM $FeSO_4$ and pH 2.

blank experiment were guaiacol, p-cumenol, vanillin, and acetovanil-

lone. Figure 4.9 b) shows that the overall p-cumenol concentration increases steeply at first and flattens after 2 h of reaction time. This behavior can be explained by the nature of the Fenton process and the p-cumenol extracted by lignin. In this work, Fe^{2+} was used as a catalyst. At the beginning of the process, many OH radicals can be generated due to the high abundance of Fe^{2+}. However, once the initial amount of Fe^{2+} is oxidized to Fe^{3+}, the Fenton reaction slows down substantially, due to the slow reduction of ferric iron to ferrous iron (Equation 2.17) [Pign2006].

Additionally, the rate of extracted products from lignin is higher at the beginning of the process and will naturally decline over time due to decreasing chemical potential differences. From the SEC data it was concluded that the concentration of LMWC increases with increasing H_2O_2 flow rate due to an increased radical generation following Equation 2.16. However, the GC analysis for p-cumenol depicted in Figure 4.9 b) shows a higher p-cumenol yield for lower H_2O_2 flow rates. This trend is similar for the total amount of GC products. Higher yields for lower flow rates are observed for the lignin degradation as well as the SCS blank degradation. It is hypothesized that with a lower flow rate of hydrogen peroxide there is more time for the extraction into the organic phase, preventing overoxidation. Nonetheless, the yield of aromatics is very low considering an initial lignin concentration of $5\,g\,L^{-1}$ and a total of identified GC products of the sample of about $150\,mg\,L^{-1}$ (even 5 - $30\,mg\,L^{-1}$ taking into account the corrected sample, see Figure 4.9). A yield of $150\,mg\,L^{-1}$ aromatics corresponds to 0.025 $g_{aromatics}/g_{H2O2}$, which is low and highlights the need for optimization. As stated before, SCS, but also other aromatic compounds, can be degraded by the Fenton process [Pign1997; Osie2013]. The products, which were identified via GC analysis, are not likely to be the only LMWC the Fenton reaction yields. Other, potentially more stable products may be formed, e.g., organic acids [Zazo2005; Schu2018]. The organic acids represent the major product fraction, which will be shown in the last section of this work. Even though in situ extraction of aromatics was performed, the mass transport from the aqueous to the organic phase may be the limiting

step to achieve higher yields. An optimization of H_2O_2 dosing, Fe_2^+ and SCS concentration should lead to a higher aromatics yield and a higher lignin concentration in the solution will additionally increase the selectivity as the substrate to product ratio increases, offering more targets for the radicals. Nonetheless, literature suggests that C-C scission cannot be avoided completely in an oxidative treatment [Klet2017].

4.3.3. Sequential Lignin Extraction and Fenton Reaction in Hydrotropic Solutions

In Chapter 3 raw beech wood was pretreated in 400 g L^{-1} hydrotropic solutions of SCS and SXS for 6 h at different temperatures (120, 150, 200 °C). In this chapter, the extracted hydrotropic lignin is treated with Fenton's reagent. A sketch of the proposed process is depicted in Figure 4.10. After lignin extraction, the pretreatment solution

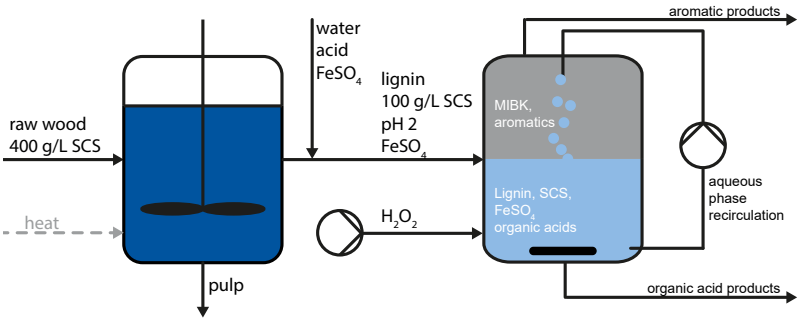

Figure 4.10.: Process sketch of sequential lignin extraction and Fenton reaction facilitated by hydrotropic solvents. Hydrogen peroxide is continuously added to the reaction vessel. The aqueous phase is recirculated through the organic phase for aromatic product extraction.

was diluted 1:4 v:v, the pH was adjusted to 2 and $FeSO_4$ was added. A treatment with the Fenton process in the continuous set-up was performed with the best parameters from the experiments with Kraft

lignin: pH 2 for a stable system without iron precipitation and a flow rate of 1 mL h^{-1} H_2O_2, which showed a slightly higher yield for aromatics than 2 mL h^{-1}. During the Fenton process, the peak of LMWCs increased while the typical superposition of polymerization and depolymerization was observed for HMWCs, as can be seen in Figure 4.11. Apparently, the depolymerization slows down after the first 2 h, which is in agreement with the observations for Kraft lignin depolymerization, Figure 4.5 b). The molar mass distributions indicate more pronounced changes for hydrotropic lignin originating from a pretreatment with 150 °C, whereas the changes for 120 °C and 200 °C are smaller. In the case of hydrotropic lignin extracted at 120 °C, the lignin concentration in the reaction solution is very low (˜0.09 g/L). Thus, it is likely that the OH radicals mainly attack the hydrotropic salt, or decay in parasitic reactions. For high concentrations of lignin (˜3 g L^{-1}), the change may not be as pronounced due to limited H_2O_2 supply and thus, limited degradation.

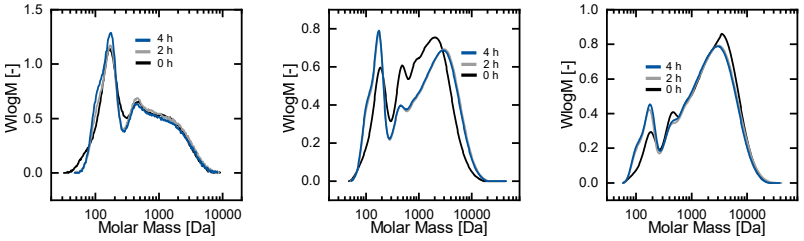

(a) Pretreatment at 120 °C.

(b) Pretreatment at 150 °C.

(c) Pretreatment at 200 °C.

Figure 4.11.: SEC results of Fenton treatment of hydrotropic lignin, which was extracted at 120, 150 and 200 °C and 400 g L^{-1} SCS. The hydrotropic salt concentration was then diluted to 100 g L^{-1}, the pH value was adjusted to 2 and the hydrogen peroxide flow rate was adjusted to 1 mL h^{-1}.

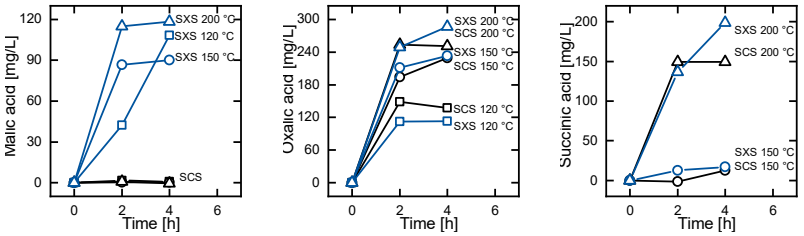

(a) LC results for the malic acid yield.

(b) LC results for the oxalic acid yield.

(c) LC results for the succinic acid yield.

Figure 4.12.: Yield of organic acids via continuous Fenton reaction of hydrotropic lignin obtained with pretreatment temperatures of 120, 150 and 200 °C.

The Fenton experiments with Kraft lignin led to the conclusion that the yield of aromatics is rather low. Thus, for the Fenton experiments with hydrotropic lignin, the aqueous phase was tested for organic acids such as oxalic acid, malic acid, and succinic acid. Reports in literature suggest that ether bond cleavage and aromatic ring degradation occur simulateneously [Kent2018] and that organic acids are the main product of the Fenton chemistry with lignin [Mae2000]. Figure 4.12 shows the concentrations of malic acid (Fig. 4.12 a)), oxalic acid (Fig. 4.12 b)) and succinic acid (Fig. 4.12 c)) in dependence of the reaction time. All concentrations were corrected by the initially present acid amount from the pretreatment. For 120 °C, no succinic acid could be detected. Figure 4.12 shows that oxalic acid is the main product of the Fenton reaction. With increasing pretreatment temperature, more product can be obtained. This observation is due to the fact that more lignin is available in the solution at higher pretreatment temperatures. Additionally, a higher pretreatment temperature may yield lignin with different functional groups and different bonds, which can be seen from the results of the NMR measurements in Figures 3.8 and 3.9 in Chapter 3. For hydrotropic lignin (150 °C pretreatment) up to 30% yield of oxalic acid based on the initial lignin concentration were obtained. This value was calculated based on LC measurements for oxalic acid and the determination of initial lignin concentration via UV-Vis. It

highlights that a mere characterization of the Fenton reaction by SEC is not sufficient, as the high yield is not apparent here (Figure 4.11 b)). The SEC is not calibrated for, e.g., oxalic acid. All in all, 0.04 $g_{OrganicAcid}/g_{HydrogenPeroxide}$ were obtained. Thus, even though the yield of organic acids compared to the initially present lignin was decent, the hydrogen peroxide should be valorized more effectively. This could be achieved by increasing the lignin concentration so that the chance of a radical attacking lignin is increased.

It cannot be ruled out that the hydrotrope or even extracted xylan is degraded to oxalic acid. On the other hand a blank experiment with a hydrotropic solution was performed (results not shown here), where organic acids such as malic acid or succinic acid were detected, but no oxalic acid. Also, the strong temperature dependence of the oxalic acid and succinic acid concentration indicates that these products do not originate from the hydrotrope, as the hydrotrope concentration was the same for every pretreatment. Additionally, a batch experiment with Kraft lignin ($5\,g\,L^{-1}$, 1 mL H_2O_2 every hour, 5 mM $FeSO_4$) was performed. Other than malic acid and succinic acid, up to about 190 mg/l oxalic acid were detected. Consequently, it can be concluded that indeed products by a Fenton treatment of hydrotropic lignin solutions were obtained. However, more experiments are needed to establish reaction mechanisms and kinetics to tune the reaction towards high yields and to gain a deeper insight into the process.

4.4. Conclusion and Outlook

The valorization of lignin in biorefineries requires solvents that extract the polymer at high yields and which ideally can be used in subsequent process steps. In this chapter, hydrotropic lignin from Chapter 4, and Kraft lignin were treated with Fenton's reagent in hydrotropic solvents. The unique properties of hydrotropic solutions, which allow for lignin dissolution at acidic pH values, are an enabler of the integrated process. It was shown that lignin was attacked and altered by SEC

analysis. In contrast to a purely aqueous solution for the Fenton process, a pH value below three was critical for long-term operation in hydrotropic solvents. Otherwise iron precipitated. The aromatic products of the oxidative degradation were not stable and detected in low concentrations. Organic acids such as oxalic or succinic acid were the main products of this study. With increasing pretreatment temperature of the wood, more lignin was extracted from beech wood and consequently more organic acids are obtained. For a pretreatment temperature of 150 ℃ up to 30% yield of oxalic acid were obtained relative to the initial lignin content.

The proposed integrated process can be a platform for lignin valorization studies. Alternatives to the Fenton reaction could be implemented. Additionally, the mechanism of Fenton's reagent in hydrotropic lignin solutions and the interplay between hydrotrope, lignin and iron catalyst should be further explored. In this study, carboxylic acids were found to be the main product. However, in situ separation of products should be intensified, e.g., by adjustment of the residence time of the aqueous droplets in the organic phase, to potentially increase the space-time yield of aromatic compounds. Additionally, the hydrotropic solvent allows an increase of the lignin concentration of up to 350 g/L, which can increase the selectivity to valuable products.

5. Depolymerization of Cellobiose with Fenton's Chemistry

5.1. Introduction

In nature, brown rot fungi employ the non-enzymatic Fenton chemistry for the degradation of biomass [Aran2012]. Two of the main constituents of biomass, cellulose and hemicellulose, are degraded through fragmentation or oxidative cleavage [Aran2012]. Inspired by nature, Fenton processes have been integrated more and more into biorefineries in the last decade: a preceding Fenton treatment improves the enzymatic hydrolysis [Jeon2016; He2015]. In fact, the complete solubilization of cellulose by Fenton chemistry was demonstrated in the 60s by Halliwell et al. [Hall1965]. Thus, cleavage of the glycosidic bond of cellulose oligomers can lead to the formation of soluble carbohydrates such as glucose [Kwon2012]. The conversion of cellulose to glucose via Fenton-related processes as an alternative to the enzymatic hydrolysis is gaining attention, as glucose may then be further converted to value-added chemicals via biotechnological routes [Kwon2012; Wang2011; Meng2011; Yang2014].

To date, knowledge gaps exist on the conversion of cellulose to glucose via OH radicals. In general, Halliwell et al. [Hall1965] demonstrated the dissolution of cotton fibers via Fenton's chemistry, which is supported by other authors [Aran2012; Aran2006; Xu2001]. Even though a successful breakdown of the fibers was demonstrated, the individual products were not identified. Total carbon determination showed that only 10% of the initial mass was retained in the supernatant. Different catalysts for the Fenton reaction were studied, and ferrous and ferric iron were identified as the most promising candidates. Kwon et al. [Kwon2012] studied the breakdown of the model compound cellobiose using the Fenton reaction as an alternative to the acid hydrolysis. The authors found that the activation energy based on Arrhenius plots for the radical based conversion is only half of the activation energy found for acidic hydrolysis. They thus emphasize the potential of the Fenton process. Furthermore, Kwon et al. [Kwon2012] investigated the influence of temperature and hydrogen peroxide concentration on the conversion. Increasing each

enhances the reaction rate but lowers the selectivity. The selectivity was always limited to values below 30%: the oxidation of glucose to organic acids and aldehydes was observed. Next to the homogeneous Fenton reaction, radical generation by electrochemical means, e.g., the electro-Fenton process or anodically generated OH radicals, was also studied [Kwon2012; Wang2011; Yang2014; Meng2011]. Even though the anodic generation of radicals yields a high selectiviy at low conversions of cello-oligomers [Kwon2012; Meng2011], oxidation to low molecular weight compounds is also observed [Kwon2012]. From a reaction engineering point of view, the Fenton process has a significant advantage compared to the radicals generated at electrode surfaces: It provides radicals throughout the solution and will not be limited by mass transport limitations as strongly, especially when a degradation of cellulose dispersions is envisaged.

This chapter focuses on the degradation of cellobiose with OH-radicals using Fenton's chemistry. In order to assess the viability of the conversion of cellulose to glucose, the model substance cellobiose is chosen as a well defined substance, which will enable an assessment of influencing parameters on the maximum attainable selectivity and reaction rate. The process parameters pH value, hydrogen peroxide, iron, Na_2SO_4 and cellobiose concentration, as well as the presence of a chelator and dissolved oxygen will be evaluated. The results of this chapter lay the foundation for an integrated degradation and separation strategy of cellobiose, which will be presented in Chapter 7.

5.2. Experimental

Cellobiose solutions were obtained by dissolving the appropriate amount of cellobiose ($\geq$ 99%, Sigma-Aldrich), iron sulfate ($FeSO_4 \cdot 7\,H_2O$, $\geq$ 99%, Sigma-Aldrich), sodium sulfate (Na_2SO_4, $\geq$ 99%, Honeywell Fluka) and 2,3-dihydroxbenzoic acid (DHBA, 99%, Sigma-Aldrich) in deionized water. Before the addition of $FeSO_4$ to the solution, the

pH value was adjusted to 3 with sulfuric acid (H_2SO_4, 97%, Sigma-Aldrich). From the prepared stock solutions 10 mL were transferred to 15 mL reaction tubes (Falcon tubes). Each experimental run was performed in duplicate and the error bars in the diagrams represent the standard deviation. The reaction tubes were placed in a thermo-shaker (MHR 23, Ditabis AG), which was set to 25 °C and 700 rpm. To initiate the reaction, an appropriate amount of hydrogen peroxide was added. The hydrogen peroxide stock solution was obtained by diluting concentrated hydrogen peroxide (H_2O_2, $\geq$ 30%, Sigma-Aldrich) with deionized water. The hydrogen peroxide solutions were stabilizer-free and stored at 4 °C. For the experiments with vayring oxygen concentrations, the reaction tubes were gassed with nitrogen (N_2, 99.9992%, Air Products) or pure oxygen (O_2, 99.95%, Westfalengas). The dissolved oxygen concentration was measured via a FireSting optical sensor by Pyroscience. Samples were taken in regular intervals throughout the reaction. The samples were quenched 1:1 v/v with a 3% aqueous sodium sulfite (Na_2SO_3) solution, similar to Kwon et al. [Kwon2012]. Na_2SO_3 efficiently eliminates hydrogen peroxide from the reaction solution and stops the reaction. Liu et al. [Liu2007] found that a stoichiometric addition of Na_2SO_3 leaves significant residues of peroxide and recommend the addition of an excess of the former. In this study, Na_2SO_3 was always at least in 2-fold excess of the initially present H_2O_2. HPLC measurements showed that Na_2SO_3 did not influence the measurement of cellobiose or glucose. The quenching solutions were always freshly prepared, as Na_2SO_3 reacts with atmospheric oxygen. The calculation of the selectivity of cellobiose conversion towards glucose is based on the assumption that a maximum of two glucose molecules can be obtained when cellobiose is cleaved [Kwon2012].

5.2.1. Sugar Quantification

Cellobiose and glucose were analyzed via high-performance liquid chromatography (HPLC); the method parameters are listed in Table

5.1. Prior to analysis, each sample was quenched 1:1 v/v with 3 wt.-% Na_2SO_3 to eliminate excess H_2O_2 [Kwon2012]. Each sample was filtered with a 0.45 µm regenerated cellulose syringe filter.

Table 5.1.: HPLC parameters for cellobiose and glucose

Parameter	**Value**
System	Agilent Technologies, Series 1200
Column	Organic acid resin 300 mm x 8 mm and guard column
Eluent	5 mM H_2SO_4
Eluent flow rate	0.5 mL/min
Temperature column oven	40 °C
Temperature autosampler	20 °C
Temperature RID	40 °C
Wavelength VWD	210 nm

5.3. Results and Discussion

5.3.1. Influence of the Iron Concentration

In a first step, the influence of the ferrous iron (Fe^{2+}) concentration was evaluated. Based on the work of Kwon et al. [Kwon2012], a 10 mM cellobiose solution was chosen. Additionally, the pH value of the solution was adjusted to pH 3, because this is commonly regarded as the best value for the Fenton reaction [Pign2006; Bril2009]. At pH values above 3, iron precipitates [Pign2006]. Fenton's chemistry is described in detail in Chapter 2. The range of tested ferrous iron was 0.1 mM to 0.7 mM.

Figure 5.1 shows the conversion of cellobiose to glucose via Fenton's chemistry. The cellobiose concentration in Figure 5.1 a) has

two distinct characteristics: in the first seconds of the reaction, the concentration drops significantly and then continues to decrease more slowly. This trend is typical for Fenton reactions with Fe^{2+} [Pign2006]. The first and second phase of the reaction are more pronounced, the higher the iron concentration is. The same characteristics can be observed in Figure 5.1 b) for the glucose concentration. In contrast to Kwon et al. [Kwon2012] a significant conversion can be observed after a few minutes of reaction time. Kwon et al. [Kwon2012] used a concentration of 2 mM ferrous iron, which is significantly higher than the one used in this study. At increased iron concentrations, scavenging reactions increase, as described in Chaper 2, eq 2.19). However, this is most likely not the main reason for the observed differences. Rather, the high pH value employed by Kwon et al. [Kwon2012] led to precipitation of iron. Usually, the use of very low amounts of iron is preferred, because high concentrations lead to increased ferric oxyhydroxide production [Pign2006]. Additionally, high iron concentrations showed adverse effects in the depolymerization of cellulose and lignocellulose [Hall1965; Bhan2015].

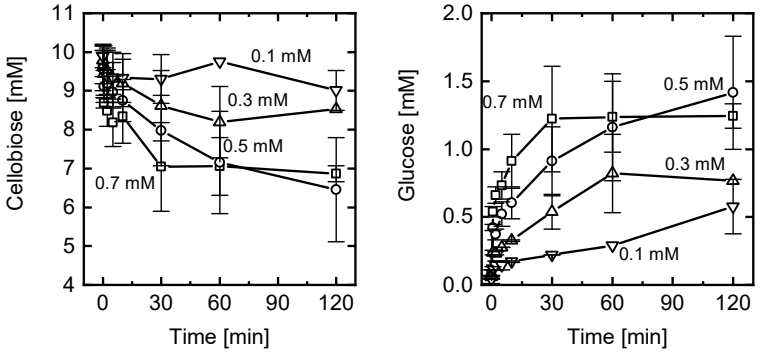

(a) Cellobiose concentration with increasing reaction time.

(b) Glucose concentration with increasing reaction time.

Figure 5.1.: Conversion of cellobiose to glucose via the Fenton's reagent with different concentrations of ferrous iron. The experimental conditions were: 10 mM cellobiose, 50 mM Na_2SO_4, pH 3.

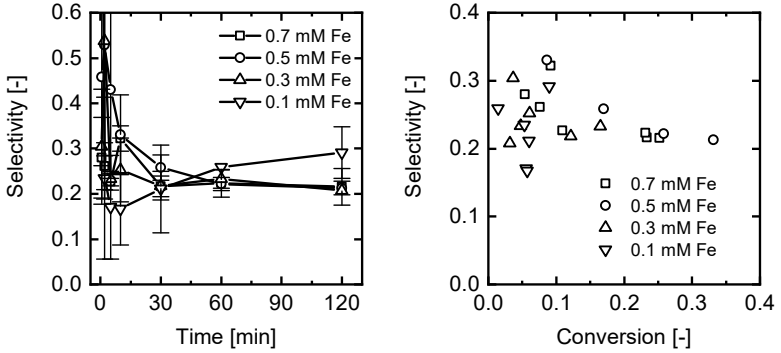

(a) Selectivity towards glucose with increasing reaction time.

(b) Selectivity towards glucose plotted in dependence of cellobiose conversion.

Figure 5.2.: Selectivity of cellobiose towards glucose via the Fenton's reagent with different concentraitons of ferrous iron. The experimental conditions were: 10 mM cellobiose, 50 mM Na_2SO_4, pH 3.

The main interest of this chapter is the conversion of cellobiose to glucose. Figure 5.2 a) shows the selectivity of the reaction towards glucose. Generally, the selectivity towards glucose decreases with increasing reaction time and is limited to values below approximately 30%. Even though there are a few data points above 30%, these have to be interpreted with care, because at very early stages of the reaction, the rate is very high and glucose concentrations are very low. This leads to some uncertainty.

Kwon et al. [Kwon2012] report the oxidation of glucose to organic acids and aldehydes, which applies to this study as well and explains the decreasing glucose selectivity with increasing reaction time. If the selectivity is plotted in dependence of the conversion, Figure 5.2 b), it is clear that the selectivity mainly depends on the conversion of cellobiose, and thus the ratio of cellobiose to glucose. As the OH radicals are an unselective species [Pign2006], it is hypothesized that a main key to steer the selectivity is the cellobiose to glucose ratio. This hypothesis is tested in Chapter 7. In the next sections an iron

concentration of 0.5 mM will be used.

In terms of the maximum of the achievable glucose selectivity, the findings in this section are supported by Kwon et al. [Kwon2012], who report a selectivity below 30% for all tested parameters. Additionally, von Sonntag et al. [Sonn1976] report that only about 1/3 of the glycosidic bonds of cellobiose are attacked by OH radical generated by radiolysis of N_2O. As the two studies from above employ different reaction conditions compared to this study, the next sections will report additional efforts in an attempt to increase the selectivity above 30%.

5.3.2. Influence of the Cellobiose Concentration

The reaction rate of degradation via OH radicals is dependent on the concentration of substrate as described in Chapter 2. Thus, it is expected that an increased cellobiose concentration will lead to an increased reaction rate for cellobiose degradation and thus a higher selectivity for glucose. Figure 5.3 a) shows the cellobiose conversion for systems with 10, 50 and 100 mM of initial cellobiose concentration. The last data point of the series for 10 mM cellobiose shows a lower cellobiose conversion than at the data point before. This is a surprising behavior, which can only be explained by a measurement error. As expected from theory, the highest cellobiose conversion is achieved in the case of the highest cellobiose concentration. Accordingly, most glucose is formed at the highest initial cellobiose concentration, see Figure 5.3 b). It can be expected that a high cellobiose concentration leads to a high selectivity, because less OH radicals are scavenged by glucose. However, the selectivity, which is plotted in Figure 5.4, does not show a clear trend. Nonetheless, the selectivity is always below 30%, independet of the cellobiose concentration. In Chapter 7 additional data and modeling results will be presented, which support the hypothesis of an increased selectivity for high cellobiose to glucose ratios.

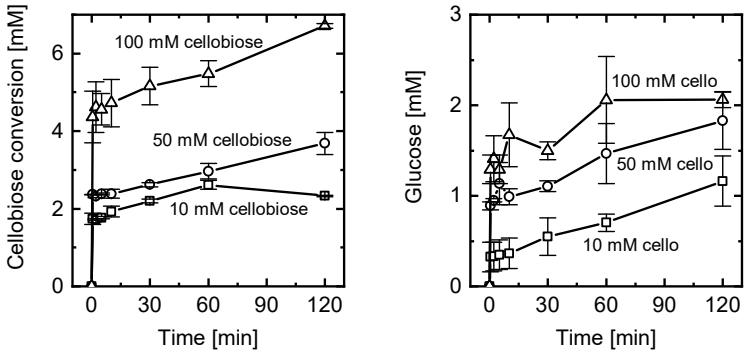

(a) Cellobiose conversion with increasing reaction time.

(b) Glucose concentration with increasing reaction time.

Figure 5.3.: Conversion of cellobiose to glucose via the Fenton's reagent with different initial cellobiose concentrations. The experimental conditions were: 10 mM H_2O_2, 0.5 mM $FeSO_4$, 50 mM Na_2SO_4, pH 3.

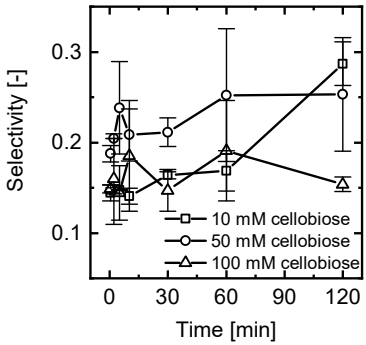

Figure 5.4.: Selectivity of cellobiose towards glucose via the Fenton's reagent with different initial cellobiose concentrations. The experimental conditions were: 10 mM H_2O_2, 0.5 mM $FeSO_4$, 50 mM Na_2SO_4, pH 3.

5.3.3. Influence of the Hydrogen Peroxide Concentration

Figure 5.5 shows the influence of an increasing H_2O_2 concentration on cellobiose conversion and glucose formation. In general, a higher concentration leads to an increased conversion of cellobiose and also an increased formation of glucose. However, the selectivity towards glucose is not influenced by a variation in H_2O_2, see Figure 5.6. Kwon et al. [Kwon2012] state that an increasing H_2O_2 concentration leads to a decreased selectivity. However, it seems likely that not the H_2O_2 concentration, but the cellobiose to glucose ratio determines the selectivity as stated in Section 5.3.1. Thus, Figure 5.6 does not show a strong correlation of selectivity and H_2O_2 concentration, because the cellobiose to glucose ratio is high in all cases (≥ 7). As will be shown in Chapter 7, the selectivity starts to drop sharply below a cellobiose to glucose ratio of five. Even though the exact value will not be the same for the Fenton and electro-Fenton process, it is reasonable to assume that the mechanism is similar for the electro-Fenton and Fenton process. Some studies in literature report a decreasing degradation rate, if the peroxide concentration is too high [Aran2006; Derb2004; Torr2003]. H_2O_2 reacts with OH radicals, and especially at high H_2O_2 concentrations this reaction becomes more pronounced, see eq 2.20 [Derb2004; Torr2003]. Also, if all iron is present in the ferric species and the reduction to ferrous iron is limiting, an increase in H_2O_2 concentration may not show a linear effect on the degradation of the target compound [Aran2006]. For this work, the limiting H_2O_2 value has not been reached and an additional increase is still viable.

5.3.4. Influence of Sodium Sulfate

Na_2SO_4 was added to the reaction solutions in order to facilitate a comparison between the Fenton (Chapter 5) and electro-Fenton (Chapter 7) experiments. Because the electro-Fenton process is ultimately envisaged, a supporting electrolyte such as Na_2SO_4 has to be

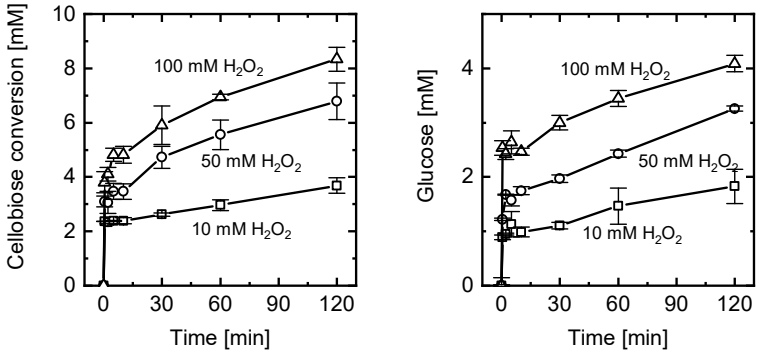

(a) Cellobiose conversion over time. **(b)** Glucose concentration over time.

Figure 5.5.: Conversion of cellobiose to glucose via the Fenton's reagent with different initial H_2O_2 concentrations. The experimental conditions were: 50 mM cellobiose, 0.5 mM $FeSO_4$, 50 mM Na_2SO_4, pH 3.

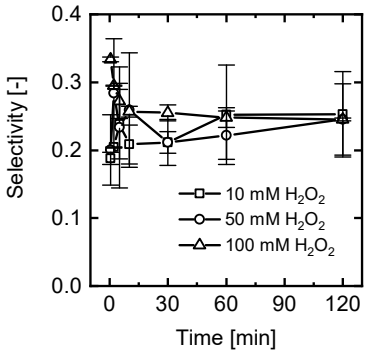

Figure 5.6.: Selectivity of cellobiose towards glucose via the Fenton's reagent with different initial H_2O_2 concentrations. The experimental conditions were: 50 mM cellobiose, 0.5 mM $FeSO_4$, 50 mM Na_2SO_4, pH 3.

added to the solution to ensure a sufficient conductivity. Thus, it is worthwhile to investigate the influence of Na_2SO_4 on the process. It is known that sulfate influences the Fenton reaction and may act as radical scavenger and complexing agent for iron [Pign2006; De L2005; Laat2004; Truo2004]. Whereas the decomposition of H_2O_2 by ferric iron (Fe^{3+}) is diminished when sulfate ions are present [De L2005], it is enhanced for ferrous iron (Fe^{2+}) [Laat2004]. Two different sets of experiments were performed: First, 50 mM cellobiose was degraded upon addition of 10 mM H_2O_2. In another experiment, the H_2O_2 concentration was increased to 100 mM. In both cases, the experiments were performed with and without the addition of 50 mM Na_2SO_4.

Figures 5.7 and 5.8 show the cellobiose conversion, glucose formation, and selectivity towards glucose for the reactions where 10 mM H_2O_2 was added. The conversion of cellobiose and formation of glucose are both enhanced when Na_2SO_4 is absent. This observation fits to the theory of a diminished radical generation when Na_2SO_4 is present. The selectivity, however, is not affected by Na_2SO_4. Figure 5.8 shows that similar to the observations in the other sections the selectivity is limited to values below 30%.

In the experiment with a high H_2O_2 concentration of 100 mM, the reaction is faster with sulfate, see Figure 5.9. Even though this does not fit to theories described in literature [De L2005; Laat2004; Truo2004], this chapter employs different experimental conditions than the cited studies. The reason for the difference to literature is unknown. Nonetheless, the main figure of merit of this work, the selectivity, remains unchanged: initially, the selectivity of the reaction is high, and declines with decreasing cellobiose concentration. The selectivity is limited to values $< 30\%$ (Figure 5.10).

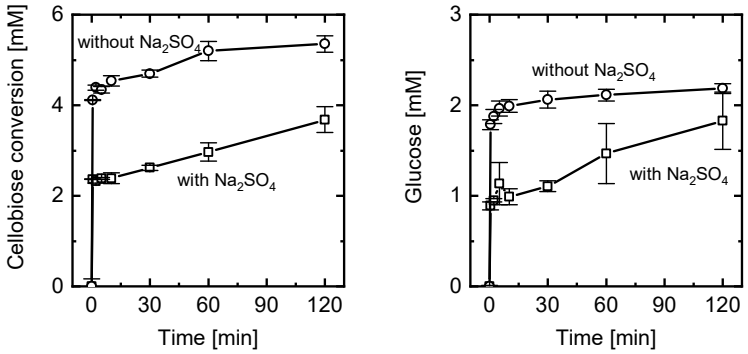

(a) Cellobiose conversion with increasing reaction time.

(b) Glucose concentration with increasing reaction time.

Figure 5.7.: Conversion of cellobiose to glucose via the Fenton's reagent with and without 50 mM $NaSO_4$ in the solution. The experimental conditions were: 50 mM cellobiose, 10 mM H_2O_2, pH 3.

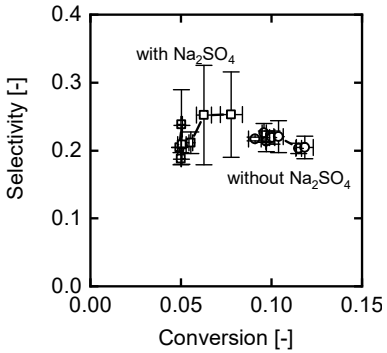

Figure 5.8.: Selectivity of cellobiose towards glucose via the Fenton's reagent with and without 50 mM $NaSO_4$ in the solution. The experimental conditions were: 50 mM cellobiose, 10 mM H_2O_2, pH 3.

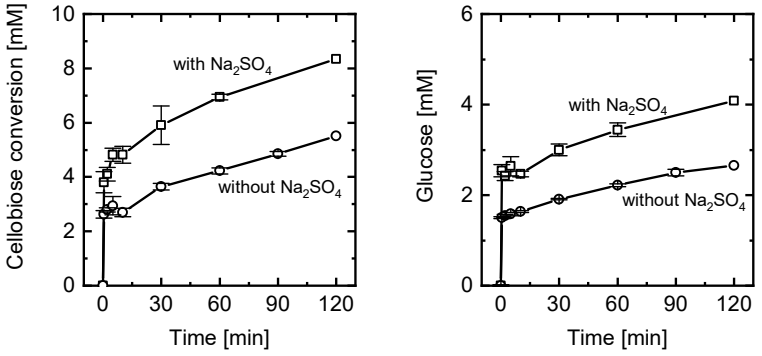

(a) Cellobiose conversion over time. **(b)** Glucose concentration over time.

Figure 5.9.: Conversion of cellobiose to glucose via the Fenton's reagent with and without 50 mM $NaSO_4$ in the solution. The experimental conditions were: 50 mM cellobiose, 100 mM H_2O_2, pH 3.

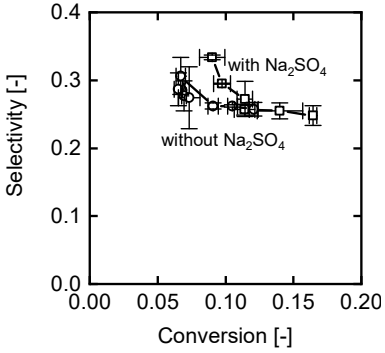

Figure 5.10.: Selectivity of cellobiose towards glucose via the Fenton's reagent with and without 50 mM $NaSO_4$ in the solution. The experimental conditions were: 50 mM cellobiose, 100 mM H_2O_2, pH 3.

5.3.5. Influence of the Chelator 2,3-Dihydroxybenzoic Acid

(Bio-)chelators play a decisive role in the degradation of cellulosic substances in nature. The chelators are able to reduce ferric iron to ferrous iron and increase the rate of reaction [Xu2001; Aran2006]. Additionally, chelators can decrease the amount of adsorbed ferric iron on cellulose [Xu2001]. In this section, the use of 2,3-dihydroxybenzoic acid (DHBA) was tested as chelator. Two concentrations of chelator were tested, which gave a ratio of iron:chelator of either 25:1 or 2.5:1. The chelator concentration should not be too low, as it will not have a measurable contribution in this case. If it is too high, the chelator scavanges radicals [Xu2001].

Figures 5.11 and 5.12 show the cellobiose conversion, glucose concentration as well as the selectivity. Indeed, at the low concentration of DHBA the difference to a system without DHBA is not pronounced. However, if the DHBA concentration is increased to 0.2 mM, the conversion of cellobiose and formation of glucose is accelerated. Overall, the chelator to decreases the selectivity towards glucose to even smaller values, see 5.12.

5.3.6. Influence of Dissolved Oxygen

Oxygen generally acts in two ways in Fenton reactions: it can be a supplemental oxidant and it leads to an accelerated degradation [Pign2006]. Oxygen can react with organic radicals, which are formed during the reaction [Pign2006]. Wang et al. [Wang2011] and Meng et al. [Meng2011] proposed a reaction scheme for the depolymerization of cellulose via Fenton's chemistry, in which oxygen has a central role. However, Kwon et al. [Kwon2012], who studied the cellobiose degradation in an oxygen free environment, reported the degradation of the model compound to glucose. In this chapter, the influence of dissolved oxygen on the degradation of cellobiose to glucose is

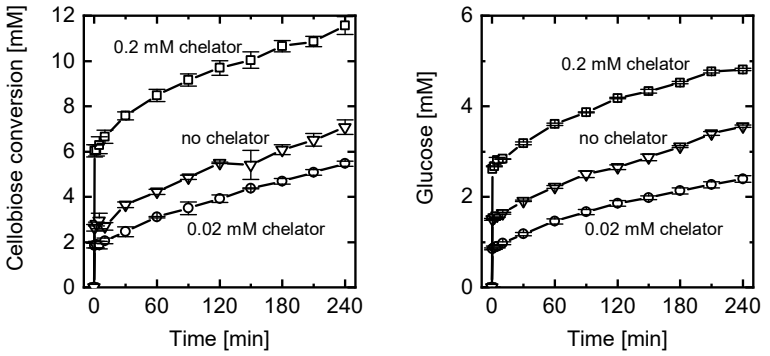

(a) Cellobiose conversion with increasing reaction time.

(b) Glucose concentration with increasing reaction time.

Figure 5.11.: Conversion of cellobiose to glucose via the Fenton's reagent with and without the chelator 2,3-DHBA. The experimental conditions were: 50 mM cellobiose, 100 mM H_2O_2, pH 3.

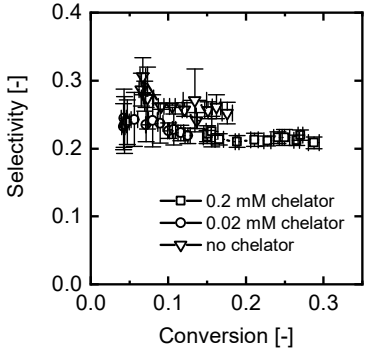

Figure 5.12.: Selectivity of cellobiose towards glucose via the Fenton's reagent with and without the chelator 2,3-DHBA. The experimental conditions were: 50 mM cellobiose, 100 mM H_2O_2, pH 3.

studied. Therefore, the reaction solution is gassed with pure O_2 before the reaction is initiated to increase the O_2 concentration to approximately $30\,\mathrm{mg\,L^{-1}}$, and also degassed with N_2, to decrease the oxygen concentration to values $\leq 1\,\mathrm{mg\,L^{-1}}$. Figure 5.13 shows the conversion of cellobiose and the formation of glucose with varying O_2 concentrations. If the O_2 concentration is $\leq 1\,\mathrm{mg\,L^{-1}}$, the reaction rate is enhanced. The difference between $8\,\mathrm{mg\,L^{-1}}$ and $30\,\mathrm{mg\,L^{-1}}$ is barely detectable. The selectivity, again, is not affected by the oxygen concentration, see Figure 5.14. Thus, oxygen may indeed protect the glycosidic bond as proposed by Schuchmann and von Sonntag [Schu1978]. However, this section shows that mainly the reaction rate is decreased. The selectivity remains almost unaffected; a small decrease can be detected in the case of $30\,\mathrm{mg\,L^{-1}}$ O_2.

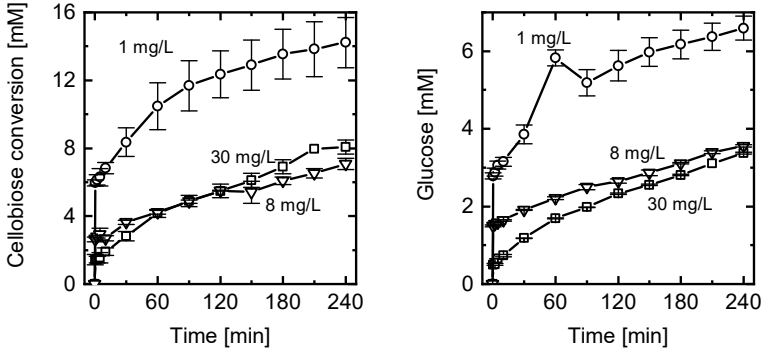

(a) Cellobiose conversion with increasing reaction time.

(b) Glucose concentration with increasing reaction time.

Figure 5.13.: Conversion of cellobiose to glucose via the Fenton's reagent in dependence of the disolved oxygen concentration. The experimental conditions were: 50 mM cellobiose, 100 mM H_2O_2, pH 3.

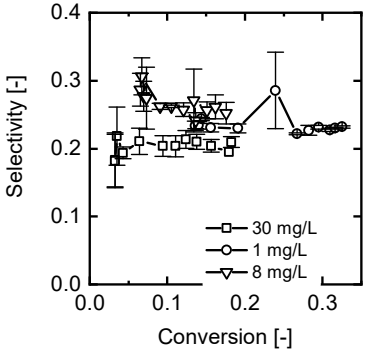

Figure 5.14.: Selectivity of cellobiose towards glucose via the Fenton's reagent in dependence of the disolved oxygen concentration. The experimental conditions were: 50 mM cellobiose, 100 mM H_2O_2, pH 3.

5.4. Conclusion and Outlook

The chapter presented the influence of different process conditions on the conversion and selectivity of cellobiose to glucose using Fenton's chemistry. Overall, the selectivity was always limited to values below 30%. This finding is supported by other studies that investigated the radical-facilitated conversion of cellobiose, but employed different reaction conditions and radical sources [Kwon2012; Sonn1976]. A high concentration of dissolved oxygen and the chelator 2,3-dihydroxybenzoic acid decreased the selectivity even further. The presented data show that the decrease of selectivity towards glucose with increasing reaction time is connected to the decreasing cellobiose to glucose ratio. As cellobiose is consumed and glucose produced, glucose scavenges radicals and is oxidized to low molecular weight acids and aldehydes. A high cellobiose, H_2O_2, and Fe^{2+} concentration and a low dissolved O_2 concentration increased the reaction rate. The OH radical based depolymerization of cellobiose is thus strongly limited in terms of selectivity and does not seem to be a viable alternative to the enzymatic hydrolysis.

In Chapter 7 the electro-Fenton will be tested for the conversion of cellobiose to glucose. Studies on the anodic conversion of cellobiose to glucose with radicals suggest a positive effect of electrode-substrate interactions, which may also be relevant in the electro-Fenton. Additionally, an in-situ separation can help to retain the selectivity at high values throughout the reaction time. Overall, future work should focus on the pretreatment of lignocellulose via Fenton's chemistry, which may then aid a subsequent enzymatic hydrolysis [Jeon2016].

Acknowledgements Indra Marth is acknowledged for her experimental support.

6. Electro-Fenton Reactors: Electrochemical Hydrogen Peroxide Synthesis

Parts of this chapter have been published as:
Robert G. Keller, Julia Weyand, Jan-Bernd Vennekötter, Johannes Kamp, Matthias Wessling *An electro-Fenton process coupled with nanofiltration for enhanced conversion of cellobiose to glucose*,
Catalysis Today, 2021
DOI: 10.1016/j.cattod.2020.05.059

6.1. Introduction

In light of the advent of renewable electricity, the electrochemical hydrogen peroxide (H_2O_2) synthesis is a promising technology for the substitution of the state of the art production process, the *anthraquinone process* [Perr2019; Camp2006]. In addition, the emerging *Advanced Oxidation Processes*, such as the electro-Fenton, rely on on-site electrochemical H_2O_2 synthesis [Pign2006; Bril2009]. The on-site generation of the oxidant not only saves costs for transport and circumvents the storage of hazardous H_2O_2 solutions, but also enhances the slow reduction of ferric iron to ferrous iron of the Fenton process [Bril2009]. Chapter 2.2.3 elucidates the vivid history of electrochemical H_2O_2 generation from its origins via the electrolysis of sulfuric acid in 1853 [Meid1853] towards the first direct cathodic reduction of oxygen in 1882 [Trau1882] and the development of the Dow-Huron trickle bed reactor [McIn1984; McIn1985; Foll1995]. Even though the history of the electrochemical H_2O_2 synthesis is more than a century old, the technology remains a niche application with many challenges.

The development of modern ion exchange membranes, advanced catalysts, and novel reactor concepts promotes an increasing interest in the electrochemical H_2O_2 synthesis as well as the electrification of the chemical industry via renewable energy [Xia2019; Kim2018; Mudd2020; Camp2006; Verd2014; Perr2019]. In this regard, the homogeneous electro-Fenton described in Chapter 2.2.4 presents a special case: many of the state of the art high performance reactors for H_2O_2 generation rely on a caustic electrolyte, which promotes the catalytic activity and ensures a high conductivitiy of the electrolyte [Mudd2020; Yeag1984; Tara1983]. However, the homogeneous electro-Fenton process should be operated at a pH value of 3 [Pign2006; Bril2009]. Neither caustic electrolytes are feasible due to too high pH values, nor a classical MEA approach is promising due to the very acidic surface of cation exchange membranes that promotes H_2 generation [Venn2019a]. In this chapter, a planar reactor is investigated and developed with

a focus on the application in the electro-Fenton catalyzed cellobiose degradation in Chapter 7. The reactor is characterized at different operating parameters and conditions such as current density (CD), type of catalyst, liquid and gas flow, and the choice of spacer for the catholyte channel. Additionally, a tubular reactor was designed with a carbon-nanotube-based gas diffusion electrodes (GDE) inspired by the work of Gendel et al. [Gend2014a; Gend2014b]. As discussed in Chapter 2, tubular reactors offer advantages over their planar counterpart. The tubular electrodes were modified with different catalysts, but also the polymeric binder PTFE to promote the formation of H_2O_2. An all tubular reactor comprising a tubular cation exchange membrane is introduced.

6.2. Planar Electrodes

In this section, a planar plate and frame reactor is developed and characterized for H_2O_2 electrosynthesis. In Chapter 7, this reactor will be used to depolymerize cellobiose towards glucose via the electro-Fenton process.

6.2.1. Experimental

All error bars reported in this section represent the standard deviation of experiments which were conducted at least in duplicate.

Electrochemical Reactor

An electrochemical plate and frame reactor was fabricated in house. The reactor is sketched in Figure 6.1 and consisted of three compartments: 1) a gas supply compartment for oxygen supply to the cathode 2) a catholyte compartment for the H_2O_2 synthesis, and

3) an anolyte compartment for the oxygen evolution reaction. Similar reactors are frequently employed in electrochemical processes with gas diffusion electrodes [Venn2019a; Liu2019]. The catholyte and anolyte were separated by a cation exchange membrane (CEM, Fumapem F-14100, Fumatech). A carbon paper was used as the gas diffusion electrode on the cathode side (QuinTech Fuel Cell Technology, Freudenberg, H2315 I2C6), and an iridium-coated titanium felt (Bekaert ST/Ti/20/150/85) was used as the anode. The geometrical area of both electrodes was 24 cm^2. The anode was operated in a zero-

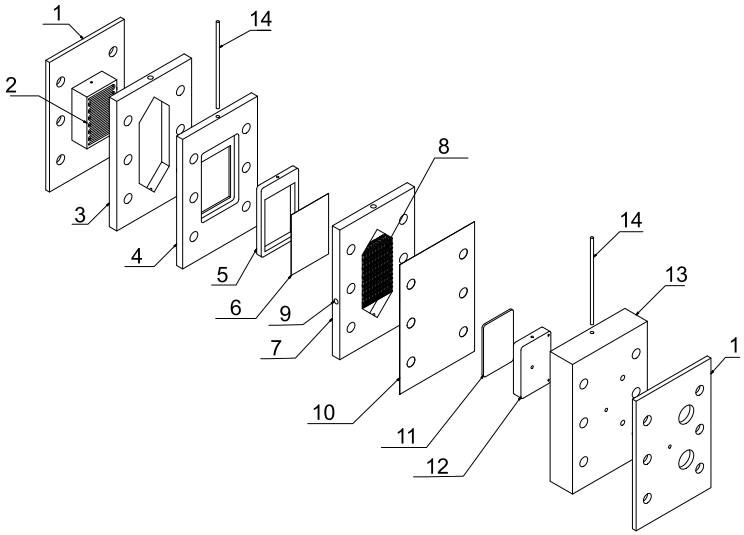

Figure 6.1.: The electrochemical cell without gaskets. 1) reinforcement plates 2) gas distributor 3) levelling layer 4) cathode holder 5) GDE current collector 6) GDE 7) catholyte compartment 8) separator 9) RE connection 10) CEM 11) iridium felt on titanium sinter plate 12) anode current collector with anolyte distributor 13) anode holder 14) power connections

gap assembly: the iridium-coated titanium felt was pressed against the cation exchange membrane with a titanium sinter plate (GKN T10 filter metal) on a self-made titanium current collector featuring a meandering flow path. On the cathode side, a catholyte compartment separated the cathode and the membrane. The catholyte compart-

ment was 10 mm wide and either a static mixer or a mere separator was installed, see Figure 6.3.

Oxygen (O_2, 99.95% Westfalen) was fed to the GDE via a flow meter (Wagner Mess- und Regeltechnik, WAKS-SV(E)S) either in dead-end or cross-flow mode. In the dead-end mode, the gas compartment was sealed on the outlet, forcing the gas through the GDE. In the cross-flow mode the outlet of the gas compartment was open to ambient conditions. In this case, oxygen supply towards the GDE was exclusively via diffusion. In some experiments, the catalyst 2-ethylanthraquinone (EAQ, $\geq$ 97%, Sigma Aldrich) was sprayed onto the GDE. For the application of the catalyst onto the carbon paper, first 7.2 mg (0.3 mg/cm^2 with a GDE surface of 24 cm^2) of EAQ were added to 3 ml of ethanol and then placed in an ultrasonic bath for 15 minutes in order to obtain a well-mixed dispersion. Subsequently, the carbon paper was mounted onto the heated vacuum table and a template shield was used to define the area where the catalyst was applied. The EAQ dispersion was sprayed onto the GDE via an air brush pistol (Harder & Steenbeck Airbrush, Evolution), which was operated with nitrogen. Due to the heated vacuum table, the ethanol evaporated quickly, leaving a uniform layer of EAQ on the GDE. After the spraying process, the GDE was left on the vacuum table until it cooled down to room temperature. As catholyte, a 100 mM sodium sulfate supporting electrolyte (Na_2SO_4, $>$ 99%, Honeywell Fluka) was prepared. The pH was adjusted to 3 with sulfuric acid (H_2SO_4, 98%, Carl-Roth). The catholyte volume was either 80 or 100 mL. The anolyte volume was 60 mL deionized water adjusted to pH 2.5 with H_2SO_4. Anolyte and catholyte were recirculated at 40 mL min^{-1} with a peristaltic pump (Cole-Parmer, ISM831C). A Knick Portamess 911 with a pH probe (SE 102N) was used to monitor pH changes in the catholyte. A process sketch is depicted in Figure 6.2.

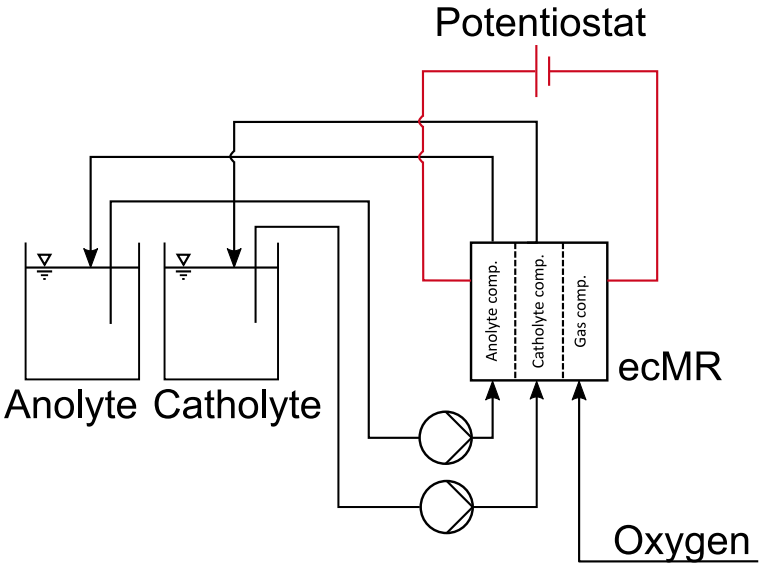

Figure 6.2.: A sketch of the process for hydrogen peroxide synthesis with the electrochemical membrane reactor (ecMR)

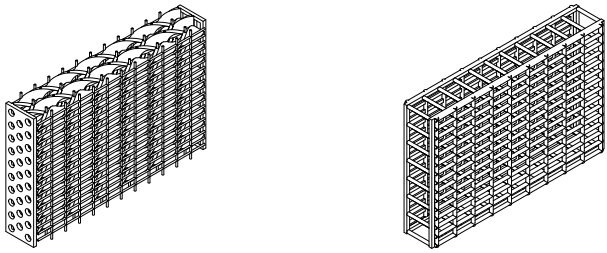

(a) 3D printed static mixer installed between cathode and membrane.

(b) 3D printed spacer installed between cathode and membrane.

Figure 6.3.: Different separators installed in the catholyte flow channel between cathode and membrane.

Electrochemical Methods

A PGSTAT302N from Metrohm was used for all electrochemical experiments. As reference electrodes, a home-made Ag/AgCl in 3 M KCl reference electrodes (more details in Section A.1) and a Hg/Hg_2SO_4 in 0.5 M H_2SO_4 (Meinsberg) were used. The reference electrodes were directly connected to the catholyte compartment via a small hole in the cell structure. All potentials are reported as Volt vs. Standard Hydrogen Electrode (SHE). Prior to and after each experiment, cyclic voltammetry (CV) measurements (−0.35 V to 1.5 V vs. SHE or −1.3 V to 1.7 V vs. SHE) were performed as pre- and post-treatment to activate and clean the GDE.

Constant potential experiments were used for the H_2O_2 synthesis. A constant potential of −0.8 V, −1.2 V, −2 V or −3 V vs. SHE was applied. The stoichiometric oxygen excess factor λ is calculated with the average current density (CD) of each experiment and the assumption of a current efficiency (CE) of 100%. The calculation of λ is explained in detail in Chapter 2. Polarization plots were obtained from multiple constant potential experiments. Each potential was held for 300 s. The final current was taken as steady state current. Electrochemical impedance spectroscopy (EIS) was performed in a two-point (impedance between working electrode and counter electrode) and three-point (impedance between reference electrode and working electrode) set-up to determine the resistance of the cell and of the catholyte channel. EIS measurements were conducted in galvanostatic mode with 1 mA amplitude from 10 kHz to 10 Hz.

Hydrogen Peroxide Quantification

The H_2O_2 concentration was determined with a method proposed by Nogueira et al. [Nogu2005] using UV-Vis spectroscopy. The method is based on the reaction of metavanadate anions and H_2O_2 to peroxovanadium cations, which can be detected at a wavelength of 450

nm. The solution was stored at 4 °C. The UV-Vis measurements were performed with a Genesys 10S UV-Vis spectrophotometer (Thermo Fisher Scientific). Each time a new metavanadate stock solution was produced, a new calibration curve was determined. Calibration curves were obtained with H_2O_2 from Sigma-Aldrich ($\geq$ 30%). With the help of the measured H_2O_2 concentrations, the CE was calculated. The CE was calculated using eq 2.7.

6.2.2. Results and Discussion

Influence of the Electrode Potential

The electrochemical membrane reactor (ecMR) depicted in Figure 6.2 was characterized for its ability to reduce O_2 to H_2O_2. In a first series of experiments, 20 mL/min oxygen was fed to the GDE in dead-end mode to ensure a sufficient reactant supply for the H_2O_2 synthesis. The static mixer was installed in the catholyte compartment. Four different potentials were investigated, namely -0.8, -1.2, -2, and -3 V vs. SHE. As expected, the carbon based gas diffusion electrode produces H_2O_2: the more negative the potential, the higher the amount of produced H_2O_2 due to the increased driving force and reaction rate, see Figure 6.4 a) [Reis2012; Li2016]. The GDE enables high current densities due to an efficient oxygen supply to the catalytically active sites. The CE was approximately 80%, even at a high potential of -3 V vs. SHE (-0.4 vs. SHE IR-drop corrected), which corresponds to 27 mA cm^{-2}. Throughout the experimental time for 90 min, no significant decrease in performance could be observed. The pH value of the catholyte usually increased slightly from 3 to about 3.4 in the early stages of the reaction and then decreased to values slightly below 3. It is not clear, why the pH increases at the beginning of the experiment. Even though protons are consumed at the GDE to form H_2O_2, these protons migrate through the CEM from the anolyte to close the charge balance. Since H_2O_2 is only a weak acid with a pK_a of about 11, it should not influence the pH value to a large extent. The decrease in pH

value can be explained from the cross-over of H_2SO_4 from the anolyte, which has been reported in literature [Venn2019b]. The observed high selectivity relies on different factors: the selective catalyst, sufficient reactant supply, and the cation exchange membrane, which separates the catholyte from the anolyte. Unwanted cross-over of peroxide to the anode can be prevented with a ion exchange membrane [Schm2012, pp. 286–292][Bril2009; Mudd2020], and thus, the CE remains high throughout an experiment. The importance of sufficient O_2 supply will be highlighted in the next sections.

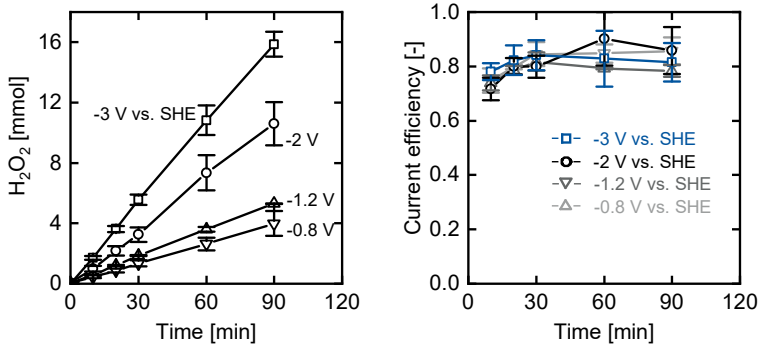

(a) Electrochemical H_2O_2 production with increasing reaction time.

(b) Current efficiency with increasing reaction time

Figure 6.4.: Electrochemical H_2O_2 synthesis at -0.8, -1.2, -2, and -3 V vs. SHE, 100 mM Na_2SO_4 at 40 mL/min, pH 3, 20 mL/min O_2 in dead-end mode.

Influence of the Gas Flow Mode

In the last section, the synthesis of H_2O_2 was performed with O_2 supply in dead-end mode, and high current efficiencies were obtained across a wide potential range, see Fig. 6.4 a). If the gas-supply is switched to cross-flow mode, see Figure 6.5 a) and b), high current

efficiencies are only obtained for low potentials, i.e., low current densities. Accordingly, for higher current densities (high potentials), the performance of the cross-flow mode drops, and the CE for H_2O_2 falls below 50% and 10% for -2 V and -3 V vs. SHE, respectively. Apparently oxygen is not sufficiently supplied to the GDE at high current densities, or more precisely, to the three phase boundary. Duarte et al. [Duar2019] have made similar observations for CO_2 reduction. In general, the cross-flow mode may be improved by adjusting differential pressure between gas and liquid phase across the GDE [De M2019; Duar2019; Jean2018; Mudd2020].

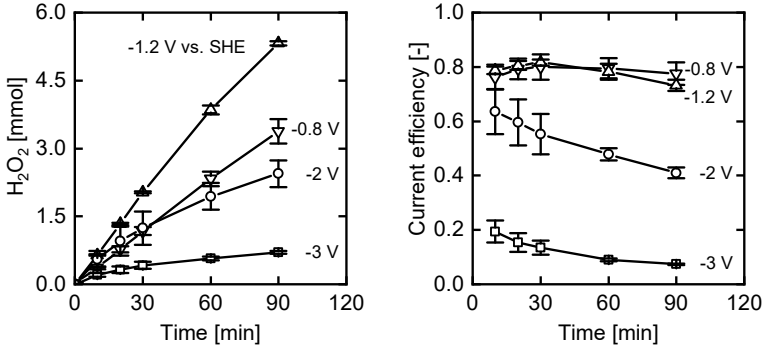

(a) Electrochemical H_2O_2 production with increasing reaction time.

(b) Current efficiency with increasing reaction time.

Figure 6.5.: Electrochemical H_2O_2 synthesis at -0.8, -1.2, -2, and -3 V vs. SHE, 100 mM Na_2SO_4 at 40 mL/min, pH 3, 20 mL/min O_2 in cross-flow mode.

6

Influence of the Catholyte Channel Separator

In order to achieve a well-mixed catholyte channel for the final application of the electrochemical membrane reactor, the depolymerization of cellulose, a static mixer was designed as separator, see Figure 6.3

a). The influence of the mixer on the performance of the reactor was compared to a mere separator, which was designed to create a defined gap between gas diffusion electrode and cation exchange membrane, see Figure 6.3 b). Figure 6.6 shows a polarization plot for the system with and without a static mixer. Apparently, the design without a mixer leads to a better performance, because about a two-fold increase in CD can be achieved. However, it has to be kept in mind that the performance should to be reevaluated for the electro-Fenton system with a cellulose slurry as substrate. A static mixer may be advantageous if slurries are used. Figure 6.7 a) shows that the two-fold increase in CD leads to a two-fold increase in the produced amount of H_2O_2. Thus, the reaction continues to run at high current efficiencies, as Figure 6.7 b) confirms. In contrast to the results for the static mixer (compare Fig. 6.4 b)), a more negative potential leads to a decreasing CE in the set-up with spacer. Apparently, the CD of about 68 mA/cm^2 at - 3 V vs. SHE for a design with spacer leads to mass transfer limitations. In order to elucidate the origin of the decreased CE, the influence of the gas supply and electrolyte flow rate will be analyzed in the coming sections. To analyze the increase in performance of the system with spacer, an electrochemical impedance spectroscopy was performed. As the mixer decreases the void fraction of the catholyte channel, it may lead to an increase in ionic resistance in the channel. The resistance of the electrochemical cell and of the catholyte channel were measured with electrochemical impedance spectroscopy measurements. The two-point EIS of the electrochemical cell shows a resistance (x-axis intercept) of about 5.9 Ω for the set-up with spacer and of about 10.6 Ω for the set-up with static mixer, as can be seen in Figure 6.8 a). Thus, the static mixer approximately doubles the resistance. Three-point measurements confirm this trend, where the impedance was measured between the reference electrode and gas diffusion electrode. Here, a resistance of 1.8 Ω for the set-up with spacer and a resistance of 4.5 Ω for the set-up with static mixer was obtained (see Figure 6.8 b)), which is even more than a two-fold increase. As the reference electrode was placed in the middle of the catholyte channel, the total resistance of the catholyte is 3.6 Ω and

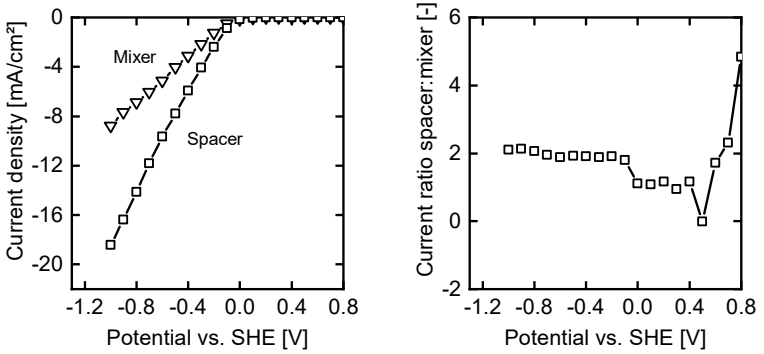

(a) Polarization plot of an ecMR with static mixer compared to an ecMR with spacer.

(b) Ratio of current density achieved in the ecMR with spacer compared to the set-up with static mixer.

Figure 6.6.: Electrochemical H_2O_2 synthesis for an ecMR with spacer or static mixer. The experimental conditions were: 100 mM Na_2SO_4 at 40 mL/min, pH 3, 20 mL/min O_2 in dead-end mode.

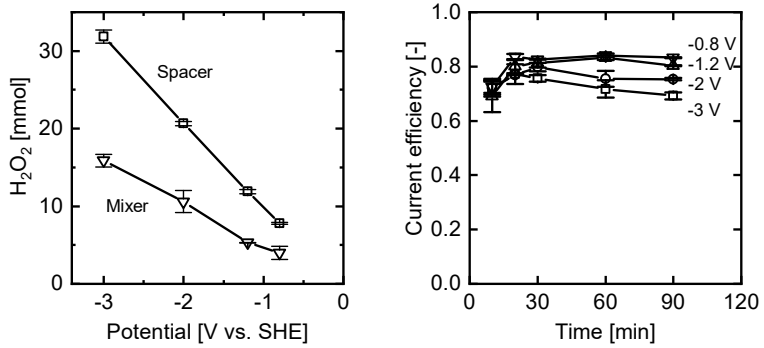

(a) Comparison between produced H_2O_2 with and without mixer after 90 min.

(b) Current efficiency of H_2O_2 synthesis at different potentials with increasing reaction time for the set-up with spacer.

Figure 6.7.: Electrochemical H_2O_2 synthesis for an ecMR with spacer or static mixer. The experimental conditions were: 100 mM Na_2SO_4 at 40 mL/min, pH 3, 20 mL/min O_2 in dead-end mode.

9 Ω, respectively. Thus, the catholyte channel represents the main resistance of the system: the low ionic strength and broad channel geometry lead to a high resistance.

The anolyte channel resistance was mitigated by design (zero-gap assembly) and the membrane has a fixed resistance of about 0.053 Ω [Venn2019a]. The impedance results confirm the results of the polarization plot and H_2O_2 measurements. Apparently, the mixer does not bring a benefit of enhanced mass transfer, but increases the catholyte resistance due to added tortuosity and decreased void fraction.

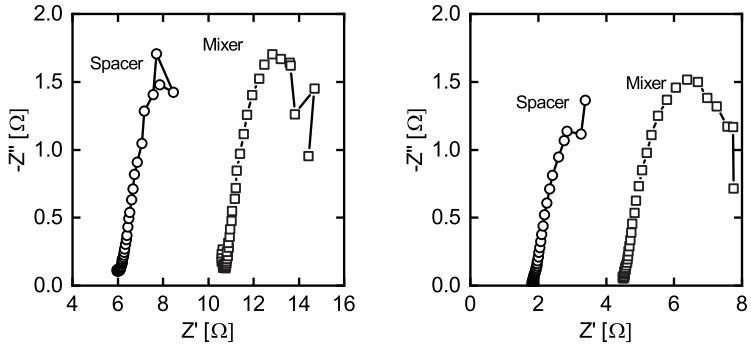

(a) 2-point impedance spectroscopy of the ecMR.

(b) 3-point impedance spectroscopy of the ecMR.

Figure 6.8.: Electrochemical impedance spectroscopy. The experimental conditions were: 10 kHz - 10 Hz, 1 mA amplitude, 100 mM Na_2SO_4 at 40 mL/min, pH 3, 20 mL/min O_2 in dead-end mode.

Influence of the Gas Flow Rate

In the last section, it was shown that the CE decreases slightly when a spacer is implemented instead of a static mixer for potentials more negative than -2 V vs. SHE. Figure 6.9 a) shows the CE for different gas flow rates (dead-end mode), and different catholyte separators. For

most of the cases, the CE is between 75 - 80%. However, it decreases in the set-up with spacer for potentials more negative than -2 V vs. SHE. The decrease in CE is especially pronounced for 10 mL/min O_2 supply, where the CE drops to about 40%. This behavior can be explained by the insufficient supply of the GDE with O_2. In Figure 6.9 b) the CE is plotted over λ, the stoichiometric excess of O_2. If λ equals 1, just as much oxygen is supplied as is theoretically consumed at 100% CE. It is thus not surprising that the CE drops to 40% for - 3 V vs. SHE and 10 mL/min in the set-up with spacer. In this case, λ is 0.79, which means the maximum CE is intrinsically limited to 79% and severe mass transfer limitations are the consequence. Interestingly, an increase of gas supply from 20 mL/min to 40 mL/min does not lead to an increase CE, but a decrease. It is known, however, that to many gas bubbles in dead-end mode can obstruct the electrolyte channel and lead to process instabilities [Duar2019]. Above an stoichiometric excess of about 2, no significant improvement in CE was achieved for a flow rate of 10 or 20 $\mathrm{mL\,min^{-1}}$. These findings are supported by literature, where the stoichiometric excess was between 1.7 - 1.8 and an increase of λ did not lead to an enhancement of the CE [Foll1995; Mudd2020].

Influence of the Electrolyte Flow Rate

The flow rate of the liquid electrolyte can be important because it determines the boundary layer thickness and diffusion pathways of reactants and products. Figure 6.10 shows the influence of the catholyte flow rate on the achievable CD. Apparently, with the applied conditions, mass transport has a minor effect. Even though the highest current densities can be reached with 40 mL/min of electrolyte flow rate for the set-ups with spacer and static mixer, the differences between a flow rate of 10, 20, and 40 mL/min are small: The CD increases by 13% for the set-up with mixer when the flow rate is increased from 10 to 40 mL/min. For the set-up with spacer the increase is 5%. It may be that mass transport limitations are

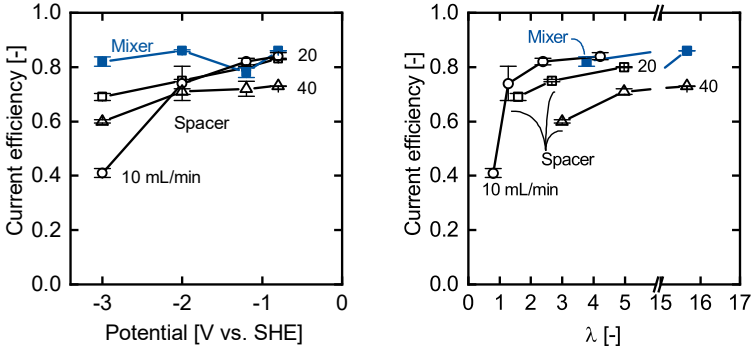

(a) Current efficiency after 90 minutes for different gas flow rates, separators and potentials.

(b) Current efficiency after 90 minutes for different gas flow rates, separators and stoichiometric O_2 excess.

Figure 6.9.: Influence of O_2 flow rate on the current efficiency. The experimental conditions were: 100 mM Na_2SO_4 at 40 mL/min, pH 3.

reached if even higher potentials are applied. A higher liquid flow rate rate could also lead to the observed incremental performance enhancement, because the gas bubbles are more efficiently removed from the liquid channel. Mass transport limitations are known to occur when transferring catalysts from lab scale tests on, e.g. rotating ring disk electrodes to flow reactors [Yang2018a]. In reactors, care must be taken when increasing the flow-rate in order to maintain the delicate pressure difference across the GDE [Li2016]. In this study it is clear that the gas side has the highest impact on the cell performance.

Influence of the Catalyst 2-Ethylanthraquinone

In order to increase the H_2O_2 production even more, the GDE was modified with the catalyst EAQ, as described in section 6.2.1. The results will be compared to the set-up with the standard GDE, the spacer, 40 mL/min electrolyte flow rate, and 20 mL/min gas flow rate

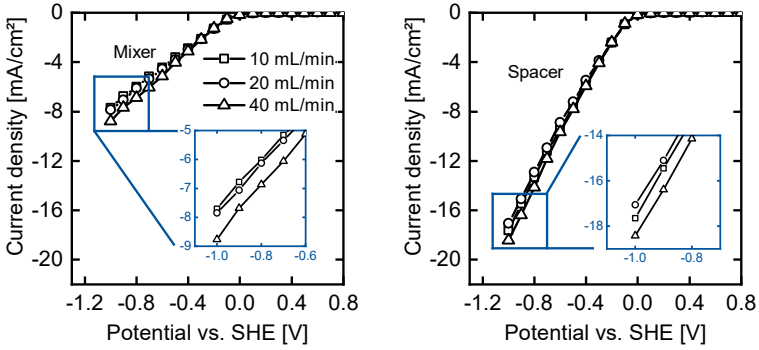

(a) Polarization plot for the set-up with static mixer.

(b) Polarization plot for the set-up with spacer.

Figure 6.10.: Polarization plots for different electrolyte flow rates and separators. The experimental conditions were: 100 mM Na_2SO_4 at 10, 20, 40 mL/min, pH 3, 20 mL/min O_2 in dead-end mode.

in dead-end configuration. Figure 6.11 a) shows a polarization plot indicating that the resulting current was notably lower for the modified GDE. Forti et al. [Fort2007] found that a certain on-set potential needs to be crossed for EAQ to be active. Additionally, it may be that the catalyst layer increased the resistance of the gas diffusion electrode. The H_2O_2 yield was slightly higher than with the plain GDE. A maximum production rate of 32.5 $\frac{\text{mg}}{\text{h cm}^2}$, compared to 30.1 $\frac{\text{mg}}{\text{h cm}^2}$ for the unmodified GDE. Additionally, the CE rose form 69.2% for the plain GDE to 76.1% EAQ-GDE. Overall, current efficiencies and maximum concentrations were higher for each potential that was tested. Thus, the use of EAQ as catalyst has a trade-off: the energy consumption is higher due to the higher potential, which is needed for electrolysis. On the other hand, more H_2O_2 is obtained at the same CD. Thus, a clear conclusion can only be drawn if the system is evaluated in a production process with a defined application.

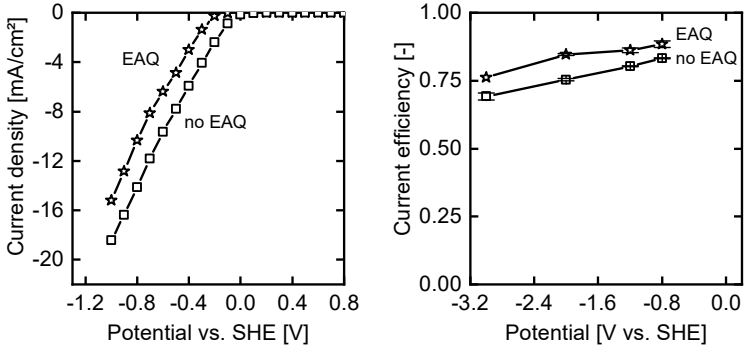

(a) Polarization plot for the set-up with and without EAQ catalyst.

(b) Current efficiency after 90 min over potential for a set-up with and without EAQ catalyst.

Figure 6.11.: Influence of the EAQ catalyst on the current density and current efficiency. The experimental conditions were: 100 mM Na_2SO_4 at 40 mL/min, pH 3, 20 mL/min O_2 in dead-end mode, spacer.

Summary

The planar electrochemical membrane reactor, which was described in this section, showed high current efficiencies of up to 70% even at a comparably high current density of 70 mA/cm^2. In general, the current efficiency remained high, as long as the excess of oxygen compared to the stoichiometrially needed oxygen was greater than 2. A dead-end mode gas supply was superior to the cross-flow mode, which did not supply sufficient O_2 to the gas diffusion electrode. If a slight overpressure relatively to the catholyte is applied to the gas compartment, an increase in performance can be expected [Jean2018]. The dead-end mode showed an optimum performance for the tested parameters at 20 mL/min. A lower flow rate led to mass transfer limitations, and a higher flow rate led to a decreased performance, which was attributed to gas bubbles in the catholyte compartment. The static mixer implemented in this work did not lead to a performance enhancement. On the contrary, the decreased catholyte channel poros-

ity and increased tortuosity led to an increase of catholyte resistance by a factor of two compared to the spacer. The electrolyte flow rate did not show a significant impact on the cell performance. In general, the Reynolds numbers, calculated for the empty channel, were low: for the highest flow rate tested, the Reynolds number was 30. As the channel length was small, one can expect a developing boundary layer. No mass transfer limitations could be observed on the liquid side. As stated above, the reaction was limited by the supply of O_2. The catalyst EAQ led to an increase of current efficiency of about 5-10 percent points. However, lower current densities were achieved for EAQ. Thus, there is a trade-off between high current efficiency and high current density, which needs to be analyzed in future studies.

Compared to other studies, the system of this work performs well [Li2016; Reis2012; Yu2015; Barr2013]. Due the pH value constraints of the electro-Fenton, the current density and current efficiency of the reactor of this work cannot reach state of the art results for H_2O_2 synthesis in caustic electrolytes such as presented by Muddemann et al. [Mudd2020]. However, with an additional or modified catalysts, the selectivity may be increased in future [Kim2018; Vali2013]. An optimization of the reactor design could lead to an increase in energy efficiency, current density, and H_2O_2 concentrations [Xia2019]. The reactor presented herein is well suited to study the electro-Fenton reaction, as it a) encompasses a catholyte compartment with stable pH conditions for the homogeneous Fenton catalyst and substrate cellobiose and b) enables a steady operation at a comparably high current density and selectivity.

6.3. Tubular Electrodes

In the following section, tubular carbon-based gas diffusion electrodes are evaluated for their application in electrochemical H_2O_2 synthesis based on the work of Gendel et al. [Gend2014a; Gend2014b]. These so-called microtubes are freestanding hollow fibers made of multi-

walled carbon nanotubes (MWCNT). This section reports the results of two separate studies:

- Modification of microtubes with a metal catalyst or a chinon catalyst for enhanced catalytic activity and selectivity (*CNT:Cat*)
- Modification of microtubes with a polymeric binder for enhanced performance as a gas diffusion electrode (*CNT:PTFE*)

The two studies are named *CNT:Cat* and *CNT:PTFE*.

6.3.1. Experimental

CNT:Cat Microtubes: Fabrication and Experiments

Tubular microtubes made of carbon nanotubes (CNT) were fabricated following the work of Gendel et al. [Gend2014a; Gend2014b]. The *CNT:Cat* microtubes were produced with MWCNT from Sigma-Aldrich. In contrast to Gendel et al. [Gend2014a], a pressure vessel was used instead of a syringe pump to drive the suspension through the membrane (5 bar trans membrane pressure (TMP)).

Tubular test-electrodes were fabricated by glueing a titanium wire inside a 5 cm long microtube with conductive glue (Leit-C, Fluka). The electrodes are coined test-electrodes to differentiate them from tubular gas diffusion electrodes, which are described in the next section. A shrinking tube was used to provide 4 cm of active length, which yields 2.1 cm^2 of surface area. For the H_2O_2 synthesis, experiments up to four electrodes were used in parallel to reach higher concentrations. A photo of a test-electrode can be seen in Figure 6.12. A glass H-cell was used for the electrochemical characterization. The anolyte (150 mL) and catholyte (150 mL) were separated by a cation exchange membrane (F-14100, Fumatech BWT). The anolyte was prepared by adjusting deionized water to pH 2 with H_2SO_4 (95-97%, Merck), while the catholyte was a 50 mM Na_2SO_4

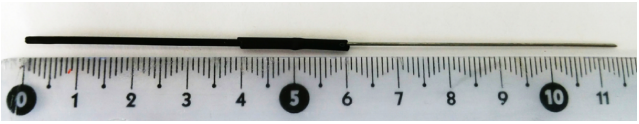

Figure 6.12.: A microtube test-electrode for the *CNT:Cat* trials

solution, which was adjusted to pH 3, again with H_2SO_4. Prior to each measurement, the catholyte was gassed with 100 mL/min oxygen (99.95%, Westfalen) or nitrogen (99.999%, Air Liquide). Gassing was continued during the electrochemical measurements and the catholyte was stirred continuously at 400 rpm. A platinized titanium mesh and a Hg/Hg_2SO_4 electrode in 0.5 M H_2SO_4 were used as counter and reference electrodes, respectively.

Tubular gas diffusion electrodes for testing of *CNT:Cat* were fabricated as described by Gendel et al. [Gend2014a]. As a current collector, a stainless steel rod (0.7 mm) was inserted into the microtube and another stainless steel wire (0.15 mm) was spirally wound around the rod, see Figure 6.13. The gas diffusion electrodes were tested in a divided cell, which is depicted in Figure 6.14 and described in detail in [Gend2014b]. A cation exchange membrane (Fumapem F-14100, Fumatech) separated anolyte and catholyte. The anode was a titanium plate (15 x 195 x 3 mm) coated with $Pt_{70}Ir_{30}$ catalyst from Magneto. The active length of the inserted microtube was approximately 20 cm, which yielded a surface area of 10 cm^2. Anolyte and catholyte were the same as in the H-cell experiments with volumes of 80 mL and 150 mL, respectively. The catholyte was recirculated through a glas flask with a gear pump (Cole-Parmer, ISM405A) at 50 mL min^{-1}. Pure oxygen was supplied to microtube from the lumen side in cross-flow mode with a pressure of 300 $mbar_g$. The microtubes were functionalized with catalysts for H_2O_2 synthesis. A wet impregnation method was chosen in order to obtain a mono-metallic nano-particulate gold catalyst. Typically, 100 mg of microtube were immersed in a 5 mL gold(III)-chloride (99.0%, Sigma-Aldrich) solution of ethanol ($>$ 99.8%, Sigma-Aldrich), which was previously sonicated

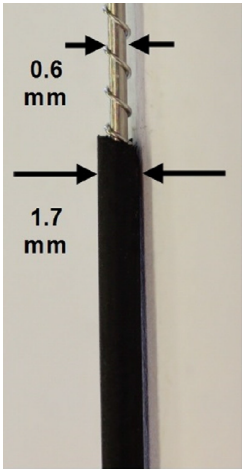

Figure 6.13.: Current collector and gas distributor in microtube gas diffusion electrode as used in the *CNT:Cat* trials. Reprinted from Electrochemistry Communications, 46, Y. Gendel, H. Roth, A. Rommerskirchen, O. David, M. Wessling, A microtubular all CNT gas diffusion electrode, 44-47, © (2014), with permission from Elsevier.

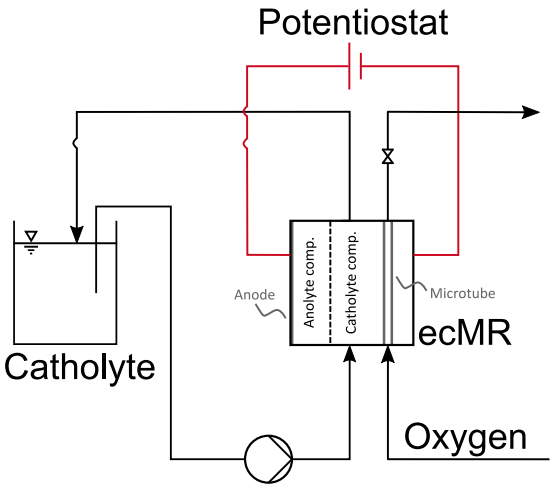

Figure 6.14.: Divided cell for testing of CNT-microtube gas diffusion electrodes (*CNT:Cat*)

for 15 min (Hielscher, UP 200S). Ethanol was chosen as solvent due to the favorable wetting properties in respect to the MWCNT compared to water. After 24 h impregnation in a rotator, the adsorbed ionic catalyst was reduced via impregnation of the microtube in an aqueous 0.01 M sodium borohydride solution (> 96 %, Sigma-Aldrich) for 1 min. The microtubes were subsequently dried in a vacuum oven over night at 30 °C and 80 mbar. Typically, the metal concentrations were chosen so that 5 wt.-% of total metal loading relative to the microtube weight was achieved. The organic catalyst 2-ethyl-anthraquinone (EAQ, > 97%, Sigma-Aldrich) was immobilized on the microtubes via a wet impregnation method. EAQ was first dissolved in ethanol while vigorously stirring the solution. Then, a microtube was impregnated with the solution (100 mg microtube, 5 mL solution) for 1 h. The EAQ concentration of the solution was varied such that 5%, 10% or 15% EAQ relative to the microtube weight were achieved. Subsequently, the microtube was dried as described above.

CNT:PTFE Microtubes: Fabrication and Experiments

The *CNT:PTFE* microtubes, which were examined for the influence of the polymeric binder polytetrafluorethylene (PTFE) , were produced with MWCNT from Bayer (Baytubes, C150HP). The polymeric binder was expected to increase the hydrophobicity of the microtubes and was added to the dispersion after sonication. In order to obtain a suspension with 90 wt.-% CNT and 10 wt.-% PTFE, the corresponding mass of PTFE suspension (60 wt.-%, Sigma-Aldrich) was added. The CNT dispersion was inserted into a syringe and subsequently filtered through a polymeric membrane via a syringe pump with an injection rate of 1.5 mL/min. The syringe pump as feed supply provided better results than the pressure vessel described previously, because it circumvented precipitation issues of the PTFE observed in the pressure vessel. This was the only modification of the microtube fabrication procedure described in 6.3.1 *CNT:Cat Microtubes: Fabrication and Experiments*. After drying of the PTFE-containing microtubes, they

were sintered in a furnace (Carbolite, AAF1100) for one hour at either 310 °C or 340 °C. Gas diffusion electrodes were subsequently produced by inserting a wound silver-plated copper wire (Conrad) through the microtube. In order to achieve a conducting connection between wire and microtube, the wire was coiled to a diameter slightly above the microtubes diameter. Afterwards, the so created "silver spring" was pulled through the microtube. This method of introducing a current collector in the GDE proved to damage the microtubes less during assembly compared to the method of Gendel et al. [Gend2014a] described in Section 6.3.1 *CNT:Cat Microtubes: Fabrication and Experiments*. Additionally, the assembly was accelerated with the new method. The computer tomography images in Figure 6.15 reveal that the wire retained the spiral geometry to function as current collector.

(a) Wound silver wire current collector inside a CNT-microtube.

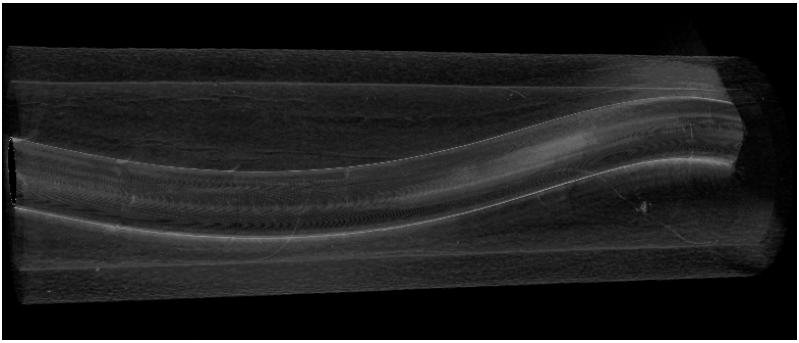

(b) CNT-microtube with wound silver wire current collector.

Figure 6.15.: Computer tomography images of the silver wire current collector inside the microtube for the *CNT:PTFE* trials

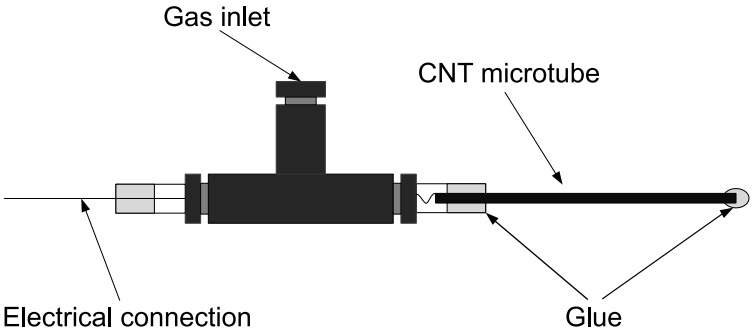

Figure 6.16.: Sketch of the connection of the CNT-microtube gas diffusion electrodes for the *CNT:PTFE* trials.

The CNT microtube gas diffusion electrodes were connected to a T-shaped tube connector for oxygen supply and the electrical connection, see Figure 6.16. Gases were supplied to the GDE in dead-end mode with either 0.25 or 0.5 bar_g.

The active length of the tubes was 4 cm and the geometrical surface are was 2.1 cm^2. As a reference electrode, a Hg/Hg_2SO_4 in saturated K_2SO_4 was used. Similar to the *CNT:Cat* trials in an H-cell, 0.05 M Na_2SO_4 adjusted to pH 3 was used as catholyte (120 mL), and an aqueous H_2SO_4 solution at pH 2 was used as anolyte (80 mL). The electrolyte compartments were separated by a F-14100 cation exchange membrane (Fumatech BWT). Additionally to the H-cell experiments, a tubular electrochemical reactor was constructed as a prototype reactor, see Figure 6.17.

In the reactor, the CNT-microtube GDE was at the center, concentrically surrounded by a liquid catholyte. A tubular proton exchanger membrane (Permapure, TT700, Nafion) then separated catholyte and anolyte compartment. The membrane was separated from the platinum-coated titanium anode (Magneto) by an anolyte layer. The active electrode length in the reactor was 10 cm. The regions of the microtube, which were not in contact with the cathode reaction cham-

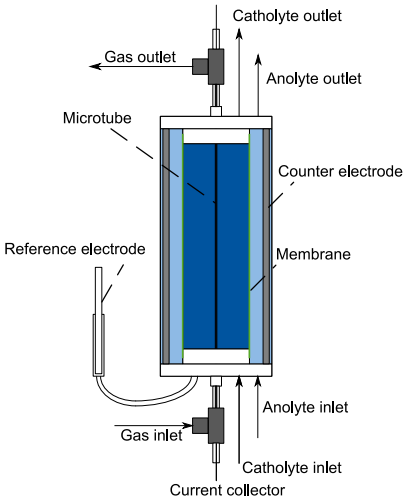

Figure 6.17.: Sketch of the tubular reactor.

ber, were covered with a shrinking tube in order to obtain a clearly defined active area. The ends of the CNT-microtube GDE were glued into a T-connector as described before. The tubular membrane was mounted as follows: the membrane was wetted with ethanol in order to achieve a swelling degree of approximately 44%. The swollen membrane was mounted on a 3D-printed socket and immersed in water. The swelling degree retracted to 20%, which yielded a membrane diameter slightly below the socket diameter and ensured a tight fit. As an additional fixation, o-rings were placed on the membrane. The membrane-socket-unit was pushed into the tubular grid anode and glued into the plastic reactor shell (Sofort fest, UHU). The reference electrode was connected to the catholyte via a salt bridge. A process sketch is depicted in Figure 6.18.

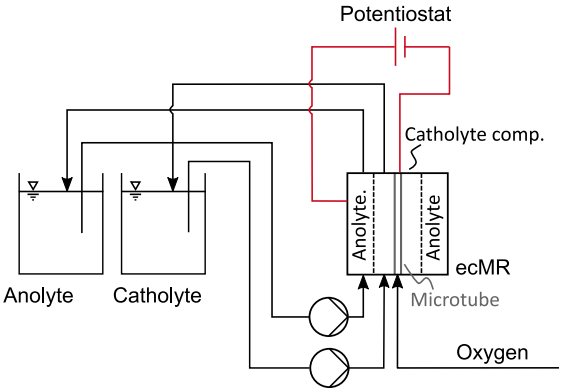

Figure 6.18.: Process sketch for the *CNT:Cat* experiments with the tubular reactor.

Surface and Volume Characterization

The surface area of the *CNT:PTFE* microtubes was determined via nitrogen adsorption measurements at 77 K (ASAP 2020, Micromeritics) according to Brunauer, Emmett and Teller (BET). All samples were degassed under vacuum (5 mmHg) at 80 °C for 24 h and weighed. To obtain the BET surface area only data points of the linear region of the adsorption isotherm were taken into account. Therefore, the region $0.05 < p/p_0 < 0.3$ was used for each surface area calculation. Scanning electrode microscopy (SEM) and energy-dispersive x-ray spectroscopy (EDX) measurements were performed with a Hitachi SEM S3000 and a S4800. A Bruker Skyscan 1272 with 50 kV and 200 μA was used for the tomography scans of the microtube.

Hydrogen Peroxide Quantification

The concentration of hydrogen peroxide was determined as described in Section 6.2.

Electrochemical Measurements

Cylcic voltammetry, constant voltage and constant current measurements were performed in order to characterize the electrochemical properties of the microtubes. A PGSTAT302N from Metrohm was used for all electrochemical experiments. As reference electrodes Hg/Hg_2SO_4 in 0.5 M H_2SO_4 or in saturated K_2SO_4 (Meinsberg) were used. All potentials are reported as V vs. Standard Hydrogen Electrode (SHE). For the *CNT:Cat* microtubes, CVs were performed with a scan rate of $10\,mV\,s^{-1}$ and in a potential range from -1.02 to 0.68 V vs. SHE. Polarization plots were obtained from multiple chronoamperometry measurements. Each potential was held until steady-state was reached. The final current was taken as steady-state current.

6.3.2. Results and Discussion

CNT:Cat Microtubes

The CNT microtubes were tested for oxygen reduction reaction (ORR) activity in cyclic voltammetry measurements. The voltamogramm in Fig. 6.19 a) shows that the microtube shows ORR activity, similar as reported by Gendel et al. [Gend2014a]. A sharp increase in cathodic current can be observed at approximately 0.5 V vs. SHE, which is close to the equilibrium potential of 0.52 V vs. SHE of H_2O_2 at pH 3 (calculated via eq 2.5 assuming a 1 M surface concentration of H_2O_2, 1 bar O_2 partial pressure, and ideal activity coefficients). In the voltammogram of the nitrogen-purged solution, a cathodic branch emerges below 0 V vs. SHE, which is a hint that competing reactions such as HER take place. Gendel et al. [Gend2014a] tested the microtubes for the two-electron oxygen reduction reaction and reported current efficiencies below 50%. In the next sections, the influence of different catalysts on the CE will be shown, and how it can be enhanced. Gold nanoparticles were deposited on the CNT microtubes in order to increase the activity and selectivity towards

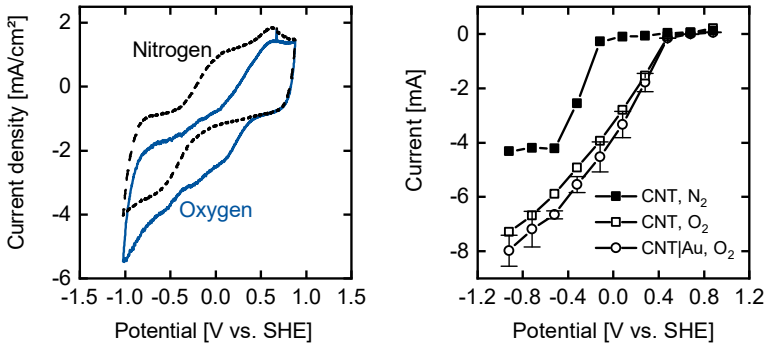

(a) Cyclic voltammogram of a CNT microtube in a oxygen saturated solution and a solution which was purged with nitrogen.

(b) Polarizations plots of pure and gold-modified microtubes.

Figure 6.19.: Cyclic voltammetry and polarization plots with pure and gold-modified CNT microtubes. The experimental conditions were: 50 mM Na_2SO_4, pH 3, 100 mL min^{-1} O_2 bubbled in solution.

H_2O_2. The SEM images in Figure 6.20 show that even though some gold was deposited in micrometer size, most of the CNT network is covered by nanoparticles in the range of 5–20 nm. The gold catalyst increases the activity of the microtubes slightly compared to the pure CNT microtubes, as shown in the polarization plot in Figure 6.19 b). The polarization plot also indicates that the pure CNTs are active for hydrogen evolution reaction starting between -0.1 and -0.3 V vs. SHE, which agrees with the findings of the cyclic voltammetry reported in Figure 6.19 a). However, it cannot be ruled out that some oxygen remained trapped in the CNT network even when gassing with nitrogen. Sanchez-Sanchez et al. [Sánc2009] have shown that oxygen can be reduced to H_2O_2 in acidic solutions. However, at potentials below approximately 0.2 V vs. RHE, the number of transferred electrons per oxygen starts to increase and the share of water as a side product to H_2O_2 increases (four-electron ORR). Figure 6.21 a) shows the increase in H_2O_2 concentration for pure and gold modified

microtubes during a constant potential experiment at 0.08 V vs. SHE (0.257 V vs. RHE at pH 3). Even though the increase of the H_2O_2 concentration is steaper initially with the gold modified electrode, the curve flattens with increasing reaction time. This trend is confirmed by the CE, which is plotted in Figure 6.21 b). On the one hand, the CE for the gold-modified electrode is overall below the pure CNT microtube. Additionally, the CE for both electrodes decreases with time, even more pronounced for the gold electrode. These observations show that even though the gold catalyst yields a higher CD, a high CE cannot be sustained. One reason could be that the potential of 0.08 V vs. SHE was not high enough to yield a two-electron ORR [Sánc2009]. Thus, the H_2O_2 production was investigated at potentials of 0.48, 0.28, 0.08, -0.12 and -0.32 V vs. SHE. At the highest potential of 0.48 V vs SHE, hardly any H_2O_2 is produced, see Figure 6.22 a). This observation is in agreement with the polarization curve in Figure 6.19 b), which shows that the current is very low at 0.48 V vs. SHE. Thus, even though the CE may be high at 0.48 V vs. SHE, the CD is too low to measure any substantial amounts of H_2O_2. If the overpotential is increased and a potential of 0.28 V vs. SHE is applied, the concentration of H_2O_2 increases linearly with increasing reaction time, see Figure 6.22 a). The CE remains high over the entire reaction time at approximately 76%. A further increase in overpotential to 0.08 V vs. SHE yields the highest H_2O_2 concentration. However, the concentration does not increase linearly, which indicates a decreasing CE, as confirmed in Figure 6.22 b). A further increase of the driving force at potentials of - 0.12 and - 0.32 V vs SHE leads to very low current efficiencies and consequently low H_2O_2 concentration (Figure 6.22). Overall, these findings confirm the work of Sanchez-Sanchez et al. [Sánc2009] that the CE for the two-electron oxygen reduction reaction drops below a potential of approximately 0.2 V vs. RHE. Additionally, there is a trade-off between CD and CE which needs to be considered for the practical application.

In a next step, the loading of the gold catalyst was varied. In order to keep the costs of the electrodes to a minimum, the loading should be as low as possible while achieving high current densities and

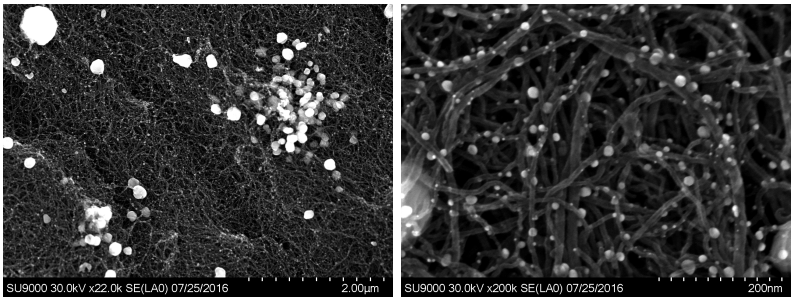

(a) Magnification of 22,000 x **(b)** Magnification of 200,000 x

Figure 6.20.: SEM image of microtube surface modified with gold catalyst.

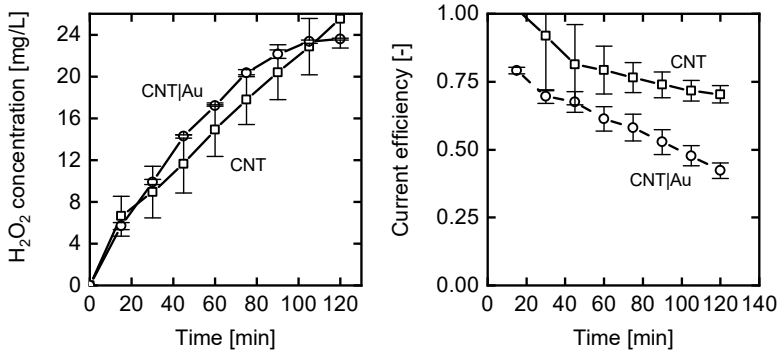

(a) H_2O_2 concentrations with and without gold catalyst.

(b) Current efficiency with increasing reaction time with and without gold catalyst.

Figure 6.21.: Concentration and current efficiency with increasing reaction time of the electrochemical synthesis with and without 5 wt.-% gold catalyst on the CNT microtubes at a constant potential of 0.08 V vs. SHE. The experimental conditions were: 50 mM Na_2SO_4, pH 3, 100 mL min^{-1} O_2 bubbled in solution.

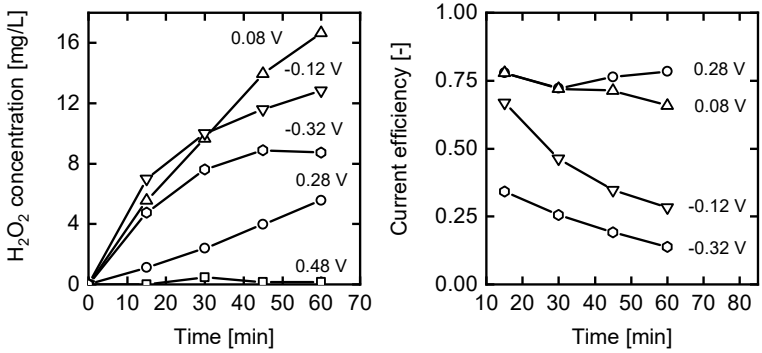

(a) H_2O_2 concentrations with increasing reaction time.

(b) Current efficiency with increasing reaction time.

Figure 6.22.: H_2O_2 synthesis at different potentials for a CNT microtube with 5 wt.-% gold catalyst. The experimental conditions were: 50 mM Na_2SO_4, pH 3, 100 mL min^{-1} O_2 bubbled in solution.

current efficiencies. Figures 6.23 show the concentration of H_2O_2 and the CE with increasing reaction time for gold-modified microtubes with loadings of 1.25, 2.5, 5, 10 and 20 wt.-% . A low gold loading of 1.25 wt.-% yields the lowest H_2O_2 concentrations. Apparently, not enough catalytically active sites are available 1.25 wt.-% gold loading. An increase in catalyst loading leads to higher H_2O_2 concentrations, which does not differ much for 2.5, 5, 10 and 20 wt.-% gold loading, see Figure 6.23 a). However, Figure 6.23 b) shows that a gold loading of 10 and 20 wt.-% mitigates the CE. Thus, these findings indicate that the optimum gold loading is between 2.5 and 5 wt.-% .

Gold is an expensive catalyst, which only enables a two-electron oxygen reduction reaction in a narrow potential window. Quinone catalysts, such as 2-ethylanthraquinone, were shown to be active catalysts for the electrochemical H_2O_2 synthesis [Fort2007; Wang2012; Yang2018a]. Figure 6.24 shows the concentration of H_2O_2 and CE with increasing reaction time for constant potential (-0.12 V vs. SHE) experiments with EAQ loadings of 5, 10 and 15 wt.-% . Compared to the gold

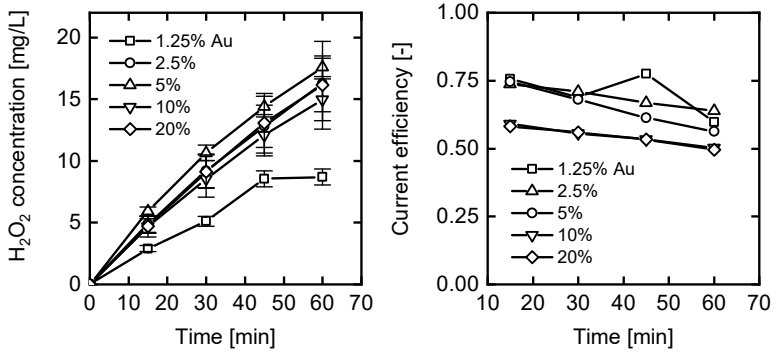

(a) H_2O_2 concentrations with increasing reaction time.

(b) Current efficiency with increasing reaction time.

Figure 6.23.: H_2O_2 synthesis at -0.08 V vs. SHE with different gold loadings of CNT microtubes. The experimental conditions were: 50 mM Na_2SO_4, pH 3, 100 mL min^{-1} O_2 bubbled in solution.

catalyst or pure CNT microtube, the EAQ catalysts yield constant current efficiencies, which do not decline with increasing reaction time. Overall, 10 wt.-% EAQ yields the highest H_2O_2 concentration and CE. A lower loading of 5 wt.-% leads to a decreased CE as apparently not enough active sites for the synthesis were available. A higher loading of 15 wt.-% reaches the same CE of approximately 80% as the 10 wt.-% loading. However, the attainable H_2O_2 concentration is lower, see Figure 6.24 a). This may be caused by a too high loading, which may impair the conductivity of the microtube. For the 15 wt.-% EAQ loading, a lower CD was reached compared to the 5 and 10 wt.-% loadings. Forti et al. [Fort2007] immobilized EAQ on glassy carbon electrodes, and found an increasing H_2O_2 production up to 10 wt.-% EAQ. However, they did not test higher concentrations, for which a decreasing performance was found in this work. Additionally, Forti et al. [Fort2007] investigated the performance of the the EAQ-modified electrode at potentials from -0.2 to -0.7 V vs. SHE in an electrolyte with pH 1 (-0.141 to -0.641 V vs. RHE). This potential range was chosen because the authors only found significant ORR currents below

approximately 0 V vs. SHE (0.059 V vs. RHE) [Fort2007]. Thus, the EAQ catalysts requires a higher overpotential than the gold catalyst. This trend could be confirmed in this thesis with EAQ-modified microtubes. Experiments with constant potentials of 0.08, −0.06 and −0.16 V vs. SHE (0.257, 0.177 and 0.017 V vs. RHE) were applied. At the most positive potential the production rate of H_2O_2 and the CE are low, whereas the higher overpotentials yields a selectivity of approximately 70%. It should be noted that experiments with potentials of -0.06 V and -0.016 V yield the same current, which can be explained by slightly different positions of the reference electrodes. Thus, even though a different potential was applied, the same H_2O_2 concentration and CE was reached for these two potentials. These results support the findings of Forti et al. [Fort2007] that a certain potential needs to be crossed to make the EAQ catalyst active.

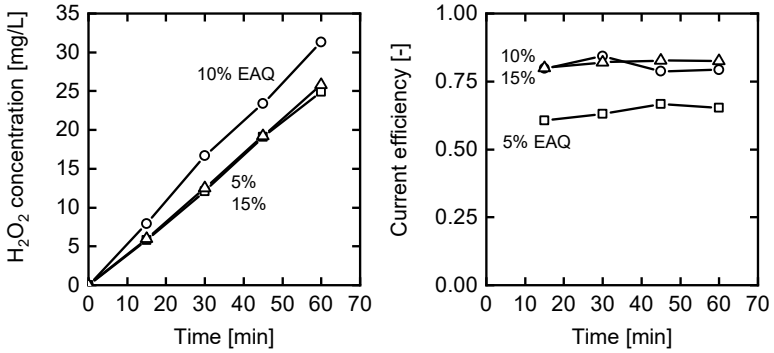

(a) H_2O_2 concentrations with increasing reaction time.

(b) Current efficiency with increasing reaction time.

Figure 6.24.: H_2O_2 synthesis at -0.12 V vs. SHE with CNT microtube with different EAQ loadings. The experimental conditions were: 50 mM Na_2SO_4, pH 3, 100 mL min^{-1} O_2 bubbled in solution.

The most promising catalysts loadings (5 wt.-% Au and 10 wt.-% EAQ) were subsequently applied on 10 cm long microtubes, which were tested as gas diffusion electrode. Figure 6.26 a) shows the polarization

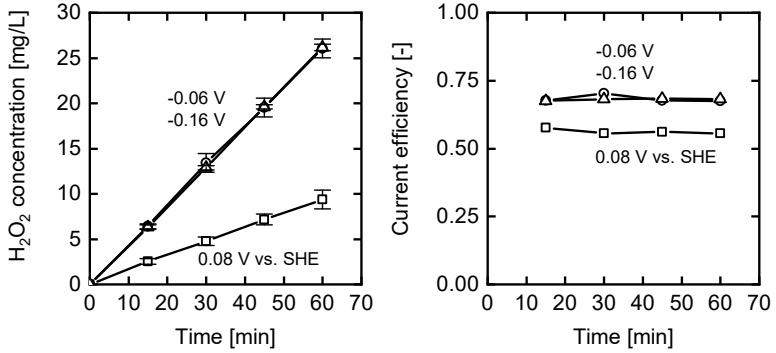

(a) H_2O_2 concentrations with increasing reaction time.

(b) Current efficiency with increasing reaction time.

Figure 6.25.: H_2O_2 synthesis with a 10 wt.-% EAQ CNT microtube at different potentials. The experimental conditions were: 50 mM Na_2SO_4, pH 3, 100 mL min^{-1} O_2 bubbled in solution.

plots for a pure and the catalyst-modified microtubes in a solution either bubbled with nitrogen or with the supply of oxygen to the GDEs. The results show that without oxygen the catalysts are not active. When oxygen is supplied to the GDEs, the CD increases. Gold exhibits the highest activity, followed by EAQ and the pure CNT microtube. H_2O_2 synthesis experiments were subsequently measured in potential ranges, which yielded the highest current densities in the experiments with the tubular test-electrodes.

The gold catalyst performed poorly, yielding current efficiencies below 50%, see Figure 6.26 b). Similarly, the pure CNT microtubes yielded low current efficiencies with values below 50% after 60 min in agreement with Gendel et al. [Gend2014b]. Only the EAQ modified gas diffusion electrodes performed at a similar CE as the tubular test-electrodes. On reason for the poor CE of all catalysts could be mass transport limitations, e.g., an insufficient supply of protons to the active sites. Alternatively, studies have shown that insufficient removal of H_2O_2 from the catalyst surface can lead to a reduction

of H_2O_2 to H_2O [Yang2018a]. Figure 6.27 a) and b) show that an increase in liquid flow rate can increase the CD twofold and even more at very negative potentials. This behaviour is a hint for mass transfer limitations. Another, reason for the poor performance of the microtubes is wetting of the gas diffusion electrodes, which mitigates the O_2 transport to the surface. Frequently, water was observed inside the microtubes after experiments. Apparently, electrolyte penetrates through the GDE network during experiments. In the worst case, the entire GDE would be flooded and mass transport of oxygen impaired. Gendel et al. [Gend2014a] report similar current densities and current efficiencies in a system where the electrolyte was saturated with pure oxygen, but where no oxygen was supplied to the GDE. The wetting behavior of CNT microtubes will be investigated in more detail in Section 6.3.2 *CNT:PTFE Microtubes*.

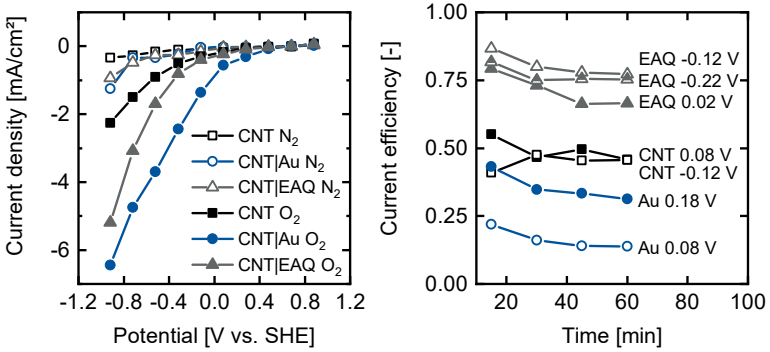

(a) Polarization plot.

(b) Current efficiency for H_2O_2 with increasing reaction time for different potentials.

Figure 6.26.: H_2O_2 electrosynthesis with pure CNT GDEs and GDEs modified with gold and EAQ catalyst. The experimental conditions were: 50 mM Na_2SO_4, pH 3, 0.3 bar_g O_2 in cross-flow mode.

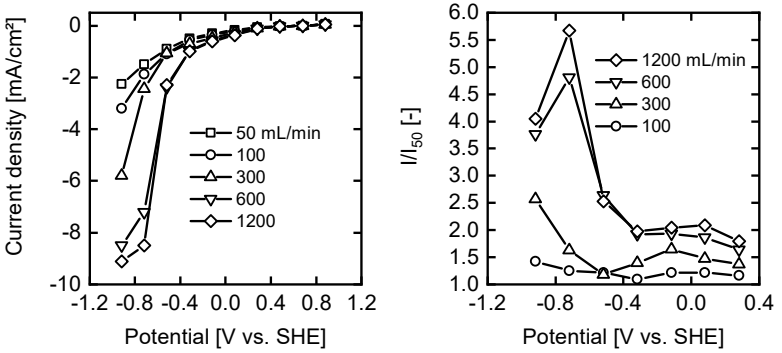

(a) Influence of the flow rate on the current density.

(b) Increase in current density with increasing flow rate compared to $50\,\mathrm{mL\,min^{-1}}$

Figure 6.27.: Influence of the liquid flow rate on the current density for pure CNT microtube GDEs. The experimental conditions were: 50 mM Na_2SO_4, pH 3, $0.3\,\mathrm{bar_g}$ O_2 in cross-flow mode.

CNT:PTFE Microtubes

Gas diffusion electrodes (GDE) are usually multi-layered structures, which consist of a catalyst layer (CL) and a gas diffusion layer (GDL), as explained in detail in Section 2.2.2 based on the work of Zhang et al. [Zhan2008]. The desired electrochemical reaction takes place in the CL. The GDL is designed for efficient transport of reactants, electrons, and heat, and provides mechanical support. PTFE is a frequently used additive in the GDL, which ensures binding of the carbon particles and enhances the hydrophobicity of the GDE. This ensure open pathways for the gas to reach the interface of catalyst and liquid electrolyte. In Section 6.3.2 *CNT:Cat Microtubes*, leakage of electrolyte through the gas diffusion electrode was observed, which was identified as one reason for the low CE of the gas diffusion microtubes. This section discusses the influence of PTFE as hydrophobic binder on the physicochemical properties of CNT-based microtubes. In general, GDLs are treated thermally after PTFE deposition to remove the surfactant and

melt the polymer, which can then uniformly distribute throughout the layer [Xing2008; Park2012]. The sintering temperature is often chosen slightly above the melting point of PTFE, which is 321 °C [GmbH2020]. The sintering temperature should not be too high, as, e.g., Rohendi et al. [Rohe2014] show that the hydrophobicity decreases above 350 °C. Carbon nanotubes show promising performance enhancements when incorporated into the microporous layer of GDLs together with PTFE [Khat2011; Lau2012; Gall2010; Soeh2008]. In this work, the gas diffusion electrode is a single layer electrode: gas diffusion layer and catalyst layer have the same properties. Thus, PTFE was added to the dispersion for fabrication of microtubes, as explained in Section 6.3.1 *CNT:PTFE Microtubes: Fabrication and Experiments*.

In Figure 6.28, the contact angle between a 100CNT microtube (microtube contains 100 wt.-% CNT) and a water droplet can be seen in the lower left corner. After the completion of an electrochemical measurement, the contact angle decreases from approximately 120° to 30°. The decrease in contact angle can be due to changes in surface functional groups [Soeh2008], but also remains of hydrophilic substances like salts on the electrode surface [Leon2020]. Additionally, so-called electro-wetting may decrease the the contact angle if the electrode is polarized [Kaka2008]. Even though CNTs are more stable than other frequently used carbon-based catalysts like Vulcan XC-72 against oxidation, they still do oxidize [Shao2006]. Because cyclic voltammetry was applied to the GDE in this work, oxidation of the catalyst may have taken place. The stability of the CNTs also depends on their fabrication method [Musa2005]. The *CNT:PTFE* microtubes have an initial contact angle of approximately 120°. After electrochemical H_2O_2 synthesis, the contact angle decreases to 95°, but remains hydrophobic. EDX analysis of the microtubes with and without the addition of PTFE reveals a fluorine peak in the case where PTFE was added to the microtube, see Figure 6.29. Carbon (CNT) and Al (sample holder) could also be identified. Mapping of the EDX analysis shows that PTFE is evenly distributed throughout the cross-section, see Figure 6.30. The BET surface area decreases for microtubes with PTFE, see Figure 6.31 a), which can be explained by

pore blocking through the additive [Kell2018]. In accordance with the BET surface area, the pore size distribution shows that the pore size in general decreases, see Figure 6.31 b). Only the smallest fraction between 1 nm to 2 nm increases. As the PTFE binds to the carbon nanotubes it will narrow the voids and lead towards smaller pore values.

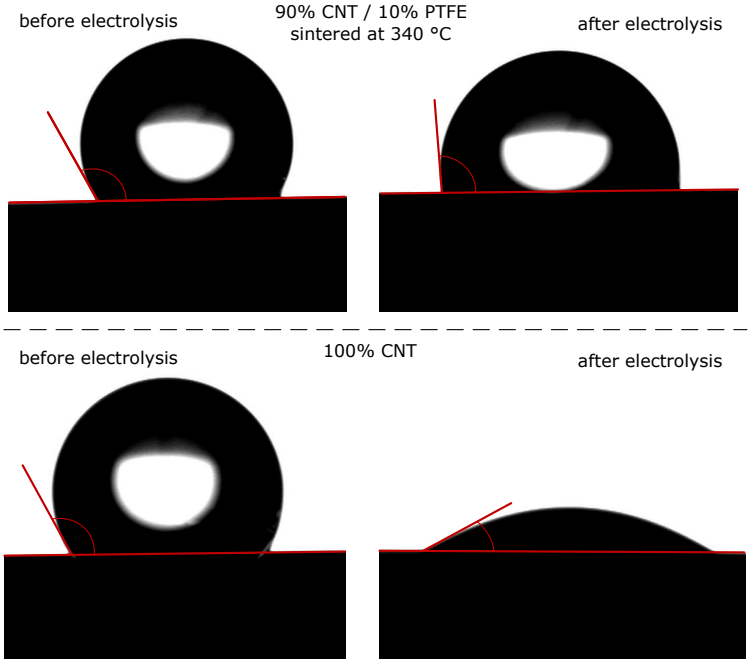

Figure 6.28.: Contact angle on CNT microtubes with and without PTFE binder before and after electrolysis.

Additionally to the physico-chemical properties studied in the previous paragraph, the electrochemical properties were evaluated. Figure 6.32 shows a comparison of microtubes without PTFE (100CNT), and microtubes with 10 wt.-% PTFE, where no gas was supplied from

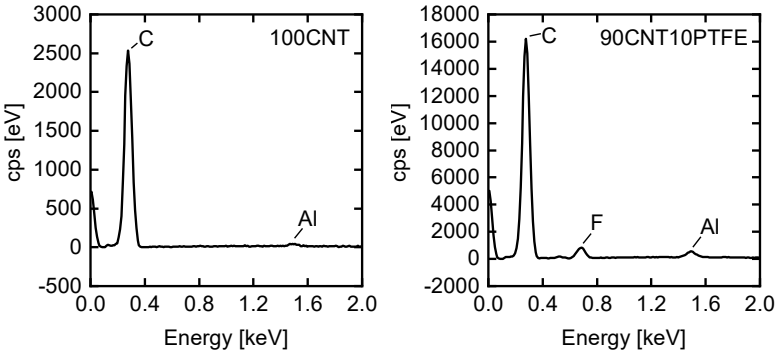

(a) EDX spectrum of the cross-section of a 100CNT microtube.

(b) EDX spectrum of the cross-section of a 90CNT10PTFE microtube, sintered at 340 °C.

Figure 6.29.: EDX spectra of microtubes with and without the addition of PTFE.

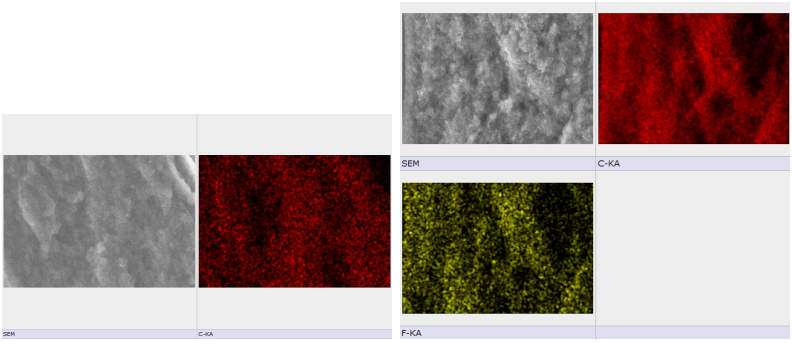

(a) EDX mapping of the cross-section of a 100CNT microtube.

(b) EDX mapping of the cross-section of a 90CNT10PTFE microtube, sintered at 340 °C.

Figure 6.30.: EDX mapping of microtubes with and without the addition of PTFE.

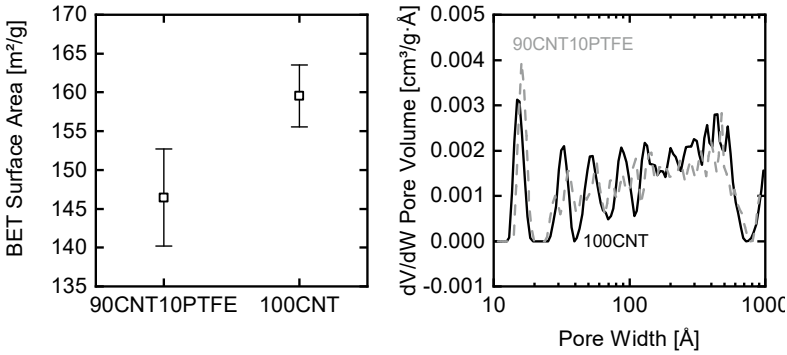

(a) BET surface area of microtubes with and without PTFE.

(b) BET pore size distribution of microtubes with and without PTFE obtained by NLDFT.

Figure 6.31.: BET surface area and pore size distribution of microtubes with and without the addition of PTFE obtained from nitrogen adsorption isotherms at 77 K. The microtube with PTFE was sintered at 340 °C.

the lumen side. The only available oxygen was supplied as dissolved oxygen from the electrolyte solution.

The tubes with PTFE were either used without further treatment (RT), or sintered at 310 °C, or 340 °C, respectively. As explained above, sintering promotes a thorough connection between the carbon nanotubes and PTFE, because the PTFE is melted. In Figure 6.32 a), the oxygen concentration in the electrolyte was below $1\,\mathrm{mg\,L^{-1}}$. Thus, hardly any activity for ORR can be observed. Only at potentials below -0.6 V vs. SHE can an increase in CD be observed. This marks the onset potential of the HER on the microtubes. An increase in oxygen concentration to $7\,\mathrm{mg\,L^{-1}}$ pushes the onset potential to approximately 0 V vs. SHE. In this case, the oxygen reduction reaction takes place. It will be shown in the next sections that most of the supplied electrons are converted to H_2O_2. It is noteworthy that the microtubes without PTFE shows the highest CD. Because no gas was supplied from the lumen side, the PTFE binder cannot act as promoter for gas transport.

The pure CNT microtubes shows the highest CD, because is has the highest specific surface are. Thus, even though all tested microtubes had the same geometrical surface area, the 100CNT provided the most active sites and thus the highest CD. All measurements in 6.32 b) indicate mass transport limitations in a flattening of the cathodic branch at potentials below -0.4 V vs. SHE.

Mass transport limitations are mitigated when oxygen is supplied through the lumen side of the gas diffusion electrodes, see Figure 6.33. Compared to the results without gas supply through the lumen, no flattening of the cathodic branch is observed and higher current densities are reached. Interestingly, only a small difference in CD can be observed between experiments, where the oxygen concentration in the electrolyte was $7\,\mathrm{mg\,L^{-1}}$ or $\geq 30\,\mathrm{mg\,L^{-1}}$, compare Figures 6.33 a) and b). This observation shows how important the gas diffusion layer and three phase boundary is: In a well designed system, the reactant is supplied via the gas phase in proximity to the location of consumption. In this case, the bulk concentration of reactant in the liquid electrolyte is not significant. Interstingly, the 100% CNT tubes show a higher CD close to the onset potential of approximately 0 V vs. SHE. However, as the potential becomes more negative, the tube with PTFE achieves higher CD than the 100CNT. Thus, the influence of PTFE seems to become more important at high CDs. The sintering temperature did not have a pronounced effect on the performance of the tubes, while the unsintered shows a decline in CD in Figure 6.33 b). All further experiments with PTFE-containing tubes were performed with electrodes sintered at 340 °C. Overall, the 100CNT microtube again performs very well compared to the PTFE containing microtubes. Due to the short measurements, pore flooding was not pronounced. However, compared to the experiments without gas supply to the lumen side, the 100CNT did not yield the highest CDs. It is hypothesized that the increase specific surface area of the 100CNT is counterbalanced by the positive effects of PTFE for the gas supply.

Figure 6.34 shows that the influence of the oxygen partial pressure

in the studied CD range does not have a significant effect on the CD. The only electrochemical activity in a system with nitrogen gassing of the electrolye ($c_{O_2} \leq 1$) is the HER with an onset potential more negative than -0.6 V vs. SHE. If oxygen is exclusively supplied via the electrolyte with a concentration of $7\,\mathrm{mg\,L^{-1}}$, mass transport limitations can be observed. A supply of oxygen via the lumen side of the GDE mitigates mass transport limitations. An increase in partial pressure of O_2 from $0.25\,\mathrm{bar_g}$ to $0.5\,\mathrm{bar_g}$ does not lead to an increase in CD, compare Figures 6.34 a) and b). This observation is supported by Gendel et al. [Gend2014b], who even observed a decrease in CD with increasing lumen side pressure. Thus, a pressure of $0.25\,\mathrm{bar_g}$ ensures a sufficient supply of reactant. At higher current densities, the stoichiometric excess λ of O_2 may drop below 1, leading to a compromised performance as described in Section 6.2.2 *Influence of the Gas Flow Rate*.

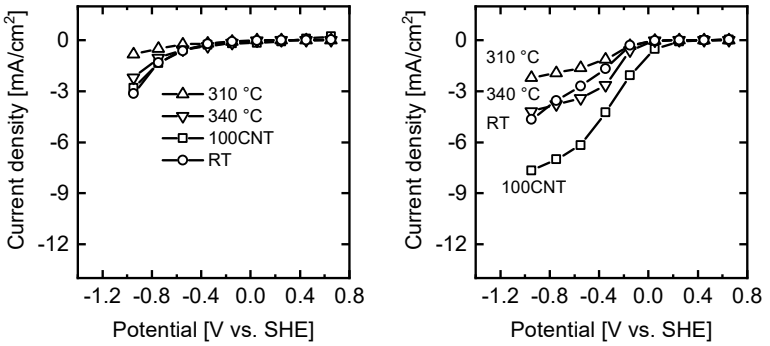

(a) Comparison of microtubes with an oxygen concentration of $\leq 1\,\mathrm{mg\,L^{-1}}$ in the electrolyte.

(b) Comparison of microtubes with an oxygen concentration of $7\,\mathrm{mg\,L^{-1}}$ in the electrolyte.

Figure 6.32.: Comparison of a 100% CNT microtube with PTFE-containing microtubes which were not sintered (RT) or sintered at 310 °C or 340 °C. No oxygen was supplied from the lumen side of the gas diffusion electrodes. The experimental conditions were: 50 mM Na_2SO_4, pH 3.

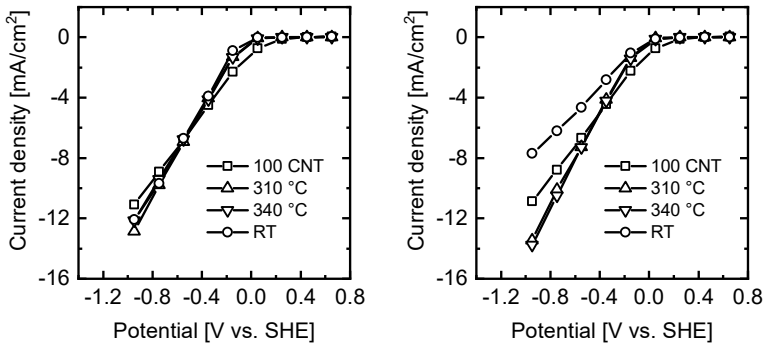

(a) Comparison of microtubes with an oxygen concentration of $7\,\mathrm{mg\,L^{-1}}$ in the electrolyte.

(b) Comparison of microtubes with an oxygen concentration of $\geq 30\,\mathrm{mg\,L^{-1}}$ in the electrolyte.

Figure 6.33.: Comparison of a 100% CNT microtube with PTFE-containing microtubes which were not sintered (RT) or sintered at 310 °C or 340 °C. Oxygen was supplied from the lumen side of the gas diffusion electrodes in dead-end mode with $0.5\,\mathrm{bar_g}$. The experimental conditions were: 50 mM Na_2SO_4, pH 3.

The polarization behaviour of microtubes made of 100% carbon nanotubes and microtubes with 10% PTFE did not show significant differences in the most cases, as described in the previous section. However, the polarization measurements are short measurements in the order of minutes. When 100% CNT electrodes were operated in longterm experiments, less and less bubbles were observed on the surface until the microtube ruptured. PTFE-containing microtubes, on the other hand, did not rupture and a constant oxygen support was ensured to the three phase boundary. Thus, for a long-term operation, the binder PTFE is essential to keep the gas flow paths open.

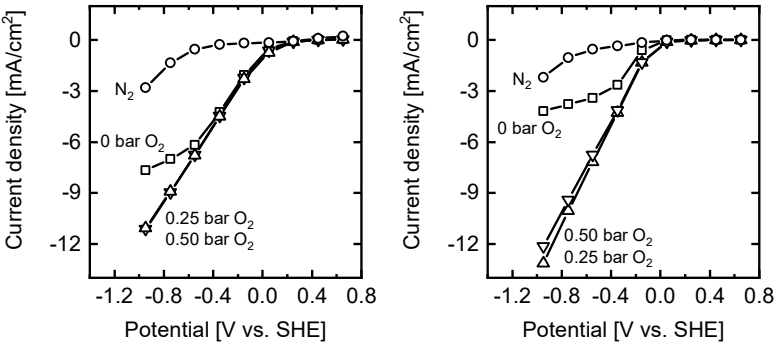

(a) Comparison of the influence of the oxygen pressure in 100CNT microtubes with an oxygen concentration of $7\,\mathrm{mg\,L^{-1}}$ in the electrolyte, and $\leq 1\,\mathrm{mg\,L^{-1}}$ with nitrogen gassing.

(b) Comparison of the influence of the oxygen pressure in 90CNT10PTFE (340 °C sintering temperature) microtubes with an oxygen concentration of $7\,\mathrm{mg\,L^{-1}}$ in the electrolyte, and $\leq 1\,\mathrm{mg\,L^{-1}}$.

Figure 6.34.: Comparison of a 100CNT microtube with a PTFE-containing microtube for different gas pressures on the lumen side. Oxygen was supplied from the lumen side of the gas diffusion electrodes in dead-end mode with 0, 0.25 or $0.5\,\mathrm{bar_g}$. The experimental conditions were: 50 mM Na_2SO_4, pH 3.

The following experiments for H_2O_2 generation with a 100% CNT microtube and a 90% CNT / 10% PTFE microtube will be used in

the next paragraph to strengthen the observation and conclusion from the previous paragraph. The experiments show the influence of the binder PTFE, of the partial pressure of oxygen in the microtube, and of the electrolyte concentration of oxygen. Figures 6.35 a) and b)

Table 6.1.: Experimental parameters for H_2O_2 generation with a 100CNT and a 90CNT10PTFE microtube. The microtube was gassed either with oxygen (O_2), synthetic air (SA), or nitrogen (N_2).

No.	**Gas**	**Lumen Pressure** bar_g	**Electrolyte O_2 Conc.** $mg\ L^{-1}$
1	O_2	0.5	8
2	SA	0.5	8
3	O_2	0.5	1
4	SA	0.5	1
5	O_2	0	8
6	N_2	0.5	1

show the potential with increasing reaction time for constant current experiments with a 100% CNT microtube and a 90CNT10PTFE microtube.

A constant current of $2.3\,mA\,cm^{-2}$ was applied for 30 min and the oxygen supply was adjusted as specified in Table 6.1. As reported before, the pure CNT microtube has a higher activity at potentials close to the onset potential. For experiments 1 and 3, where pure oxygen was supplied to the microtube lumen, the potential is slightly above 0 V vs. SHE and slightly below 0 V vs. SHE for the pure electrode and for the PTFE-containing microtube, respectively. However, for the experiments with synthetic air (Exp. no 2 & 4), the PTFE-containing electrodes show a more positive working potential, and thus a better performance. In contrast to the polarization experiments (Figures 6.33 and 6.32), which ran less than minute, the constant current experiments ran for 30 min each. Over this period of time, flooding of the 100% CNT microtubes is much more pronounced. Thus, the CE for the PTFE-containing electrodes is constantly above 90%, in-

dependently whether oxygen is supplied pure or as synthetic air, as can be seen in Figure 6.36 b). However, a more negative potential of about -40 mV must be applied when using synthetic air, which can be partially explained by the Nernst equation (eq 2.5) and has been observed by other authors [Mudd2020]. The potential difference between the use of pure oxygen ($p_{O_2} = 1.5$ bar) and synthetic air ($p_{O_2} = 0.21 * 1.5 = 0.32$ bar) is 20 mV assuming activity coefficients of 1 in the Nernst equation. The oxygen concentration of the electrolyte is not important, as long as the gas is supplied sufficiently via the gas diffusion electrode, as experiment no. 2 in Figure 6.36 b) shows. In contrast, the CE of the 100% CNT microtube is above 90% in experiment no. 1 and is lower in all other experiments. For the experiments with synthetic air, no. 2 and 4, the CE was below 15%. Interestingly, both microtubes had a CE below 25% for experiment no. 5, where no oxygen was supplied via the lumen. As shown in Section 6.3.1 *CNT:Cat Microtubes: Fabrication and Experiments*, the CE drops quickly at potentials below approximately 0 V vs. SHE. Also, the CNTs supplied by Sigma-Aldrich (Section 6.3.2) showed a lower CE compared to the Baytubes, which were used in this section. In Section 6.3.2 it was also shown that a catalyst like ethylanthraquinone or gold can lead to higher CEs. However, even if these catalysts are used, there will be mass transfer limitations at high CDs. This section clearly showed that this gas diffusion electrode needs PTFE as binding polymer to enhance the hydrophobicity and to generate open channels for the gas reactant supply. The 90% CNT / 10% PTFE microtube was tested at higher current densities and multiple times in a next step. The CD remains at approximately 80%, as can be seen in Figure 6.37. Thus, compared to the results presented in Section 6.3.2, the incorporation of PTFE into the CNT network improves the tubular electrode, which can be operated at up to 14 mA cm^{-2} at 80% CE without the application of an additional catalyst.

As an outlook, the electrode was modified with a catalyst, which increased the activity. Kim et al. [Kim2018] introduced a graphene-based catalyst, which can readily adsorb on carbon surfaces. This catalyst was mixed into the CNT suspension prior to the microtube

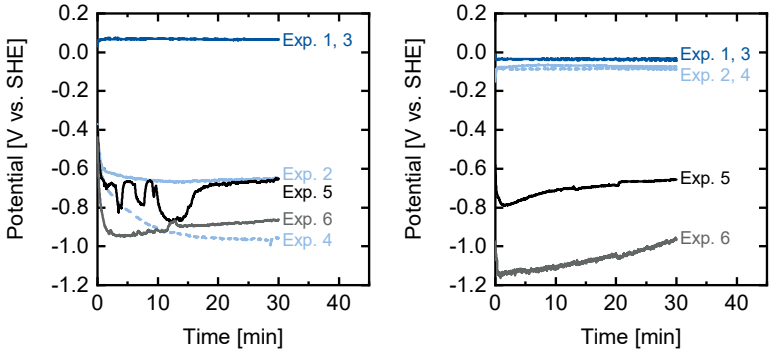

(a) Potential with increasing reaction time for a 100% CNT microtube for 2.3 mA cm^{-2}.

(b) Potential with increasing reaction time for a 90% CNT / 10% PTFE microtube for 2.3 mA cm^{-2}.

Figure 6.35.: Comparison of a 100% CNT microtube with a PTFE-containing microtube at constant current operation with varying oxygen pressures in the lumen of the microtube and varying oxygen concentrations in the electrolyte. Potentials were IR-drop compensated. The experimental conditions were: 50 mM Na_2SO_4, pH 3, O_2 concentrations according to Table 6.1

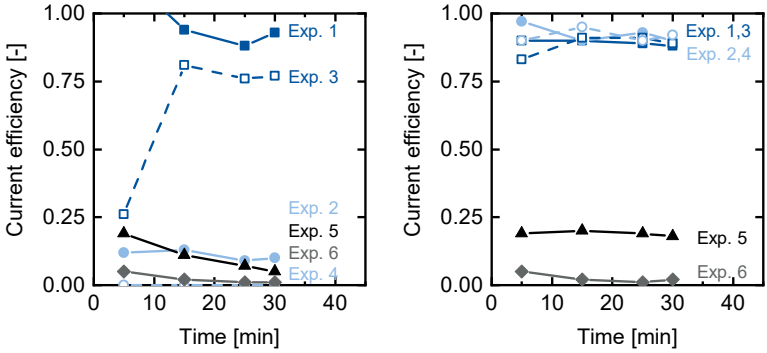

(a) Current efficiency with increasing reaction time for a 100% CNT microtube for 2.3 mA cm^{-2}.

(b) Current efficiency with increasing reaction time for a 90% CNT / 10% PTFE microtube for 2.3 mA cm^{-2}.

Figure 6.36.: Comparison of the current efficiency for H_2O_2 of a 100% CNT microtube with a PTFE-containing microtube at constant current operation with varying oxygen pressures in the lumen of the microtube and varying oxygen concentrations in the electrolyte. The experimental conditions were: 50 mM Na_2SO_4, pH 3, O_2 concentrations according to Table 6.1

fabrication.The polarization plot of this catalyst reveals the high activity it provides, see Figure 6.38 a). Additionally, the microtube can be scaled-up and incorporated in a tubular module as described in Section 6.3.1. A first test with the PTFE-containing microtube in the tubular module revealed a comparable polarization behaviour as the H-cell tests, see Figure 6.38 b).

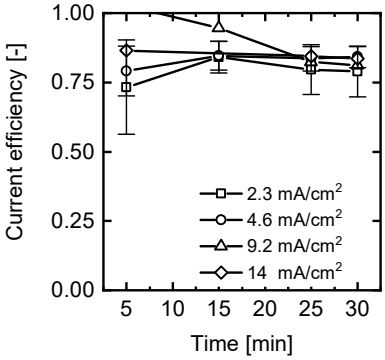

Figure 6.37.: Constant current experiments with a 90% CNT / 10% PTFE microtube. The experimental conditions were: 50 mM Na_2SO_4, pH 3, 0.5 bar_g O_2 in dead-end mode.

Summary

In comparison to the previous work by Gendel et al. [Gend2014b], the CE could be significantly increased, especially with the addition of PTFE to the microtube fabrication process. A gold catalyst increased the onset potential for the ORR compared to the pure GDEs and enabled an operation at a reduced overpotential, at least for low current densities. However, in order to achieve industrially viable current densities above 10 mA cm^{-2}, preferentially above 100 mA cm^{-2}, the working electrode operating potential drops below 0.2 V vs. RHE. In this region, the electron transfer number increased above two and O_2

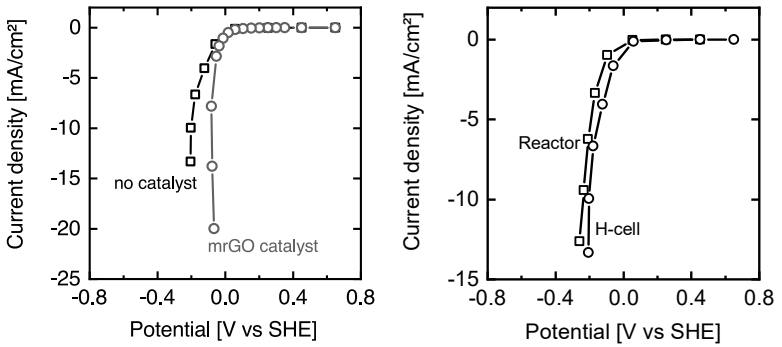

(a) Comparison between a 90% CNT / **(b)** Comparison between a microtube in 10%PTFE microtube with and without an H-cell and in a tubular reactor. mrGO catalyst.

Figure 6.38.: Comparison between microtubes with and without additional catalysts and in a reactro scale-up. Potentials were IR-drop compensated. The experimental conditions were: 50 mM Na_2SO_4, pH 3, 0.5 bar_g O_2 in dead-end mode.

was reduced to H_2O. A quinone-based catalyst, on the other hand, enabled operation at a higher current efficiency of 75% compared to the gold catalyst. The general viability of the catalyst-coated gas diffusion electrodes in a scale-up reactor was shown and the importance of the liquid flow rate was highlighted. However, the CE of the gas diffusion electrode was diminished in contrast to test electrodes, which were only supplied with oxygen via the electrolyte. This observation led to the conclusion that the microtubes were not suitable for a gas diffusion operation. Thus, in a next step, the microtubes were fabricated with hydrophobic PTFE as binder to overcome limitations of flooding and mass transport. Section 6.3.2 demonstrated that the incorporation of PTFE is essential in order to achieve a stable long-term performance of the microtube gas diffusion electrodes. The influence of the sintering temperature after PTFE-addition did not show a strong influence on the electrochemical performance. Even though the BET surface was decreased with the PTFE binder, the polymer-containing microtubes could outperform the one without, especially in a long-term operation and at high current densities. It was shown that the concentration of oxygen in the electrolyte was not relevant, as long as sufficient oxygen was supplied via the gas side. Excellent current efficiencies between 80 and 90% were achieved, even if synthetic air was used instead of pure oxygen. The high current efficiencies were obtained at current densities up to $14\,\mathrm{mA\,cm^{-2}}$.

6.4. Conclusion and Outlook

In this chapter, planar and tubular electrode geometries were investigated for their ability to synthesize H_2O_2 at high current densities and efficiencies. In Section 6.2 *Planar Electrodes* it was shown that a commercially available microporous layer (MPL) can yield high current efficiencies of approximately 80% over a wide range of current densities. However, at about $70\,\mathrm{mA\,cm^{-2}}$, a decrease in current efficiency was observed, which was attributed to the non-sufficient

availability of of oxygen at the active sites caused by a too low gas flow rate. In agreement with work in the field of electrochemical CO_2 reduction [Jean2018], it was shown that the stoichiometric excess of the gaseous reactant should be above 2. The gas supply strategy — dead-end or cross-flow — was shown to be very important for the current efficiency. The dead-end mode showed a superior performance; however, care must be taken not to supply too much gas. The appliance of a pressure gradient in the cross-flow mode could potentially overcome the shortcomings of the dead-end mode [De M2019]. In the studied *Re*-number range, an increase in liquid flow-rate lead to a decrease in overpotential. This effect is ascribed to the improved mass-transport. The coating of the MPL with the organic catalyst ethylanthraquinone showed an increased current efficiency. However, simultaneously the energy efficiency decreased due to an increased ohmic resistance of the coating. In Section 6.3 *Tubular Electrodes*, microtubes based on carbon nanotubes were investigated. Different catalysts (gold, graphene oxide, ethylanthraquinon) were investigated. Compared to the state of the art in literature [Gend2014b; Roth2016], the current efficiency could be increased significantly up to 80-90%. However, the strongest effect on the current efficiency was not achieved by changing the catalyst. It was achieved with the incorporation of PTFE in the CNT network as hydrophobic binder. The polymer ensured open pores for an effective gas supply to the GDE surface. As outlook, the PTFE-containing microtubes were impregnated with a moderately reduced graphene oxide catalyst provided by Kim et al. [Kim2018]. The catalyst increased the activity for ORR significantly. Further, an all-tubular reactor with a tubular membrane was introduced, which can be used in future in different processes, e.g., an electro-Fenton process. Even though current efficiency of the tubular system was tremendously increased compared to the work of Gendel et al. [Gend2014b], the microtubes are at a lower technical maturity than the commercially available carbon-based microporous layers. In the next chapter the planar system will be investigated for electro-Fenton reactions, as it is more mature and facilitates higher reaction rates. Nonetheless, the tubular system may provide opportunities in future

for new reactor designs.

Acknowledgements R.K. thanks Jan-Bernd Vennekötter for many fruitful discussions and H.W. Kim for supplying the mrGO catalyst. Marcel Welz, Daniel Bell, Julia Weyand, Hannah Rosenthal, and Sebastian Holtwerth are acknowledged for their experimental support.

7. Electro-Fenton Reactors for Cellobiose Depolymerization

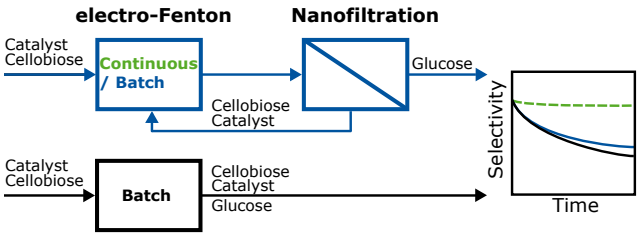

Parts of this chapter have been published as:
Robert G. Keller, Julia Weyand, Jan-Bernd Vennekoetter, Johannes Kamp, Matthias Wessling *An electro-Fenton process coupled with nanofiltration for enhanced conversion of cellobiose to glucose*,
Catalysis Today, 2021
DOI: 10.1016/j.cattod.2020.05.059

7.1. Introduction

The so-called *electrobiorefinery* represents the electrification of biorefineries: in a synergetic fashion, renewable electricity drives electrochemical reactors in which biomass and its constituents and derivatives are converted to value-added products [Harn2018]. Fenton's chemistry is part of biomass degradation in the natural environment [Aran2011], and has been shown to degrade cellulose and cellobiose to low molecular weight compounds such as glucose [Kwon2012; Hall1965]. The electrification of the Fenton process is called *electro-Fenton*, as described in Section 2.2.4. Based on the studies for the degradation of cellobiose via Fenton's chemistry in Chapter 5 and the planar electrochemical reactor in Chapter 6, this chapter combines electrochemistry, Fenton's chemistry, and cellobiose conversion. Additionally, an in situ separation strategy is presented.

Even though studies exist for the conversion of cellooligomers to glucose via the electro-Fenton or other OH radical generating processes, most of them cleave long-chained polymers [Wang2011; Meng2011; Yang2014; She2015]. On the one hand, long-chained polymers are the substrate, which should ultimately be used in a biorefinery process. On the other hand, the use of cellobiose simplifies analytics, and can enable a higher experimental throughput. Wang et al. [Wang2011] employed an electro-Fenton process with graphite/PTFE electrodes modified with 2-ethylanthraquinone. During the experiment, the degree of polymerization of cellulose decreased steadily and soluble sugars and 5-hydroxymethylfurfural were detected with yields of up to 10% and 6%, respectively. Kwon et al. [Kwon2012] simplified the approach to gain a deeper understanding of the kinetics and mechanism of the radical catalyzed degradation. Cellobiose was used instead of long-chained cellulose. The Fenton process was compared to the degradation by electrochemically generated acid and OH radicals via a boron doped diamond (BDD) electrode. Cellobiose degradation follows a first-order reaction with varying activation energies for either acid or radical promoted degradation. The selectivity in the

Fenton-catalyzed process was below 30% for all temperatures and H_2O_2 concentrations that were tested. Studies with the BDD electrode clearly showed that the OH radical degrades glucose further to organic acids and aldehydes, as the radical is not selective [Kwon2012]. Related approaches include the electrochemical degradation of cellulose with lead anodes [Meng2011] or oligosaccharides with manganese dioxide modified electrodes [Yang2014]. Meng et al. [Meng2011] reported low soluble sugar yields of 2.5%, which is in agreement with the low yields of the studies reported above [Wang2011; Kwon2012]. Interestingly, Yang et al. [Yang2014] found up to 100% selectivity with the MnO_2 electrodes, which may be attributed to the specific adsorption of cellooligomers with the β-1,4-glycosidic bond on the electrode. This reaction, however, is surface limited in comparison with a homogeneous electro-Fenton process and, therefore, not as effective with non-soluble cellulose.

Because of the unselective nature of the OH radicals, in situ separation strategies may help to increase the glucose yield [Kwon2012] and can enable a continuous process [Ocha2016]. Membrane reactors increase the product yield when small products are separated from oligomers, e.g., during the oxidative depolymerization of lignin [Bawa2018]. A continuous Fenton process requires the retention of the catalyst (e.g., Fe^{2+} or Fe^{3+}) and the acid in the reactor. The acid is usually added to keep the pH at a value below or at 3 in order to prevent iron precipitation [Pign2006]. In electro-Fenton processes, the supporting electrolyte should additionally be retained. Nowadays, not many concepts exist to achieve this goal: the acid is often neutralized and iron is removed, e.g., by precipitation, which leads to high process costs [Robl2018]. Robles et al. [Robl2018] report an electro-Fenton process where the acid and iron are retained by an ion exchange resin in a cyclic process. Roth et al. [Roth2016] describe a process where the electro-Fenton step is coupled with adsorption in a cyclic manner. Another strategy is the use of a heterogeneous electro-Fenton process, in which iron is immobilized on the electrode which enables neutral pH values [Rahi2014]. In this case, however, the reaction is limited to the electrode surface. A promising approach for the retention of the

iron catalyst in the Fenton reactor was presented by Ochando-Pulido et al. [Ocha2016], who demonstrated the potential of nanofiltration membranes to retain the iron catalyst of a Fenton process with a rejection close to 100%. Additionally, nanofiltration membranes are well-known for the separation of sugars [Shi2013; Feng2009]. In this study, in addition to the retention of catalyst and acid, glucose should be separated from the reaction vessel to avoid further degradation. Appendix A.2 gives a detailed background of separation of ionic mixtures containing mono- and disaccharides.

This chapter reports the depolymerization of cellobiose to glucose in an electro-Fenton reactor, which is coupled with a nanofiltration membrane module to increase the selectivity towards glucose. In a first step, the performance of the electrochemical reactor for the Fenton-aided degradation of cellobiose is investigated. The plate and frame reactor features a gas diffusion electrode for efficient electrochemical H_2O_2 synthesis, which was described in detail in Chapter 6. Different experimental parameters such as applied potential, substrate concentration, and catalyst concentration were varied to obtain high rates and a high selectivity towards glucose. Subsequently, a layer-by-layer nanofiltration membrane module was fabricated and coupled with the electrochemical reactor, in order to increase the selectivity towards glucose. The in situ membrane separation retains catalyst and cellobiose while glucose permeates. The potential of the coupled process is investigated experimentally and with a modeling approach.

7.2. Experimental

All error bars reported in this chapter represent the standard deviation of experiments, which were conducted at least in duplicate.

7.2.1. Electrochemical Reactor

A self-made electrochemical plate and frame reactor was used for the electro-Fenton process, as described in Section 6.2.1. The reaction system was operated either with or without a nanofiltration membrane module. A process sketch is depicted in Figure 7.1. As catholyte, a 100 mM Na_2SO_4 supporting electrolyte (Honeywell Fluka, >99%) was prepared with deionized water and the desired concentration of the catalyst $FeSO_4 \cdot 7\,H_2O$ (Sigma-Aldrich, >99%). The pH was adjusted to 3 with H_2SO_4 (Carl-Roth, 98%). D-(+)-cellobiose (Sigma-Aldrich, >99%) and glucose (Merck) were dissolved in the desired concentrations. Glucose was only added in two experiments: to determine its stability against H_2O_2 and its degradation kinetics via Fenton's chemistry. The catholyte and anolyte were temperature-controlled to 25 °C via jacketed feed tanks, which were cooled with a Julabo F25-ME thermostat and continuously stirred. The catholyte volume was either 80 mL for electro-Fenton experiments without the coupled membrane process or 275 mL with the coupled membrane process. The anolyte volume was always 60 mL for which deionized water was adjusted to pH 2.5 with sulfuric acid (Carl-Roth, 98%). Anolyte and catholyte were recirculated at $40\,mL\,min^{-1}$ with a peristaltic pump (Cole-Parmer, ISM831C). A pH probe from Metrohm (Unitrode) was used to monitor any changes in the catholyte. Oxygen (Westfalen, 99.95%) was supplied with 20 mL/ min to the cathode in dead-end mode via a gas flow meter (Wagner Mess- und Regeltechnik, WAKS-SVES). For the experiments with the coupled nanofiltration membrane module, the catholyte was additionally pumped through the membrane module with 45 mL/ min retentate flow controlled by a flow meter (Bronkhorst, M14 & C5I). The transmembrane pressure (TMP) was adjusted by increasing the speed of rotation of the recirculation pump (Cole-Parmer, ISM405A) until a TMP of 2 bar was reached. The pressure was monitored and recorded with a pressure sensor (WIKA, P-31). The permeate was collected in a vessel and the increase in permeate weight was recorded via a scale (Sartorius, AX6202).

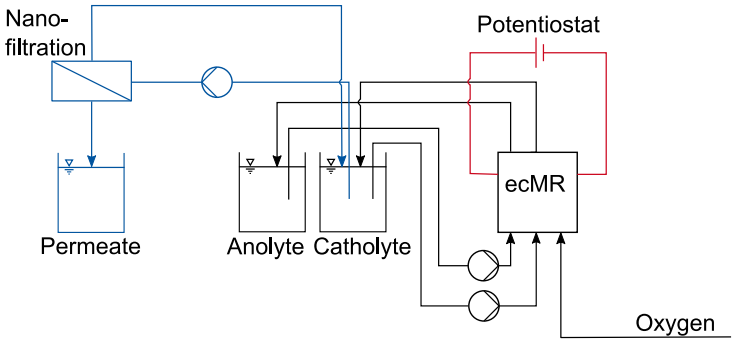

Figure 7.1.: A sketch of the electrochemical membrane reactor (ecMR) coupled with a nanofiltration stage.

7.2.2. Electrochemical Methods

A PGSTAT302N from Metrohm was used for all electrochemical experiments. As reference electrodes, a self-made Ag/AgCl in 3 M KCl reference electrodes and a Hg/Hg_2SO_4 in 0.5 M H_2SO_4 (Meinsberg) were used. The reference electrodes were directly connected to the catholyte compartment via a small hole in the cell structure. All potentials in this work are reported vs. Standard Hydrogen Electrode (SHE). Prior to and after each experiment, cyclic voltammetry (CV) measurements from $-0.35\,V$ to $1.5\,V$ vs. SHE were performed as pre- and post-treatment to activate and clean the GDE. A constant potential of $-0.8\,V$, $-1.2\,V$, $-2\,V$ or $-3\,V$ vs. SHE was applied was applied for H_2O_2 synthesis and cellobiose degradation experiments without a downstream membrane separation. Considering the high selectivity of the chosen electro-catalyst over a wide range of potentials, the constant current mode enables a controlled H_2O_2 production rate and thus theoretically a steady cellobiose degradation and glucose production. A constant current is thus potentially more attractive for an in situ separation with constant flux. The constant current mode was consequently applied during the cellobiose degradation

experiments with combined downstream membrane separation.

7.2.3. Hydrogen Peroxide and Iron Quantification

The H_2O_2 concentration was determined as described in Chapter 5. A method for simultaneous iron(II) and iron(III) detection via UV/Vis spectroscopy was introduced by Harvey et al. [Harv1955]. With the help of this method, the total iron concentration can be measured at 396 nm. Fe^{2+} shows a peak at 512 nm, Fe^{3+} absorbs weakly at this wavelength. Through an iteration, the individual concentrations can be obtained. The UV-Vis measurements were performed with a Genesys 10S UV-Vis spectrophotometer (Thermo Fisher Scientific). This method was used for the experiments with the hollow fiber membranes. For the experiments with flat sheet membranes, the retention of iron was calculated with the help of calibration curves for the conductivity and pH value of an acidic ferrous iron solution. The accuracy of the method was validated via ICP-OES measurements and the maximum deviation was approximately 10%.

7.2.4. Sugar, Organic Acid and Salt Quantification

The concentration of cellobiose, glucose and formic acid was analyzed via HPLC as described in Chapter 5. Sodium and sulfate were additionally determined via HPLC with the parameters listed in Tables 7.1 and 7.2. Prior to analysis, the samples were quenched with Na_2SO_3 to eliminate excess H_2O_2, as described in Chapter 5. Each sample was filtered with a 0.45 µm regenerated cellulose syringe filter.

Table 7.1.: HPLC parameters for sodium.

Parameter	**Value**
System	Agilent Technologies, Series 1100
Column	Metrosep C4 250 mm x 4 mm
Eluent	1 mM oxalic acid + 1.2 mM HNO_3
Eluent flow rate	1.4 mL/min
Temperature column oven	35 °C
Detector type	Conductivity detector (CD) Shodex CD-5
Temperature CD	45 °C

Table 7.2.: HPLC parameters for sulfate.

Parameter	**Value**
System	Agilent Technologies, Series 1200
Column	PRP X100 125 mm x 4 mm
Eluent	2 mM $C_8H_5KO_4$ pH 6 with KOH
Eluent flow rate	1.2 mL/min
Temperature column oven	30 °C
Temperature autosampler	20 °C
Wavelength VWD	280 nm

7.2.5. Membrane Characterization

Flat Sheet Membranes

Commercially available flat sheet membranes and self-fabricated layer-by-layer membranes were tested for the retention of cellobiose, glucose and iron. For the NF experiments, a model solution was used containing 10 mM of glucose (Sigma-Aldrich, >99.9%), 10 mM of cellobiose (Sigma-Aldrich, >99%) and 3.33 mM of $FeSO_4 \cdot 7\,H_2O$ (Sigma-Aldrich, >99%). The solutions were prepared with deionized water. The pH of the aqueous solution was adjusted to 3 with concentrated H_2SO_4 (Carl Roth). Nitrogen gas from Westfalen was used to generate the feed pressure. For the LbL assembly, two polyelectrolyte solutions were prepared. PDADMAC (Sigma-Aldrich) with an average high molecular weight of $400 - 500$ kDa was chosen as the polycation and PSS (Sigma-Aldrich) with an average molecular weight of 1000 kDa as the polyanion. The coating solutions of each polyelectrolyte was $1\,g\,L^{-1}$ (PE) with 0.25 M NaCl (Sigma-Aldrich, >99.5%) in deionized water. The investigated membranes and their properties are listed in Table 7.3. The hydrophilic NF270 from Dow Filmtec is a polyamide (PA) based thin-film composite NF membrane [Dow]. The isoelectric point is at pH 3.2, and the PWP is >10 LMH/bar [Dalw2011a]. NP010 and NP030 are both hydrophilic NF membranes produced by Microdyn-Nadir with polyethersulfone (PES) as the active layer material. NP010 has a sodium sulfate retention of 35 % to 75 %, and the PWP is >5 LMH/bar, while NP030 has a retention of 80 % to 95 % and a PWP >1 LMH/bar [Micra; Micrb]. The GE membrane is a dense composite UF membrane from GE Osmotics with an $MWCO = 1000\,Da$. Bargeman et al. [Barg2005] reported a PWP of 0.9 LMH/bar. The US100 from Microdyn-Nadir is a hydrophilic polysulfone (PSUH) based UF membrane with a PWP > 100 LMH/bar and a nominal MWCO of 100 kDa [Micrc]. It was used as the support membrane for the self fabricated PE membranes. Prior to the use for the NF experiments, each membrane was immersed in deionized water for at least 24 h. After the filtration experiments, the

membranes were rinsed and stored in deionized water.

A dead-end cell with a maximum capacity of 2 L was used for filtration experiments. A metal sinter plate acts as the support for the membrane. The membrane has an effective membrane surface area of approximately 135 cm^2. The stainless steel test cell is equipped with a retentate valve and a permeate valve to take samples. The collected permeate was recorded with a balance during filtration. The feed side of the system was compressed by N_2 to apply a TMP of up to 30 bar. The TMP was regulated with an analogous pressure regulator (Linde) and the pressure relief valve of the cell. The solution was mixed with a magnetic stirring bar which was installed inside the cell just above the membrane surface. The gap between the stirring bar and the membrane was approximately 1 cm. The suspended stirring bar had a length of 7 cm and a diameter of 1.2 cm. All experiments were performed at ambient temperature. The TMP was set to 9 bar the initial feed volume was 1.5 L. The feed solution in the batch filtration cell was continuously mixed with a magnetic stirring bar at 250 rpm. A retentate sample was taken with each collected permeate sample. The samples were taken at every 100 g of permeate. The filtration experiments were performed up to a permeate yield of 50%, which is defined in eq 7.1. In this case, the figures of merit can be plotted in dependence of the the so-called *permeate yield* γ

$$\gamma = \frac{V_{permeate}}{V_{initialfeed}} \tag{7.1}$$

where $V_{permeate}$ is the accumulated permeate volume and $V_{initialfeed}$ the initial feed volume. Due to a dead-zone in the long retentate pipe, the first approximately 18 mL of the retentate were discarded before a retentate sample was taken. Between every two permeate samples, the flux was measured via a scale. Before and after the retention experiments, the pure water permeability was measured. In addition to the commercially available nanofiltration membranes, self-fabricated layer-by-layer polyelectrolyte membranes were tested. The polyelectrolyte coating experiments were performed with a self-

Table 7.3.: Properties of the investigated commercial flat sheet membranes.

Name	**NF270**	**NP030**	**NP010**	**GE-GE**	**US100**
Supplier	Dow Filmtec	Microdyn-Nadir	Microdyn-Nadir	GE Osmotics	Microdyn-Nadir
Structure	TFC	-	-	-	-
Active layer	PA	PES	PES	-	PSUH
PWP [LMH/bar]	>10	>1	>5	0.9	>100
MWCO [Da]	200-400	500–600	1000–1200	1000	100,000
pH range [-]	2–11	1–14	1–14	-	1–14
References	[Dow] [Dalw2011a] [Moha2015]	[Micrb]	[Micra]	[Barg2005]	[Micrc]

constructed cell, shown in Fig. 7.2. The cell, which was a four-end-module, consisted of two casings made of poly(methyl methacrylate) (PMMA) with an outer diameter of 200 mm and a total height of 60 mm. A membrane disc with a diameter 156 mm was mounted on top of a circular metal sinter plate. The process scheme is illustrated in Fig. 7.2. The PE coating was applied via an OSMO Inspector 2 (Convergence).

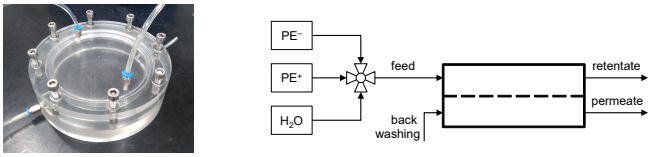

Figure 7.2.: Picture of the PE coating cell and process scheme of the PE coating

Before the membranes were coated with polyelectrolyte, they were flushed three times for 15 min with deionized water to ensure the complete removal of any impurities on the membrane surface. The procedure of coating a bilayer of a cationic and anionic PE was as follows: First, the wetted membrane was rinsed at $2.5\,\mathrm{L\,h^{-1}}$ for 5 min with the polycation solution. Thereafter, the dead-end permeation of the polycation solution was applied at a constant volume flow of $0.45\,\mathrm{L\,h^{-1}}$ for 10 min. Here, the PE was sterically rejected and adsorbed at the membrane surface. Afterwards, the membrane surface was flushed with deionized water to remove the excess and loosely-bound PEs on the membrane surface. Subsequently, the PWP was identified during filtration with deionized water at a constant volume flow of $0.45\,\mathrm{L\,h^{-1}}$ for 15 min, while the TMP was measured and reached a steady state value. These steps were repeated with the polyanion solution.

Hollow Fiber Membranes

Ultrafiltration hollow fiber membranes made of sulfonated polyethersulfone (Pentair X-Flow) were coated with three bilayers of polydiallyldimethylammonium chloride (PDADMAC) and poly-4-styrene sulfonate (PSS) in dead-end mode as described by Menne et al. [Menn2016a]. The polyelectrolyte concentrations of PDADMAC and PSS were 1 g/L and 0.25 M NaCl was added additionally. During the coating time of 10 min a flux of 30 $L/(m^2\,h)$ was applied. Each module consisted of ten membranes with an inner diameter of 0.8 mm each (total membrane surface area: 0.0101 m^2). The membrane module was characterized at a constant cross flow of 40 mL/ min and by adjusting the retentate pressure, similar to Menne et al. [Menn2016b]. Retentate and permeate were recycled to the feed tank. In order to determine the retention of the membrane for cellobiose, glucose, iron, sodium, and sulfate, a model solution with 100 mM sodium sulfate, 10 mM cellobiose, 5 mM glucose, and 5 mM iron at pH 3 (adjusted with sulfuric acid) was tested. The experiment was performed twice, once with Fe^{2+} and once with Fe^{3+} ($FeCl_3 \cdot 6\,H_2O$, 97%, Sigma-Aldrich) in the solution. The membrane retention for the salt solutions was tested at 1, 2 and 3 bar TMP. The steady-state of the system was determined via changes in conductivity of the feed, retentate and permeate stream with a conductivity meter (Mettler-Toledo, SevenCompact S230). After a steady state was reached at 1 bar, samples were taken from all three streams. Samples at 2 and 3 bar were taken about an hour after the retentate pressure had been increased.

7.2.6. Calculation

In this chapter, experimental data are fit to model equations describing the electro-Fenton process. The experimental data for cellobiose and glucose degradation were fitted to kinetic rate constants with python using the package "scipy.optimize" with the function "curve_fit". A simplified first-order model for the kinetics was applied, as, e.g., the

concentration of OH radicals was not measured in this work. Similar first-order approaches have been used in literature and are reasonable, as, e.g., the OH radical concentration is often at a low, steady-state value [Nidh2012; Liu2007]. The cellobiose and glucose degradation are described with the equations

$$\frac{\mathrm{d}c_{cello}}{\mathrm{d}t} = -k_1 c_{OH1} c_{cello} \tag{7.2}$$

$$\frac{\mathrm{d}c_{glu}}{\mathrm{d}t} = -k_2 c_{OH2} c_{glu} \tag{7.3}$$

$$\frac{\mathrm{d}c_{glu}}{\mathrm{d}t} = -k_2 c_{OH2} c_{glu} + 2sk_1 c_{OH1} c_{cello} \tag{7.4}$$

with c_{cello} and c_{glu} as cellobiose and glucose concentration, k_1 and k_2 as kinetic rate constants and c_{OH1} and c_{OH2} as hydroxyl radical concentrations. For the experiments, a first-order model was assumed with the sugar concentrations as the only variables. The product of the rate constant k_i and the OH radical concentration $c_{OH,i}$ can then be substituted by the apparent rate constant $k_{i,app}$ [Nidh2012]. equation 7.3 describes an experiment where only glucose is present, and Equation 7.4 describes the competing glucose formation and degradation when cellobiose is used as substrate. In general, the formation of two molecules glucose from one molecule cellobiose was assumed, and the selectivity was calculated according to Kwon et al. [Kwon2012], as described in Chapter 5. In the modeling equations the selectivity factor s was added, as it will be shown in the next sections that the ideal selectivity is never 100%, even at the beginning of an experiment. For the simulations of cellobiose degradation and glucose production, equations 7.2 and 7.4 were solved for systems without a membrane stage in Python using the "scipy.integrate" package with the function "odeint". For a system with membrane, the set of eqs 7.5–7.13 was solved with DAE tools (Sundials IDAS and LU solver), where $n_{cello,f}$, $n_{glu,f}$, $n_{cello,p}$, $n_{glu,p}$ and $n_{OH,f}$ are the molar amounts of cellobiose, glucose and OH radicals in the feed and permeate, with corresponding concentrations $c_{i,j}$. The apparent rate constants are $k_{i,app}$, R_{cello} and R_{glu} are the retentions for cellobiose and glucose and

V_f, V_p and $\dot{V}_p$ the feed volume, the permeate volume and the permeate volume flow through the membrane. The concentration of OH radicals was set to a constant concentration, similar to the simulations without a membrane, because the membrane is not likely to retain OH radicals due to their small size. A more detailed discussion will follow in the Results and Discussion section.

$$\frac{\mathrm{d}n_{cello,f}}{\mathrm{d}t} = -k_{1,app} n_{cello,f} - (1 - R_{cello}) c_{cello,f} \dot{V}_p \tag{7.5}$$

$$\frac{\mathrm{d}n_{glu,f}}{\mathrm{d}t} = -k_{2,app} n_{glu,f} + 2s k_{1,app} n_{cello,f} - (1 - R_{glu}) n_{glu,f} \dot{V}_p \tag{7.6}$$

$$\frac{\mathrm{d}n_{cello,p}}{\mathrm{d}t} = (1 - R_{cello}) c_{cello,f} \dot{V}_p \tag{7.7}$$

$$\frac{\mathrm{d}n_{glu,p}}{\mathrm{d}t} = (1 - R_{glu}) c_{glu,f} \dot{V}_p \tag{7.8}$$

$$\frac{\mathrm{d}V_f}{\mathrm{d}t} = -\dot{V}_p \tag{7.9}$$

$$\frac{\mathrm{d}V_p}{\mathrm{d}t} = \dot{V}_p \tag{7.10}$$

$$n_{OH,f} = c_{OH,f} V_f \tag{7.11}$$

$$n_{cello,f} = c_{cello,f} V_f \tag{7.12}$$

$$n_{glu,f} = c_{glu,f} V_f \tag{7.13}$$

7.3. Results and Discussion

7.3.1. Cellobiose Degradation via electro-Fenton

The planar reactor, which was tested for the electrochemical H_2O_2 synthesis in Section 6.2, was used to depolymerize cellobiose to glucose via the electro-Fenton process. Cellobiose was used as a well-defined model substance, which allows the study of the influence of different

reaction parameters on the selectivity towards glucose. Glucose was the main product in this study, and the aim was to find the best reactor conditions in order to achieve the highest possible selectivity. In a first step, the degradation of a solution of 8 mM cellobiose was studied at pH 3, with 100 mM Na_2SO_4 supporting electrolyte, and 5 mM $FeSO_4$ as homogeneous Fenton catalyst. Oxygen was fed to the GDE with $20\,mL\,min^{-1}$ in dead-end mode. The cellobiose concentration decreases continuously over the course of the experiment, as can be seen in Figure 7.3 a). Simultaneously, the concentration of glucose rises. However, it approaches a maximum and decreases again thereafter (Figure 7.3 a)). Even though glucose is formed by the degradation of cellobiose, it is also attacked by the OH radicals and degrades [Kwon2012]. Figure 7.8 b) shows the degradation of glucose with increasing reaction time in an electro-Fenton process. Kwon et al. [Kwon2012] also reported the over-oxidation of glucose due to the unselective nature of the radicals. Accordingly, C1 to C5 organic acids and aldehydes can be detected [Kwon2012]. In this chapter, formic acid was analyzed as product next to glucose. The concentration of formic acid increases continuously over the course of the experiment, see Figure 7.3 b). Compared to glucose, the overoxidation of formic acid to carbon dioxide is not as severe. Other authors reported a comparably high stability of formic acid under oxidative conditions, e.g., compared to aromatics [Mari2019; Kwon2012]. Similarly, the organic acids seem to be more stable than the sugars. The concentration of H_2O_2 increases at the beginning of the experiment, reaches a maximum and decreases again to approach a steady value, see Figure 7.3 b). The trend of the H_2O_2 concentration can be explained by competing reactions, which strive towards an equilibrium: While the concentration of H_2O_2 rises due to its synthesis, it is simultaneously consumed, see eqs. 2.16 and 2.17. As will be shown in the next sections, the concentration of ferrous iron undergoes significant changes (Fig. 7.18), which also influences the H_2O_2 concentration (eq. 2.16). Thus, it takes a while for the system to reach an equilibrium where H_2O_2 is synthesized as quickly as it is consumed.

H_2O_2 does not react with cellobiose without the iron catalyst, as

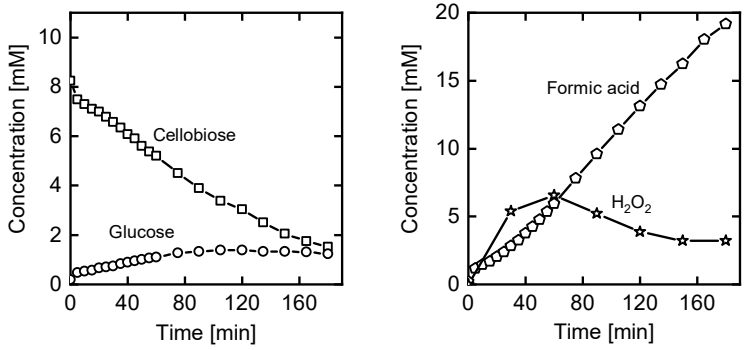

(a) Cellobiose degradation to glucose. **(b)** Formation of hydrogen peroxide and formic acid.

Figure 7.3.: Depolymerization of cellobiose via electro-Fenton. The experimental conditions were: -0.8 V vs. SHE, 100 mM Na_2SO_4, 5 mM $FeSO_4$, pH 3, 20 mL/min O_2.

can be seen in Figure 7.4 a). The H_2O_2 concentrations for the experiment without iron catalyst and cellobiose (pure H_2O_2 synthesis) and the experiment with cellobiose and without iron catalyst are the same. This is supported by blank experiments of cellobiose and glucose without iron catalyst, where each of the concentrations remains constant, which can be seen in Figure 7.5. This observation is strengthened by Kane et al. [Kane1992], who observed that H_2O_2 alone does not, or only at minimal rates, degrade cellobiose under acidic conditions. Another interesting observation is the change in pH value towards more acidic values over the reaction time once cellobiose and iron catalyst are added to the reaction, as can be seen in Figure 7.4 b). This change can be explained by the generation of organic acids, such as formic acid or oxalic acid via the degradation of cellobiose. Organic acids were also detected by other authors in the Fenton-catalyzed degradation of cellobiose [Kwon2012; Kane1992].

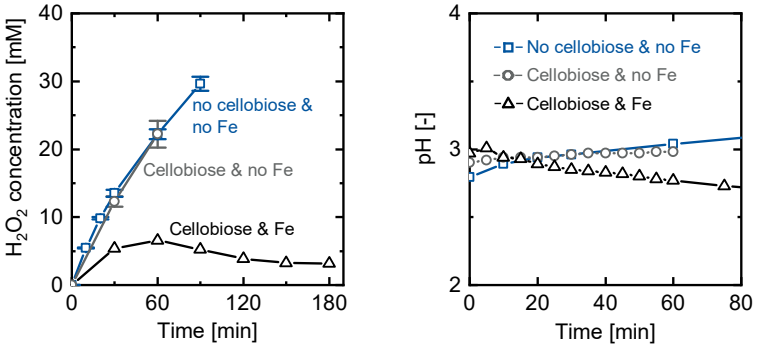

(a) H_2O_2 concentration evolution in the electrochemical reactor.

(b) pH evolution in the electrochemical reactor.

Figure 7.4.: Comparison of the H_2O_2 concentration and pH value in a system with iron catalyst and cellobiose to a system without iron catalyst and a system without iron catalyst and without cellobiose. The experimental conditions were: -0.8 V vs. SHE, 100 mM Na_2SO_4, pH 3, 20 mL/min O_2.

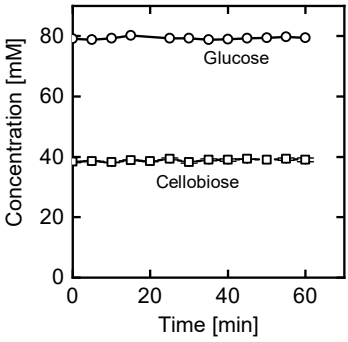

Figure 7.5.: Stability test of glucose and cellobiose in the electrochemical reactor without $FeSO_4$ as catalyst. The experimental parameters were: -0.8 V vs. SHE, 0 mM $FeSO_4$, 100 mM Na_2SO_4, pH 3.

Influence of Operating Parameters on the Glucose Selectivity

The following reaction parameters were analyzed for their influence on the selectivity towards glucose:

- catalyst concentration ($FeSO_4$)
- initial cellobiose concentration
- working potential

In Figure 7.6 a), it is apparent that the conversion rate of cellobiose increases with increasing ferrous iron concentration. This can be explained by eq. 2.16, as more radicals are generated when more iron is present. As the cellobiose concentration decreases with increasing reaction time, the probability of a glucose molecule being attacked by an OH radical increases. Degradation of organic compounds and cellobiose by OH radicals can be described by (pseudo-)first-order kinetics [Bril2009; Kwon2012]. Thus, if the concentration of one compound decreases, and the concentration of another increases, the rate of degradation of the second component will simultaneously increase. Consequently, the glucose concentration for the experiment with 5 mM ferrous iron reaches a peak after around 50 min. Subsequently, the concentration decreases again, see Figure 7.6 b), as the degradation rate exceeds the production rate. From the experiments with varying iron concentration two conclusions can be drawn: a higher Fe concentration leads to an increased reaction rate, but also to a glucose degradation at earlier times. Figure 7.7 a) shows the selectivity towards glucose of the electro-Fenton reaction for varying iron concentrations. The selectivity decreases over time, which can be expected from the previously discussed glucose concentrations. Even more, the selectivity towards glucose is low, even at the initiation of the reaction when the cellobiose to glucose ratio is high. From these results, it is hypothesized that there is an upper bound for the glucose selectivity that can obtained with the system presented in this work. Kwon et al. [Kwon2012] also found a selectivity for cellobiose

degradation towards glucose via the Fenton process below 30% in all experiments, whereas von Sonntag et al. [Sonn1976] found that only about 1/3 of the glycosidic bonds of cellobiose are cleaved by OH radicals. As both authors employed different operating conditions for the Fenton process, or even used radiolysis for the OH radical generation, a difference in the exact selectivity value is reasonable. However, both studies support the hypothesis of a limited selectivity. It may seem that higher selectivities can be reached if a low concentration of ferrous iron is used. However, the conversion of cellobiose, and thus the concentration of glucose is very low at early reaction times with low amounts of catalyst. Thus, the recorded selectivity in the first few minutes of the experiment for 1 mM catalyst is prone to measurement errors. In order to test the hypothesis, the depolymerization of cellobiose was investigated at different initial cellobiose concentrations at 5 mM iron concentration, see Figure 7.7 b). With increasing cellobiose concentration, an increased selectivity is expected, because cellobiose is in high excess of all other targets for OH radicals. However, even with a high initial cellobiose concentration, the selectivity always remains below 25%. As before, the selectivity decreases with increasing reaction time due to the decreasing cellobiose to glucose ratio.

In the next paragraphs, a simplified model will show that the trend of the selectivity towards glucose over time depends mainly on the cellobiose to glucose ratio. Individual experiments for cellobiose and glucose degradation (see Figure 7.8) were fitted to eqs. 7.2 and 7.3 in order to obtain the apparent rate constants for their degradation by OH radicals. The apparent rate constants were $k_{1,app} = 0.0193 \frac{1}{min}$ and $k_{2,app} = 0.0285 \frac{1}{min}$. The rate constants $k_{1,app}$ and $k_{2,app}$ are similar, which could be expected from the results shown so far. The apparent rate constants are further similar to other organics degraded by the electro-Fenton with comparable conditions [Bril2009]. The obtained rate constants were used to simulate the glucose formation by cellobiose degradation of an experiment with the same iron concentration and voltage as before (i.e., the same rate of H_2O_2 formation and Fe^{3+} reduction), now with eqs. 7.2 and 7.4. It is assumed that the selectivity s towards glucose is inherently limited to 0.25, which

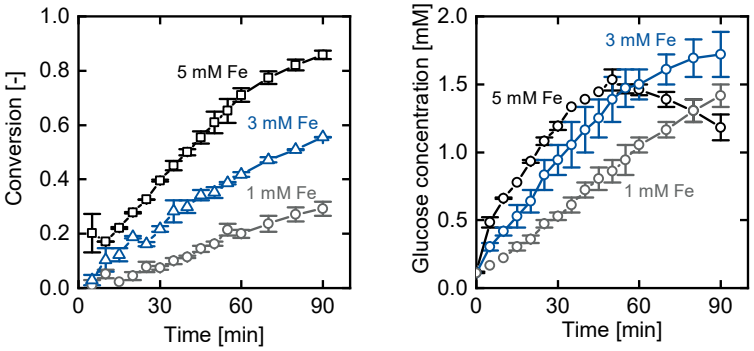

(a) Cellobiose conversion over time. **(b)** Glucose concentration over time.

Figure 7.6.: Depolymerization of cellobiose via electro-Fenton with different catalyst concentrations. Experimental conditions were: -2 V vs. SHE, 100 mM Na_2SO_4, pH 3, 20 mL/min O_2.

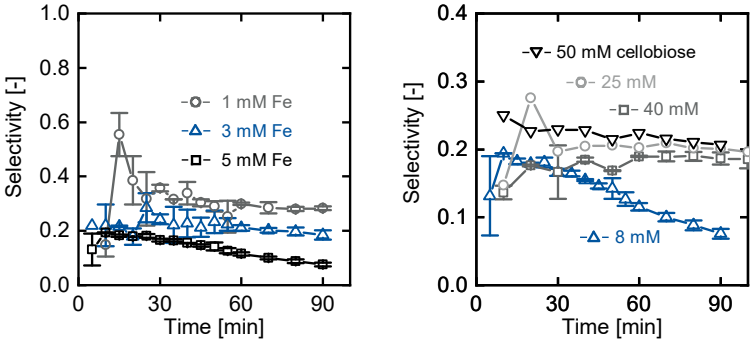

(a) Selectivity in dependence of catalyst concentration. **(b)** Selectivity in dependence of cellobiose concentration.

Figure 7.7.: Selectivity towards glucose of cellobiose depolymerization via electro-Fenton. Experimental conditions were: -2 V vs. SHE, 100 mM Na_2SO_4, pH 3, 20 mL/min O_2.

the results of this thesis suggest. As mentioned before, other authors also found an upper limit for glucose selectivity [Kwon2012; Sonn1976]. Figure 7.9 a) shows that the trend for glucose production is predicted accurately with small deviations (average deviation of the glucose concentration was <15%). In a next step, equal apparent rate constants for cellobiose and glucose degradation are assumed ($k_{1,app} = k_{2,app} = 0.0193\frac{1}{min}$). Figure 7.9 b) shows the results of the simulation, which deviate less from the experimental results. The average deviation of simulated cellobiose and glucose concentrations compared to the measured concentrations is approximately 10%. Of course, the individual apparent rate constants for glucose and cellobiose degradation obtained in individual experiments seem to be the natural choice. However, the simplified model used herein requires a new fit of the apparent rate constants every time, e.g., the current density is varied. As apparent rate constants for glucose degradation were not available for every experimental variation tested, equal apparent rate constants for cellobiose and glucose degradation are assumed. The influence of a higher apparent rate constant for glucose degradation will be discussed in the last section of the Results and Discussion. A rigorous model should incorporate all influencing parameters [Nidh2012; Liu2007]. However, the results of other studies, e.g., Liu et al. [Liu2007] cannot merely be transferred: for example, in contrast to Liu et al. [Liu2007], the H_2O_2 concentration does not strive towards a maximum in this work, but shows a more complex behavior. Also, as more and more degradation products are formed, these should be taken into account as OH radical sinks, which is often neglected. Another parameter is the oxygen concentration, which is correlated with the H_2O_2 production rate [Liu2007]. However, researchers have suggested that oxygen may also influence the degradation of cellobiose and cellulose [Schu1978; Carl2005]. Even though the advanced models provide a higher potential for an accurate description and a deeper understanding of the process, these models require many input parameters. Some of these parameters are difficult to measure, e.g., all side products of the reaction. This study shows that the simplified model can accurately describe the cellobiose and

glucose concentrations, which are the only parameters needed to calculate the main figure of merit, the selectivity. The model emphasizes the importance of a coupled membrane process and the importance of the cellobiose to glucose ratio for the selectivity.

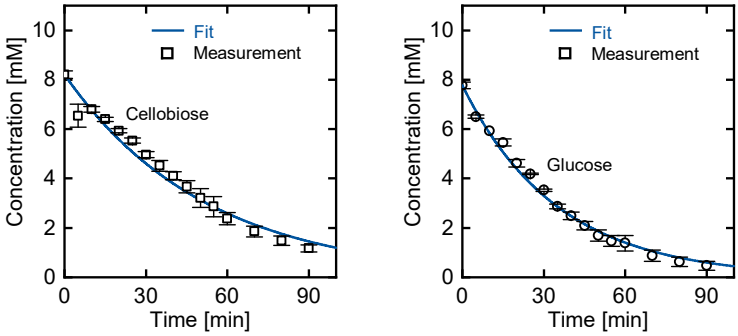

(a) Fit of cellobiose degradation kinetics. **(b)** Fit of glucose degradation kinetics.

Figure 7.8.: Fit of kinetic rate constants for cellobiose and glucose degradation. The experimental conditions were: -2 V vs. SHE, 100 mM Na_2SO_4, 5 mM $FeSO_4$, pH 3, 20 mL/min O_2.

It can be seen in Figure 7.10 a) that the simulation results for conversion and selectivity towards glucose fit well to the experimental data. Subsequently, different experimental results (varying potential, cellobiose and catalyst concentration) were plotted as selectivity over the ratio of cellobiose to glucose, see Figure 7.10 b). It is apparent that the selectivity strongly depends on the ratio of cellobiose to glucose, which is to be expected from the non-selective nature of OH radicals. This behavior is also predicted by the simulation (blue line). Even though it does not seem feasible to increase the selectivity above 25–30%, it is worthwhile to investigate whether the selectivity can be held constant at the highest possible level if an in situ membrane separation is applied.

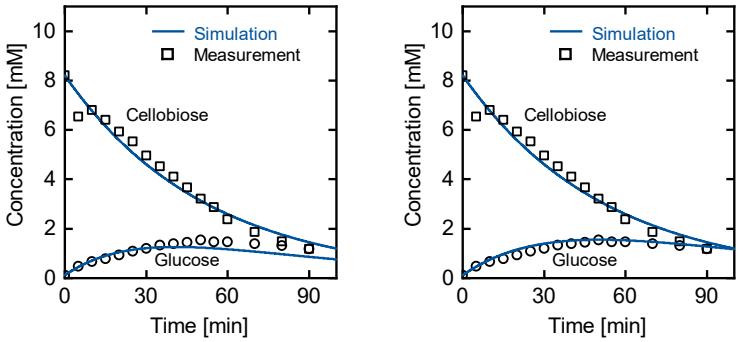

(a) Results obtained with individual kinetic parameters for glucose and cellobiose degradation.

(b) Results obtained with the same kinetic parameters obtained from cellobiose degradation.

Figure 7.9.: Simulation of glucose production with fitted kinetic parameters. The experimental conditions were: -2 V vs. SHE, 100 mM Na_2SO_4, 5 mM $FeSO_4$, pH 3, 20 mL/min O_2

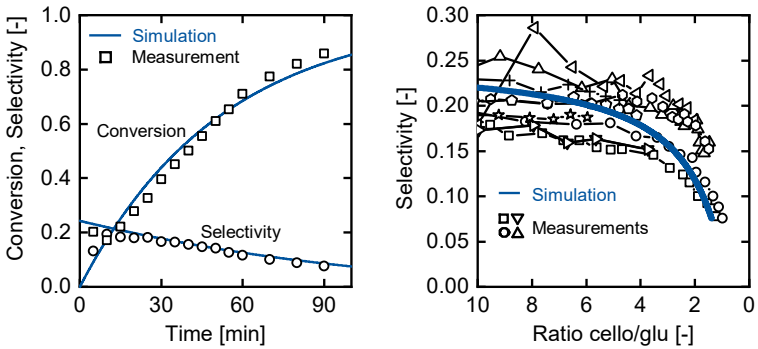

(a) Simulation of conversion and selectivity with fitted kinetic rate constants. The experimental conditions were: -2 V vs. SHE, 100 mM Na_2SO_4, 5 mM $FeSO_4$, pH 3, 20 mL/min O_2.

(b) All experimental results for cellobiose degradation plotted over the cellobiose to glucose ratio. The solid line represents a simulation.

Figure 7.10.: Simulation results of cellobiose degradation via E-Fenton.

7.3.2. Characterization of Nanofiltration Membranes

Flat Sheet Membranes

In order to find a suitable membrane for the in situ separation of glucose from the reaction solution, four commercially available and two self-made layer-by-layer polyelectrolyte flat sheet membranes were tested in a dead-end filtration. The NF270 membrane has a molecular weight cut-off of approximately 300 Da [Esca2014]. According to literature, the rejection for glucose is 97% for a 5.6 mM solution at 5 bar TMP [Barg2014]. However, the rejection of sugar solutions is also dependent on the concentration of the ionic species and decreases to less than 70% when NaCl is added to the solution [Barg2014]. Thus, the membranes were tested in a dead-end cell according to the specifications described in Section 7.2.5. Figure 7.11 a) shows the results for the retention of glucose, cellobiose and iron, whereas Figure 7.11 b) shows the permeability with increasing permeate yield. The rejection of cellobiose is approximately 96%, and the rejection of ferrous iron is 85%. These high values are desired for the targeted separation and in agreement with literature [Esca2014]. However, the rejection for glucose is also high with 85%, which is in between the values reported by Bargeman et al. [Barg2014] for a pure glucose solution and one where sodium chloride was added. In Figure 7.11 b) it can be seen that the permeability of the membrane decreases with increasing permeate yield. Due to the high rejection of the membrane, the osmotic pressure increases from approximately 0.5 bar at the beginning of the experiment to approximately 1.3 bar at the end of the experiment. However, even if the TMP is corrected for the osmotic pressure, the permeability is not constant. Mass transport limitations could lead to a decreased flux at high permeate yields [Barg2005]. Even though the selectivity $S_{glu:cello}$ (glucose to cellobiose) is approximately 4, the selectivity of $S_{glu:Fe}$ (glucose to iron) is 1 and thus, the solution cannot be separated as desired. The main results for the membrane characterization experiments are summarized in Table A.2 in the Appendix. The retention values and the permeability of the NP010

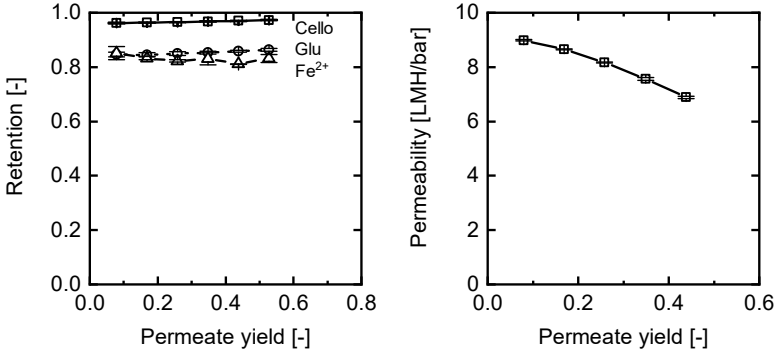

(a) Retention of cellobiose, glucose and ferrous iron as a function of permeate yield. **(b)** Permeability as a function of permeate yield.

Figure 7.11.: Characterization of the NF270 membrane. The experimental conditions were: 10 mM cellobiose, 10 mM glucose, 3.33 mM $FeSO_4$, 9 bar TMP, 250 rpm.

membrane are depicted in Figures 7.12 a) and b). The membrane does not show any significant rejection for cellobiose, glucose or ferrous iron. Even more, the retention for ferrous iron shows negative values, which are associated with the method to determine the iron rejection: small inaccuracies in the pH measurement can lead to high deviations if the rejection is close to zero. The measured PWP of 15 LMH/bar in Table A.2 is higher than provided by the manufacturer (PWP $>$ 5 LMH/bar, [Micra]), but in line with another report from literature [Nord2014]. Nordvang et al. [Nord2014] also reported a rejection of less than 20% for disaccharides for the NP010. Figure 7.12 b) shows that the PWP declines with increasing permeate yield and that the standard deviation is quite high. One reason for this observation could be internal fouling of the membrane. As the solutes are not retained, fouling in the pores may occur. Compared to the NP010 membrane, the NP030 is a tighter variation and thus, the retention values for the three solutes are higher, see Figure 7.13 a).

The retentions of cellobiose, iron, and glucose are 35%, 44%, and 18%, respectively. Consequently, the sugar selectivity $S_{glu:cello}$ is 1.3 and the iron selectivity $S_{glu:Fe}$ is 1.5, see Table A.2. Bargeman et al. [Barg2014] found a glucose rejection of <20% for a TMP of 5 bar and approximatley 30% for 10 bar, which is in a similar range (compare Table A.1). Thus, a separation of the solutes is theoretically possible. However, the losses of cellobiose and glucose would be high and, overall, higher rejections are desired. Additionally, the permeability and pure water permeability are low with 2.7 LMH/bar and 3.2 LMH/bar, similar to the values reported by Bargeman et al. [Barg2014]. The ultrafiltration membrane GE from GE Osmonics

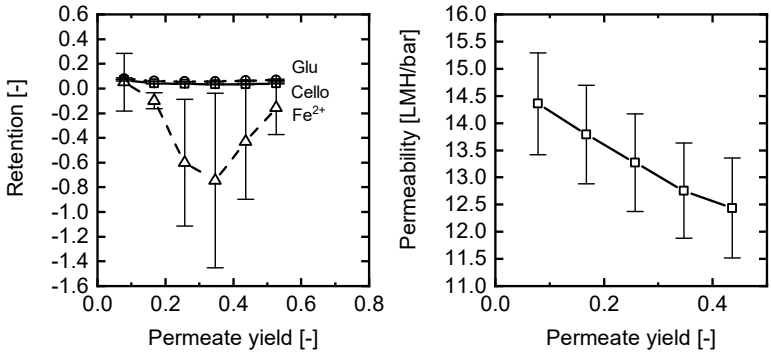

(a) Retention of cellobiose, glucose and ferrous iron as a function of permeate yield.

(b) Permeability as a function of permeate yield.

Figure 7.12.: Characterization of the NP010 membrane. The experimental conditions were: 10 mM cellobiose, 10 mM glucose, 3.33 mM $FeSO_4$, 9 bar TMP, 250 rpm.

exhibits a comparably high retention of 54% for cellobiose and 56% for ferrous iron, while glucose is retained to 26%, see Figure 7.14. Goulas et al. [Goul2002] reported a rejection of 8% for monosaccharides and 41% for dissaccharides. Even though these values are lower than the results in this study, they support the findings that the GE membrane can reject the sugars. The corresponding selectivity for

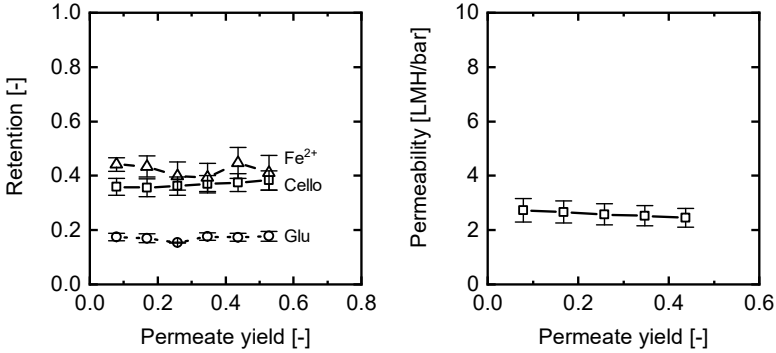

(a) Retention of cellobiose, glucose and ferrous iron as a function of permeate yield. **(b)** Permeability as a function of permeate yield.

Figure 7.13.: Characterization of the NP030 membrane. The experimental conditions were: 10 mM cellobiose, 10 mM glucose, 3.33 mM $FeSO_4$, 9 bar TMP, 250 rpm.

the sugar separation is 1.6, and for glu:iron 1.7. However, a very low permeability of 2.1 LMH/bar (2.58 LMH/bar PWP) is observed, see Figure 7.14 b). Bargeman et al. [Barg2005] reported an even lower PWP of 0.9 LMH/bar, which shows that the results of this work are reasonable.

Even though the commercially available membranes NF270 and NP030 are in general acceptable for the separation desired in this work, a tailor-made layer-by-layer membrane may yield better results. A high selectivity for glucose in relation with a dissaccharide was demonstrated by Shi et al. [Shi2013]. The selectivity could be varied by coating different numbers of bilayers. Similarily, Menne et al. [Menn2016a] were able to tailor the retention of bivalent salts. According to the procedure described in Section 7.2.5, a two-bilayer and a three-bilayer polyelectrolyte membrane were fabricated. The two-bilayer membrane is characterized by a high permeability of approximately 9.4 LMH/bar, as can be seen in Figure 7.15 b). At the

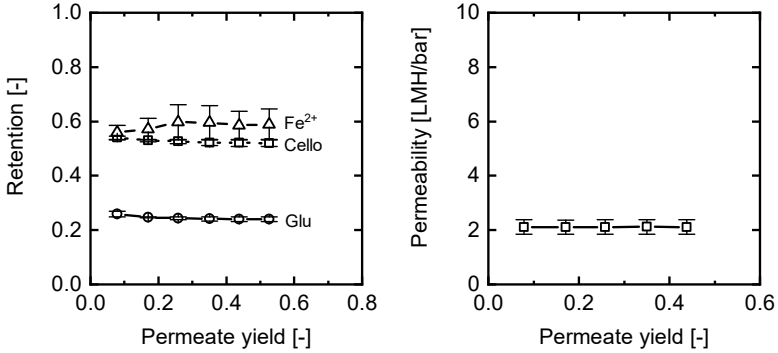

(a) Retention of cellobiose, glucose and ferrous iron as a function of permeate yield.

(b) Permeability as a function of permeate yield.

Figure 7.14.: Characterization of the GE membrane. The experimental conditions were: 10 mM cellobiose, 10 mM glucose, 3.33 mM $FeSO_4$, 9 bar TMP, 250 rpm.

same time, the cellobiose and ferrous iron retention is 54%, and the glucose retention is 26% (Figure 7.15 a)). The sugar and iron selectivity were both 1.7. Thus, even though this membrane has a higher flux than the commercially available NF270, NP010, NP030 and GE, the selectivity is not impaired. The permeability shows a relatively high standard deviation compared to the other membranes, see Figure 7.15 b). The two-layer membrane does not seem to have a perfectly homogeneous coating and its performance varies during the individual experiments. Thus, it is hypothesized that the layers were not sufficiently stable. Due to the circular membrane geometry a circular cell was designed for the membrane coating, see Figure 7.2. The fluid flow during coating and flushing was not distributed homogeneously. An additional bilayer increases the selectivity at the cost of the permeability, see Figure 7.16 and Table A.2. Also, the three-bilayer membrane exhibits a decreased standard deviation of the measured flux and retention and seems to be more stable. The PWP and the rejection of bivalent ions are comparable to previously pub-

lished results [Menn2016a]. Overall, the three-bilayer LbL membrane provides the highest selectivity towards iron ($S_{glu:Fe} = 1.7$) and the second highest selectivity towards cellobiose ($S_{glu:cello} = 2.2$) with a medium permeability. In a next step, this approach was transferred to a hollow fiber membrane, for which a reliable coating procedure has been established [Menn2016a].

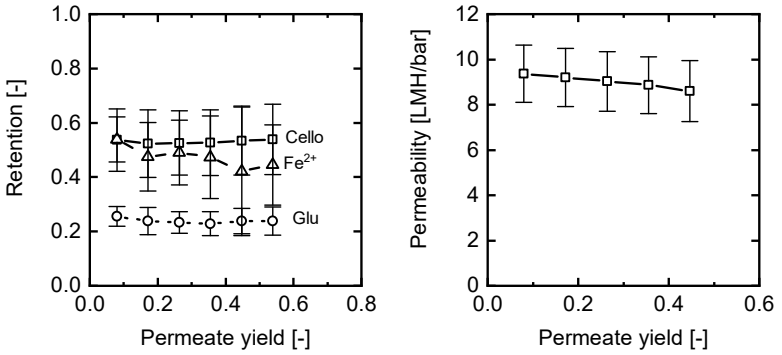

(a) Retention of cellobiose, glucose and **(b)** Permeability as a function of permeferrous iron as a function of permeate ate yield.
yield.

Figure 7.15.: Characterization of the two-bilayer polyelectrolyte membrane. The experimental conditions were: 10 mM cellobiose, 10 mM glucose, 3.33 mM $FeSO_4$, 9 bar TMP, 250 rpm.

Hollow Fiber Membranes

A layer-by-layer nanofiltration hollow fiber membrane was fabricated in house to facilitate the separation between cellobiose, glucose, and ferrous/ferric iron. The retention of cellobiose and iron catalyst, as well as the permeation of glucose to prevent over-oxidation were desired. The three-bilayer LbL membrane was characterized in constant pressure experiments as described in Section 7.2.5. Before the salt retention experiments, the pure water flux and permeability were

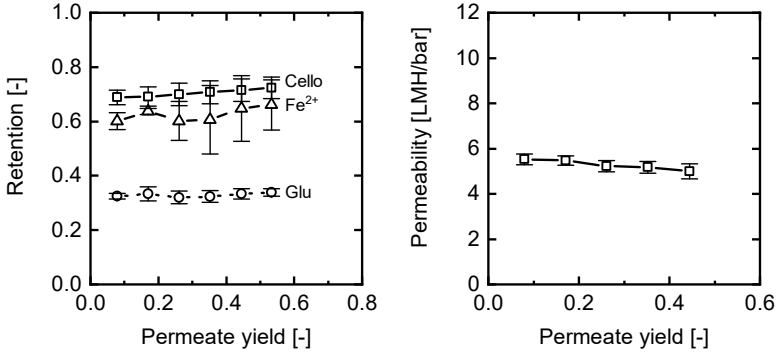

(a) Retention of cellobiose, glucose and ferrous iron as a function of permeate yield. **(b)** Permeability as a function of permeate yield.

Figure 7.16.: Characterization of the three-bilayer polyelectrolyte membrane. The experimental conditions were: 10 mM cellobiose, 10 mM glucose, 3.33 mM $FeSO_4$, 9 bar TMP, 250 rpm.

tested. The membranes had a pure water permeability of approximately 20 LMH/bar, which was constant in a TMP range of 0.5 bar to 3 bar.

The permeability was higher than in the original work by Menne et al. [Menn2016a]. One reason for this observation could be deterioration of the active membrane layer, because the membrane was stored for several months before use. However, the main figure of merit for this work is the retention of cellobiose, glucose, and iron, which was tested subsequently. As long as a satisfactory selectivity can be achieved, the high flux is even favorable. Figure 7.17 a) shows the results for the retention. It can be seen that cellobiose is retained to more than 90% when a transmembrane pressure of 2 bar is applied, and that the retention increases with increasing TMP as expected by theory [Meli2007, pp. 294–299]. Ions are retained due to the charge of the layer-by-layer membrane [Menn2016a]. Apparently, ferric iron is retained to a higher degree than ferrous iron. Even though the out-

ermost layer of the LbL membrane is a negative PSS polyanion layer, the interdiffusion of the polycation PDADMAC may overcompensate the negative charges and lead to a positive excess charge [Reur2018], or at least no excess negatively-charged PSS [Ghos2013]. However, there are also examples of the opposite, e.g., a three-bilayer PSS/PDADMAC membrane, which has a negative zeta potential at pH 5.5 [Mala2011]. Nonetheless, at pH 3 the surface charge will be different and other authors report that the zeta potential moves towards less negative values at decreasing pH values [Laak2015]. In general, the surface charge depends on many factors such as the concentrations in the deposition solution, the pH value, or the storage conditions [Reur2018; Adam2004; Aria2016]. In this case, it is hypothesized that the combined effects of Donnan-repulsion and the steric/diffusive hindrance of the hydrated iron ions lead to a strong rejection of Fe^{3+} and a lower rejection of Fe^{2+}. In contrast, glucose permeates quite well through the membrane due to its rather low molecular weight, i.e., the retention is 27% at 2 bar TMP. Thus, in terms of uncharged molecules, the membrane behaves as is to be expected: small, uncharged molecules permeate to a higher degree than large, uncharged molecules [Meli2007, pp. 305–306]. The selectivity of glucose over cellobiose is approximately 9 at 2 bar TMP, while the selectivity of glucose to ferrous iron is 2.7 and of glucose to ferric iron 4.9. In Figure 7.17 b), the retention of sulfate and sodium is depicted. Both are retained to a very low degree. It can be reasoned that this effect is due to the low charge and the size of sodium. Due to electro-neutrality conditions, sulfate has to permeate as well [Meli2007, pp. 290–294]. In order to understand the rejection of the ions in detail, especially in this multi-solute system, further investigations are necessary. Of course, retention of all salts would be desirable. An optimization of the coating procedure may lead to an increased retention [Menn2016a]. The permeability of the tested membrane was between 6 LMH/bar to 8 LMH/bar. The flux and selectivity of the membrane are thus superior to all tested commercially available membranes. It should be noted that a strong flux decline was observed towards the end of the rejection test with the ferric iron solution. Apparently, local

pH changes led to a precipitation of iron. In the electro-Fenton experiments described later, this phenomenon was not observed. The measured permeabilities and retentions for flat-sheet and hollow-fiber membranes are compiled in the Appendix in Tables A.2 and A.3.

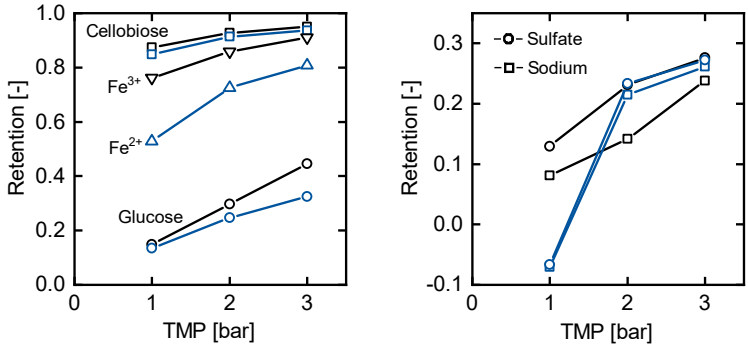

Figure 7.17.: Retention of cellobiose, glucose, Fe^{2+}, Fe^{3+}, Na^{+}, $SO_4{}^{2-}$. The blue and black curves represent two different experiments.

As shown, ferrous and ferric iron are retained to different degrees. It is thus of interest whether the iron is in its ferrous or ferric form during the degradation of cellobiose. Figure 7.18 shows that ferrous iron is oxidized to ferric iron in the first 10 min of an experiment at a constant current of -500 mA, which corresponds to approximately -2 V vs. SHE. After 10 min, more than 90% of the total iron are in the ferric form. The decrease of ferrous iron and increase of ferric iron is typical for an electro-Fenton reaction [Qiu2015]. On the one hand, this means that the membrane will perform well for iron retention. On the other hand, it also means that the reaction is limited by the reduction of ferric iron to ferrous iron. Additionally, it can be seen that some iron is lost throughout the reaction. At the beginning of the experiment, 5 mM of Fe^{2+} is present. After 10 min, the total iron amounts to approximately 4 mM.

In addition to iron precipitation, adsorption on the electrode can be a

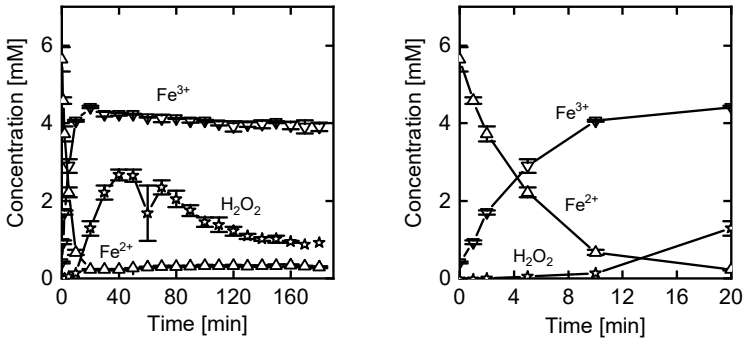

Figure 7.18.: Speciation of iron in an electro-Fenton reactor. The experimental conditions were: - 500 mA, 100 mM Na_2SO_4, 5 mM $FeSO_4$, pH 3, 20 mL/min O_2.

reason for the decreasing concentration, which has been described by other authors [Qiu2015]. Due to the high current density, the pH value increases in the vicinity of the electrode. A higher pH value leads to precipitation of iron [Pign2006]. In this study, no degradation of the membrane performance over time was observed. However, even if the radicals attacked the membrane, the layer-by-layer architecture would allow for the regeneration of the membrane properties [Menn2016b].

7.3.3. Electro-Fenton Coupled with Nanofiltration for In Situ Separation

In a next step, the nanofiltration membrane module was coupled with the electro-Fenton reactor. In order to directly compare a process with and without a membrane, experiments with increased feed volume were conducted. In the process with the membrane stage, the feed volume decreased continuously due to the permeation through the membrane. A constant current of -500 mA was applied to the cathode.

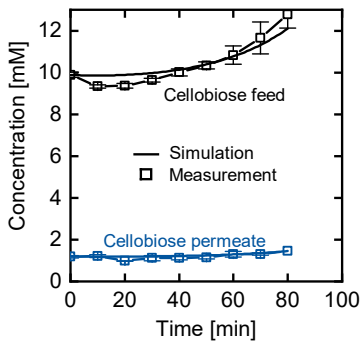

(a) Concentrations of cellobiose.

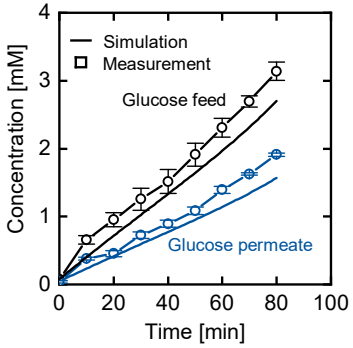

(b) Concentrations of glucose.

Figure 7.19.: Concentrations of cellobiose and glucose in the feed and permeate stream of the coupled electro-Fenton and nanofiltration process. The experimental conditions were: -500 mA, 100 mM Na_2SO_4, 5 mM $FeSO_4$, pH 3, 20 mL/min O_2, 2 bar TMP.

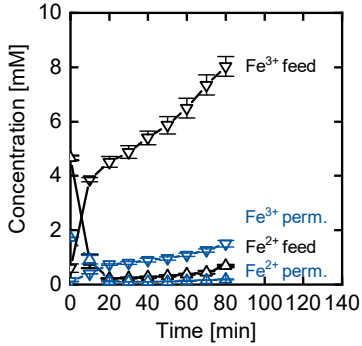

(a) Concentrations of ferric and ferrous iron.

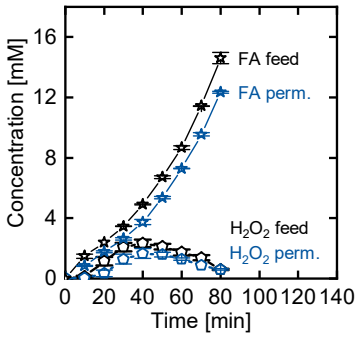

(b) Concentrations of formic acid (FA) and H_2O_2.

Figure 7.20.: Concentrations of iron, H_2O_2 and formic acid (FA) in the feed and permeate stream of the coupled electro-Fenton and nanofiltration process. The experimental conditions were: -500 mA, 100 mM Na_2SO_4, 5 mM $FeSO_4$, pH 3, 20 mL/min O_2, 2 bar TMP.

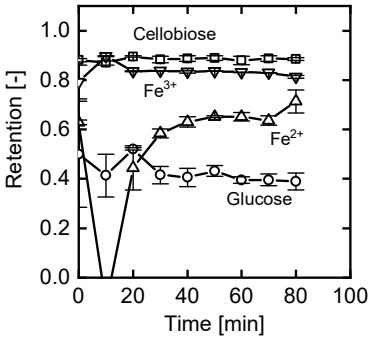

Figure 7.21.: Retention of cellobiose, glucose, ferrous and ferric iron in the coupled process of electro-Fenton and nanofiltration membrane. The experimental parameters were: -500 mA, 10 mM cellobiose, 5 mM $FeSO_4$, 100 mM Na_2SO_4, pH 3, 20 mL/min O_2, 2 bar TMP

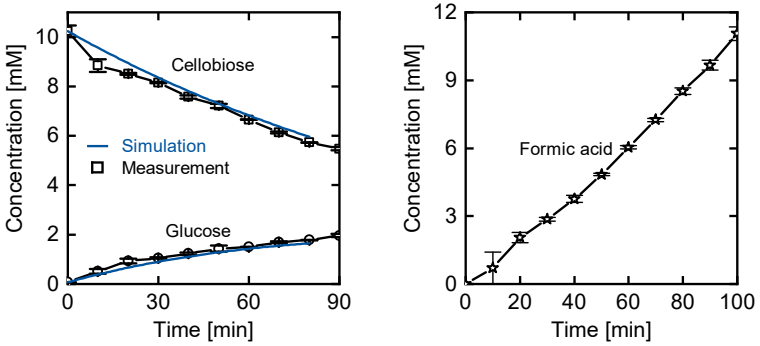

Figure 7.22.: Concentrations of cellobiose, glucose (a) and formic acid (b) in an electro-Fenton reactor. The experimental parameters were: -500 mA, 10 mM cellobiose, 5 mM $FeSO_4$, 100 mM Na_2SO_4, pH 3, 20 mL/min O_2.

Figures 7.19 and 7.20 show the cellobiose and glucose concentration in the feed and permeate as well as the concentrations of the iron species, H_2O_2, and formic acid. Compared to a process with the same current density, initial volume, and without nanofiltration membrane, see Figures 7.22 and 7.18, the cellobiose concentration in the feed remains high, due to the rejection of the membrane and decreasing feed volume. Likewise, the glucose concentration is higher in the system with coupled membrane. Ferric iron is the main iron species in the system, see Figure 7.20 a). As in the process without a coupled membrane (Figure 7.18), the initially present ferrous iron is oxidized in the first minutes of the process. Formic acid is a nearly not retained side product. Due to its small size and the low pH value, at which it is only partially dissociated, it can permeate through the membrane [Rege2018]. The H_2O_2 concentration approaches a maximum at about 40 min, after which it decreases again, see Figure 7.20 b), similar to the system without the membrane. The retention over time of cellobiose, glucose, ferrous and ferric iron in the coupled process is depicted in Figure 7.21. It can be seen that cellobiose and glucose are retained to similar levels as in the membrane characterization experiments, see Section 7.3.2. The ferrous iron retention is lower in the coupled process (R = 0.53) compared to the characterization experiments (R = 0.72), and the glucose retention is higher (R = 0.42 vs. 0.27). In the membrane characterization experiments, the entire system was in equilibrium. In the coupled degradation and filtration, however, the concentrations of all solutes vary over time. Additionally, the concentrations of ferrous iron and glucose are significantly different than in the membrane characterization. It is known that dynamic and changing concentrations affect the retention [Meli2007, pp. 294–295][Shi2013]. Still, the membranes retain cellobiose and ferric iron to a high degree, as desired, while glucose permeates. At the end of the here reported experiment, the glucose concentration reaches about 2 mM. This concentration is not high enough for an input stream of a fermentation in, e.g., a biorefinery. However, the glucose concentration could potentially be increased by an additional subsequent nanofiltration or even reverse osmosis step [Rege2018].

Alternatively, the cellobiose concentration could be increased, which would enable higher glucose concentrations in a continuous process. This will be discussed in the next paragraphs. Kinetic parameters were fitted in order to describe the changed experimental conditions. The experimental results could again be well described by the model, see Figure 7.22 a) and Figure 7.23 a). If a membrane is coupled with the process, the experimental results for the selectivity in Figure 7.23 b) show slightly improved values for the set-up with the membrane. The improved selectivity was confirmed by a simulation of the process with the coupled membrane (Figure 7.23 b)). For the simulation the cellobiose retention (R = 0.88) and glucose retention (R = 0.42) were adjusted compared to the membrane characterization experiments. The simulation shows a less pronounced benefit of the membrane compared to the experiment, as can be seen in Figure 7.23 b). The reason for the deviation is that the simulation underestimates the glucose concentration in the feed and permeate, see Figure 7.19 b), and thus underestimates the selectivity. The cellobiose concentration is predicted accurately, on the other hand (Figure 7.19 a)). One reason for the discrepancy is the changing feed volume in the membrane process. This leads to, e.g., an increasing ferric iron concentration (see Figure 7.20 a)), which in turn influences the reaction kinetics (Equations 2.16, 2.17 and 2.18). Additionally, other variations, which were observed in the experiments with membrane, e.g., the non-constant retentions, were not accounted for in the simulation. Thus, some deviation from the experiment can be expected. All in all, the final deviation of the simulated selectivity from the experimental data is 9.5% in the simulation with membrane separation and 2.6% in the simulation without membrane separation. Thus, it can be concluded from the experiments and the simulations that the membrane separation enables an increased selectivity towards glucose. In order to demonstrate the potential of fully continuous operation, a process was simulated with a continuous supply of cellobiose solution to the electrochemical reactor. As described above, the model used in this study is more accurate when a constant reactor volume is applied, which is the case in the fully continuous operation.

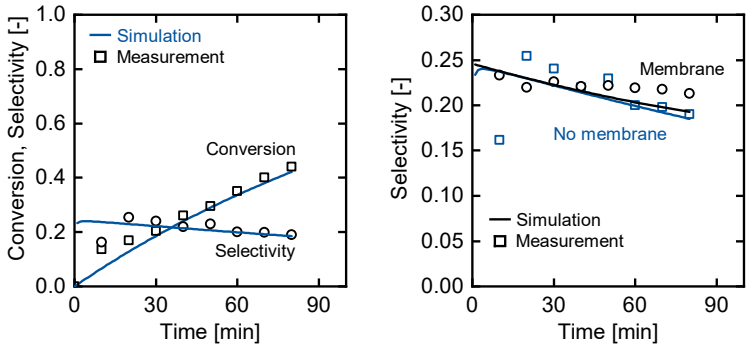

Figure 7.23.: Experimental and simulation results for constant current experiments. a) Validation of model for constant current experiment without membrane. b) Comparison of the selectivity with and without a coupled membrane process.

According to the reaction kinetics for cellobiose and glucose, the ratio of cellobiose to glucose should be as high as possible in the reactor to obtain a high selectivity, see Figure 7.10 b). Thus, the initial cellobiose concentration in the reactor was set close to the solubility limit of about 300 mM. The initial glucose concentration in the reactor was set to 10 mM. Three simulations were performed: one with a membrane with ideal retention ($R_{cello} = 1$, $R_{glu} = 0$), one with the measured retentions (non-ideal retention) and one with ideal retentions but with different apparent rate constants for cellobiose and glucose degradation ($k_{2,app}/k_{1,app} = 1.47$). The separate apparent rate constants show the influence of an enhanced glucose degradation compared to cellobiose. A continuous supply of a 30 mM (ideal cases) or a 65 mM (non-ideal case) cellobiose solution was fed to the reactor. The feed of cellobiose in the ideal case was chosen such that it matches the expected degradation rate in the reactor. The cellobiose supply was higher in the non-ideal case, as some cellobiose permeates through the membrane. The permeate flow was chosen such that it is close to the expected glucose production rate in the reactor. Figure 7.24 a) shows the concentrations of cellobiose and

glucose in the electrochemical reactor over time. It can be seen that the estimations of supply of cellobiose and permeation of glucose were accurate for the systems with ideal retention, as the process is close to steady-state. In the case of the non-ideal (or measured) retention, the glucose increases at the beginning and then strives towards a steady value. This is due to the fact that the membrane retains some of the glucose. As higher glucose concentrations are reached, a steady-state is approached because of the increased degradation of glucose. The selectivity towards glucose can be continuously kept very close to 25% with the ideal membrane and equal apparent rate constants, see Figure 7.24 b), which is the highest obtainable value in the simulation. The simulation with non-ideal membrane yields slightly lower selectivities, as some glucose is retained in the reactor, accumulates and is partially degraded by OH radicals. As a remedy, the permeate and feed volume flow could be adjusted. Additionally, some cellobiose is lost in the case with the non-ideal membrane. The simulation with an increased glucose degradation rate also shows some selectivity losses. However, even here the membrane enables a steady, relatively high selectivity. If the concentrations of cellobiose and glucose in the reactor were adjusted, the selectivity could even reach higher values. Even though the coupled membrane process can increase the selectivity, the electro-Fenton process with the parameters studied here and in other studies shows an upper limit for the selectivity towards glucose [Kwon2012; Sonn1976]. However, other degradation products of cellobiose can also be value-added products, such as formic acid, and the scope of target products could be expanded. As small molecules such as formic acid are only retained to a very low degree by the membrane presented in this work, the here proposed process could be employed. Alternatively, She et al. [She2015] have demonstrated high yields of the value-added product glycolic acid via Fenton treatment of cellulose. Furthermore, the proposed process has implications beyond the degradation of cellobiose: it could be implemented as a continuous pre-treatment stage of biomass. Fenton pre-treatment of biomass has been shown to enhance the enzymatic hydrolysis [Jeon2016]. The process can also be transferred to wastewater treatment or other electro-Fenton processes

as a next step towards the implementation of these processes in the industry.

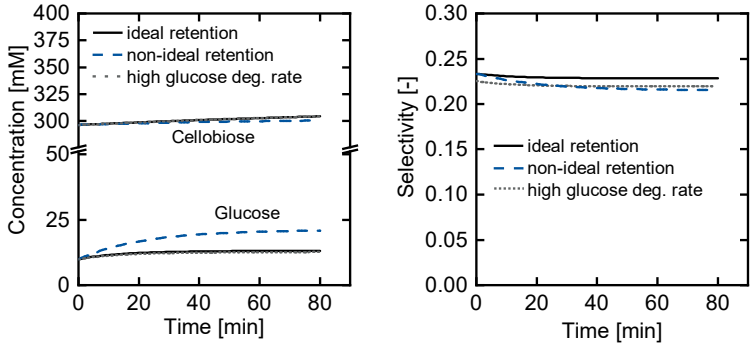

(a) Concentrations of cellobiose and glucose in the reactor.

(b) Selectivity towards glucose.

Figure 7.24.: Simulation of a fully continuous process for the degradation of cellobiose to glucose.

7.4. Conclusion and Outlook

Membrane reactors provide selectivity enhancement to chemical reactions due to the removal of, e.g., intermediate products. In this chapter, an electro-Fenton process was introduced, in which OH radicals from the Fenton reaction convert cellobiose to glucose. With the parameters tested in this work, the selectivity was limited to about 25–30% and decreased with increasing time in a batch process. The non-selective nature of the radicals oxidizes glucose to organic acids and aldehydes. As a remedy, a membrane reactor consisting of a coupled electro-Fenton process and layer-by-layer nanofiltration stage was established, which maintained high selectivities throughout the reaction time. A tailor-made layer-by-layer polyelectrolyte membrane

showed an improved selectivity for glucose and iron compared to commercially available nanofiltration membranes. The retention of cellobiose and iron catalyst was 80–90%, while glucose permeated through the membrane (R= 42%). Additionally, a modeling approach was developed, which allowed to fit and simulate the conversion of cellobiose to glucose. Simulations demonstrate that the electro-Fenton reactor coupled with a membrane separation stage can enable a fully continuous process, which runs close to the highest achievable selectivity. Future work should focus on establishing a continuous process with higher cellobiose and glucose concentrations. Further, the membrane rejection should be improved and optimized. It is well known that the rejection decreases with increasing concentrations of the solutes [Meli2007, pp. 294–295][Shi2013]. Thus, the membrane rejection needs to be reevaluated at the high sugar concentrations chosen for the continuous process. In order to obtain an input stream for a fermentation, an additional concentration step for glucose should be added to the process. Further, the model needs to be expanded to include the electrochemical reaction and detailed kinetics for cellobiose degradation in order to facilitate a detailed process optimization.

Acknowledgements Sahel Khanna, Oktay Altunok, Moritz Becker, Sebastian Holtwerth, Alexander Schmitz, and Jan Schulze are acknowledged for their experimental support.

8. Conclusions and Outlook

Exploitive use of fossil resources such as oil, gas, and coal to satisfy an ever increasing demand for energy and materials has led to the anthropogenic climate change, which poses a major threat to human life and prosperity. The mitigation of green house gas emissions requires an advent of new, renewable-resource-based technologies. Among the manifold approaches currently discussed in science, politics, and society, biorefineries and Power-to-X technologies are identified as two promising routes to achieve said goal. In this work, both approaches were pursued to convert woody biomass to intermediate products of the (bio-)chemical industry. As a grand vision, on the one hand integrated processes were pursued, which do not merely focus on one process step, but encompass pre- and posttreatment as well. On the other hand, the benefits of Power-to-X and biorefinery technologies were merged to exploit the potential of electro-Fenton processes for the conversion of lignin and cellobiose.

In **Chapter 3** deep eutectic and hydrotropic solvents were used to extract lignin from beech wood chips. Both types of solvents are capable of extracting lignin up to 80%, especially at high temperatures of 120 °C (deep eutectic solvent) and 200 °C (hydrotropic solvent). Additionally, a decrease in wood chip size leads to an increased lignin yield. The DES pretreated biomass shows a very poor enzymatic conversion, possibly due to the formation of inhibitors at high temperatures or the DES adsorption on the biomass. The enzymatic hydrolysis for the hydrotropic solvents shows promising results, when moderate pretreatment temperatures between 120 °C to 150 °C for lignin extraction are applied, while at 200 ℃ pretreatment temperature, no conversion

was observed. Overall, the hydrotrope shows the best pretreatment characteristics: Lignin is dissolved from biomass and the enzymatic digestibility is ensured. Additionally, the hydrotropic solution enables a Fenton treatment. The unique properties of hydrotropic solutions, which allow lignin dissolution at acidic pH values, are an enabler for a Fenton-based degradation of the biopolymer.

In **Chapter 4** size exclusion chromatography results show how lignin is attacked and degraded by OH radicals from the Fenton process. In contrast to purely aquaeous solutions, the hydrotropic solvent requires a pH value below three for a successful long-term operation. Aromatic products are not stable towards the oxidative environment and even an in situ extraction provides low yields. However, organic acids, which are more stable against oxidation than the aromatics, were found to be the major product of the lignin degradation, yielding up to 30% oxalic acid relative to the initial lignin content. Together, Chapters 3 and 4 introduced an integrated approach to lignin valorization.

Fenton's chemistry is known from natural wood degradation to cleave the glycosidic bonds of cellulose. **Chapter 5** explored the feasibility of cellulose conversion to glucose via Fenton's chemistry with the model substance cellobiose. The variation of cellobiose, hydrogen peroxide, iron, oxygen, chelator, and sodium sulfate concentration showed that a low concentration of oxygen is beneficial to the reaction rate whereas all the other parameters have a positive correlation on the reaction rate in the studied range. However, the selectivity towards glucose does not surpass 30%. Over time, the selectivity decreases due to oxidation of glucose by OH radicals. Thus, the OH radical based depolymerization of cellobiose is strongly limited in terms of selectivity and is no viable alternative to the enzymatic hydrolysis.

The Fenton processes described in Chapters 4 and 5 can be electrified and are then coined electro-Fenton. **Chapter 6** introduced planar and tubular reactor geometries for the electrochemical synthesis of hydrogen peroxide. These reactors are the basis for an electro-Fenton

process. In planar reactors, commercially available gas diffusion electrodes yield high current efficiencies of approximately 80%. However, at $70\,\mathrm{mA\,cm^{-2}}$ a sharp decrease in current efficiency was observed. The influence of gas flow rate, gas flow mode, liquid flow rate, catalyst, and spacer type was tested. Overall, the gas flow rate and mode have the greatest effect on the current efficiency. It is critical that oxygen is always supplied at a stoichiometric excess greater than two and that a pressure gradient between gas phase and liquid phase is ensured. Tubular microtubes based on carbon nanotubes were investigated as an alternative to the planar counterpart. Among the different tested parameters (catalysts, flow rates, gas pressure), the polymeric binder PTFE showed the greatest influence. The hydrophobic polymer ensures open pores in the gas diffusion electrode for a sustainable gas reactant supply.

The findings of Chapters 5 and 6 were combined in **Chapter 7**, where the conversion of cellobiose to glucose was studied in an electro-Fenton reactor. Similar to the findings of Chapter 5, the selectivity is limited to values below 30% in the electro-Fenton process. It was shown that a further decrease in selectivity with increasing reaction time is connected to the ratio of cellobiose to glucose. As less cellobiose is available in the reactor, more glucose is degraded. As a remedy, a layer-by-layer nanofiltration stage was coupled to the electro-Fenton reactor in order to separate glucose from the OH radicals. A tailor-made layer-by-layer polyelectrolyte membrane shows an improved selectivity for glucose and iron compared to commercially available nanofiltration membranes. Cellobiose and iron catalyst can be retained up to 80–90%, while glucose permeates through the membrane with a retention of 42%. Additionally, a modeling approach was developed, which allowed to fit and simulate the conversion of cellobiose to glucose. Simulations demonstrate that the electro-Fenton reactor coupled with a membrane separation stage can enable a fully continuous process close to the initial selectivity.

The main findings of this thesis are:

- Hydrotropic solvents facilitate an integrated process for lignin extraction from biomass and subsequent Fenton-based degradation to organic acids.
- The conversion of cellobiose to glucose via Fenton's chemistry is limited to a selectivity below 30% for all parameters tested in this work and decreases with increasing reaction time.
- Tubular and planar electrochemical reactors are well suited to produce hydrogen peroxide. However, a highly selective catalyst does not suffice: special attention must be paid to enable sufficient oxygen supply to the reactive interface.
- Layer-by-layer membranes outperform commercially available membranes, because they can be tailored to the specific needs of the electro-Fenton process: they retain iron catalyst and large molecules (cellobiose), while small molecules (glucose) can permeate.

Future work should consider an intensified investigation of the **limits of a Fenton-based lignin conversion in hydrotropic solvents**. Based on the results for cellobiose degradation, an increase in reactant concentration prevents the products from overoxidation and thus, the lignin concentration must be increased. In this thesis, the lignin concentration was $5\,\mathrm{g\,L^{-1}}$, which could theoretically be increased up to $350\,\mathrm{g\,L^{-1}}$. Further, a change in hydrotropic solvent to one that performs well at moderate temperatures below 100 °C may prove to be more energy efficient and less altering to the lignin and residual biomass. The preservation of the original lignin bonds is essential in the lignin-first approach. Additionally, a low pretreatment temperature will likely boost the enzymatic digestibility of the solid residue. Finally, Fenton's chemistry with lignin in hydrotropic solvents must be understood in more detail: How does the hydrotrope interact with the iron catalyst and the OH radicals? What is the fate of xylan

compounds? At last, the electrification of the Fenton process and a coupling to a separation stage are landmarks.

Electrochemical reactors for the synthesis of hydrogen peroxide must be developed for neutral and acidic solvents, but also organic solvents, to substitute the state of the art anthraquinone process and establish a hydrogen peroxide production based on renewable electricity. Additional work on stable and selective catalysts is necessary. The influence of operating parameters, such as the trans GDE pressure, must be further elucidated with a special focus on a scale-up. Mitigation strategies for losses at the electrodes, electrolytes and membrane need to be developed to reduce the cell voltage and obtain an economically viable process.

The herein developed **coupled process of electro-Fenton and tailored layer-by-layer membrane stage** is applicable beyond biorefineries. The process developed within this thesis can be transferred to the wastewater industry, in which Fenton's chemistry is frequently employed. Further efforts in modeling and experiments must be made to understand the electrode / electrolyte interface. How high can current densities climb, before iron precipitates due to a caustic boundary layer? How can the reduction of ferric iron be accelerated? The retention of the supporting electrolyte must be improved for a viable process. Interestingly, layer-by-layer membranes not only provide the chance to tailor rejections characteristics for the Fenton process. The coating can also be regenerated, which is of particular interest in the challenging oxidative environment of Fenton processes.

In this thesis, Fenton's chemistry was explored as valorization technology for lignin and cellobiose. The limitations for both biomass constituents were thoroughly discussed. The findings broaden the decision basis in an effort to develop integrated, electrified, environment-friendly, and cost-efficient biorefineries. The electrodes, reactors, and processes developed in this thesis can be transferred to develop a sustainable hydrogen peroxide production by renewable energy and

integrated wastewater treatment processes.

A. Appendix

A.1. Fabrication of Reference Electrodes

Reference electrodes were fabricated by treating a silver wire in a sodium hypochlorite solution for about 30 min. The chlorinated silver wire was then inserted into a tube, protruding at the bottom and the top of the tube. This wire-in-tube-assembly was subsequently inserted into another tube filled with $3\,\mathrm{mol\,L^{-1}}$ KCl and which was sealed with a glass frit. The two tubes were sealed so that no electrolyte could leak. A thread connection was placed above the sealing. A schematic view of the RE and a picture of the RE can be seen in Figure A.1.

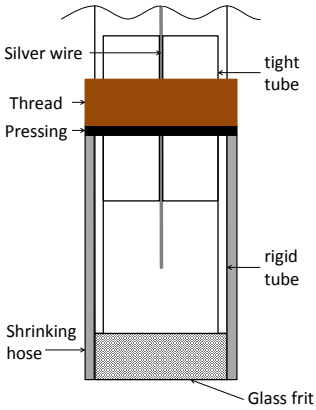

(a) *Schematic view of the self-made reference electrode*

(b) *Photo of the self-made reference electrode*

Figure A.1.: *Self-made Ag/AgCl reference electrode*

A.2. Separation of Ionic Mixtures of Mono- and Disaccharides

In Chapter 7 the separation of the monosaccharide glucose from the dissaccharide cellobiose and the salts sodium sulfate and iron sulfate is studied. This sections provides a detailed background on the separation of ionic mixtures containing mono- and disaccharides. Feng et al. [Feng2009] investigated the separation of galacto-oligosaccharides with the help of nanofiltration. The saccharide mixture consisted of 18 wt.-% glucose, 1 wt.-% galactose, 45 wt.-% lactose (same molecular weight as cellobiose) and 36 wt.-% oligosaccharides. Four commercial membranes were tested: NF-2 (MWCO: 500–600 Da) and NF-3 (MWCO: 800–1000 Da) by Sepro, NF-1812-50 (MWCO: 150–300 Da) by Dow Chemical and HBRO-1812-2 (MWCO: 800–1000 Da) by Beijing Ande [Feng2009]. The effect of applied pressure, temperature and feed concentration on the flux and retention of the saccharides was studied. All membranes rejected glucose to more than 50% at

a total sugar concentration of $20\,g\,L^{-1}$ and 2 bar retentate pressure. An increase of pressure to 8 bar led to an increase of rejection up to over 70% for all membranes. Lactose, as the larger molecule, was rejected to over 80% at 2 bar pressure and over 90% at 8 bar. An increase in temperature led to a decrease of the rejection of all solutes. The total concentration of the sugars in the feed significantly affected the rejection. For the NF-3 membrane, the lactose rejection dropped from approximately 95% to 85% at 6 bar pressure when the sugar concentration was increased from 5 to $60\,g\,L^{-1}$. The glucose rejection was affected even more and dropped from about 80% to 45%. The authors explain the decrease of rejection with increasing sugar concentration by a decrease in driving force due to an increased osmotic pressure. Goulas et al. [Goul2002] studied the rejection of mono-, di- and oligosaccharides in a commercial oligosaccharide mixture (Vivinal® GOS) with the membranes Desal 51-HL, 5-DL, and GE by GE Osmonics. The influence of sugar concentration, temperature and pressure on the rejection and flux were studied. The flux increased with pressure from 6.9 bar to 27.6 bar and the rejection of solutes increased. The total sugar concentration was in the range of $50\,g\,L^{-1}$ to $76\,g\,L^{-1}$, with equal concentrations of fructose, sucrose and raffinose. The increasing retention can be explained by a greater solvent flux through the membrane and higher membrane compaction due to pressure. A rising temperature led to a decreasing rejection. An increase in total sugar concentration led to a decrease of the rejection at constant TMP, similar to Feng et al. [Feng2009]. Rejection values for different membranes can be found in Table A.1. Almazán et al.[Alma2015] characterized Desal DL and Desal DK membranes by GE Osmonics for their rejection of glucose solutions with concentrations between $5\,g\,L^{-1}$ to $100\,g\,L^{-1}$ at pressures from 4 bar to 28 bar at 50 °C. They found a decreasing rejection with increasing glucose feed concentration at constant TMP. E.g., at 4 bar TMP, the retention for the DL membrane was $> 80\%$ for a $5\,g\,L^{-1}$ glucose concentration and $< 40\%$ for a $100\,g\,L^{-1}$ solution. However, when the TMP was corrected for the osmotic pressure, no concentration dependence could be observed anymore. Almazán et al. [Alma2015] thus support the

argument of Feng et al. [Feng2009].

A.2.1. Mixtures of Charged and Non-Charged Solutes

Bargeman et al.[Barg2005; Barg2014; Barg2015] studied the influence of multi-component feeds on the rejection of the individual solutes. In particular, the glucose rejection was studied under the influence of various salts containing chloride as anion. The following membranes were investigated: Desal 5DK, Desal 5DL (GE Osmonics), Desal G5 (GE Osmonics), NF (Dow Chemicals) and NTR-7450 (Nitto Denko). In single solute experimentes, a decreasing rejection of NaCl was found for an increasing salt concentration, as expected from theory [Meli2007, pp. 285–307]. Additionally, in multi solute experiments, the glucose rejection decreased with increasing salt concentration. Two possible explanations were proposed by Bargeman et al. [Barg2005]. On the one hand, a high salt concentration leads to pore swelling. The increase in pore size leads to a decrease in rejection of neutral solutes. On the other hand, an increase in salt concentration leads to a higher membrane charge density. This in turn leads to more friction of the components in the membrane, which lowers the flux. Bargeman et al. [Barg2005] found that the flux of small pores is lowered to a greater extend than the flux of bigger pores. Thus, in the presence of a salt the bigger pores become more dominant in the rejection characeristics of the membrane and the rejection for uncharged solutes decreases. Mohammad et al. [Moha2010] investigated Desal DK and CK membranes by GE Osmonics for their rejection of glucose and mixtures of glucose and sodium chloride. The rejection of glucose followed the trends, which were discussed previously. When glucose was added to an aqueous solution of sodium chloride, the retention of sodium chloride decreased with increasing salt concentration. This can be expected due to the decreasing electrostatic repulsion with increasing salt concentration [Meli2007, pp. 285–307][Moha2010]. Moreover, the salt concentration affected the rejection of glucose, especially

for the CK membranes. For the DK membranes, Mohammad et al. [Moha2010] could not observe a clar influence of salt on the sugar retention. In contrast, Bouchoux et al. [Bouc2005] report a decreasing glucose rejection mixtures with salt for DK membranes. According to Bargeman et al. [Barg2005], the high salt concentration leads to pore swelling, especially for membranes with a high charge density. The CK membrane has a higher charge density than the DK membrane, and thus, the Mohammad et al. [Moha2010] argue that pore swelling has a higher impact with the CK membranes.
The rejection of NaCl decreased with increasing glucose concentration [Moha2010]. The authors argue that back diffusion of the salt from the membrane boundary to the bulk is impeded by an increasing glucose concentration, which diminishes the rejection [Moha2010]. According to Vellenga and Trägardh [Vell1998], a high sugar concentration leads to an increased viscosity, which impairs the diffusion. In contrast, Bouchoux et al. [Bouc2005] did not find any influence of sodium lactate on the retention of sodium chloride with a Desal DK membrane. Thus, the effect is dependent on the used membrane, salt and non-salt concentrations.

A.2.2. The Influence of the pH Value on the Membrane Retention

Chilyumova [Chil2014] reported that divalent cations were stronger retained with pH values below the isoelectric point due to stronger electrostatic repulsion with NF and NF90 membranes (Dow Filmtech). Effects of the pH value on nanofiltration performance of charged solutes are well known [Mänt2006; Chil1996]. However, the influence of the pH value on the surface charge and thus the retention is superimposed by an additonal effect: Nordvang et al. [Nord2014] studied the separation of lactose (uncharged, MW = 342 g/mol) and 3'-sialyllactose (charged, MW = 634 g/mol) with varying pH value for the membranes NP010 (Microdyn-Nadir) and NF45 (Dow Filmtech). Even though a higher rejection of 3'-sialyllactose was expected at

high pH values, which corresponded to high charge densities for the investigated membranes, it was not observed. The authors argue that pore swelling superimposed the stronger electrostatic repulsion of ions, yielding no net change in retention. On the other hand, Qi et al. [Qi2011] found a reduced retention of furfural for an NF90 and xylose and glucose for a NF270 membrane (Dow Filmtech) with increasing pH value. These uncharged solutes can pass more easily through the membrane, if it is swollen at high pH values [Qi2011; Mänt2006; Dalw2011b]. Escalona et al. [Esca2014] investigated the degradation of bisphenol A (MW = 228 g/mol) during Fenton process with a following NF operation of the Fenton solution. Here, the NF membranes (CK, NF270, NF90) showed a high rejection of $> 90\%$ for ferrous iron. The BPA rejection was between 80 to 90 % at a TMP of 6 bar and a pH of approximately 3.

Layer-by-layer polyelectrolyte membranes offer the chance to tailor the membrane properties by adjusting the number of bilayers, the polyelectrolyte and coating conditions [Menn2016a]. Thus, they have a high potential for the separation envisaged in this work. Menne et al. [Menn2016a] investigated PEM hollow fibers with different bilayers. Polydiallyldimethylammonium chloride / polysodiumstyrene sulfonate (PDADMAC/PSS) membranes with a constant coating flux $J_{coating} > 20\,LMH$ showed could be tuned for the retention of magnesium sulfate. With two bilayers, 40% rejection was reached while three bilayers even enabled a rejection of 80%. The pure water permeability of the membranes were 14 LMH/bar and 13 LMH/bar. Self-fabricated polyelectrolyte multilayer membranes showed a promising potential for separation of mono- and disaccharides. As a support membrane, a hydrolyzed polyacrylonitrile (PAN) membrane was coated with a layer of polyethyleneimine (PEI). Subsequently, either a number of bilayers composed of poly(allylamine hydrochloride) (PAH) and poly(styrene sulfonic acid) sodium salt (PSS) or PSS and chitosan was coated in dead-end mode. Additionally, a C-PEM denoted membrane with a middle layer comprised of 3 bilayers chitosan/PSS and a top layer comprised of two bilayers PAH/PSS was fabricated. The C-PEM membrane reached a flux of 3.7 LMH at 3 bar. Maltose,

which is a dissaccharide with the same molecular weight as cellobiose, was separated from glucose. The selectivity of the maltose/glucose separation was 46 with the best membrane as reported by Shi et al [Shi2013]. The rejection of glucose was 63% and the rejection of maltose was 99%. Depending on the polyelectrolyte layers, the rejection of glucose was as low as 25% and the rejection of maltose dropped to 72%. The experiments in this work were performed at a pH value of 3, which is considered as the optimum for electro-Fenton processes [Pign2006; Bril2009]. Many nanofiltration membranes such as Desal DK, NF270, NF45, NP010 and NP030 will be positively charged at $pH = 3$, as their isoelectric point is above 3 [Hagm1999; Semi2011; Xu1999; Kose2018]. However, as e.g. the isoelectric points of the NP010 and NP030 membranes, which are 3.3 and 3.2, are only slightly above the desired value, a detailed investigation on the retention for the in this thesis described system is necessary.

Table A.1.: Literature review of nanofiltration membranes

Membrane	c_{ms} [mM]	c_{ds} [mM]	c_{di} [mM]	R_{ms} [%]	R_{ds} [%]	R_{di} [%]	TMP [bar]	T [°C]	MWCO [Da]	PWP $[\frac{L}{m^2 hbar}]$	References
CK			17[2]			97[2]	16	25			[GE Wa]
CK			0.016[1]			91[1]	6	30	150–300	1.6	[Esca2014]
CK	5.6			90			9	25		2.4	[Moha2010]
CK	5.6†			90†			9	25			[Moha2010]
Desal DK			17[2]			98[2]	7.6	25	150–300		[Sueza]
Desal DK	27.8			< 80			8	50		10	[Alma2015]
Desal DK	5.6			95			9	25		3.06	[Moha2010]
Desal DK	5.6†			95†			9	25			[Moha2010]
Desal DK			1.3[4]			96[4]		25		5.1	[Chil2014]
Desal 5DK	5.6			> 90			5	20		4.5	[Barg2014]
Desal 5DK	5.6†			< 80†			5	20			[Barg2014]
Desal 5HL			17[2]			98[2]	7.6	25	150–300		[GE Wb]
Desal 5HL	5.6			93			5	20		11.6	[Barg2014]
Desal 5HL	5.6†			< 80†			5	20			[Barg2014]
Desal 51-HL	70	70		51	77		6.9	25			[Goul2002]
Desal DL			17[2]			96[2]	7.6	25	150–300		[Suezb]
Desal DL	27.8						8	50		16	[Alma2015]
Desal 5-DL								20		5.69	[Barg2005]
Desal 5-DL	39	39		54	99		6.9	25			[Goul2002]
Desal GE	70	70		8	41		6.9	25	1000		[Goul2002]
Desal G5	8.3			20–60			2–30	20	1000	0.9	[Barg2005]
ESNA1-LF2			0.016[1]			98[1]	6	30	100–300	9.7	[Esca2014]
ETNA01PP		0.5			< 20		4	RT	1000	30.5	[Nord2014]

Continued on the next page

Continued of table A.1

Membrane	c_{ms} [mM]	c_{ds} [mM]	c_{di} [mM]	R_{ms} [%]	R_{ds} [%]	R_{di} [%]	TMP [bar]	T [°C]	MWCO [Da]	PWP $[\frac{L}{m^2 hbar}]$	References
HBRO1812-2	19.9	26.2		79	91		8	25	800–1000	22	[Feng2009]
NF1812-50	19.9	26.2		78	99		8	25	150–300	42	[Feng2009]
NF2	19.9	26.2		89	94		8	25	500–600	18–20	[Feng2009]
NF270			17[2]			> 97[2]	4.8	25			[Dow]
NF270	5.6			97			5	20		13.5	[Barg2014]
NF270	5.6[†]			< 70[†]			< 5	20			[Barg2014]
NF270			0.016[1]			92[1]	6	30	300	14.4	[Esca2014]
NF3	19.9	26.2		72	91		8	25	800–1000	18–20	[Feng2009]
NF45		0.5			> 95		4	RT	200–400	4.1	[Nord2014]
NF90			0.016[1]			96[1]	6	30	200	11	[Esca2014]
NF90			1.3[4]			99[4]		25		1.9	[Chil2014]
NF			1.3[4]			93[4]		25		2.2	[Chil2014]
NFD			0.016[1]			82[1]	6	30	≤ 200	8	[Esca2014]
NP010			35[3]			35–75[3]	40	20	1000–1200	> 5	[Micra]
NP010		0.5			< 20		4	RT	1000–1400	19.3	[Nord2014]
NP030			35[3]			80–95[3]	40	20	500–600	> 1	[Micrb]
NP030	5.6			< 20			5	20		4.4	[Barg2014]
NP030	5.6			30			10	20			[Barg2014]
C-PEM	22	7		63	99		3	25			[Shi2013]
$(PAH/PSS)_3$	22	7		60	95		3	25			[Shi2013]
$(PAH/PSS)_5$	22	7		79	99.5		3	25			[Shi2013]
$(PDADMAC/PSS)_2$			5[2]			40[2]	3.5	25		14	[Menn2016a]
$(PDADMAC\,/\,PSS)_3$			5[2]			> 80[2]	3.5	25		13	[Menn2016a]

Continued on the next page

Continued of table A.1

Membrane	c_{ms} [mM]	c_{ds} [mM]	c_{di} [mM]	R_{ms} [%]	R_{ds} [%]	R_{di} [%]	TMP [bar]	T [°C]	MWCO [Da]	PWP $[\frac{L}{m^2 hbar}]$	References

Abbreviations: ms: monosaccharide, ds: disaccharide, di: divalent cation

[1] Retention of Fe^{2+}, [2] Retention of $MgSO_4$, [3] Retention of Na_2SO_4, [4] Retention of $Ni(NO_3)_2$ at pH 3
[†] Salt added in solution

A.2.3. Membrane Properties

Table A.2.: Pure water permeability (PWP), permeability, retentions and selectivities for all investigated flat-sheet membranes in Chapter 7.

	Permeability		Retention[2]			Selectivity[2]	
	PWP[1]	Perm.[2]	Cellobiose	Glucose	Fe^{2+}	Glu:cello	Glu:Fe
	[LMH/bar]		[-]	[-]	[-]	[-]	[-]
NF270	17.21± 0.71	8.99±0.03	0.96 ± 0.0018	0.85 ± 0.0084	0.85 ± 0.0246	4.07 ± 0.0309	1.07 ± 0.2339
NP030	3.15 ± 0.61	2.74±0.43	0.36 ± 0.0308	0.18 ± 0.0139	0.44 ± 0.0244	1.29 ± 0.0402	1.48 ± 0.0397
NP010	15.32 ± 1.82	14.36±0.94	0.08 ± 0.0072	0.07 ± 0.0064	0.05 ± 0.2327	1.01 ± 0.0011	1.05 ± 0.2634
GE	2.58 ± 0.14	2.11±0.27	0.54 ± 0.0062	0.26 ± 0.0107	0.56 ± 0.0269	1.61 ± 0.0014	1.69 ± 0.0787
2-bilayer	13.39 ± 1.18	9.37±1.26	0.54 ± 0.1143	0.26 ± 0.0359	0.54 ± 0.0829	1.69 ± 0.3392	1.65 ± 0.2200
3-bilayer	10.18 ± 1.88	5.53±0.24	0.69 ± 0.0270	0.32 ± 0.0099	0.60 ± 0.0313	2.18 ± 0.1578	1.70 ± 0.1089

Additional information:
[1] The pure water permeability was measured before and after each experiment
[2] The permeability, retentions and selectivities correspond to the first sample in the batch experiments, where the concentrations in the feed were still close to the initial concentrations
[3] All values are given with their standard deviation.

Table A.3.: Pure water permeability (PWP), permeability, retentions and selectivities for the self-made hollow fiber LbL membrane in Chapter 7.

3-bilayer HF	Permeability PWP [LMH/bar]	Perm.[1]	Cellobiose [-]	Retention Glucose [-]	Fe^{2+} [-]	Fe^{3+} [-]	Selectivity Glu:cello [-]	Glu:Fe2+ [-]	Glu:Fe3+ [-]
1 bar TMP	20.1 ± 0.08	6.5	0.86 ± 0.013	0.14 ± 0.006	0.53	0.76	6.23 ± 0.53	1.83	3.56
2 bar TMP	19.6 ± 0.11	7.1	0.92 ± 0.006	0.27 ± 0.025	0.72	0.86	9.24 ± 0.43	2.74	4.93
3 bar TMP	19.2 ± 0.10	7.4	0.94 ± 0.007	0.39 ± 0.061	0.81	0.91	10.95 ± 0.29	3.51	6.18

Additional information:

[1] Only one data set was taken into consideration because of precipitation in the second run.

* Errors are given as standard deviation.

Nomenclature

AGU Anhydroglucose

AO process Autooxidation process

BET Brunauer, Emmett and Teller

CD Current density

CE Current efficiency

CEM Cation exchange membrane

CL Catalyst layer

CNT Carbon nanotube

CV Cyclic voltammetry

DCA Dicarboxylic acids

DES Deep eutectic solvent

DHBA 2,3-dihydroxybenzoic acid

EAQ 2-ethylanthraquinone

ecMR Electrochemical membrane reactor

EDX energy-dispersive x-ray spectroscopy

EIS Electrochemical impedance spectroscopy

GC Gas chromatography

GC-MS Gas chromatography mass spectrometry

GDE Gas diffusion electrode

GHG Greenhouse gas

HMWC High molecular weight compounds

HPLC High-performance liquid chromatography

LbL Layer-by-layer

LC Liquid chromatography

LMWC Low molecular weight compounds

MMWC Medium molecular weight compounds

MPL Microporous layer

MWCNT multi-walled carbon nanotubes

NF Nanofiltration

ORR Oxygen reduction reaction

P2X Power-to-X

PAH poly(allylamine hydrochloride)

PAN	polyacrylonitrile
PE	Polyelectrolyte
PEI	Polyethyleneimine
PSS	poly(styrene sulfonic acid) sodium salt
PTFE	polytetrafluorethylene
SCS	Sodium cumene sulfonate
SEC	Size exclusion chromatography
SEM	scanning electrode microscopy
SHE	Standard hydrogen electrode
SL	Substrate layer
SXS	Sodium cumene sulfonate
TMP	Trans membrane pressure

Bibliography

[Abel1952] E. Abel. "Über die Selbstzersetzung von Wasserstoffsuperoxyd". *Monatshefte für Chemie und verwandte Teile anderer Wissenschaften* 83.2 (1952). DOI: 10.1007/BF00938566 (cit. on p. 25).

[Abu-2020] Mahdi M. Abu-Omar, Katalin Barta, Gregg T. Beckham, Jeremy Luterbacher, John Ralph, Roberto Rinaldi, Yuriy Roman-Leshkov, Joseph Samec, Bert Sels, and Feng Wang. "Guidelines for performing lignin-first biorefining". *Energy & Environmental Science* (2020). DOI: 10.1039/D0EE02870C (cit. on pp. 11, 12, 15).

[Adam2004] Z. Adamczyk, M. Zembala, P. Warszyński, and B. Jachimska. "Characterization of polyelectrolyte multilayers by the streaming potential method". *Langmuir* 20.24 (2004). DOI: 10.1021/la040064d (cit. on p. 182).

[Agla2007] G. R. Agladze, G. S. Tsurtsumia, B. I. Jung, J. S. Kim, and G. Gorelishvili. "Comparative study of hydrogen peroxide electro-generation on gas-diffusion electrodes in undivided and membrane cells". *Journal of Applied Electrochemistry* 37.3 (2007). DOI: 10.1007/s10800-006-9269-x (cit. on pp. 27, 29).

[Akha2020] Sneha A. Akhade, Nirala Singh, Oliver Y. Gutiérrez, Juan Lopez-Ruiz, Huamin Wang, Jamie D. Holladay, Yue Liu, Abhijeet Karkamkar, Robert S. Weber, Asanga B. Padmaperuma, Mal-Soon Lee, Greg A. Whyatt, Michael Elliott, Johnathan E. Holladay, Jonathan L. Male, Johannes A. Lercher, Roger Rousseau, and Vassiliki-Alexandra Glezakou. "Electrocatalytic Hydrogenation of Biomass-Derived Organ-

ics: A Review". *Chemical Reviews* (2020). DOI: 10.1021/acs.chemrev.0c00158 (cit. on p. 2).

[Alma2015] Jorge Emilio Almazán, Estela María Romero-Dondiz, Verónica Beatriz Rajal, and Elza Fani Castro-Vidaurre. "Nanofiltration of glucose: Analysis of parameters and membrane characterization". *Chemical Engineering Research and Design* 94 (2015). DOI: 10.1016/j.cherd.2014.09.005 (cit. on pp. 201, 206).

[Aran2006] Valdeir Arantes and a. M F Milagres. "Degradation of cellulosic and hemicellulosic substrates using a chelator-mediated Fenton reaction". *Journal of Chemical Technology and Biotechnology* 81.3 (2006). DOI: 10.1002/jctb.1417 (cit. on pp. 78, 86, 91).

[Aran2011] Valdeir Arantes, Adriane M F Milagres, Timothy R. Filley, and Barry Goodell. "Lignocellulosic polysaccharides and lignin degradation by wood decay fungi: The relevance of nonenzymatic Fenton-based reactions". *Journal of Industrial Microbiology and Biotechnology* 38.4 (2011). DOI: 10.1007/s10295-010-0798-2 (cit. on p. 152).

[Aran2012] Valdeir Arantes, Jody Jellison, and Barry Goodell. "Peculiarities of brown-rot fungi and biochemical Fenton reaction with regard to their potential as a model for bioprocessing biomass". *Applied Microbiology and Biotechnology* 94.2 (2012). DOI: 10.1007/s00253-012-3954-y (cit. on pp. 18, 46, 51, 54, 78).

[Argy2016] D. S. Argyropoulos and C. Crestini. "A Perspective on Lignin Refining, Functionalization, and Utilization". *ACS Sustainable Chemistry & Engineering* 4.10 (2016). (Cit. on p. 15).

[Aria2016] Carlos J. Arias, Richard L. Surmaitis, and Joseph B. Schlenoff. "Cell Adhesion and Proliferation on the "living" Surface of a Polyelectrolyte Multilayer". *Langmuir* 32.21 (2016). DOI: 10.1021/acs.langmuir.6b00784 (cit. on p. 182).

[Ashr2017] Muhammad Tahir Ashraf and Jens Ejbye Schmidt. "Process Simulation and Economic Assessment of Hydrothermal Pretreatment and Enzymatic Hydrolysis of Multi-feedstock

Lignocellulose — Separate vs Combined Processing". *Bioresource Technology* 249 (2017). DOI: 10.1016/j.biortech.2017.10.088 (cit. on pp. 11, 17).

[Assu2011] M. H.M.T. Assumpção, R. F.B. De Souza, D. C. Rascio, J. C.M. Silva, M. L. Calegaro, I. Gaubeur, T. R.L.C. Paixão, P. Hammer, M. R.V. Lanza, and M. C. Santos. "A comparative study of the electrogeneration of hydrogen peroxide using Vulcan and Printex carbon supports". *Carbon* 49.8 (2011). DOI: 10.1016/j.carbon.2011.03.014 (cit. on p. 30).

[Ausf2019] Florian Ausfelder and Hanna Ewa Dura. *Optionen für ein nachhaltiges Energie-System mit Power-to-X-Technologie*. Tech. rep. DECHEMA, 2019, p. 204 (cit. on p. 1).

[Barb1949] W. G. Barb, J. H. Baxendale, Philip George, and K. R. Hargrave. "Reactions of ferrous and ferric ions with hydrogen peroxide". *Nature* 163.4148 (1949). DOI: 10.1038/163692a0 (cit. on p. 30).

[Barb1951a] W. G. Barb, J. H. Baxendale, P. George, and K. R. Hargrave. "Reactions of ferrous and ferric ions with hydrogen peroxide. Part II.—The ferric ion reaction". *Trans. Faraday Soc.* 47.0 (1951). DOI: 10.1039/TF9514700591 (cit. on p. 30).

[Barb1951b] W.G. Barb, J.H. Baxendale, P George, and K.R. Hargrave. "Reactions of ferrous and ferric ions with hydrogen peroxide Part I.-The ferrous ion reaction". *Trans. Faraday Soc.* 47 (1951). (Cit. on p. 30).

[Bard1985] Allen J Bard, Roger Parsons, and Joseph Jordan. *Standard Potentials in Aqueous Solution*. Vol. 6. CRC Press, 1985 (cit. on pp. 20, 25).

[Barg2005] G. Bargeman, J. M. Vollenbroek, J. Straatsma, C.G.P.H. Schroën, and R. M. Boom. "Nanofiltration of multi-component feeds. Interactions between neutral and charged components and their effect on retention". *Journal of Membrane Science* 247.1-2 (2005). DOI: 10.1016/j.memsci.2004.05.022 (cit. on pp. 159, 161, 175, 178, 202, 203, 206).

[Barg2014] G. Bargeman, J. B. Westerink, O. Guerra Miguez, and M. Wessling. "The effect of NaCl and glucose concentration on retentions for nanofiltration membranes processing concentrated solutions". *Separation and Purification Technology* 134 (2014). DOI: 10.1016/j.seppur.2014.07.025 (cit. on pp. 175, 177, 202, 206, 207).

[Barg2015] G. Bargeman, J. B. Westerink, C.F.H. Manuhutu, and A. ten Kate. "The effect of membrane characteristics on nanofiltration membrane performance during processing of practically saturated salt solutions". *Journal of Membrane Science* 485 (2015). DOI: 10.1016/j.memsci.2015.03.039 (cit. on p. 202).

[Barr2013] Willyam R P Barros, Rafael M Reis, Robson S Rocha, and Marcos R V Lanza. "Electrogeneration of hydrogen peroxide in acidic medium using gas diffusion electrodes modified with cobalt ({II}) phthalocyanine". *Electrochimica Acta* 104 (2013). DOI: 10.1016/j.electacta.2013.04.079 (cit. on p. 114).

[Bawa2018] Bander Bawareth, Davide Di Marino, T Alexander Nijhuis, Tim Jestel, and Matthias Wessling. "Electrochemical membrane reactor modelling for lignin depolymerization". (2018). DOI: 10.1021/acssuschemeng.8b04670 (cit. on p. 153).

[Behl2016] R. Behling, S. Valange, and G. Chatel. "Heterogeneous catalytic oxidation for lignin valorization into valuable chemicals: what results? What limitations? What trends?" *Green Chemistry* 18.7 (2016). DOI: 10.1039/C5GC03061G (cit. on pp. 15, 16).

[Bent1999] G. Bentivenga, C. Bonini, M. D'Auria, A. De Bona, and G. Mauriello. "Singlet oxygen mediated degradation of Klason lignin". *Chemosphere* 39.14 (1999). (Cit. on p. 54).

[Bent2003] G. Bentivenga, C. Bonini, M. D'Auria, and A. De Bona. "Degradation of steam-exploded lignin from beech by using Fenton's reagent". *Biomass & Bioenergy* 24.3 (2003). (Cit. on p. 54).

[Bhan2015] V. P. Bhange, S. P. M. P. William, A. Sharma, J. Gabhane, A. N. Vaidya, and S. R. Wate. "Pretreatment of garden biomass using Fenton's reagent: Influence of Fe2+and H2O2 concentrations on lignocellulose degradation". *Journal of Environmental Health Science and Engineering* 13 (2015). (Cit. on pp. 18, 54, 62, 82).

[BMU2016] BMU. *Klimaschutzplan 2050*. Tech. rep. Bundesministerium für Umwelt, Naturschutz und nukleare Sicherheit, 2016, pp. 1–96 (cit. on p. 1).

[Bouc2005] A. Bouchoux, H. Balmann, and H. Lutin. "Nanofiltration of glucose and sodium lactate solutionsVariations of retention between single- and mixed-solute solutions". *Journal of Membrane Science* 258.1-2 (2005). DOI: 10.1016/j.memsci.2005.03.002 (cit. on p. 203).

[Bret2020] Simone Brethauer, Robert L Shahab, and Michael H Studer. "Impacts of biofilms on the conversion of cellulose". *Applied Microbiology and Biotechnology* 104.12 (2020). DOI: 10.1007/s00253-020-10595-y (cit. on p. 12).

[Bril2009] Enric Brillas, Ignasi Sire, and Mehmet A. Oturan. "Electro-Fenton Process and Related Electrochemical Technologies Based on Fenton's Reaction Chemistry". *Chem. Rev* 109 (2009). DOI: 10.1021/cr900136g (cit. on pp. 30, 31, 81, 98, 105, 169, 170, 205).

[Camp2006] Jose M. Campos-Martin, Gema Blanco-Brieva, and Jose L.G. Fierro. "Hydrogen peroxide synthesis: An outlook beyond the anthraquinone process". *Angewandte Chemie - International Edition* 45.42 (2006). DOI: 10.1002/anie.200503779 (cit. on pp. 23, 24, 98).

[Carl2005] Magnus Carlsson and David Stenman. "A comparative study on the degradation of cotton linters induced by carbonate and hydroxyl radicals generated from peroxynitrite A comparative study on the degradation of cotton linters induced by carbonate and hydroxyl radicals generated from peroxynitri". August 2016 (2005). DOI: 10.1515/HF.2005.020 (cit. on p. 172).

[Chan2018] Anuj Kumar Chandel, Vijay Kumar Garlapati, and Akhilesh Kumar Singh. "The path forward for lignocellulose biorefineries: Bottlenecks, Solutions, and perspective on commercialization". *Bioresource Technology* 264 (2018). DOI: 10.1016/j.biortech.2018.06.004 (cit. on pp. 1, 2, 10, 11, 17).

[Chat2014] G. Chatel and R. D. Rogers. "Review: Oxidation of Lignin Using Ionic Liquids-An Innovative Strategy To Produce Renewable Chemicals". *ACS Sustainable Chemistry & Engineering* 2.3 (2014). (Cit. on p. 16).

[Chen2017] Zhihua Chen, Shucheng Chen, Samira Siahrostami, Pongkarn Chakthranont, Christopher Hahn, Dennis Nordlund, Sokaras Dimosthenis, Jens K. Nørskov, Zhenan Bao, and Thomas F. Jaramillo. "Development of a reactor with carbon catalysts for modular-scale, low-cost electrochemical generation of H_2O_2". *Reaction Chemistry and Engineering* 2.2 (2017). DOI: 10.1039/c6re00195e (cit. on pp. 14, 36, 37, 43).

[Chil1996] Amy E. Childress and Menachem Elimelech. "Effect of solution chemistry on the surface charge of polymeric reverse osmosis and nanofiltration membranes". *Journal of Membrane Science* 119 (2 1996). (Cit. on p. 203).

[Chil2014] Evgenia Chilyumova. "Rückgewinnung zweiwertiger Kationen aus Komplexmedien durch prozessintegrierte Nanofiltration". Dissertation. Bremen: Universität Bremen, 2014 (cit. on pp. 203, 206, 207).

[Ciri2016] Rosaria Ciriminna, Lorenzo Albanese, Francesco Meneguzzo, and Mario Pagliaro. "Hydrogen Peroxide: A Key Chemical for Today's Sustainable Development". *ChemSusChem* 9.24 (2016). DOI: 10.1002/cssc.201600895 (cit. on p. 23).

[Cron2017] Dylan J. Cronin, Xiao Zhang, John Bartley, and William O. S. Doherty. "Lignin Depolymerization to Dicarboxylic Acids with Sodium Percarbonate". *ACS Sustainable Chemistry & Engineering* 5.7 (2017). DOI: 10.1021/ACSsuschemeng.7b01208 (cit. on pp. 55, 62).

[Dabr2015] Saumya Dabral, Jakob Mottweiler, Torsten Rinesch, and Carsten Bolm. "Base-catalysed cleavage of lignin β-O-4 model compounds in dimethyl carbonate". *Green Chemistry* 17.11 (2015). (Cit. on pp. 40, 46).

[Dalw2011a] M. R. Dalwani. "Thin film composite nanofiltration membranes for extreme conditions". PhD thesis. Twente: University of Twente, 2011 (cit. on pp. 159, 161).

[Dalw2011b] Mayur Dalwani, Nieck E. Benes, Gerrald Bargeman, Dimitris Stamatialis, and Matthias Wessling. "Effect of pH on the performance of polyamide/polyacrylonitrile based thin film composite membranes". *Journal of Membrane Science* 372.1-2 (2011). DOI: 10.1016/j.memsci.2011.02.012 (cit. on p. 204).

[De L2005] Joseph De Laat and Truong Giang Le. "Kinetics and modeling of the Fe(III)/H2O2 system in the presence of sulfate in acidic aqueous solutions". *Environmental Science and Technology* 39.6 (2005). DOI: 10.1021/es0493648 (cit. on p. 88).

[De L2019] Phil De Luna, Christopher Hahn, Drew Higgins, Shaffiq A Jaffer, Thomas F Jaramillo, and Edward H Sargent. "What would it take for renewably powered electrosynthesis to displace petrochemical processes?" *Science* 364.6438 (Apr. 2019). DOI: 10.1126/science.aav3506 (cit. on p. 1).

[De M2019] Bert De Mot, Jonas Hereijgers, Miguel Duarte, and Tom Breugelmans. "Influence of flow and pressure distribution inside a gas diffusion electrode on the performance of a flow-by CO2 electrolyzer". *Chemical Engineering Journal* 378.July (2019). DOI: 10.1016/j.cej.2019.122224 (cit. on pp. 106, 148).

[Dean2008] Bill Dean, Tim Dodge, Fernando Valle, and Gopal Chotani. "Development of Biorefineries–Technical and Economic Considerations". In. *Biorefineries-Industrial Processes and Products*. John Wiley & Sons, Ltd, 2008. Chap. 3, pp. 67–83. DOI: 10.1002/9783527619849.ch3 (cit. on p. 17).

[Derb2004] Aly S. Derbalah, Nobutake Nakatani, and Hiroshi Sakugawa. "Photocatalytic removal of fenitrothion in pure and natural waters by photo-Fenton reaction". *Chemosphere* 57.7 (2004). DOI: 10.1016/j.chemosphere.2004.08.025 (cit. on p. 86).

[Deut2019] Deutscher Bundestag. *Gesetz zur Einführung eines Bundes-Klimaschutzgesetzes und zur Änderung weiterer Vorschriften (2019)*. 2019 (cit. on p. 1).

[Dhap2015] Vividha Dhapte and Piyush Mehta. "Advances in hydrotropic solutions: An updated review". *St. Petersburg Polytechnical University Journal: Physics and Mathematics* 1.4 (Dec. 2015). DOI: 10.1016/j.spjpm.2015.12.006 (cit. on p. 13).

[Di M2016] Davide Di Marino, David Stöckmann, Stefanie Kriescher, Serafin Stiefel, and Matthias Wessling. "Electrochemical depolymerisation of lignin in a deep eutectic solvent". *Green Chem.* 18.22 (2016). DOI: 10.1039/C6GC01353H (cit. on pp. 14, 51).

[Di M2019a] Daivde Di Marino. "Extraction and electrochemical valorization of lignin in novel electrolyte". Dissertation. Rheinisch-Westfälische Technische Hochschule, 2019, p. 157. DOI: 10.18154/RWTH-2019-09911 (cit. on p. 43).

[Di M2019b] Davide Di Marino, Tim Jestel, Caroline Marks, Jörn Viell, Malte Blindert, Stefanie M. A. Kriescher, Antje C. Spiess, and Matthias Wessling. "Carboxylic Acids Production via Electrochemical Depolymerization of Lignin". *ChemElectroChem* 6.5 (2019). DOI: 10.1002/celc.201801676 (cit. on pp. 15, 55, 59, 60).

[Dong1990] Dennis F. Dong and Arthur L. Clifford. "Porous diaphragm for electrochemical cell". US4921587A. 1990 (cit. on p. 28).

[Dow] Dow Filmtech. *NF270-400*. URL: https://www.lenntech.com/Data-sheets/Dow-Filmtec-NF270-400.pdf (visited on 11/19/2020) (cit. on pp. 159, 161, 207).

[Duar2019] Miguel Duarte, Bert De Mot, Jonas Hereijgers, and Tom Breugelmans. "Electrochemical Reduction of CO2: Effect of Convective CO2 Supply in Gas Diffusion Electrodes". *ChemElectroChem* 6.22 (2019). DOI: 10.1002/celc.201901454 (cit. on pp. 106, 110).

[Esca2005] Maybeth Escalante, Antonio J. Rodríguez-Malaver, Elisa Araujo, Aura M. González, Orlando J. Rojas, Nancy Peñaloza, Johnny Bullón, Mayra A. Lara, Natalia Dmitrieva, and Elizabeth Pérez-Pérez. "Effect of surfactants on Fenton's reagent-mediated degradation of Kraft black liquor". *Journal of Environmental Biology* 26.4 (2005). DOI: 10.1385/ABAB:97:2:091 (cit. on p. 56).

[Esca2014] I. Escalona, A. Fortuny, F. Stüber, C. Bengoa, A. Fabregat, and J. Font. "Fenton coupled with nanofiltration for elimination of Bisphenol A". *Desalination* 345 (2014). DOI: 10.1016/j.desal.2014.04.024 (cit. on pp. 175, 204, 206, 207).

[Fard2013] P. Fardim, R. Sarna, K. Gabov, and R. Gosselink. "Hydrotropic extraction and shaping of lignin to advanced materials". *Abstracts of Papers of the American Chemical Society* 245 (2013). (Cit. on pp. 14, 36).

[Faul2002] Larry R. Faulkner and Allen J. Bard. *Electrochemical methods: fundamentals and applications*. John Wiley and Sons, 2002 (cit. on pp. 20, 25).

[Feng2009] Y. M. Feng, X. L. Chang, W. H. Wang, and R. Y. Ma. "Separation of galacto-oligosaccharides mixture by nanofiltration". *Journal of the Taiwan Institute of Chemical Engineers* 40.3 (2009). DOI: 10.1016/j.jtice.2008.12.003 (cit. on pp. 154, 200–202, 207).

[Fent1894] H J H Fenton. "Oxidation of Tartaric Acid in presence of Iron". *Journal of the Chemical Society* 65 (1894). (Cit. on p. 30).

[Figu2018] P. Figueiredo, K. Lintinen, J. T. Hirvonen, M. A. Kostiainen, and H. A. Santos. "Properties and chemical modifications of lignin: Towards lignin-based nanomaterials for biomedical applications". *Progress in Materials Science* 93 (2018). (Cit. on p. 15).

[Foll1995] P. C. Foller and R. T. Bombard. "Processes for the production of mixtures of caustic soda and hydrogen peroxide via the reduction of oxygen". *Journal of Applied Electrochemistry* 25.7 (1995). DOI: 10.1007/BF00241923 (cit. on pp. 24, 27–29, 98, 110).

[Fort2007] J.C. Forti, R.S. Rocha, M.R.V. Lanza, and R. Bertazzoli. "Electrochemical synthesis of hydrogen peroxide on oxygen-fed graphite/PTFE electrodes modified by 2-ethylanthraquinone". *Journal of Electroanalytical Chemistry* 601.1-2 (Mar. 2007). DOI: 10.1016/j.jelechem.2006.10.023 (cit. on pp. 112, 127–129).

[Fran2012] María Francisco, Adriaan van den Bruinhorst, and Maaike C. Kroon. "New natural and renewable low transition temperature mixtures (LTTMs): screening as solvents for lignocellulosic biomass processing". *Green Chemistry* 14.8 (2012). DOI: 10.1039/c2gc35660k (cit. on pp. 14, 37).

[Fuku2012] Shunichi Fukuzumi, Yusuke Yamada, and Kenneth D. Karlin. "Hydrogen peroxide as a sustainable energy carrier: Electrocatalytic production of hydrogen peroxide and the fuel cell". *Electrochimica Acta* 82 (2012). DOI: 10.1016/j.electacta.2012.03.132 (cit. on p. 24).

[Gabo2013] K. Gabov, P. Fardim, and F. G. da Silva. "Hydrotropic Fractionation of Birch Wood into Cellulose and Lignin: A New Step Towards Green Biorefinery". *Bioresources* 8.3 (2013). (Cit. on pp. 36, 43).

[Gabo2014] K. Gabov, R. J. A. Gosselink, A. I. Smeds, and P. Fardim. "Characterization of Lignin Extracted from Birch Wood by a Modified Hydrotropic Process". *Journal of Agricultural and Food Chemistry* 62.44 (2014). (Cit. on pp. 36, 41, 43, 46).

[Gabo2017] K. Gabov, J. Hemming, and P. Fardim. "Sugarcane bagasse valorization by fractionation using a water-based hydrotropic process". *Industrial Crops and Products* 108 (2017). (Cit. on p. 36).

[Gall2010] P. Gallo Stampino, L. Omati, C. Cristiani, and G. Dotelli. "Characterisation of nanocarbon-based gas diffusion media by electrochemical impedance spectroscopy". *Fuel Cells* 10.2 (2010). DOI: 10.1002/fuce.200900126 (cit. on p. 133).

[GE Wa] GE Water & Process Technologies. *CK Series*. URL: https://www.lenntech.com/Data-sheets/GE-CK-Series-L.pdf (visited on 11/19/2020) (cit. on p. 206).

[GE Wb] GE Water & Process Technologies. *HL Series*. URL: https://www.lenntech.com/Data-sheets/GE-HL-Series-L.pdf (visited on 11/19/2020) (cit. on p. 206).

[Gend2014a] Youri Gendel, Oana David, and Matthias Wessling. "Microtubes made of carbon nanotubes". *Carbon* 68 (2014). DOI: 10.1016/j.carbon.2013.11.005 (cit. on pp. 23, 99, 114–116, 119, 123, 131).

[Gend2014b] Youri Gendel, Hannah Roth, Alexandra Rommerskirchen, Oana David, and Matthias Wessling. "A microtubular all CNT gas diffusion electrode". *Electrochemistry Communications* 46 (2014). DOI: 10.1016/j.elecom.2014.06.006 (cit. on pp. 23, 99, 114–116, 130, 138, 145, 148).

[Ghos2013] Ramy A. Ghostine, Marie Z. Markarian, and Joseph B. Schlenoff. "Asymmetric growth in polyelectrolyte multilayers". *Journal of the American Chemical Society* 135.20 (2013). DOI: 10.1021/ja401318m (cit. on p. 182).

[Giom2008] M. Giomo, A. Buso, P. Fier, G. Sandonà, B. Boye, and G. Farnia. "A small-scale pilot plant using an oxygen-reducing gas-diffusion electrode for hydrogen peroxide electrosynthesis". *Electrochimica Acta* 54.2 (2008). DOI: 10.1016/j.electacta.2008.06.038 (cit. on p. 29).

[GmbH2020] Sigma-Aldrich Chemie GmbH. *Polytetrafluorethylene*. Tech. rep. MSDS No. GF58560734. 2020 (cit. on p. 133).

[Goor2019] Gustaaf Goor, Jürgen Glenneberg, Sylvia Jacobi, Jal Dadabhoy, and Elize Candido. "Hydrogen Peroxide". In *Ullmann's Encyclopedia of Industrial Chemistry*. American Cancer Society, 2019. Pp. 1–40. (Cit. on pp. 24, 25, 27).

[Goul2002] Athanasios K. Goulas, Petros G. Kapasakalidis, Haydn R. Sinclair, Robert A. Rastall, and Alistair S. Grandison. "Purification of oligosaccharides by nanofiltration". *Journal of Membrane Science* 209 (1 2002). (Cit. on pp. 177, 201, 206).

[Groo2015] Joris de Grooth, Radek Oborný, Jens Potreck, Kitty Nijmeijer, and Wiebe M. de Vos. "The role of ionic strength and odd-even effects on the properties of polyelectrolyte multilayer nanofiltration membranes". *Journal of Membrane*

Science 475 (2015). DOI: 10.1016/j.memsci.2014.10.044 (cit. on p. 34).

[Gupt2006] Neeraj Gupta and Colin W. Oloman. "Alkaline peroxide generation using a novel perforated bipole trickle-bed electrochemical reactor". *Journal of Applied Electrochemistry* 36.2 (2006). DOI: 10.1007/s10800-005-9066-y (cit. on p. 28).

[Hagm1999] G. Hagmeyer and R. Gimbel. "Modelling the rejection of nanofiltration membranes using zeta potential measurements". *Separation and Purification Technology* 15.1 (1999). DOI: 10.1016/S1383-5866(98)00050-1 (cit. on p. 205).

[Hall1965] G Halliwell. "Catalytic Decomposition of Cellulose Under Biological Conditions." *The Biochemical journal* 95 (1965). (Cit. on pp. 18, 78, 82, 152).

[Harn2018] Falk Harnisch and Carolin Urban. "Elektrobioraffinerien: Synergien zwischen elektrochemischen und mikrobiologischen Stoffumwandlungen nutzbar machen". *Angewandte Chemie* 130.32 (2018). DOI: 10.1002/ange.201711727 (cit. on pp. 2, 152).

[Harv1955] A. E. Harvey, J. A. Smart, and E. S. Amis. "Simultaneous Spectrophotometric Determination of Iron(II) and Total Iron with 1,10-Phenanthroline". *Analytical Chemistry* 27.1 (1955). DOI: 10.1021/ac60097a009 (cit. on p. 157).

[Hasc2016] Frédéric Hasché, Mehtap Oezaslan, Peter Strasser, and Tim Patrick Fellinger. "Electrocatalytic hydrogen peroxide formation on mesoporous non-metal nitrogen-doped carbon catalyst". *Journal of Energy Chemistry* 25.2 (2016). DOI: 10.1016/j.jechem.2016.01.024 (cit. on pp. 24, 30).

[He2015] Yu-Cai He, Yun Ding, Yu-Feng Xue, Bin Yang, Feng Liu, Cheng Wang, Zheng-Zhong Zhu, Qing Qing, Hao Wu, Cheng Zhu, Zhi-Cheng Tao, and Dan-Ping Zhang. "Enhancement of enzymatic saccharification of corn stover with sequential Fenton pretreatment and dilute NaOH extraction". *Bioresource Technology* 193 (2015). DOI: 10.1016/j.biortech.2015.06.088 (cit. on pp. 18, 78).

[Hube2006] George W. Huber, Sara Iborra, and Avelino Corma. "Synthesis of Transportation Fuels from Biomass: Chemistry, Catalysts, and Engineering". *Chemical Reviews* 106.9 (Sept. 2006). DOI: 10.1021/cr068360d (cit. on p. 10).

[Ilya2015] Shazia Ilyas, Joris de Grooth, Kitty Nijmeijer, and Wiebe M. de Vos. "Multifunctional polyelectrolyte multilayers as nanofiltration membranes and as sacrificial layers for easy membrane cleaning". *Journal of Colloid and Interface Science* 446 (2015). DOI: 10.1016/j.jcis.2014.12.019 (cit. on p. 34).

[Jean2018] Philippe Jeanty, Christian Scherer, Erhard Magori, Kerstin Wiesner-Fleischer, Olaf Hinrichsen, and Maximilian Fleischer. "Upscaling and continuous operation of electrochemical CO2to CO conversion in aqueous solutions on silver gas diffusion electrodes". *Journal of CO2 Utilization* 24.November 2017 (2018). DOI: 10.1016/j.jcou.2018.01.011 (cit. on pp. 106, 113, 148).

[Jeon2016] So-Yeon Jeong and Jae-Won Lee. "Sequential Fenton oxidation and hydrothermal treatment to improve the effect of pretreatment and enzymatic hydrolysis on mixed hardwood". *Bioresource Technology* 200 (2016). DOI: 10.1016/j.biortech.2015.10.015 (cit. on pp. 18, 78, 95, 190).

[Jirk2011] Jakub S. Jirkovský, Itai Panas, Elisabet Ahlberg, Matej Halasa, Simon Romani, and David J. Schiffrin. "Single atom hot-spots at Au-Pd nanoalloys for electrocatalytic H2O2 production". *Journal of the American Chemical Society* 133.48 (2011). DOI: 10.1021/ja206477z (cit. on p. 27).

[Jose2014] Nithya Joseph, Pejman Ahmadiannamini, Richard Hoogenboom, and Ivo F. J. Vankelecom. "Layer-by-layer preparation of polyelectrolyte multilayer membranes for separation". *Polymer Chemistry* 5.6 (2014). DOI: 10.1039/c3py01262j (cit. on p. 34).

[Juri2015] F. E. Jurin, C. C. Buron, C. Magnenet, M. Quinart, S. Lakard, C. Filiâtre, and B. Lakard. "Predictive tools for selection of appropriate polyelectrolyte multilayer film for the functionalization of organic membranes". *Colloids and Surfaces A: Physicochemical and Engineering Aspects. Physic-*

ochemical and Engineering Aspects 486 (2015). (Cit. on p. 34).

[Kai2016] D. Kai, M. J. Tan, P. L. Chee, Y. K. Chua, Y. L. Yap, and X. J. Loh. "Towards lignin-based functional materials in a sustainable world". *Green Chemistry* 18.5 (2016). (Cit. on p. 15).

[Kaka2008] Bhalchandra Kakade, Rutvik Mehta, Apurva Durge, Sneha Kulkarni, and Vijayamohanan Pillai. "Electric field induced, superhydrophobic to superhydrophilic switching in multiwalled carbon nanotube papers". *Nano Letters* 8.9 (2008). DOI: 10.1021/nl801012r (cit. on p. 133).

[Kane1992] Randall W. Kane and Judy D. Timpa. "A High-Performance Liquid Chromatography Study of D-Cellobiose Degradation Under Fenton Conditions". *Journal of Carbohydrate Chemistry* 11.6 (1992). DOI: 10.1080/07328309208020092 (cit. on p. 167).

[Kato2014] Dawn M. Kato, Noelia Elía, Michael Flythe, and Bert C. Lynn. "Pretreatment of lignocellulosic biomass using Fenton chemistry". *Bioresource Technology* 162 (2014). DOI: 10.1016/j.biortech.2014.03.151 (cit. on p. 31).

[Kell2018] Laura Keller, Burkhard Ohs, Jelena Lenhart, Lorenz Abduly, Philipp Blanke, and Matthias Wessling. "High capacity polyethylenimine impregnated microtubes made of carbon nanotubes for CO2 capture". *Carbon* 126 (2018). DOI: 10.1016/j.carbon.2017.10.023 (cit. on p. 134).

[Kell2020] Robert Gregor Keller, Davide Di Marino, Malte Blindert, and Matthias Wessling. "Hydrotropic solutions enable homogeneous Fenton treatment of lignin". *Industrial & Engineering Chemistry Research* (2020). DOI: 10.1021/acs.iecr.9b06607 (cit. on p. 18).

[Kent2015] Michael S. Kent, Isaac C. Avina, Nadeya Rader, Michael L. Busse, Anthe George, Noppadon Sathitsuksanoh, Edward Baidoo, Jerilyn Timlin, Nicholas H. Giron, Mathias C. Celina, Laura E. Martin, Ronen Polsky, Victor H. Chavez, Dale L. Huber, Jay D. Keasling, Seema Singh, Blake A. Simmons, and Kenneth L. Sale. "Assay for lignin break-

down based on lignin films: insights into the Fenton reaction with insoluble lignin". *Green Chem.* 17.10 (2015). DOI: 10.1039/C5GC01083G (cit. on pp. 18, 55, 56, 65).

[Kent2018] Michael S. Kent, Jijiao Zeng, Nadeya Rader, Isaac C. Avina, Casey T. Simoes, Christopher K. Brenden, Michael L. Busse, John Watt, Nicholas H. Giron, Todd M. Alam, Mark D. Allendorf, Blake A. Simmons, Nelson S. Bell, and Kenneth L. Sale. "Efficient conversion of lignin into a water-soluble polymer by a chelator-mediated Fenton reaction: Optimization of H2O2 use and performance as a dispersant". *Green Chemistry* 20.13 (2018). DOI: 10.1039/c7gc03459h (cit. on pp. 18, 55, 74).

[Khat2011] A. R. Khataee, M. Safarpour, M. Zarei, and S. Aber. "Electrochemical generation of H2O2 using immobilized carbon nanotubes on graphite electrode fed with air: Investigation of operational parameters". *Journal of Electroanalytical Chemistry* 659.1 (2011). DOI: 10.1016/j.jelechem.2011.05.002 (cit. on p. 133).

[Kim2018] Hyo Won Kim, Michael B. Ross, Nikolay Kornienko, Liang Zhang, Jinghua Guo, Peidong Yang, and Bryan D. McCloskey. "Efficient hydrogen peroxide generation using reduced graphene oxide-based oxygen reduction electrocatalysts". *Nature Catalysis* 1.4 (2018). DOI: 10.1038/s41929-018-0044-2 (cit. on pp. 24, 26–28, 30, 98, 114, 142, 148).

[Klem2005a] Dieter Klemm, Brigitte Heublein, Hans-Peter Peter Fink, and Andreas Bohn. "Cellulose: fascinating biopolymer and sustainable raw material." *Angewandte Chemie - International Edition* 44.22 (2005). DOI: 10.1002/anie.200460587 (cit. on p. 17).

[Klem2005b] Dieter Klemm, Hans-Peter Schmauder, and Thomas Heinze. "Cellulose". In. *Biopolymers Online*. American Cancer Society, 2005. DOI: https://doi.org/10.1002/3527600035.bpol6010 (cit. on p. 16).

[Klet2017] Adam S Klett, E Foster, Aditya Bhalla, Daniel Holmes, C Thies, and David B Hodge. "Predicting lignin depolymerization yields from quantifiable properties using fraction-

ated biorefinery lignins". *Green Chemistry* 19 (2017). DOI: 10.1039/c7gc02023f (cit. on pp. 46, 72).

[Kose2018] Borte Kose Mutlu, Beatrice Cantoni, Andrea Turolla, Manuela Antonelli, Heileen Hsu-Kim, and Mark R. Wiesner. "Application of nanofiltration for Rare Earth Elements recovery from coal fly ash leachate: Performance and cost evaluation". *Chemical Engineering Journal* 349.May (2018). DOI: 10.1016/j.cej.2018.05.080 (cit. on p. 205).

[Kotr2008] Stefan Kotrel and Sigmar Bräuninger. "Industrial Electrocatalysis". In*Handbook of Heterogeneous Catalysis*. American Cancer Society, 2008. Chap. 8.1.3, pp. 1936–1958. (Cit. on p. 24).

[Kwon2012] Youngkook Kwon, Steven E. F. Kleijn, Klaas Jan P. Schouten, and Marc T. M. Koper. "Cellobiose hydrolysis and decomposition by electrochemical generation of acid and hydroxyl radicals". *ChemSusChem* 5.10 (2012). DOI: 10.1002/cssc.201200250 (cit. on pp. 18, 59, 78–84, 86, 91, 94, 152, 153, 164, 166, 167, 169, 172, 190).

[Laak2015] Timo Laakso, Mari Kallioinen, Arto Pihlajamäki, Mika Mänttäri, and John Erik Wong. "Polyelectrolyte multilayer coated ultrafiltration membranes for wood extract fractionation". *Separation and Purification Technology* 156.December (2015). DOI: 10.1016/j.seppur.2015.10.075 (cit. on p. 182).

[Laat2004] Joseph De Laat, Giang Truong Le, and Bernard Legube. "A comparative study of the effects of chloride , sulfate and nitrate ions on the rates of decomposition of H2O2 and organic compounds by Fe (II)/ H2O2 and Fe (III)/ H2O2". 55 (2004). DOI: 10.1016/j.chemosphere.2003.11.021 (cit. on p. 88).

[Lau2012] Carolin Lau, Emily R. Adkins, Ramaraja P. Ramasamy, Heather R. Luckarift, Glenn R. Johnson, and Plamen Atanassov. "Design of carbon nanotube-based gas-diffusion cathode for O2 reduction by multicopper oxidases". *Advanced Energy Materials* 2.1 (2012). DOI: 10.1002/aenm.201100433 (cit. on p. 133).

[Lede2017] Isis Ledezma-Yanez, W. David Z. Wallace, Paula Sebastián-Pascual, Victor Climent, Juan M. Feliu, and Marc T.M. Koper. "Interfacial water reorganization as a pH-dependent descriptor of the hydrogen evolution rate on platinum electrodes". *Nature Energy* 2.4 (2017). DOI: 10.1038/nenergy.2017.31 (cit. on p. 27).

[Lee2012] Ying Hui Lee, Feng Li, Kuo Hsin Chang, Chi Chang Hu, and Takeo Ohsaka. "Novel synthesis of N-doped porous carbons from collagen for electrocatalytic production of H_2O_2". *Applied Catalysis B: Environmental* 126 (2012). DOI: 10.1016/j.apcatb.2012.06.031 (cit. on p. 27).

[Leon2020] McLain E. Leonard, Lauren E Clarke, Antoni Forner-Cuenca, Steven M. Brown, and Fikile R. Brushett. "Investigating Electrode Flooding in a Flowing Electrolyte, Gas-Fed Carbon Dioxide Electrolyzer". *ChemSusChem* 13.2 (Jan. 2020). DOI: 10.1002/cssc.201902547 (cit. on p. 133).

[Lewi2006] Nathan S. Lewis and Daniel G. Nocera. "Powering the planet: Chemical challenges in solar energy utilization". *Proceedings of the National Academy of Sciences of the United States of America* 103.43 (2006). DOI: 10.1073/pnas.0603395103 (cit. on pp. 1, 24).

[Li2016] Nan Li, Jingkun An, Lean Zhou, Tian Li, Junhui Li, Cuijuan Feng, and Xin Wang. "A novel carbon black graphite hybrid air-cathode for efficient hydrogen peroxide production in bioelectrochemical systems". *Journal of Power Sources* 306 (2016). DOI: 10.1016/j.jpowsour.2015.12.078 (cit. on pp. 104, 111, 114).

[Liu2007] H Liu, X Z Li, Y J Leng, and C Wang. "Kinetic modeling of electro-Fenton reaction in aqueous solution". *Water Research* 41 (2007). DOI: 10.1016/j.watres.2006.12.006 (cit. on pp. 80, 164, 172).

[Liu2019] Kai Liu, Wilson A. Smith, and Thomas Burdyny. "Introductory Guide to Assembling and Operating Gas Diffusion Electrodes for Electrochemical CO2 Reduction". *ACS Energy Letters* (2019). DOI: 10.1021/acsenergylett.9b00137 (cit. on p. 100).

[Lute2014] J. S. Luterbacher, D. Martin Alonso, and J. A. Dumesic. "Targeted chemical upgrading of lignocellulosic biomass to platform molecules". *Green Chemistry* 16.12 (2014). DOI: 10.1039/c4gc01160k (cit. on p. 17).

[Ma2014] Ruoshui Ma, Mond Guo, and Xiao Zhang. "Selective conversion of biorefinery lignin into dicarboxylic acids". *ChemSusChem* 7.2 (2014). DOI: 10.1002/cssc.201300964 (cit. on pp. 18, 46).

[Ma2018a] C. Ma, X. W. Mei, Y. M. Fan, and Z. T. Zhang. "Oxidative Depolymerizaton of Kraft Lignin and its Application in the Synthesis of Lignin-phenol-formaldehyde Resin". *Bioresources* 13.1 (2018). (Cit. on pp. 15, 55, 62).

[Ma2018b] Qianli Ma, Junjun Zhu, Rolland Gleisner, Rendang Yang, and J Y Zhu. "Valorization of Wheat Straw Using a Recyclable Hydrotrope at Low Temperatures ($\leq$ 90 °C)". *ACS Sustainable Chemistry & Engineering* 6 (2018). DOI: 10.1021/acssuschemeng.8b03135 (cit. on pp. 14, 36, 37, 43).

[Mae2000] Kazuhiro Mae, Isao Hasegawa, Noriaki Sakai, and Kouichi Miura. "A New Conversion Method for Recovering Valuable Chemicals from Oil Palm Shell Wastes Utilizing Liquid-Phase Oxidation with H2O2 under Mild Conditions". *Energy Fuels* 14.1 (2000). DOI: 10.1021/ef0000911 (cit. on p. 74).

[Makh2008] O.A. Makhotkina, S.V. Preis, and E.V. Parkhomchuk. "Water delignification by advanced oxidation processes: Homogeneous and heterogeneous Fenton and H2O2 photo-assisted reactions". *Applied Catalysis B: Environmental* 84.3 (2008). DOI: https://doi.org/10.1016/j.apcatb.2008.06.015 (cit. on p. 31).

[Mala2011] Ramamoorthy Malaisamy, Alain Talla-Nwafo, and Kimberly L Jones. "Polyelectrolyte modification of nanofiltration membrane for selective removal of monovalent anions". *Separation and Purification Technology* 77.3 (2011). DOI: 10.1016/j.seppur.2011.01.005 (cit. on p. 182).

[Mänt2006] Mika Mänttäri, Arto Pihlajamäki, and Marianne Nyström. "Effect of pH on hydrophilicity and charge and their effect on the filtration efficiency of NF membranes at different

pH". *Journal of Membrane Science* 280 (1-2 2006). (Cit. on pp. 203, 204).

[Mari2019] Davide Di Marino, Tim Jestel, Caroline Marks, Jörn Viell, and Malte Blindert. "Carboxylic Acids Production via Electrochemical Depolymerization of Lignin". (2019). DOI: 10.1002/celc.201801676 (cit. on p. 166).

[Mass2018] Masson-Delmotte, V., P. Zhai, H.-O. Pörtner, D. Roberts, J. Skea, P.R. Shukla, A. Pirani, W. Moufouma-Okia, C. Péan, R. Pidcock, S. Connors, J.B.R. Matthews, Y. Chen, X. Zhou, M.I. Gomis, E. Lonnoy, T. Maycock, M. Tignor, and T. Waterfield (eds.) *Global Warming of 1.5°C. An IPCC Special Report on the impacts of global warming of 1.5°C above pre-industrial levels and related global greenhouse gas emission pathways, in the context of strengthening the global response to the threat of climate*. Tech. rep. Geneva: World Meteorological Organization, 2018 (cit. on p. 1).

[McIn1984] James Arthur McIntyre and Robert F. Phillips. "Method for electrolytic production of alkaline peroxide solutions". US4431494A. 1984 (cit. on pp. 28, 98).

[McIn1985] James Arthur McIntyre and Robert Floyd Philips. "Improved method of operating a liquid-gas electrochemical cell". US4511441A. 1985 (cit. on pp. 28, 98).

[McKe1946] R. H. McKee. "Use of Hydrotropic Solutions in Industry". *Industrial and Engineering Chemistry* 38.4 (1946). (Cit. on pp. 13, 14, 36).

[Meid1853] Heinrich Meidinger. "Ueber voltametrische Messungen". *Justus Liebigs Annalen der Chemie* 88.1 (1853). DOI: 10.1002/jlac.18530880103 (cit. on pp. 24, 98).

[Meli2007] Thomas Melin and Robert Rautenbach. *Membranverfahren: Grundlagen der Modul-und Anlagenauslegung*. Springer-Verlag, 2007. DOI: 10.1007/978-3-540-34328-8 (cit. on pp. 33, 181, 182, 187, 192, 202).

[Meng2011] De Fa Meng, Gang Li, Fang Yang, and Zhi Hua Liu. "Electrocatalytic Degradation of Cellulose Using Lead Dioxide Anode". *Advanced Materials Research* 233-235 (2011). DOI:

10.4028/www.scientific.net/AMR.233-235.1036 (cit. on pp. 18, 78, 79, 91, 152, 153).

[Menn2016a] Daniel Menne, Johannes Kamp, John Erik, and Matthias Wessling. "Precise tuning of salt retention of backwashable polyelectrolyte multilayer hollow fiber nanofiltration membranes". *Journal of Membrane Science* 499 (2016). DOI: 10.1016/j.memsci.2015.10.058 (cit. on pp. 163, 178, 180–182, 204, 207).

[Menn2016b] Daniel Menne, Cagri Üzüm, Arne Koppelmann, John Erik Wong, Chiel van Foeken, Fokko Borre, Lars Dähne, Timo Laakso, Arto Pihlajamäki, and Matthias Wessling. "Regenerable polymer/ceramic hybrid nanofiltration membrane based on polyelectrolyte assembly by layer-by-layer technique". *Journal of Membrane Science* 520 (2016). DOI: 10.1016/j.memsci.2016.08.048 (cit. on pp. 163, 184).

[Micra] Microdyn-Nadir. *NP010*. URL: https://www.lenntech.com/Data-sheets/Microdyn-Nadir-D-NP010-P-V1-01-L.pdf (visited on 11/19/2020) (cit. on pp. 159, 161, 176, 207).

[Micrb] Microdyn-Nadir. *NP030*. URL: https://www.lenntech.com/Data-sheets/Microdyn-Nadir-D-NP030-P-V1-L.pdf (visited on 11/19/2020) (cit. on pp. 159, 161, 207).

[Micrc] Microdyn-Nadir. *US100*. URL: https://www.lenntech.com/Data-sheets/Microdyn-Spira-Cel-L.pdf (visited on 11/19/2020) (cit. on pp. 159, 161).

[Moha2010] A. W. Mohammad, R. Kadir Basha, and C. P. Leo. "Nanofiltration of glucose solution containing salts: Effects of membrane characteristics, organic component and salts on retention". *Journal of Food Engineering* 97.4 (2010). DOI: 10.1016/j.jfoodeng.2009.11.010 (cit. on pp. 202, 203, 206).

[Moha2015] A. W. Mohammad, Y. H. Teow, W. L. Ang, Y. T. Chung, D. L. Oatley-Radcliffe, and N. Hilal. "Nanofiltration membranes review: Recent advances and future prospects". *Desalination* 356 (2015). DOI: 10.1016/j.desal.2014.10.043 (cit. on p. 161).

[Mou2014] Hongyan Mou, Elina Heikkila, and Pedro Fardim. "Topochemistry of Environmentally Friendly Pretreatments To Enhance Enzymatic Hydrolysis of Sugar Cane Bagasse to Fermentable Sugar". *Journal of Agricultural and Food Chemistry* 62.16 (2014). DOI: 10.1021/jf500582w (cit. on p. 43).

[Mou2017] Hongyan Mou and Shubin Wu. "Comparison of hydrothermal, hydrotropic and organosolv pretreatment for improving the enzymatic digestibility of bamboo". *Cellulose* 24.1 (2017). DOI: 10.1007/s10570-016-1117-5 (cit. on pp. 14, 43).

[Mudd2020] Thorben Muddemann, Dennis R. Haupt, Michael Sievers, and Ulrich Kunz. "Improved Operating Parameters for Hydrogen Peroxide-Generating Gas Diffusion Electrodes". *Chemie-Ingenieur-Technik* 92.5 (2020). DOI: 10.1002/cite.201900137 (cit. on pp. 29, 30, 98, 105, 106, 110, 114, 142).

[Musa2005] Mustafa Musameh, Nathan S. Lawrence, and Joseph Wang. "Electrochemical activation of carbon nanotubes". *Electrochemistry Communications* 7.1 (2005). DOI: 10.1016/j.elecom.2004.10.007 (cit. on p. 133).

[Nidh2012] P.V. Nidheesh and R. Gandhimathi. "Trends in electro-Fenton process for water and wastewater treatment: An overview". *Desalination* 299 (Aug. 2012). DOI: 10.1016/j.desal.2012.05.011 (cit. on pp. 164, 172).

[Nogu2005] Raquel F Pupo Nogueira, Mirela C Oliveira, and Willian C Paterlini. "Simple and fast spectrophotometric determination of H2O2 in photo-Fenton reactions using metavanadate." *Talanta* 66.1 (Mar. 2005). DOI: 10.1016/j.talanta.2004.10.001 (cit. on p. 103).

[Nord2014] Rune T. Nordvang, Jianquan Luo, Birgitte Zeuner, Rasmus Prior, Mads F. Andersen, Jørn D. Mikkelsen, Anne S. Meyer, and Manuel Pinelo. "Separation of 3-sialyllactose and lactose by nanofiltration: A trade-off between charge repulsion and pore swelling induced by high pH". *Separation and Purification Technology* 138 (2014). DOI: 10.1016/j.seppur.2014.10.012 (cit. on pp. 176, 203, 206, 207).

[Ocha2016] J Ochando-Pulido, M Víctor-Ortega, and A Martínez-Férez. "Recovery of iron after Fenton-like secondary treatment of olive mill wastewater by nano-filtration and low-pressure reverse osmosis membranes". *Grasas y Aceites* 67.3 (2016). DOI: 10.3989/gya.1001153 (cit. on pp. 153, 154).

[Olom1979] C. Oloman and A. P. Watkinson. "Hydrogen peroxide production in trickle-bed electrochemical reactors". *Journal of Applied Electrochemistry* 9.1 (1979). DOI: 10.1007/BF00620593 (cit. on p. 28).

[Orel2018] Michael J. Orella, Yuriy Román-Leshkov, and Fikile R. Brushett. "Emerging opportunities for electrochemical processing to enable sustainable chemical manufacturing". *Current Opinion in Chemical Engineering* 20 (2018). DOI: 10.1016/j.coche.2018.05.002 (cit. on pp. 1, 24).

[Osie2013] Lidia Osiewała, Adam Socha, Aleksandra Perek, Marek Socha, and Jacek Rynkowski. "Electrochemical, photochemical, and photoelectrochemical treatment of sodium p-cumenesulfonate". *Water, Air, and Soil Pollution* 224.9 (2013). DOI: 10.1007/s11270-013-1657-3 (cit. on pp. 70, 71).

[Park2010] Sunkyu Park, John O Baker, Michael E Himmel, Philip A Parilla, and David K Johnson. "Cellulose crystallinity index: measurement techniques and their impact on interpreting cellulase performance". *Biotechnology for Biofuels* 3.1 (2010). DOI: 10.1186/1754-6834-3-10 (cit. on p. 17).

[Park2012] Sehkyu Park, Jong Won Lee, and Branko N. Popov. "A review of gas diffusion layer in PEM fuel cells: Materials and designs". *International Journal of Hydrogen Energy* 37.7 (2012). DOI: 10.1016/j.ijhydene.2011.12.148 (cit. on p. 133).

[Park2014] Jisung Park, Yuta Nabae, Teruaki Hayakawa, and Masa Aki Kakimoto. "Highly selective two-electron oxygen reduction catalyzed by mesoporous nitrogen-doped carbon". *ACS Catalysis* 4.10 (2014). DOI: 10.1021/cs5008206 (cit. on p. 27).

[Perc2020] Korcan Percin, Oliver Zoellner, Deniz Rall, and Matthias Wessling. “A Tubular Electrochemical Reactor for Slurry Electrodes”. *ChemElectroChem* 7.12 (2020). DOI: 10.1002/celc.202000616 (cit. on p. 23).

[Perr2019] Samuel C. Perry, Dhananjai Pangotra, Luciana Vieira, Lénárd István Csepei, Volker Sieber, Ling Wang, Carlos Ponce de León, and Frank C. Walsh. “Electrochemical synthesis of hydrogen peroxide from water and oxygen”. *Nature Reviews Chemistry* 3.7 (2019). DOI: 10.1038/s41570-019-0110-6 (cit. on pp. 23–26, 98).

[Pign1997] Joseph J Pignatello. “Role of Quinone Intermediates as Electron Shuttles in Fenton and Photoassisted Fenton Oxidations of Aromatic Compounds”. *Environ. Scie. Technol.* 31.8 (1997). DOI: 10.1021/es9610646 (cit. on p. 71).

[Pign2006] Joseph J. Pignatello, Esther Oliveros, and Allison MacKay. “Advanced Oxidation Processes for Organic Contaminant Destruction Based on the Fenton Reaction and Related Chemistry”. *Critical Reviews in Environmental Science and Technology* 36.April 2015 (2006). DOI: 10.1080/10643380500326564 (cit. on pp. 30–32, 54, 66, 71, 81–83, 88, 91, 98, 153, 184, 205).

[Plie2015] Gema Pliego, Juan A. Zazo, Patricia Garcia-Muñoz, Macarena Munoz, Jose A. Casas, and Juan J. Rodriguez. “Trends in the Intensification of the Fenton Process for Wastewater Treatment: An Overview”. *Critical Reviews in Environmental Science and Technology* 45.24 (Dec. 2015). DOI: 10.1080/10643389.2015.1025646 (cit. on pp. 31, 32).

[Proc1971] A. R. Procter. “Review of Hydrotropic Pulping”. *Pulp and Paper Magazine of Canada* 72.8 (1971). (Cit. on pp. 14, 36).

[Proc2015] Alessandra Procentese, Erin Johnson, Valerie Orr, Anna Garruto Campanile, Jeffery a. Wood, Antonio Marzocchella, and Lars Rehmann. “Deep eutectic solvent pretreatment and subsequent saccharification of corncob”. *Bioresource Technology* 192 (2015). DOI: 10.1016/j.biortech.2015.05.053 (cit. on pp. 36, 37).

[Pu2008] Y. Q. Pu, D. C. Zhang, P. M. Singh, and A. J. Ragauskas. "The new forestry biofuels sector". *Biofuels Bioproducts & Biorefining* 2.1 (2008). (Cit. on p. 15).

[Qi2011] Benkun Qi, Jianquan Luo, Xiangrong Chen, Xiaofeng Hang, and Yinhua Wan. "Separation of furfural from monosaccharides by nanofiltration". *Bioresource Technology* 102.14 (2011). DOI: 10.1016/j.biortech.2011.04.041 (cit. on p. 204).

[Qian2002] Zhimin Qiang, Jih-Hsing Chang, and Chin-Pao Huang. "Electrochemical generation of hydrogen peroxide from dissolved oxygen in acidic solutions." *Water research* 36.1 (2002). DOI: 10.1016/S0043-1354(01)00235-4 (cit. on pp. 25, 27, 32).

[Qiu2015] Shan Qiu, Di He, Jinxing Ma, Tongxu Liu, and T. David Waite. "Kinetic Modeling of the Electro-Fenton Process: Quantification of Reactive Oxygen Species Generation". *Electrochimica Acta* 176 (2015). DOI: 10.1016/j.electacta.2015.06.103 (cit. on pp. 183, 184).

[Rahi2014] Shima Rahim Pouran, Abdul Aziz Abdul Raman, and Wan Mohd Ashri Wan Daud. "Review on the application of modified iron oxides as heterogeneous catalysts in Fenton reactions". *Journal of Cleaner Production* 64 (2014). DOI: 10.1016/j.jclepro.2013.09.013 (cit. on p. 153).

[Rege2018] Lars Regestein, Tobias Klement, Philipp Grande, Dirk Kreyenschulte, Benedikt Heyman, Tim Maßmann, Armin Eggert, Robert Sengpiel, Yumei Wang, Nick Wierckx, Lars M Blank, Antje Spiess, Walter Leitner, Carsten Bolm, Matthias Wessling, Andreas Jupke, Miriam Rosenbaum, and Jochen Büchs. "Biotechnology for Biofuels From beech wood to itaconic acid : case study on biorefinery process integration". *Biotechnology for Biofuels* 11.279 (2018). DOI: 10.1186/s13068-018-1273-y (cit. on pp. 2, 11, 187).

[Reis2012] Rafael M. Reis, André A.G.F. Beati, Robson S. Rocha, Mônica H.M.T. Assumpção, Mauro C. Santos, Rodnei Bertazzoli, and Marcos R.V. Lanza. "Use of gas diffusion electrode for the in situ generation of hydrogen peroxide in an electrochemical flow-by reactor". *Industrial and Engineering*

Chemistry Research 51.2 (2012). DOI: 10.1021/ie201317u (cit. on pp. 104, 114).

[Reur2018] Dennis M. Reurink, Jord P. Haven, Iske Achterhuis, Saskia Lindhoud, (Erik) H.D.W. Roesink, and Wiebe M. de Vos. "Annealing of Polyelectrolyte Multilayers for Control over Ion Permeation". *Advanced Materials Interfaces* 5.20 (2018). DOI: 10.1002/admi.201800651 (cit. on p. 182).

[Ried1939] Hans-Joachim Riedl and Georg Pfleiderer. "Production of hydrogen peroxide". US2158525A. 1939 (cit. on p. 24).

[Rina2016] Roberto Rinaldi, Robin Jastrzebski, Matthew T. Clough, John Ralph, Marco Kennema, Pieter C. A. Bruijnincx, and Bert M. Weckhuysen. "Paving the Way for Lignin Valorisation: Recent Advances in Bioengineering, Biorefining and Catalysis". *Angewandte Chemie International Edition* 55.29 (2016). DOI: 10.1002/anie.201510351 (cit. on p. 46).

[Robe2017] G. Philip Robertson, Stephen K. Hamilton, Bradford L. Barham, Bruce E. Dale, R. Cesar Izaurralde, Randall D. Jackson, Douglas A. Landis, Scott M. Swinton, Kurt D. Thelen, and James M. Tiedje. "Cellulosic biofuel contributions to a sustainable energy future: Choices and outcomes". *Science* 356.6345 (2017). DOI: 10.1126/science.aal2324 (cit. on pp. 1, 10).

[Robl2018] Irma Robles, Francisco J Rodríguez-valadez, Luis A Godínez, and Dennys Fern. "Novel arrangement for an electro-Fenton reactor that does not require addition of iron , acid and a final neutralization stage . Towards the development of a cost-effective technology for the treatment of wastewater". *Chemosphere* 199 (2018). DOI: 10.1016/j.chemosphere.2018.02.036 (cit. on p. 153).

[Rohe2014] D. Rohendi, E. H. Majlan, A. B. Mohamad, W. R.W. Daud, A. A.H. Kadhum, and L. K. Shyuan. "Effect of PTFE content and sintering temperature on the properties of a fuel cell electrode backing layer". *Journal of Fuel Cell Science and Technology* 11.4 (2014). DOI: 10.1115/1.4026932 (cit. on p. 133).

[Roth2016] Hannah Roth, Youri Gendel, Pompilia Buzatu, and Oana David. "Tubular carbon nanotube-based gas diffusion electrode removes persistent organic pollutants by a cyclic adsorption - electro-Fenton process". *Journal of Hazardous Materials* 307 (2016). DOI: 10.1016/j.jhazmat.2015.12.066 (cit. on pp. 148, 153).

[Sagu2018] William J. Sagues, Hanxi Bao, John L. Nemenyi, and Zhaohui Tong. "Lignin-First Approach to Biorefining: Utilizing Fenton's Reagent and Supercritical Ethanol for the Production of Phenolics and Sugars". *ACS Sustainable Chemistry and Engineering* 6.4 (2018). DOI: 10.1021/acssuschemeng.7b04500 (cit. on pp. 18, 54).

[Sánc2009] Carlos M. Sánchez-Sánchez and Allen J. Bard. "Hydrogen peroxide production in the oxygen reduction reaction at different electrocatalysts as quantified by scanning electrochemical microscopy". *Analytical Chemistry* 81.19 (2009). DOI: 10.1021/ac901291v (cit. on pp. 124, 125).

[Sany2015] Oishi Sanyal, Zhiguo Liu, Brooke M. Meharg, Wei Liao, and Ilsoon Lee. "Development of polyelectrolyte multilayer membranes to reduce the COD level of electrocoagulation treated high-strength wastewater". *Journal of Membrane Science* 496 (2015). DOI: 10.1016/j.memsci.2015.09.011 (cit. on p. 34).

[Schä2018] Tobias Schäfer, Moritz Eisenlauer, and Ulrich Teipel. "Extraction of Spruce Lignin with a Deep Eutectic Solvent in Dependence of the Particle Size". *Chemie Ingenieur Technik* 90.4 (2018). DOI: 10.1002/cite.201700104 (cit. on p. 41).

[Schi2017] Zachary J. Schiffer and Karthish Manthiram. "Electrification and Decarbonization of the Chemical Industry". *Joule* 1.1 (2017). DOI: 10.1016/j.joule.2017.07.008 (cit. on pp. 1, 24).

[Schm2012] Volkmar M Schmidt. *Elektrochemische Verfahrenstechnik: Grundlagen, Reaktionstechnik, Prozessoptimierung*. John Wiley & Sons, 2012. DOI: 10.1002/3527602143 (cit. on pp. 22, 105).

[Schu1978] M N Schuchmann and C von Sonntag. "The effect of oxygen on the OH-radical-induced scission of the glycosidic linkage of cellobiose." *International journal of radiation biology and related studies in physics, chemistry, and medicine* 34.4 (1978). (Cit. on pp. 17, 93, 172).

[Schu2018] W. Schutyser, T. Renders, S. Van Den Bosch, S. F. Koelewijn, G. T. Beckham, and B. F. Sels. "Chemicals from lignin: An interplay of lignocellulose fractionation, depolymerisation, and upgrading". *Chemical Society Reviews* 47.3 (2018). DOI: 10.1039/c7cs00566k (cit. on pp. 10, 15, 16, 46, 54, 65, 66, 71).

[Semi2011] Andrea J.C. Semião and Andrea I. Schäfer. "Estrogenic micropollutant adsorption dynamics onto nanofiltration membranes". *Journal of Membrane Science* 381.1-2 (2011). DOI: 10.1016/j.memsci.2011.07.031 (cit. on p. 205).

[Shao2006] Yuyan Shao, Geping Yin, Jian Zhang, and Yunzhi Gao. "Comparative investigation of the resistance to electrochemical oxidation of carbon black and carbon nanotubes in aqueous sulfuric acid solution". *Electrochimica Acta* 51.26 (2006). DOI: 10.1016/j.electacta.2006.03.021 (cit. on p. 133).

[She2015] Z. She, J. G. Wang, J. P. Ni, X. Q. Liu, R. Y. Zhang, H. N. Na, and J. Zhu. "Direct conversion of cellulose into glycolic acid by a zinc-stabilized UV-Fenton reaction". *RSC Adv.* 5 (2015). DOI: 10.1039/C4RA11070F (cit. on pp. 152, 190).

[Shi2013] Jiafu Shi, Wenyan Zhang, Yanlei Su, and Zhongyi Jiang. "Composite polyelectrolyte multilayer membranes for oligosaccharides nanofiltration separation". *Carbohydrate polymers* 94.1 (2013). DOI: 10.1016/j.carbpol.2013.01.044 (cit. on pp. 154, 178, 187, 192, 205, 207).

[Shi2018] X. J. Shi, X. Wang, B. Tang, Z. Dai, K. F. Chen, and J. H. Zhou. "Impact of lignin extraction methods on microstructure and mechanical properties of lignin-based carbon fibers". *Journal of Applied Polymer Science* 135.10 (2018). (Cit. on p. 15).

[Siah2013] Samira Siahrostami, Arnau Verdaguer-Casadevall, Mohammadreza Karamad, Davide Deiana, Paolo Malacrida, Björn Wickman, María Escudero-Escribano, Elisa A. Paoli, Rasmus Frydendal, Thomas W. Hansen, Ib Chorkendorff, Ifan E.L. Stephens, and Jan Rossmeisl. "Enabling direct H_2O_2 production through rational electrocatalyst design". *Nature Materials* 12.12 (2013). DOI: 10.1038/nmat3795 (cit. on p. 27).

[Silv2015] Marcos Henrique Luciano Silveira, Ana Rita C. Morais, Andre M. da Costa Lopes, Drielly Nayara Olekszyszen, Rafał Bogel-Łukasik, Jürgen Andreaus, and Luiz Pereira Ramos. "Current Pretreatment Technologies for the Development of Cellulosic Ethanol and Biorefineries". *ChemSusChem* 8.20 (Aug. 2015). DOI: 10.1002/cssc.201500282 (cit. on pp. 10–13, 36, 43).

[Sixt2006] Herbert Sixta. *Handbook of pulp*. Wiley-vch, 2006 (cit. on pp. 11, 12, 15, 17, 18).

[Smit2014] Emma L. Smith, Andrew P. Abbott, and Karl S. Ryder. "Deep Eutectic Solvents (DESs) and Their Applications". *Chemical Reviews* 114.21 (2014). DOI: 10.1021/cr300162p (cit. on pp. 14, 36).

[Soeh2008] M. Soehn, M. Lebert, T. Wirth, S. Hofmann, and N. Nicoloso. "Design of gas diffusion electrodes using nanocarbon". *Journal of Power Sources* 176.2 (2008). DOI: 10.1016/j.jpowsour.2007.08.073 (cit. on p. 133).

[Song2008] Chaojie Song and Jiujun Zhang. "Electrocatalytic oxygen reduction reaction". In*PEM Fuel Cell Electrocatalysts and Catalyst Layers: Fundamentals and Applications*. Ed. by Jiujun Zhang. London: Springer, 2008. Chap. 2, pp. 89–134. (Cit. on pp. 24, 25).

[Sonn1976] C von Sonntag, Miral Dizdaraoglu, and Dietrich Schulte-Frohlinde. "Radiation Chemistry of Carbohydrates, y-Radiolysis of Cellobiose in N 2 0 - saturated Aqueous Solution Part I I . Quantitative Measurements . Mechanisms of the Radical-induced Scission of the Glycosidic Linkage". *Zeitschrift fur Naturforschung B* 31b.6 (1976). (Cit. on pp. 84, 94, 170, 172, 190).

[Stie2016a] S. Stiefel, C. Marks, T. Schmidt, S. Hanisch, G. Spalding, and M. Wessling. "Overcoming lignin heterogeneity: reliably characterizing the cleavage of technical lignin". *Green Chemistry* 18.2 (2016). (Cit. on p. 15).

[Stie2016b] Serafin Stiefel, Annika Schmitz, Jens Peters, Davide Di Marino, and Matthias Wessling. "An integrated electrochemical process to convert lignin to value-added products under mild conditions". *Green Chem.* 18.18 (2016). DOI: 10.1039/C6GC00878J (cit. on p. 65).

[Subb2012] C. V. Subbarao, I. P.K. Chakravarthy, A. V.S.L. Sai Bharadwaj, and K. M.M. Prasad. "Functions of hydrotropes in solutions". *Chemical Engineering and Technology* 35.2 (2012). DOI: 10.1002/ceat.201100484 (cit. on pp. 13, 36).

[Sueza] Suez. *DK Series*. URL: https://www.lenntech.com/Data-sheets/GE-Osmonics-DK-Series-High-Rejection-Nanofiltration-RO-Elements-L.pdf (visited on 11/19/2020) (cit. on p. 206).

[Suezb] Suez. *DL Series*. URL: https://www.lenntech.com/Data-sheets/GE-Osmonics-DL-Series-Industrial-High-Flow-Nanofiltration-Elements-L.pdf (visited on 11/19/2020) (cit. on p. 206).

[Tade2011] Haregewine Tadesse and Rafael Luque. "Advances on biomass pretreatment using ionic liquids: an overview". *Energy & Environmental Science* 4.10 (2011). (Cit. on p. 36).

[Tang2017] Xing Tang, Miao Zuo, Zheng Li, Huai Liu, Caixia Xiong, Xianhai Zeng, Yong Sun, Lei Hu, Shijie Liu, Tingzhou Lei, and Lu Lin. "Green Processing of Lignocellulosic Biomass and Its Derivatives in Deep Eutectic Solvents". *ChemSusChem* 10.13 (2017). DOI: 10.1002/cssc.201700457 (cit. on p. 36).

[Tara1983] M. R. Tarasevich, Andrzej Sadkowski, and Ernest Yeager. "Oxygen Electrochemistry". *Comprehensive Treatise of Electrochemistry* (1983). DOI: 10.1007/978-1-4613-3584-9_6 (cit. on pp. 25–27, 98).

[Torr2003] Francesc Torrades. "Experimental design of Fenton and photo-Fenton reactions for the treatment of cellulose bleaching effluents". 53 (2003). DOI: 10.1016/S0045-6535(03)00579-4 (cit. on p. 86).

[Trau1882] Moritz Traube. “Ueber die Aktivirung des Sauerstoffs”. *Berichte der deutschen chemischen Gesellschaft* 15.2 (1882). DOI: 10.1002/cber.188201502197 (cit. on pp. 24, 98).

[Truo2004] Giang Le Truong, Joseph De Laat, and Bernard Legube. “Effects of chloride and sulfate on the rate of oxidation of ferrous ion by H2O2”. *Water Research* 38.9 (2004). DOI: 10.1016/j.watres.2004.01.033 (cit. on p. 88).

[Umwe2020] Umweltbundesamt. *Nationale Treibhausgas-Inventare 1990 bis 2018 (Stand 12/2019) und Zeitnahschätzung für 2019 aus UBA Presse-Mitteilung 15.03.2020*. 2020 (cit. on p. 1).

[Vali2013] Ricardo B. Valim, Rafael M. Reis, Pollyana S. Castro, Alex S. Lima, Robson S. Rocha, Mauro Bertotti, and Marcos R V Lanza. “Electrogeneration of hydrogen peroxide in gas diffusion electrodes modified with tert-butyl-anthraquinone on carbon black support”. *Carbon* 61 (2013). DOI: 10.1016/j.carbon.2013.04.100 (cit. on p. 114).

[Vedo2020] Vincent Vedovato, Karolien Vanbroekhoven, Deepak Pant, and Joost Helsen. “Electrosynthesis of Biobased Chemicals Using Carbohydrates as a Feedstock”. *Molecules* 25.16 (Aug. 2020). DOI: 10.3390/molecules25163712 (cit. on pp. 2, 18).

[Vell1998] Eert Vellenga and Gun Trägårdh. “Nanofiltration of combined salt and sugar solutions: Coupling between retentions”. *Desalination* 120.3 (1998). DOI: 10.1016/S0011-9164(98)00219-7 (cit. on p. 203).

[Venn2019a] Jan-bernd Vennekoetter, Robert Sengpiel, and Matthias Wessling. “Beyond the catalyst : How electrode and reactor design determine the product spectrum during electrochemical CO 2 reduction”. *Chemical Engineering Journal* 364.January (2019). DOI: 10.1016/j.cej.2019.01.045 (cit. on pp. 98, 100, 109).

[Venn2019b] Jan-bernd Vennekötter, Thomas Scheuermann, Robert Sengpiel, and Matthias Wessling. “The electrolyte matters : Stable systems for high rate electrochemical CO 2 reduction”. *Journal of CO2 Utilization* 32.February (2019). DOI: 10.1016/j.jcou.2019.04.007 (cit. on p. 105).

[Verd2014] Arnau Verdaguer-Casadevall, Davide Deiana, Mohammadreza Karamad, Samira Siahrostami, Paolo Malacrida, Thomas W Hansen, Jan Rossmeisl, Ib Chorkendor, and Ifan E L Stephens. "Trends in the Electrochemical Synthesis of H_2O_2: Enhancing Activity and Selectivity by Electrocatalytic Site Engineering". *Nano Letters* 14 (2014). (Cit. on pp. 26, 27, 98).

[Vigi2015] Karine De Oliveira Vigier, Gregory Chatel, and François Jérôme. "Contribution of Deep Eutectic Solvents for Biomass Processing: Opportunities, Challenges, and Limitations". *ChemCatChem* 7.8 (2015). DOI: 10.1002/cctc.201500134 (cit. on p. 14).

[Wage2012] Kurt Wagemann et al. *Biorefineries Roadmap as a part of the German Federal Government action plans for the material and energetic utilisation of renewable raw materials.* Tech. rep. Berlin: Federal Ministry of Food, Agriculture and Consumer Protection, 2012, p. 108 (cit. on pp. 10, 11).

[Wage2019] Kurt Wagemann and Nils Tippkötter. *Biorefineries.* Springer, 2019. DOI: 10.1007/978-3-319-97119-3 (cit. on pp. 2, 12, 17, 18).

[Wang2011] Zhong Xu Wang, Gang Li, Fang Yang, Yu Lu Chen, and Peng Gao. "Electro-Fenton degradation of cellulose using graphite / PTFE electrodes modified by 2-ethylanthraquinone". *Carbohydrate Polymers* 86.4 (2011). DOI: 10.1016/j.carbpol.2011.07.021 (cit. on pp. 18, 78, 79, 91, 152, 153).

[Wang2012] Andrew Wang, Arman Bonakdarpour, David P. Wilkinson, and Elöd Gyenge. "Novel organic redox catalyst for the electroreduction of oxygen to hydrogen peroxide". *Electrochimica Acta* 66 (2012). DOI: 10.1016/j.electacta.2012.01.086 (cit. on p. 127).

[Wang2019] Zhaojiang Wang, Shi Qiu, Kolby Hirth, Jinlan Cheng, Jialong Wen, Ning Li, Yunming Fang, Xuejun Pan, and J.Y. Zhu. "Preserving Both Lignin and Cellulose Chemical Structures: Flow-Through Acid Hydrotropic Fractionation at Atmospheric Pressure for Complete Wood Valorization". *ACS Sustainable Chemistry & Engineering* 7.12 (2019). DOI:

10.1021/acssuschemeng.9b01634 (cit. on pp. 14, 36, 37, 43, 46).

[Xia2019] Chuan Xia, Yang Xia, Peng Zhu, and Lei Fan. "Direct electrosynthesis of pure aqueous H_2O_2 solutions up to 20% by weight using a solid electrolyte". *Science* 366.October (2019). DOI: 10.1126/science.aay1844 (cit. on pp. 30, 98, 114).

[Xing2008] Wei Xing. "Catalyst layer composition optimization". In *PEM Fuel Cell Electrocatalysts and Catalyst Layers*. Ed. by Jiujun Zhang. London: Springer, 2008. Chap. 22, pp. 1003–1040. (Cit. on p. 133).

[Xu1999] Yazhen Xu and Rémi E. Lebrun. "Investigation of the solute separation by charged nanofiltration membrane: Effect of pH, ionic strength and solute type". *Journal of Membrane Science* 158.1-2 (1999). DOI: 10.1016/S0376-7388(99)00005-8 (cit. on p. 205).

[Xu2001] G. Xu and B. Goodell. "Mechanisms of wood degradation by brown-rot fungi: Chelator-mediated cellulose degradation and binding of iron by cellulose". *Journal of Biotechnology* 87 (2001). DOI: 10.1016/S0168-1656(00)00430-2 (cit. on pp. 78, 91).

[Yang2011] Bin Yang, Ziyu Dai, Shi-you Ding, and Charles E Wyman. "Enzymatic hydrolysis of cellulosic biomass". *Biofuels* 2.4 (July 2011). DOI: 10.4155/bfs.11.116 (cit. on p. 17).

[Yang2014] Fang Yang, Qian Zhang, Hong-Xian Fan, Yang Li, and Gang Li. "Electrochemical control of the conversion of cellulose oligosaccharides into glucose". *Journal of Industrial and Engineering Chemistry* 20.5 (Sept. 2014). DOI: 10.1016/j.jiec.2013.12.039 (cit. on pp. 18, 78, 79, 152, 153).

[Yang2018a] Sungeun Yang, Arnau Verdaguer-Casadevall, Logi Arnarson, Luca Silvioli, Viktor Čolić, Rasmus Frydendal, Jan Rossmeisl, Ib Chorkendorff, and Ifan E.L. Stephens. "Toward the Decentralized Electrochemical Production of H2O2: A Focus on the Catalysis". *ACS Catalysis* 8.5 (2018). DOI: 10.1021/acscatal.8b00217 (cit. on pp. 27, 111, 127, 131).

[Yang2018b] W. J. Yang, E. Fortunati, D. Q. Gao, G. M. Balestra, G. Giovanale, X. Y. He, L. Torre, J. M. Kenny, and D. Puglia. "Valorization of Acid Isolated High Yield Lignin Nanoparticles as Innovative Antioxidant/Antimicrobial Organic Materials". *ACS Sustainable Chemistry & Engineering* 6.3 (2018). (Cit. on p. 15).

[Yeag1976] E. Yeager. "Electrocatalysis on Non-Metalic Surfaces". *NBS Special Publication* 455 (1976). (Cit. on p. 26).

[Yeag1984] E Yeager. "Electrocatalysts for O_2 Reduction". *Electrochimica Acta* 29.11 (1984). (Cit. on pp. 27, 98).

[Yu2015] Xinmin Yu, Minghua Zhou, Gengbo Ren, and Liang Ma. "A novel dual gas diffusion electrodes system for efficient hydrogen peroxide generation used in electro-Fenton". *Chemical Engineering Journal* 263 (2015). DOI: 10.1016/j.cej.2014.11.053 (cit. on p. 114).

[Yun2008] Yu Yun, Lou Xia, and Wu Hongwei. "Some Recent Advances in Hydrolysis of Biomass in Hot-Compressed Water and Its Comparisons with Other Hydrolysis Methods". *Energy and Fuels* 22.1 (2008). DOI: 10.1021/ef7002969 (cit. on p. 17).

[Zakz2010] J. Zakzeski, P. C. A. Bruijnincx, A. L. Jongerius, and B. M. Weckhuysen. "The Catalytic Valorization of Lignin for the Production of Renewable Chemicals". *Chemical Reviews* 110.6 (2010). (Cit. on p. 15).

[Zazo2005] J. A. Zazo, J. A. Casas, A. F. Mohedano, M. A. Gilarranz, and J. J. Rodríguez. "Chemical pathway and kinetics of phenol oxidation by Fenton's reagent". *Environmental Science and Technology* 39.23 (2005). DOI: 10.1021/es050452h (cit. on pp. 64, 71).

[Zeng2015] J. J. Zeng, C. G. Yoo, F. Wang, X. J. Pan, W. Vermerris, and Z. H. Tong. "Biomimetic Fenton-Catalyzed Lignin Depolymerization to High-Value Aromatics and Dicarboxylic Acids". *Chemsuschem* 8.5 (2015). (Cit. on pp. 18, 46, 54).

[Zhan2008] Huamin Zhang, Xiaoli Wang, Jianlu Zhang, and Jiujun Zhang. "Conventional Catalyst Ink, Catalyst Layer and MEA Preparation". In. *PEM Fuel Cell Electrocatalysts and Catalyst Layers: Fundamentals and Applications*. Ed. by

Jiujun Zhang. London: Springer, 2008. Chap. 19, pp. 889–916. DOI: 10.1007/978-1-84800-936-3_19 (cit. on pp. 22, 132).

[Zhan2012] Qinghua Zhang, Karine De Oliveira Vigier, Sébastien Royer, and François Jérôme. "Deep eutectic solvents: syntheses, properties and applications." *Chem. Soc. Rev.* 41.21 (2012). DOI: 10.1039/c2cs35178a (cit. on p. 14).

[Zhao2010] Wei Zhao, Wen-Juan Xu, Xiao-Jing Lu, Chen Sheng, Shi-Teng Zhong, Shi-Rong Tang, Zhi-Min Zong, and Xian-Yong Wei. "Preparation and Property Measurement of Liquid Fuel from Supercritical Ethanolysis of Wheat Stalk". *Energy & Fuels* 24.1 (2010). DOI: 10.1021/ef900521k (cit. on p. 46).

[Zhen2016] Zhaoke Zheng, Yun Hau Ng, Da Wei Wang, and Rose Amal. "Epitaxial Growth of Au–Pt–Ni Nanorods for Direct High Selectivity H_2O_2 Production". *Advanced Materials* 28.45 (2016). DOI: 10.1002/adma.201603662 (cit. on p. 27).